Christian Holden

Modeling and Control of Parametric Roll Resonance

Thesis for the degree of philosophiae doctor
Trondheim, June 2011

Norwegian University of Science and Technology
Faculty of Information Technology, Mathematics and Electrical Engineering
Department of Engineering Cybernetics

NTNU
Innovation and Creativity

NTNU
Norwegian University of Science and Technology

Thesis for the degree of philosophiae doctor

Faculty of Information Technology, Mathematics and Electrical Engineering
Department of Engineering Cybernetics

ISBN 978-82-471-2896-1 (printed version)
ISBN 978-82-471-2897-8 (electronic version)
ISSN 1503-8181
ITK Report 2011-6-W

Doctoral theses at NTNU, 2011:174

Printed by Skipnes Kommunikasjon as

Til familien.

Summary

Parametric roll resonance is a dangerous resonance phenomenon affecting several types of ships, such as destroyers, RO-RO paxes, cruise ships, fishing vessels and especially container ships. Worst case, parametric roll is capable of causing roll angles of at least 50 degrees, and damage in the tens of millions of US dollars.

Empirical and mathematical investigations have concluded that parametric roll occurs due to periodic changes in the waterplane area of the ship. If the vessel is sailing in longitudinal seas, with waves of approximately the same length as the ship, and encounter frequency[1] of about twice the natural roll frequency, then parametric resonance can occur.

While there is a significant amount of literature on the hydrodynamics of parametric roll, there is less on controlling and stopping the phenomenon through active control. The main goal of this thesis has been to develop controllers capable of stopping parametric roll. Two main results on control are presented.

To derive, analyze and simulate the controllers, it proved necessary to develop novel models. The thesis thus contains four major contributions on modeling.

The main results are (presented in order of appearance in the thesis):

Six-DOF computer model for parametric roll The model is valid for non-constant speed and course and incorporates the effects of waves (first order) through integrating the pressure field over the instantaneous submerged part of the hull. Most existing models require constant speed.

The main drawback of the novel model is that it is not analytical, and thus only suitable for simulation, not analysis.

One-DOF model of parametric roll for non-constant velocity Assuming that the velocity (speed and course) of the ship changes only slowly, a quasi-steady approach is used to derive explicit expressions for the heave and pitch motion as functions of time. Inserting these functions into the known non-linear couplings between heave/pitch and roll, a 1-DOF analytical model is derived. The model was verified against the 6-DOF model and showed very good fit across a wide range of scenarios.

It was also shown that the commonly used Mathieu equation is not capable of accurately modeling parametric roll resonance if the encounter frequency (and thus speed and course) is not constant.

[1] The encounter frequency is the frequency of the waves as seen form the ship. Due to the Doppler effect, this is not the same as the actual frequency of the waves.

Three-DOF model of parametric roll Chronologically the first model derived, this model considers the nonlinear coupling between heave/pitch and roll. Using a third-order Taylor series expansion of the restoring term, the model is analytical. Parameters can be computed based on hull data. The model was verified against experiments with a 1:45 scale model of a 281 m container ship. The main drawback of the model is that it requires constant ship velocity.

Seven-DOF model for ships with u-tanks of arbitrary shape U-tanks are anti-roll tanks consisting of two fluid-filled reservoirs (one port side and one starboard side) with a duct connecting them. The weight and motion of the tank fluid is used to damp out roll. Existing models require a particular tank shape, only take into account some degrees of freedom and are largely linear.

The new model has all seven DOFs (six for the ship and one for the tank), captures all the inherent nonlinearities of the system and can handle u-tanks of arbitrary shape. The model was derived with Hamiltonian mechanics.

The model was verified against experimental data.

Frequency detuning controller Parametric resonance can only occur if the encounter frequency is approximately twice the natural roll frequency. The encounter frequency can be changed by changing the ship's speed or course via the Doppler effect. Frequency detuning control is exploiting this phenomenon to drive the encounter frequency away from the dangerous values.

The model was derived using the 1-DOF parametric roll model, and mathematically proven to stop parametric roll resonance. The controller was verified in simulation against both the 1-DOF model and the 6-DOF computer model. The controller is quite simple, and does not require any special hardware or software on the ship.

There are two main drawbacks of the controller: It requires that the controller be turned on quite early during parametric resonance, when the roll angle is still small. Furthermore, it requires that the ship is capable of fairly rapid speed changes.

Active u-tank based controller for parametric roll Using a 2-DOF (roll and tank state) version of the 7-DOF u-tank model, we derived a controller capable of stopping parametric roll. The validity of the model was proven mathematically, and verified in simulation using two different models of varying complexity. The control system uses almost no resources.

For comparison, the system was also simulated with the controller turned off in the same scenario (that is, a ship with a passive u-tank in parametric roll resonance). The passive u-tank did reduce the roll motion, but was not capable of driving it to zero. A passive u-tank is also highly dependent on correct tuning of the u-tank's natural frequency (which should equal the ship's natural roll frequency). However, it is quite difficult to tune this correctly.

An active u-tank does not have this drawback. Given the modest resource consumption, it is probably advantageous to use an active u-tank.

Contents

List of figures

List of tables

List of models

Preface

This thesis is submitted in partial fulfillment of the requirements for the degree of philosophiae doctor (PhD) at the Norwegian University of Science and Technology (NTNU).

This thesis presents the results of my doctoral studies, carried out at the Department of Engineering Cybernetics and the Centre for Ships and Ocean Structures, both part of NTNU, in the period June 2006–June 2011. My supervisor has been Professor Thor I. Fossen of the Department of Engineering Cybernetics/Centre for Ships and Ocean Structures, NTNU and my co-supervisor Associate Professor Tristan Perez of the Mechatronics Program & Robotics Research at the University of Newcastle, Australia.

During my time as a PhD student I was given the opportunity to collaborate with Professor Marcelo Almeida Santos Neves at the Department of Naval Architecture and Ocean Engineering, LabOceano/COPPE, Federal University of Rio de Janeiro, Brazil. I was also lucky enough to visit him and his colleagues in Rio a short week in February, 2007. I also spent two months (October–November 2007) with Professor Henk Nijmeijer and his colleagues at the Department of Mechanical Engineering, Eindhoven University of Technology, the Netherlands. I am very grateful for the their hospitality. I learnt a lot and had a great time.

Acknowledgments

No work is done in a vacuum, and so also with my thesis. There are several people I would like to thank, who, in some way or another, have contributed to me being able to present my thesis and obtain the fancy title of "doctor" (but not the kind that does anyone any good).

While there will certainly be someone I've forgotten to mention – my profuse apologies – I would especially like to thank the following wonderful people:

Firstly, big thanks to my supervisor, Professor Thor I. Fossen of the Department of Engineering Cybernetics/Centre for Ships and Ocean Structures, NTNU and my co-supervisor Associate Professor Tristan Perez of the Mechatronics Program & Robotics Research at the University of Newcastle, Australia. Without their help and support (and willingness to hire me in the first place) there would be no thesis, certainly not this one. I can't say there wouldn't be any Dr Holden without them, because there's quite the number of Dr Holdens already.

I would like to thank the Department of Engineering Cybernetics (ITK) and the Centre for Ships and Ocean Structures (CeSOS), both part of NTNU, who

have been my employers while I was working on my thesis. I like to think that I have given something back to them, but they have certainly given a lot to me (an office and a paycheck, and support when I needed it).

On the same note, I would like to thank my many friends and coworkers, both those who've finished before I did and those who're still slaving away at their keyboards, for cooperation and friendship during long working days and longer coffee breaks. I would especially like to thank my office mates Arnfinn Aas Eielsen and Dr Gullik Jensen who have been as great office mates as I could hope for. I would also like to thank Dr Roberto Galeazzi and Dominik Breu with whom I've collaborated extensively and whose company is enjoyable both in and out of the office.

SINTEF Marintek deserves thanks for the use of their laboratory. Doing experiments is always a pain in the neck (but frequently fun and usually rewarding), and I'm very grateful to Kjetil Berget for helping me out of the quagmire. The experimental results were invaluable.

My gratitude goes to SINTEF Marintek and especially Dr Ingo Drummen for having provided the experimental facilities and performing the experiments in the towing tank. I can't imagine it was any easier than my u-tank experiments (but hopefully fun and rewarding for them, too; it was certainly indispensable for me).

The Research Council of Norway (Norges forskningsråd) footed the bill (via ITK and CeSOS and the Strategic University Program (Strategisk universitetsprogram) on Computational Methods in Nonlinear Motion Control, administered by Professor Tor Arne Johansen) for which I am of course grateful.

A big, big thanks goes of course to the Norwegian taxpayers for ultimately funding my work. I couldn't have done it without your unknowing but tacit support for fundamental research in general and my research in particular. Since almost none of you are going to actually read this thesis, I guess these words are kind of futile, but my thanks are heartfelt.

Last, but certainly not least, I would like to thank my family. My father (always there with helpful advice and anything else that is needed); my mother; my three brothers Mads, Frederik and Daniel; my four grandparents, especially Bestemor; and more extended family than I can count to.

Christian Holden

Trondheim, April 2011

I think we may safely say that the studies preliminary to the construction of a great theory should be at least as deliberate and thorough as those that are preliminary to the building of a dwelling-house.

Charles Sanders Peirce,
The Architecture of Theories

Part I

Preliminaries

Chapter 1

Introduction

In this thesis, the phenomenon of parametric roll resonance is investigated, and two control strategies presented that attempts to solve the problem. To be able to derive, analyze and simulate the controllers, a significant amount of modeling work was also done. Some background material, strictly speaking not new research but necessary to understand the rest of the work, is also included.

1.1 Motivation

This thesis is motivated largely by several spectacular maritime disasters, of which two will here be described in detail.

1.1.1 The *APL China* incident

> "Cargo, container and vessel owners and their underwriters confronted the largest container casualty in history." France et al. [27]

In late October 1998, the M/V *APL China* was traveling from Kaohsiung, South Korea to Seattle, USA carrying over 4 000 containers full of cargo for the Christmas season. The *APL China* is no small vessel; it is a post-Panamax C11 container ship, with a length of 260 m, breadth of 40 m and draft of 24.5 m.

Off Alaska's Aleutian Islands it was overtaken by a violent storm. The encounter with the storm lasted about 12 hours, and the master reduced speed and attempted to steer into the increasingly high waves off the vessel's starboard bow.

The storm was severe, and officers reported green water at bridge level during the worst of it. Even worse than the violence of the seas were reports of extreme and violent ship motions during the worst parts of the storm. There were significant pitch amplitudes, and simultaneously port and starboard roll angles reached approximately 35 to 40 degrees.

The following morning, the damage could be assessed: Of the 1 300 containers on deck, 300 had been lost overboard with their cargo. Another 400 had been damaged. Containers hung over the sides of the vessel, and the *APL China* itself had suffered structural damage. See Figure 1.1 for pictures of her when she arrived in Seattle.

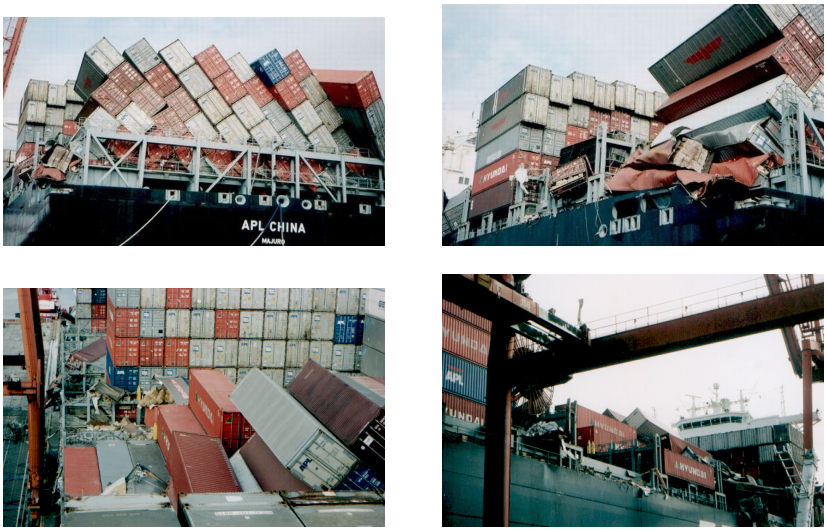

Figure 1.1: The *APL China* incident. Images from cargolaw.com.

Insurance lawyers estimated that the lost cargo was worth more than the total value of the ship. To limit liability, the ship's owners, APL, got New York's federal district court to limit its liability to USD 50 million, the total value of the ship. It is regarded as the greatest container disaster in history.

(Account taken from France et al. [27], Ginsberg [35].)

1.1.2 The *Mærsk Carolina* incident

> "The crew described the onset as a sudden departure from the normal rolling motion of the vessel [...] building to the maximum [of more than 47 degrees] in only a few roll cycles." Carmel [12]

In January 2001, the *Mærsk Carolina* sailed from Algeciras, Spain to Halifax, Nova Scotia, Canada. She carried 675 containers of 20 ft and 1 505 containers of 40 ft, with a total cargo of 36 021 metric tons. At 290 m length, 32 m breadth and 13.5 m draft, the *Mærsk Carolina*, too, is a very large vessel.

During worsening weather east of Nova Scotia, and in increasingly heavy seas, the ship followed standard procedure and reduced speed and turned directly into the waves. At around 2000 hours local time, the vessel experienced extraordinarily heavy roll, in excess of 47 degrees. The actual roll angle is impossible to know; the on-board inclinometer saturates at that value. Simultaneously, the ship experienced heavy heave and pitch motion, and the crew reported that the roll motion had come from seemingly nowhere, building up in just a few cycles. Massive amounts of green water were observed boarding the vessel as the bow pitched down into successive waves.

When the *Mærsk Carolina* finally arrived in Halifax (Figure 1.2), an investigation found that 133 containers were lost at sea, and 50 containers were damaged. In

total, cargo claims exceeded USD 4 million. The vessel itself also suffered structural damage, and indicated that the ship had been placed under considerable stress.

(Account paraphrased from Carmel [12].)

Figure 1.2: The *Mærsk Carolina* incident. Images from cargolaw.com.

1.2 Parametric roll resonance

While other examples exist (such as the 2005 incident with the Horizon Navigation-owned cruise ship *Voyager*[1]), the above examples should provide ample motivation for why parametric roll should be investigated. However, the examples do not explain what is happening.

As research has shown, the incidents described (and others like them) were caused by parametric roll resonance [12, 27, 32]. Parametric roll resonance is, as the name implies, a resonance phenomenon.

Parametric resonance is distinct from "normal" resonance, which is characterized by external forces. It is perhaps best explained with the help of a differential equation:

$$\ddot{x} + d\dot{x} + k(t)x = u \tag{1.1}$$

where x is the state and $d > 0$ is a constant parameter. u is external forcing and $k = k_0 + k_t \cos(\omega_k t)$ with $k_0 > k_t \geq 0$ and $\omega_k > 0$ constant.

If $k_t = 0$ and $u = u_0 \cos(\omega_u t)$ with $u_0 \neq 0$, then the system will be resonating if $\omega_e \approx \sqrt{k_0}$ [63]. This is a well-known problem, and x can reach dangerously high values, as seen in Figure 1.3(a).

However, if $k_t \neq 0$, $u = 0$ and $\omega_k \approx 2\sqrt{k_0}$, then as long as d is not too large and $x(t_0), \dot{x}(t_0)$ are not both zero, the system will parametrically resonate. There are several possible responses, but a typical one is an exponentially increasing oscillating motion, with frequency of $\sqrt{k_0}$, as seen in Figure 1.3(b). [63]

[1] See www.youtube.com/watch?v=1hUqt2acbm8 or news.bbc.co.uk/2/hi/europe/4264661.stm.

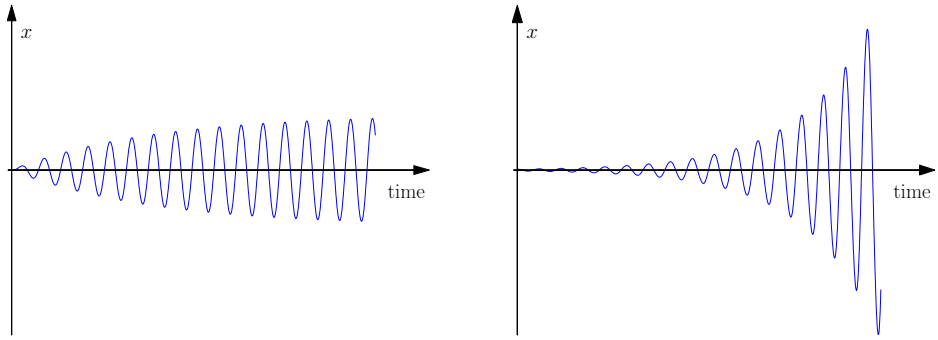

(a) "Ordinary" resonance ($u_0 \neq 0, k_t = 0$). (b) Parametric resonance ($u_0 = 0, k_t \neq 0$).

Figure 1.3: Two types of resonance (x and y axes on the same scale).

A closer examination of Figure 1.3 shows important differences and similarities between the two types of resonance. Apart from the values of k_t and u_0, both simulations used the same parameters. In both cases, x resonates at the same frequency (specifically, at the natural frequency $\sqrt{k_0}$), despite the fact that the frequency of excitation are different in the two cases ($\omega_u = \sqrt{k_0}$ while $\omega_k = 2\sqrt{k_0}$). It is also worth noting that the externally forced resonance causes x to grow fairly slowly to a maximum (but high) value. Parametric resonance, on the other hand, builds exponentially[2], and – for the linear ODE (1.1) – grows unbounded.

It has been known since the 19th century that several systems are capable of experiencing parametric resonance [22, 30, 31, 59, 60]. Some ships are susceptible to parametric resonance, principally in roll [1, 5, 10, 15, 28, 30–32, 38, 46–48, 56, 64, 66–68, 72, 76, 80, 84–86, 89, 90]. This was first described in 1861 [30].

To explain why ships are susceptible, we first note that, commonly, the coefficient of the restoring moment in roll is considered proportional to the waterplane area (i.e., the 2-D plane created by cutting the hull at the waterline) [24].[3]

Consider the following scenario (Figure 1.4):

1. A ship is sailing in longitudinal waves, of wave length approximately the length of the ship. At this instant in time, the ship has a small, non-zero roll angle, and the wave trough amidships. If the ship's hull is correctly shaped, there will be a very large waterplane area at this time instant. Therefore, the restoring moment coefficient in roll is quite large, and a large moment forces the ship upright.

2. Some time later, when the ship is upright and the roll angle – but, crucially, not roll velocity – is zero, the wave crest is amidships. Due to the shape of the hull, the waterplane area is now much smaller, and so is the restoring moment coefficient. Due to this, there is very little resistance to further rolling. And

[2] This exponential growth explains why sailors stated that the high rolling came "from nowhere"; the time it takes to go from noticeable to dangerous is very short with exponential growth.

[3] Technically, this analysis is a simplification, using only hydrostatics.

since the ship still has roll velocity and thus angular momentum, it will keep going.

3. Still later, the ship will be at maximum roll angle. If this coincides with when the wave through is amidships, the waterplane area and the restoring moment coefficient will be large. So is the roll angle, and an even larger moment forces the ship upright again.
4. Once upright, angular momentum is still higher, and the moment stopping the ship from rolling further very small, and so the ship rolls even further to the other side.

Over a few cycles, this motion builds up to very high roll values, easily up to 50° as seen in the *Mærsk Carolina* incident [12]. The exact value reached depends on conditions and the hull shape.

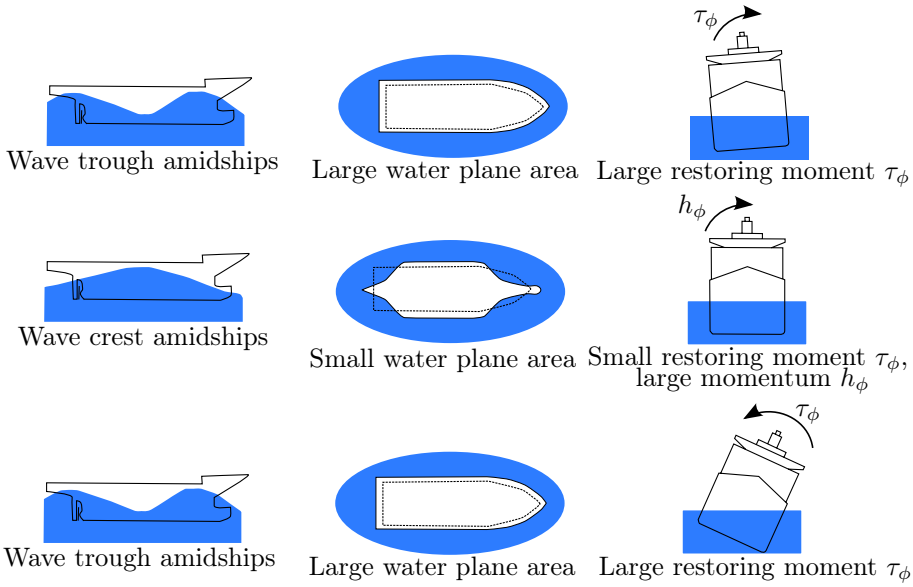

Figure 1.4: Parametric roll resonance.

From the above explanation, we can formulate certain empirical criteria for the onset of parametric roll resonance [27]:

Encounter frequency equal to twice the natural roll frequency This ensures the timing necessary for the waterplane area to change in time with the roll motion.[4]

Wave length equal to the ship length This is necessary to get sufficiently large changes in waterplane area.

Sufficient wave height This is necessary to get sufficiently large changes in waterplane area.

[4]The encounter frequency is the frequency of the waves as seen from the ship. Due to the Doppler effect, this is not the same as the actual frequency of the waves.

Sufficiently low roll damping If the damping is too high, the roll motion will be quickly damped out. Unfortunately, roll damping is usually low.

Worth noting is that if the seas are irregular, it reduces the likelihood of parametric roll resonance, as it interrupts the precise timing of waterplane area changes necessary.

As a side note, parametric resonance can also be described in a different manner. Consider the following equations:

$$\ddot{z} + d_z\dot{z} + k_z z = u_0 \cos(\omega_u t) \tag{1.2}$$

$$\ddot{x} + d_x\dot{x} + k_x x + k_{xz} xz = 0 \tag{1.3}$$

Since z of (1.2) is not affected by x, z will eventually reach a steady-state motion of $z = z_0 \cos(\omega_u t + \alpha_z)$ [3]. Eventually, then, (1.3) will become

$$\ddot{x} + d_x\dot{x} + [k_x + k_{xz} z_0 \cos(\omega_u t + \alpha_z)]\, x = 0. \tag{1.4}$$

This is the same as (1.1), and can parametrically resonate if $\omega_u \approx 2\sqrt{k_x}$ [63, 88].

As it turns out, heave and pitch are coupled nonlinearly with roll in the restoring moment, giving rise to equations similar to (1.2)–(1.3) [6, 64–66, 68–71, 73, 78, 88]. But, as we have seen, these two ways of looking at the phenomenon are effectively the same [88].

As mentioned, a crucial necessity for parametric roll to occur is a hull shape such that the waterplane area can change significantly depending on the position of the wave crest. Several different types of ship do have this unfortunate shape (so designed due to other concerns, such as maximizing cargo space and minimizing drag) and are known to be susceptible to parametric roll. Examples are destroyers [28], RO-RO paxes [29], PCTCs [72] and fishing vessels [64, 66–68]. Container carriers, however, are extremely prone to parametric roll because of the hull shape, i.e., large bow flares and stern overhangs. This makes them particularly prone to changes in waterplane area. Consequently, significant research has gone into investigating container ships specifically [5, 11, 32, 38, 46–48, 56, 76, 80, 80, 86, 89, 90], no doubt also spurred by the *APL China* and *Mærsk Carolina* incidents.

For an in-depth mathematical investigation of parametric resonance, the reader might consult Nayfeh and Mook [63]. Tondl et al. [88] gives a thorough overview of the phenomenon in mechanical systems. The reader might also enjoy Fossen and Nijmeijer [25].

1.3 Main contributions

There are six main contributions in this thesis, four on modeling and two on control.

1.3.1 Modeling contributions

While the main goal of the thesis work has been to develop control systems that can stop parametric roll resonance, accurate and powerful models are needed to derive and test the control schemes. To this effect, four novel models have been

developed. Three of these are for ships in parametric roll, and the third for ships equipped with a u-tank (suitable for ships in and out of parametric roll).

One-DOF models (uncoupled roll) have been a popular choice for analyzing the critical parameters of the phenomenon and derive stability conditions [27, 38, 51, 80, 89]. The very simplest model suitable for parametric roll is the Mathieu equation [88]

$$m_{44}\ddot{\phi} + d_{44}\dot{\phi} + [k_{44} + k_{\phi t}\cos(\omega_e t + \alpha_\phi)]\,\phi = 0 \tag{1.5}$$

where ϕ is the roll angle, m_{44} is the sum of the rigid-body moment of inertia and added mass in roll, d_{44} is a linear damping parameter, k_{44} a linear spring term and ω_e the encounter frequency (i.e., the Doppler-shifted frequency of the waves as seen from the ship). $k_{\phi t}$ gives the amplitude of the change in the linear spring term, and α_ϕ the phase. All the parameters are constant. Note that (1.5) is equivalent to (1.1) and (1.4).

The Mathieu equation has the advantage of great simplicity, and is quite capable of displaying behavior similar to that of a ship suffering parametric roll if the parameters are given the corrects value. The Mathieu equation will oscillate if $\omega_e \approx 2\sqrt{k_{44}/m_{44}}$; d_{44}, k_{44} are not too big; and $\phi(t_0), \dot{\phi}(t_0)$ are not both zero [88].[5]

Unfortunately, while simple, the Mathieu equation has certain limitations. One is its lack of accuracy. While experience shows that parametric roll resonance is limited in amplitude (although that amplitude can be quite large), the standard Mathieu equation will grow unbounded (Figure 1.3(b)). Adding a nonlinear spring term such as $k_{\phi^3}\phi^3$ with $k_{\phi^3} > 0$ to the left-hand side of (1.5) takes care of this problem [63], and gives the model higher accuracy. It is still only valid for regular waves and constant forward speed and heading and the accuracy could still be further improved.

By assuming quasi-steady heave and pitch and the dynamic interaction between the vertical motions and the roll oscillations, Bulian [9] proposed a 1.5-DOF model. Moreover, that assumption also allowed an analytical description of the so-called $\overline{\mathrm{GZ}}$ curve (see, e.g., Faltinsen [20], Fossen [24]) that was approximated as a surface varying with roll angle and wave crest position. Considered valid for moderate ship speed in head seas, the model has lead to reasonable results in predicting parametric roll.

A 3-DOF (heave, roll, pitch) nonlinear fully coupled model was first developed by Neves [65]. There, restoring forces and moment nonlinearities were Taylor expanded up to second-order. Although the model provided a thorough description of the nonlinear interactions of the different modes, it tended to overestimate the roll oscillations. Therefore third-order Taylor series expansion of the restoring forces and moment was used in Neves and Rodriguez [64]. In that model, the nonlinear coefficients were mathematically derived as functions of the characteristics of the hull shape. That 3-DOF model was used for prediction parametric roll in a transom stern fishing vessel [66, 67], and provided a better match to experimental results than the second-order model.

This leads us to the first major contribution:

[5] Other parameter combinations will also give parametric resonance of the Mathieu equation [63], but these are the one that is most useful for modeling ship behavior [88].

Contribution 1 (3-DOF parametric roll model)**.** In Chapter 6, we present a 3-DOF model (heave, roll and pitch) for ships in parametric resonance, suitable for regular seas.

The results of Neves and Rodriguez [64] was applied to describe the dynamics of a container ship during parametric roll resonance in head seas with regular waves. The model parameters were identified based upon the ship line drawings and loading conditions.

The reliability of the implemented model in simulating parametric roll was verified against experimental data gathered from model scale tests in SINTEF Marintek's facilities in Trondheim, Norway.[6] The verification showed good agreement with the experimental results for roll both in the experiments where parametric roll resonance occurred, and in the experiments where it did not occur.

The model has been published in Holden et al. [40], Rodriguez et al. [77].

However, the 3-DOF model is only valid for regular waves and constant forward speed/course. Its main advantage over simpler model is greater accuracy, but it is not capable of modeling fundamentally different scenarios. Furthermore, it has the disadvantage the the model parameters are computed only for a certain fixed sea states and forward speeds. Change any of these, and the parameters would have to be re-computed.

A new model was therefore developed:[7]

Contribution 2 (6-DOF parametric roll model)**.** In Chapter 5, we present a 6-DOF model for ships in parametric roll resonance, suitable for both regular and irregular seas.

External forces due to the surrounding ocean are taken into account by integrating the instantaneous pressure field of the surrounding ocean over the instantaneous submerged part of the ship. Some of these forces are computed off-line, but some are computed on-line. An analytical expression is not derived, which means that this model can only be used in simulation on a computer. Although our implementation was done using regular seas, the framework is quite capable of handling other sea states. Wave-induced forces are effectively included as first-order forces via the pressure field.

The model is capable of handling a wide range of maneuvers, including both speed and course changes. This makes the model quite suitable to study the effects of such changes.

The model has been published in Breu et al. [8].

An unfortunate downside to the 6-DOF model is that it is not analytical. While the 3-DOF model is, it is not capable of handling different sea states. A compromise model between the 3-DOF and 6-DOF models was needed:

Contribution 3 (1-DOF parametric roll model for non-constant speed)**.** In Chapter 5, we present a 1-DOF model for ships in parametric roll resonance, suitable for non-constant forward speed in regular seas.

[6] Experiments performed by Dr Ingo Drummen.

[7] Although the 6-DOF and 1-DOF models appear earlier in the thesis than the 3-DOF model, they were developed later.

Assuming that the speed changes only slowly (a fairly valid assumption for high-inertia ships such as the container vessel used in this thesis (76 500 metric tons)), we use a quasi-steady approach to derive explicit time-domain solutions to the heave and pitch motions. Inserting these into the known heave and pitch couplings in roll yields a 1-DOF roll model.

The model is analytical, fairly easy to analyze mathematically, reasonably accurate compared to the 6-DOF model and can handle non-constant forward speeds. This makes the model suitable for designing a frequency detuning controller (changing encounter frequency to violate the frequency condition for parametric resonance, see Contribution 5).

The model has been published in Breu et al. [8].

A possible avenue of control was frequency detuning – changing the speed of the vessel to change the encounter frequency (see Contribution 5). The 6-DOF and 1-DOF parametric roll models allows us to investigate the effectiveness of this method. The effects of changes in surge have beens investigated before [32–34, 47, 83] but not with models of the accuracy 6-DOF model, and with different goal [47, 83] or different detail [32–34] than that found in Contribution 5.

While frequency detuning can be used to control parametric roll (as seen in Chapter 11), there are some concerns regarding the effectiveness of this method. Using direct actuation in roll allows one to set up a counter moment that drives the roll angle to zero. Most ships aren't equipped with direct actuators in roll [24], but there are several options. Among these are u-tanks (see Figure 1.5(a)), fins and gyro stabilizers (see, e.g., Perez [75]). In this thesis, we have focused on u-tanks (sometimes known as u-tube tanks or u-shaped anti-roll tanks).

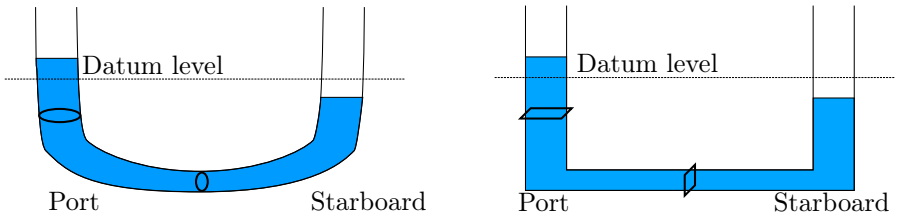

(a) A generic u-tank.

(b) A rectangular-prism u-tank.

Figure 1.5: U-tank design.

As the ship rolls, the fluid inside the u-tank (usually water) moves. Ideally, for an un-actuated tank, the fluid should move with the same frequency as the rolling motion of the ship, but lagging a quarter of a period behind the roll motion [58]. This moment attains its maximum values when the ship passes through its vertical position. Thus, the vessel's roll kinetic energy is transformed into kinetic and potential energy of the tank fluid. Part of the energy is dissipated by vortex shedding and fluid viscous effects related to skin friction on the walls of the tank [4].

There are two main advantages of u-tanks: They have medium to high performance in terms of roll reduction (estimated to be in the range of 20–70 % (RMS)),

and their performance is independent of the speed of the vessel. This makes u-tanks the preferred option for vessels that spend large amounts of time at zero or low speeds, such as fishing vessels [61].

There are, unfortunately, also disadvantages [4, 58]. Chief among these is that they take up room that could otherwise have been used for machinery, cargo or passengers; and that they can (at least if passive, i.e., uncontrolled) have averse effects on the stability of the ship. Part of this is due to the free surface effect, but another is because they are, if passive, only designed to reduce roll in certain frequency bands. In others, they actually increase roll.

From a control perspective, another disadvantage of u-tanks compared to other potential actuators, is that the roll and tank modes are tightly coupled, and only indirectly give a control moment in roll. Output stabilization (with roll as output and the tank state as internal state) tends to not leave the tank in its equilibrium position, at least in the presence of parametric roll, as seen in Holden et al. [42].

Anti-roll tanks can be either passive or active. In passive tanks, the fluid flows freely from side to side. The tank is dimensioned so that the tank fluid's natural period equals the natural roll period of the ship [57, 58]. In the presence of waves, however, the roll period is determined by the frequency of the waves, not the natural frequency in roll [63]. Therefore, active control is necessary to maintain performance across a wider range of conditions.

Active tanks operate in a similar manner to their passive counterparts, but they incorporate a control system which modifies the period of the tank to match the actual ship roll period, and can also ensure optimal phase difference. Control can be achieved by adjusting the air that flows from one reservoir to the other by means of an air duct and a controlled valve, high-pressure air, or by pumps located in the fluid duct [79].

Several models of u-tanks exist. One of the oldest [62] is that of Goodrich [37]. The model is fairly simple; the tank's effect on roll is attributed to a single linear term proportional to the difference in fluid volume in the two reservoirs. Kagawa et al. [49, 50] developed a model based on Lagrangian mechanics for the purpose of controlling the swaying of skyscrapers during earthquakes. However, they only modeled the tank's effect on sway, not on roll. The most commonly used model is that of Lloyd [57, 58]. This model includes sway, roll, yaw and a single degree of freedom for the tank fluid.

All these models have in common that they are derived for rectangular-prism u-tanks, as seen in Figure 1.5(b) [44, 50, 57, 58, 62, 79], while several actually installed tanks do not match this shape [74, 75, 79]. A model for more generic tank shapes is therefore useful. In addition, most models are linear, and technically only valid for small roll angles [26, 37, 50, 57, 58, 62]. During parametric resonance, the roll angle can reach 40 to 50 degrees [27, 32, 34, 40, 42].

All these drawback necessitated a new model:

Contribution 4 (7-DOF nonlinear model for generic u-tanks)**.** In Chapter 7, we present a 7-DOF model of u-tanks of arbitrary shape.

The model was derived using Hamiltonian mechanics, and exclusively models the tank–ship interactions. Other forces, such as those exerted by the ocean, are added afterwards in a Newtonian framework. The model assumes one-dimensional

tank flow, but captures the inherent nonlinearities of the dynamics. It is valid for almost arbitrary conditions.

The model was experimentally verified (Chapter 9) and compared to the model of Lloyd [57, 58] (Chapter 8).

The model has not yet been published, but is a generalization of that found in Holden and Fossen [39], Holden et al. [44]. Verification results have been published in Holden et al. [44] (for a special case of the general model).

1.3.2 Contributions in automatic control

Although deriving new models proved necessary, the main goal of the thesis work has been to derive controllers that are capable of stopping parametric roll.

There are two basic approaches to control parametric roll; we can call them *direct* and *indirect*.

Indirect methods attempt to ensure that the conditions necessary for parametric roll to develop are violated, as seen in Breu and Fossen [7], Jensen et al. [47, 48], Ribeiro e Silva et al. [76]. Perhaps the simplest one of these is to change the ship's speed or course, which changes the encounter frequency ω_e via the Doppler effect.

The direct method, as seen in Holden and Fossen [39], Holden et al. [42], Umeda et al. [90] uses actuators to set up a counter-acting moment in roll, and use this to drive roll to zero. Direct methods can be *active* or *passive*. Active methods use active control, while passive does not. Examples are controlled (active) versus uncontrolled (passive) u-tanks.

A combination of direct and indirect methods is also possible, as seen in Galeazzi [32], Galeazzi and Blanke [33], Galeazzi et al. [34].

Although separately, direct (active) and indirect approaches are used in this thesis.

We investigated an indirect method we have called frequency detuning control. As mentioned previously in the introduction, ships can parametrically roll if the encounter frequency is about twice the natural roll frequency. The encounter frequency can be changed via Doppler shift by changing speed and/or course. Thus, we detune the encounter frequency away from the (potentially) dangerous values.

Frequency detuning has the advantage of great simplicity. As long as the helmsman is aware that the ship is in danger of parametrically rolling, performing a speed and/or course change is fairly straightforward and requires no complicated or expensive control systems.

This leads us to the first control contribution:

Contribution 5 (Frequency detuning control)**.** In Chapter 11, we present a frequency detuning controller capable of stopping parametric roll by changing the speed of the vessel, and thus Doppler shifting the encounter frequency away from the dangerous values.

The controller is based on the model listed as Contribution 3. The validity of the controller is proven mathematically, and verified by simulation against both the simplified model of Contribution 3 and the 6-DOF model of Contribution 2.

This controller has been published in Holden et al. [43].

The main disadvantage of frequency detuning control is that it relies on two key assumptions, that may or may not hold: Firstly, it is vital for the helmsman to detect parametric roll early, or parametric roll will have time to develop fully before the controller has had time to become effective (recall that parametric roll builds exponentially). Secondly, the ship must have the ability to change speed fairly fast. For high-inertia ships such as container ships and cruise ships (which are susceptible to parametric roll) or vessels at rest (such as fishing vessels, also susceptible to parametric roll), this is unlikely to be true.

An active, direct control system is not affected by these drawbacks. This leads us to the final major contribution of this thesis:

Contribution 6 (Active u-tank control)**.** In Chapter 12, we present a control system capable of stopping parametric roll. The control system uses u-tanks as actuators.

The controller was based on a 2-DOF simplification of the model described in Contribution 4. The stability properties of the controller was proven mathematically, and verified in simulation using a higher-fidelity model than the one used to derive the controller.

This controller has been published in Holden and Fossen [39].

The two control schemes can fairly easily be combined, which should further increase the ship's ability to stop parametric roll. However, due to time constraints, this was not investigated during the course of my PhD studies.

1.4 Publications

The thesis work has resulted in nine international publications.

1.4.1 Journal papers

[40] C. Holden, R. Galeazzi, C. A. Rodriguez, T. Perez, T. I. Fossen, M. Blanke, and M. A. S. Neves. Nonlinear container ship model for the study of parametric roll resonance. *Modeling, Identification and Control*, 28(4), 2007.

[44] C. Holden, T. Perez, and T. I. Fossen. A Lagrangian approach to nonlinear modeling of anti-roll tanks. *Ocean Engineering*, 38:341–359, 2011.

1.4.2 Book chapters

[39] C. Holden and T. I. Fossen. A u-tank control system for ships in parametric roll resonance. In T. I. Fossen and H. Nijmeijer, editors, *Parametric Resonance in Dynamical Systems*. Springer-Verlag, 2011.

[43] C. Holden, D. A. Breu, and T. I. Fossen. Frequency detuning control by doppler shift. In T. I. Fossen and H. Nijmeijer, editors, *Parametric Resonance in Dynamical Systems*. Springer-Verlag, 2011.

[8] D. A. Breu, C. Holden, and T. I. Fossen. Ship model for parametric roll incorporating the effects of time-varying speed. In T. I. Fossen and H. Nijmeijer, editors, *Parametric Resonance in Dynamical Systems*. Springer-Verlag, 2011.

1.4.3 Conference papers

[41] C. Holden, T. Perez, and T. I. Fossen. Frequency-motivated observer design for the prediction of parametric roll resonance. In *Proceedings of the IFAC Conference on Control Applications in Marine Systems*, 2007.

[42] C. Holden, R. Galeazzi, T. I. Fossen, and T. Perez. Stabilization of parametric roll resonance with active u-tanks via Lyapunov control design. In *Proceedings of the 10th European Control Conference*, 2009.

[34] R. Galeazzi, C. Holden, M. Blanke, and T. I. Fossen. Stabilisation of parametric roll resonance by combined speed and fin stabiliser control. In *Proceedings of the 10th European Control Conference*, 2009.

[77] C. A. Rodriguez, C. Holden, T. Perez, I. Drummen, M. A. S. Neves, and T. I. Fossen. verification of a container ship model for parametric rolling. In *Proceedings of the 9th International Ship Stability Conference*, 2007.

1.4.4 Papers that are part of this thesis

[8] Makes up the majority of Chapter 5.

[39] Makes up the majority of Chapter 12. Chapter 7 presents a generalization of the model found in [39].

[40] Makes up the majority of Chapter 6 and Appendix C.

[42] Referred to in the text, but does not form a significant part of the thesis.

[43] Makes up the majority of Chapter 11 and Appendix D.

[44] Makes up part of Chapter 8 and the majority of Chapter 9. Chapter 7 presents a generalization of the model found in [44].

[77] Makes up parts of Chapter 6.

1.5 Thesis organization

The rest of this thesis is organized as follows:

Chapter 2 This chapter explains the nomenclature used in this thesis.

Part II This part contains the modeling section of this thesis. Most models used in the thesis are found here.

- **Chapter 3** This chapter presents some basic results on kinematics; it is presented as necessary background and contains no novel contributions.
- **Chapter 4** In this chapter, the equations of motion for a rigid body freely translating and rotating in $\mathbb{R}^3$ is presented. Hamiltonian mechanics is used in the derivation. The results of this chapter are unpublished, but are used as basis for Chapters 5 and 6.
- **Chapter 5** This chapter extends the model of Chapter 4 by including the forces and moments that specifically act on ships. Assuming regular, longitudinal waves, a 1-DOF simplified model is also presented. Both the full and simplified models are valid for ships with non-constant velocity, and the full model is also valid for a wide range of sea states. The chapter is based on Chapter 4 and Breu et al. [8].

Chapter 6 This chapter simplifies the model of Chapter 5 to three degrees of freedom, and presents experimental verification of the reduced-order model. The chapter is based on Chapters 4 and 5, and Holden et al. [40], Rodriguez et al. [77].

Chapter 7 This chapter presents a 7-DOF nonlinear model for ships with u-tanks of arbitrary shape. The ship–tank system is not rigid, and the model is derived using Hamiltonian mechanics. This chapter presents unpublished results (specifically, a generalization of the models of Holden and Fossen [39], Holden et al. [44]).

Chapter 8 This chapter presents the equations for a rectangular-prism u-tank, such as used in Faltinsen and Timokha [21], Holden et al. [44], Lloyd [58], and compares it to the model of Lloyd [57, 58]. Results in this chapter are based on Chapter 7 and Holden et al. [44].

Chapter 9 In this chapter, the model of Chapter 7 is experimentally verified. This chapter is based on Chapter 7 and Holden et al. [44].

Part III This part contains the control results presented in this thesis.

Chapter 10 This chapter gives a brief introduction to the many ways of controlling parametric roll resonance. It contains no novel results.

Chapter 11 In this chapter, parametric roll is controlled using frequency detuning; by changing the speed of the vessel, the encounter frequency is driven away from the resonant conditions. The validity of the controller is proven mathematically and shown in simulation. The results of this chapter are based on Holden et al. [43].

Chapter 12 Based on the model of Chapter 7 and some results from Chapter 9, this chapter presents a u-tank-based controller that is capable of driving the ship out of parametric roll resonance with almost trivial energy expenditure. The validity of the controller is proven mathematically and shown in simulation. This chapter is based on Chapter 7 and Holden and Fossen [39].

Chapter 13 This chapter presents the conclusions and lists avenues for future work.

Appendices Here are found some auxiliary results.

Appendix A This appendix contains rules for differentiating matrices with respect to vectors. It contains unpublished results.

Appendix B This appendix summarizes the basics of Hamiltonian mechanics. It contains no novel contributions, and is presented here only as necessary background.

Appendix C This appendix contains tables of parameters for the model presented in Chapter 6. Results are published in Holden et al. [40].

Appendix D In this appendix, a lemma required for Chapter 11 is proved. It was published in Holden et al. [43].

References Lists the references used in this thesis.

Chapter 2

Nomenclature

This chapter lists the variables used in this thesis. Note that not every symbol used will be defined here; only those that are used in more than one chapter are listed.

In general, matrices will be written in uppercase with italic typeface, e.g., A. Coordinate vectors and scalars are typically written in lowercase with italic typeface, e.g., a. Whether it is a vector or scaler will be stated in the text, but should largely be clear from context.

If the vector has an interpretation as a point, velocity or angular velocity in physical $\mathbb{R}^3$, a superscript will typically denote which reference frame is used to describe the vector, e.g., r^n would denote that r is given in the n-frame. Only two frames are used, the b-frame (fixed to the ship) and the n-frame (fixed to the mean ocean surface and considered inertial). See Chapter 3.

General

$I_n \in \mathbb{R}^{n \times n}$**:** The n-by-n identity matrix.

$0_{m \times n} \in \mathbb{R}^{m \times n}$**:** The m-by-n zero matrix.

$e_x = [1, 0, 0]^{\mathrm{T}}$**:** Unit vector in the x-direction (in $\mathbb{R}^3$).

$e_y = [0, 1, 0]^{\mathrm{T}}$**:** Unit vector in the y-direction (in $\mathbb{R}^3$).

$e_z = [0, 0, 1]^{\mathrm{T}}$**:** Unit vector in the z-direction (in $\mathbb{R}^3$).

$S(\cdot) \in \mathrm{SS}(3) \subset \mathbb{R}^{3 \times 3}$**:** A skew-symmetric matrix representing the cross-product in $\mathbb{R}^3$. $S(x)y = x \times y$ if $x, y \in \mathbb{R}^3$.

t**:** The time.

t_0**:** The initial time.

Rigid body dynamics

$R \in \mathrm{SO}(3) \subset \mathbb{R}^{3 \times 3}$**:** Rotation matrix representing the orientation of the b-frame relative to the n-frame. If r is a vector in physical $\mathbb{R}^3$, then $r^n = Rr^b$.

$x^n = [x, y, z]^{\mathrm{T}} \in \mathbb{R}^3$**:** The position of the origin of the b-frame, described in the n-frame.

$\eta = [\eta_r, \eta_i^{\mathrm{T}}]^{\mathrm{T}} \in \mathbb{R}^4$**:** Quaternion describing the orientation of the b-frame relative to the n-frame. $\eta_r = \mathrm{Re}\,\eta \in \mathbb{R}$, $\eta_i = \mathrm{Im}\,\eta \in \mathbb{R}^3$.

$\Theta = [\phi, \theta, \psi]^{\mathrm{T}} \in \mathbb{R}^3$**:** Vector of roll ($\phi$), pitch ($\theta$) and yaw ($\psi$) angles.

$q = [x^{n\mathrm{T}}, \eta^{\mathrm{T}}]^{\mathrm{T}} \in \mathbb{R}^7$**:** Generalized position of the body frame.

v^b**:** The velocity of the b-frame relative to the n-frame, described in the b-frame.

ω^b**:** The angular velocity of the b-frame relative to the n-frame, described in the b-frame.

$\nu = [v^{n\mathrm{T}}, \omega^{b\mathrm{T}}]^{\mathrm{T}}$**:** Generalized velocity of the body frame.

$G(\eta) \in \mathbb{R}^{3\times4}$**:** Matrix relating $\dot{\eta}$ to ω^b; $\dot{\eta} = \frac{1}{2}G^{\mathrm{T}}(\eta)\omega^b$.

$G_\Theta(\Theta)$**:** Matrix relating $\dot{\Theta}$ to ω^b; $\dot{\Theta} = G_\Theta(\Theta)\omega^b$.

$\mathcal{P}(\eta) \in \mathbb{R}^{7\times6}$**:** Matrix relating $\dot{q}$ to ν; $\dot{q} = \mathcal{P}^{\mathrm{T}}(\eta)\nu$.

$M_{\mathrm{RB}} = M_{\mathrm{RB}}^{\mathrm{T}} > 0 \in \mathbb{R}^{6\times6}$**:** Generalized inertia of the rigid body.

$C_{\mathrm{RB}}(\omega^b) = -C_{\mathrm{RB}}^{\mathrm{T}}(\omega^b) \in \mathbb{R}^{6\times6}$**:** Coriolis/centripetal matrix of the rigid body.

$p = [p_l^{\mathrm{T}}, p_r^{\mathrm{T}}]^{\mathrm{T}} \in \mathbb{R}^6$**:** Generalized momentum of the rigid body; $p = M_{\mathrm{RB}}\nu$. $p_l \in \mathbb{R}^3$ and $p_r \in \mathbb{R}^3$ are the first and last three elements.

$\tau \in \mathbb{R}^6$**:** Generalized forces on the rigid body.

The environment

$g > 0 \in \mathbb{R}$**:** The acceleration of gravity.

$\rho > 0 \in \mathbb{R}$**:** Density of the ocean.

$\zeta \in \mathbb{R}$**:** A function describing the ocean surface.

$\zeta_0 > 0 \in \mathbb{R}$**:** The amplitude of the waves.

$\omega_0 > 0 \in \mathbb{R}$**:** The frequency of the waves as seen by an observer in the n-frame.

$k_w \in \mathbb{R}$**:** The wave number of the waves as seen by an observer in the n-frame.

$\alpha_\zeta \in \mathbb{R}$**:** The phase of the waves as seen by an observer in the n-frame.

The ship

$m > 0 \in \mathbb{R}$**:** Mass of the ship.

$J = J^{\mathrm{T}} > 0 \in \mathbb{R}^{3\times3}$**:** The ship's moment of inertia in the body frame.

$r_g^b = [x_g^b, y_g^b, z_g^b]^{\mathrm{T}}$**:** Position of the ship's center of gravity, in the b-frame.

$M_A \in \mathbb{R}^6$ **:** Added mass of the ship.

$M = M^{\mathrm{T}} > 0 \in \mathbb{R}^{6\times6}$**:** Total inertia of the ship.

$C(\omega^b) = -C^{\mathrm{T}}(\omega^b) \in \mathbb{R}^{6\times6}$**:** Coriolis/centripetal matrix of the ship.

$D(\nu) \in \mathbb{R}^{6\times6}$**:** Damping matrix of the ship.

$k(q) \in \mathbb{R}^6$**:** Restoring force on the ship.

$\tau_e \in \mathbb{R}^6$**:** Unmodeled generalized forces on the ship.

$\tau_c \in \mathbb{R}^6$**:** Generalized control forces on the ship.

$u \in \mathbb{R}^6$**:** Control input to the ship.

$m_{44} > 0 \in \mathbb{R}$**:** Total moment of inertia (rigid body and added mass) of the ship in roll.

$d_{44} > 0 \in \mathbb{R}$**:** Linear damping parameter in roll.

$k_{44} > 0 \in \mathbb{R}$**:** Linear restoring parameter in roll.

$k_{\phi^3} > 0 \in \mathbb{R}$**:** Nonlinear restoring parameter in roll.

$k_{\phi t} > 0 \in \mathbb{R}$**:** Amplitude of the changes in the linear restoring parameter in roll.

$\alpha_\phi > 0 \in \mathbb{R}$**:** Phase of the changes in the linear restoring parameter in roll.

ω_ϕ**:** The ship's natural roll frequency; $\omega_\phi = \sqrt{k_{44}/m_{44}}$.

$\omega_e \in \mathbb{R}$**:** The encounter frequency; the Doppler-shifted frequency of the waves as seen from the ship.

U-tanks

$\sigma \in \mathbb{R}$**:** Parameter describing the geometry of the tank.

$r_t^b(\sigma) = [x_t^b, y_t^b(\sigma), z_t^b(\sigma)]^{\mathrm{T}} \in \mathbb{R}^3$**:** A function describing the centerline of the u-tank, in the b-frame.

$A(\sigma) > 0 \in \mathbb{R}$**:** Cross-sectional area of the tank.

$\rho_t > 0 \in \mathbb{R}$**:** Density of the tank fluid.

$\varsigma_0 > 0 \in \mathbb{R}$**:** Mean level of tank fluid.

$\varsigma_p \in \mathbb{R}$**:** Instantaneous position of the tank fluid surface in the port side reservoir.

$\varsigma_s \in \mathbb{R}$**:** Instantaneous position of the tank fluid surface in the starboard side reservoir.

$q_t \in \mathbb{R}$**:** Generalized position of the tank fluid.

$A_0 > 0 \in \mathbb{R}$**:** An arbitrary parameter.

$V_t > 0 \in \mathbb{R}$**:** Total volume of the tank fluid.

$m_t > 0 \in \mathbb{R}$**:** Total mass of the tank fluid; $m_t = \rho_t V_t$.

$\bar{m}_t > 0 \in \mathbb{R}$**:** Inertial mass of the tank fluid. Note that $\bar{m}_t \neq m_t$.

$M_t(q_t) = M_t^{\mathrm{T}}(q_t) > 0 \in \mathbb{R}^{7\times 7}$**:** Inertia of a ship with a u-tank.

$\tilde{q} = [q^{\mathrm{T}}, q_t]^{\mathrm{T}} \in \mathbb{R}^8$**:** Generalized position of a ship with a u-tank.

$\tilde{\nu} = [\nu^{\mathrm{T}}, \dot{q}_t]^{\mathrm{T}} \in \mathbb{R}^7$**:** Generalized velocity of a ship with a u-tank.

$\tilde{\mathcal{P}}(\eta) \in \mathbb{R}^{7\times 6}$**:** Matrix relating $\dot{\tilde{q}}$ to $\tilde{\nu}$; $\dot{\tilde{q}} = \tilde{\mathcal{P}}^{\mathrm{T}}(\eta)\tilde{\nu}$.

$\tilde{M}(q_t) \in \mathbb{R}^{7\times 7}$**:** Total inertia of a ship with a u-tank.

$\tilde{C}(q_t, \tilde{\nu}) = -\tilde{C}^{\mathrm{T}}(q_t, \tilde{\nu}) \in \mathbb{R}^{7\times 7}$**:** Total Coriolis/centripetal matrix of a ship with a u-tank.

$\tilde{D}(\tilde{\nu}) \in \mathbb{R}^{7\times 7}$**:** Total damping matrix of a ship with a u-tank.

$\tilde{k}(\tilde{q}, t) \in \mathbb{R}^7$**:** Restoring forces on a ship with a u-tank.

$\tilde{\tau}_e \in \mathbb{R}^7$**:** Unmodeled forces on a ship with a u-tank.

$\tilde{B}$**:** Defines which states are directly controllable for a ship with a u-tank.

u_t**:** Control input to the u-tank.

$\tilde{u} = [u^{\mathrm{T}}, u_t^{\mathrm{T}}]^{\mathrm{T}}$**:** Control input to the ship with a u-tank.

$A_r > 0 \in \mathbb{R}$**:** The cross-sectional area of the reservoirs.

$A_d > 0 \in \mathbb{R}$**:** The cross-sectional area of the duct.

$w > 0 \in \mathbb{R}$**:** The width of the u-tank, measured from the center of one reservoir to the other.

$r_d > 0 \in \mathbb{R}$**:** The distance along the z-axis from the ship's center of gravity to the geometric center of the u-tank.

$h_t > 0 \in \mathbb{R}$**:** The fluid depth in the u-tank.

In theory, there is no difference
between theory and practice.
But, in practice, there is.

Yogi Berra

Part II

Modeling

Chapter 3

Kinematics

In this chapter, we will focus on kinematics, the mathematical relationship between two (or more) reference frames. The contents of this chapter are quite general, and hold true for any reference frames in $\mathbb{R}^3$.

The contents of this chapter is largely gathered from Altmann [2], Conway and Smith [14], Egeland and Gravdahl [19], Fossen [24], Shivarama [81], Shivarama and Fahrenthold [82] and is presented here merely as necessary background for the remaining chapters.

3.1 Reference frames

In this thesis, we will use two reference frames. One is fixed to the Earth, and considered inertial. While not technically true, this approximation is fairly good for vessels not moving extremely far or extremely fast [24]. The other (non-inertial) frame is fixed to the vessel, and moves with it. The inertial frame will be labelled as n, while the body-fixed frame is labelled as b.

The n-frame has its z-axis pointing down towards the center of the earth (i.e., parallel to and in the same direction as the gravity field), and its xy-plane at the mean sea level. Its origin may otherwise be arbitrarily placed.

The b-frame has its origin in the ship. Transversally, the origin is midships. Vertically, the origin is in the waterline when the ship is at rest in calm seas. Longitudinal position is arbitrary. The x-axis points forward, the y-axis to starboard and the z-axis towards the keel. See Figure 3.1.

A vector in $\mathbb{R}^3$ that can be interpreted as a point in physical space (i.e., a position) or the time derivative of such a point (i.e., a velocity) will be written as $\vec{r}$. Decomposed in either coordinate system, it will be written as r^b or r^n. These two coordinate vectors are related by the relationship

$$r^n = Rr^b \tag{3.1}$$

where R is a rotation matrix satisfying $\det(R) = 1$ and $R^{-1} = R^{\mathrm{T}}$ [19].

At any given instant in time, the b-frame may be translated and rotated relative to the n-frame. The translational part gives the position of the ship relative to the inertial frame, and can be fairly straightforwardly handled mathematically. If the

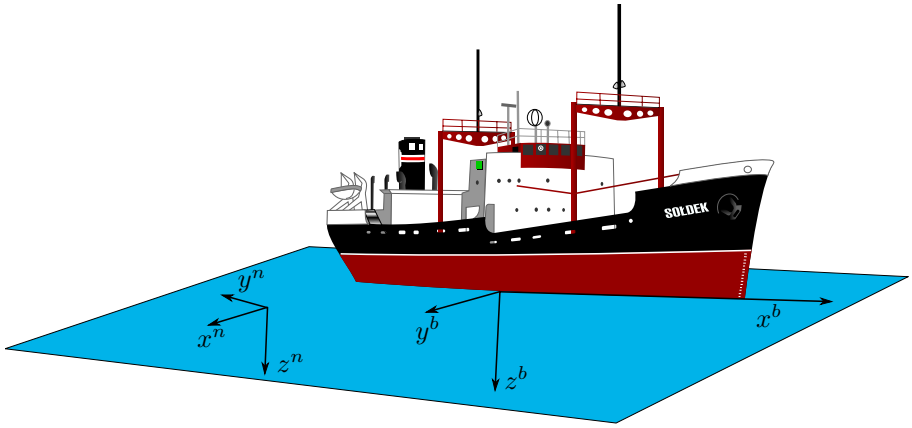

Figure 3.1: Reference frames used in this thesis.

position of the body origin in the inertial frame is $x^n = [x, y, z]^{\mathrm{T}}$, then the (linear) velocity of the body origin (in the inertial frame) is $\dot{x}^n = [\dot{x}, \dot{y}, \dot{z}]^{\mathrm{T}}$.

In the body frame,

$$x^b = R^{\mathrm{T}} x^n \;\Leftrightarrow\; x^n = R x^b. \tag{3.2}$$

However,

$$\dot{x}^b = R^{\mathrm{T}} \dot{x}^n + \dot{R}^{\mathrm{T}} x^n = R^{\mathrm{T}} \dot{x}^n + \dot{R}^{\mathrm{T}} R x^b. \tag{3.3}$$

The velocity of the ship is $v^n \triangleq \dot{x}^n$ in the inertial frame, and $v^b = R^{\mathrm{T}} v^n$. Thus,

$$\dot{x}^b = v^b + \dot{R}^{\mathrm{T}} R x^b \quad \Leftrightarrow \quad v^b = \dot{x}^b - \dot{R}^{\mathrm{T}} R x^b. \tag{3.4}$$

We define

$$v^b \triangleq [v_1^b, v_2^b, v_3^b]^{\mathrm{T}}. \tag{3.5}$$

3.2 Rotation matrices

Before we continue, the rotation matrix R needs further investigation. Before we do that, we also need to define the cross-product matrix S.

Definition 3.1. For any two vectors $x, y \in \mathbb{R}^3$, we define the cross-product matrix S so that

$$S(x)y = x \times y. \tag{3.6}$$

From this definition follows several properties for vectors $x, y, z \in \mathbb{R}^3$ [19]:

Property 3.1. If $x = [x_1, x_2, x_3]^{\mathrm{T}}$, then

$$S(x) = \begin{bmatrix} 0 & -x_3 & x_2 \\ x_3 & 0 & -x_1 \\ -x_2 & x_1 & 0 \end{bmatrix} \in \mathbb{R}^{3\times 3}. \tag{3.7}$$

Property 3.2. S is skew-symmetric, i.e., $S^{\mathrm{T}}(x) = -S(x)$.

Property 3.3. For any skew-symmetric matrix $\mathcal{S} \in \mathbb{R}^{n\times n}$ and vector $\bar{y} \in \mathbb{R}^n$, $\bar{y}^{\mathrm{T}}\mathcal{S}\bar{y} = 0$. As a special case, $y^{\mathrm{T}}S(x)y = 0$.

Property 3.4. $S(x)y = -S(y)x$.

Property 3.5. $S(x)x = 0$.

Property 3.6. $S(x)S(y)z = x \times (y \times z) = \left(yx^{\mathrm{T}} - x^{\mathrm{T}}yI_3\right) z$.

Property 3.7 (The Jacobi identity)**.** $S(x)S(y)z + S(y)S(z)x + S(z)S(x)y = 0$.

Property 3.8. $S(S(x)y) = S(x)S(y) - S(y)S(x)$.

3.2.1 General properties of the rotation matrix

A rotation matrix transforms a vector from one reference frame to another. It is equivalent to rotating the vector about some axis, but it can also be interpreted as keeping the vector still and rotating the frame itself.

No matter the interpretation, rotation matrices have certain useful properties (from Egeland and Gravdahl [19]):

Property 3.9. $R \in \mathrm{SO}(n) \subset \mathbb{R}^{n\times n}$, where $\mathrm{SO}(n)$ is the special orthogonal group of order n for rotations in Euclidean n-space. The special orthogonal group is characterized by

- R is orthogonal, i.e., all column vectors are orthogonal and all row vectors are orthogonal.
- $R^{\mathrm{T}} = R^{-1}$.
- $\det(R) = 1$.

Property 3.10. If R_α^β is a rotation matrix from reference frame α to frame β, and R_β^α is a rotation matrix from frame β to frame α, then $R_\beta^\alpha = \left(R_\alpha^\beta\right)^{-1} = \left(R_\alpha^\beta\right)^{\mathrm{T}}$.

Property 3.11. If R_α^β is a rotation matrix from reference frame α to frame β, R_β^γ is a rotation matrix from frame β to frame γ, and R_α^γ is a rotation matrix from frame α to frame γ, then $R_\alpha^\gamma = R_\beta^\gamma R_\alpha^\beta$.

Property 3.12. In $\mathbb{R}^3$, the time derivative of the rotation matrix R_α^β from frame α to frame β is given by

$$\dot{R}_\alpha^\beta = R_\alpha^\beta S(\omega^\alpha) = S(\omega^\beta)R_\alpha^\beta$$

where $\vec{\omega}$ is the angular velocity vector of frame α relative to frame β and S is the cross-product matrix of Definition 3.1.

From here on, we will concentrate on rotation matrices in $\mathbb{R}^3$, the matrix R will be the rotation matrix from the body-fixed frame to the inertial frame (i.e., $R = R_b^n$) and $\vec{\omega}$ will be the angular velocity of the body frame relative to the inertial frame.

By Property 3.12, we write

$$\dot{R} = RS(\omega^b) \tag{3.8}$$

and define

$$\omega^b \triangleq [\omega_1^b, \omega_2^b, \omega_3^b]^{\mathrm{T}}. \tag{3.9}$$

We can then expand (3.4) as

$$\dot{\mathrm{x}}^b = v^b + S(\omega^b)x^b \quad \Leftrightarrow \quad v^b = \dot{x}^b - S(\omega^b)x^b. \tag{3.10}$$

3.2.2 Parametrizing the rotation matrix

The rotation matrix R has nine elements, but it can be shown that they are not independent [19]. Thus, R can be parametrized to be a function of fewer than nine parameters. There are several ways, three of which will be addressed here. It is worth noting that the lowest possible number of parameters necessary to describe an arbitrary rotation is three [19].

Angle-axis representation

For any rotation matrix R, there exists vectors $\bar{n}$ such that

$$R\bar{n} = \bar{n}. \tag{3.11}$$

An $\bar{n}$ satisfying this property is called a rotation axis. Since, for any scalar k, $Rk\bar{n} = k\bar{n}$, there clearly exists an infinite number of rotation axes. However, it can be shown [19] that all rotation axes are parallel.

Choosing a rotation axis that satisfies $\|\bar{n}\|_2 = 1$, there exists a $\vartheta \in \mathbb{R}$ so that

$$R = I_3 + \sin(\vartheta)S(\bar{n}) + (1 - \cos(\vartheta))S^2(\bar{n}). \tag{3.12}$$

Note that we don't have to specify in which coordinate system $\bar{n}$ is given, as $\bar{n}^b = \bar{n}^n$, by virtue of (3.11). This gives a four-parameter representation of the rotation matrix (three parameters of $\bar{n}$, plus ϑ).

The parameter ϑ has a physical interpretation. The rotation of the b-frame relative to the n-frame can be seen as a rotation of ϑ around the axis $\bar{n}$, which is why this parametrization is known as the angle-axis (or axis-angle) representation.

Note that, if $\vartheta = 2\pi k, k \in \{0, \pm 1, \pm 2, \ldots\}$ (corresponding to no rotation) then $R = I_3$, regardless of choice of $\bar{n}$. In the case of no rotation, the axis is therefore poorly defined. Also note that $\bar{n}$ is not unique, even when $\vartheta \neq 2\pi k, k \in \{0, \pm 1, \pm 2, \ldots\}$, as both $\bar{n}$ and $-\bar{n}$ are valid choices for rotation axis.

In general, both $\bar{n}$ and ϑ my be time-varying.[1] The derivative of the angle-axis parameters satisfies

$$\dot{\vartheta} = \bar{n}^{\mathrm{T}}\omega^b \tag{3.13}$$

$$\dot{\bar{n}} = \frac{1}{2}\left(S(\bar{n}) - \frac{1}{\tan(\vartheta/2)}S^2(\bar{n})\right)\omega^b, \quad \tan(\vartheta/2) \neq 0. \tag{3.14}$$

[1] If $\bar{n}$ is constant in time, then the rotation is a simple rotation, and R can be parametrized by only one parameter, ϑ.

Unit quaternions

Based on the angle-axis representation, we can define another four-parameter parametrization of R that avoids some of the drawbacks of the angle-axis representation by using unit quaternions.

A quaternion is a generalization of complex numbers. While complex numbers have one real and one imaginary part, quaternions have one real and three imaginary parts. Alternately, one can view the imaginary part of the quaternion as a vector in $\mathbb{R}^3$. In effect, a quaternion η is a vector in $\mathbb{R}^4$ to which we assign special properties and operators. [2, 14, 19]

We define

$$\eta_r \triangleq \operatorname{Re}\eta \in \mathbb{R} \tag{3.15}$$

$$\eta_i \triangleq \operatorname{Im}\eta \in \mathbb{R}^3 \tag{3.16}$$

giving $\eta = [\eta_r, \eta_i^{\mathrm{T}}]^{\mathrm{T}} \in \mathbb{R}^4$. A unit quaternion is a quaternion that satisfies

$$\eta^{\mathrm{T}}\eta = 1. \tag{3.17}$$

We will only be focusing on unit quaternions, as they (but no other quaternions) can be used to parametrize R and thus be interpreted as rotations in $\mathbb{R}^3$ [2, 14, 19].

Unit quaternions satisfy several interesting properties (function arguments have been dropped for brevity):

Property 3.13. The rotation matrix R can be written as [19, 81, 82]

$$R = EG^{\mathrm{T}} \tag{3.18}$$

where

$$E \triangleq \begin{bmatrix} -\eta_i & \eta_r I_3 + S(\eta_i) \end{bmatrix} \in \mathbb{R}^{3\times 4} \tag{3.19}$$

$$G \triangleq \begin{bmatrix} -\eta_i & \eta_r I_3 - S(\eta_i) \end{bmatrix} \in \mathbb{R}^{3\times 4}. \tag{3.20}$$

Alternate representations of the rotation matrix are

$$R = I_3 + 2\eta_r S(\eta_i) + 2S^2(\eta_i) \tag{3.21}$$

$$= (\eta_r^2 - \eta_i^{\mathrm{T}}\eta_i)I_3 + 2\eta_i\eta_i^{\mathrm{T}} + 2\eta_r S(\eta_i) \tag{3.22}$$

$$= (2\eta_r^2 - 1)I_3 + 2\eta_i\eta_i^{\mathrm{T}} + 2\eta_r S(\eta_i) \tag{3.23}$$

$$= (1 - 2\eta_i^{\mathrm{T}}\eta_i)I_3 + 2\eta_i\eta_i^{\mathrm{T}} + 2\eta_r S(\eta_i). \tag{3.24}$$

Property 3.14. The matrix G satisfies

$$GG^{\mathrm{T}} = I_3. \tag{3.25}$$

Proof. From the definition, we have

$$\begin{aligned} GG^{\mathrm{T}} &= \begin{bmatrix} -\eta_i & \eta_r I_3 - S(\eta_i) \end{bmatrix} \begin{bmatrix} -\eta_i^{\mathrm{T}} \\ \eta_r I_3 + S(\eta_i) \end{bmatrix} \\ &= \eta_i\eta_i^{\mathrm{T}} + \eta_r^2 I_3 - S^2(\eta_i) = \eta_i\eta_i^{\mathrm{T}} + \eta_r^2 I_3 - \eta_i\eta_i^{\mathrm{T}} + \eta_i^{\mathrm{T}}\eta_i I_3 \\ &= \eta^{\mathrm{T}}\eta I_3 = I_3 \end{aligned} \tag{3.26}$$

where it has been used that $\eta_r^2 + \eta_i^{\mathrm{T}}\eta_i = \eta^{\mathrm{T}}\eta = 1$. □

Property 3.15. The matrix G satisfies

$$G\eta = 0. \tag{3.27}$$

Proof. From the definition,

$$\begin{aligned} G\eta &= \begin{bmatrix} -\eta_i & \eta_r I_3 - S(\eta_i) \end{bmatrix} \begin{bmatrix} \eta_r \\ \eta_i \end{bmatrix} \\ &= -\eta_r\eta_i + \eta_r\eta_i - S(\eta_i)\eta_i = 0 \end{aligned} \tag{3.28}$$

where it has been used that $S(x)x = 0 \; \forall \; x \in \mathbb{R}^3$. □

Property 3.16. The matrix G satisfies

$$G\dot{\eta} = -\dot{G}\eta. \tag{3.29}$$

Proof. From Property 3.15 we have $G\eta = 0$. Differentiating on both sides with respect to time gives $\dot{G}\eta + G\dot{\eta} = 0 \;\Rightarrow\; \dot{G}\eta = -G\dot{\eta}$. □

Property 3.17. From Egeland and Gravdahl [19], Shivarama [81], Shivarama and Fahrenthold [82] we have that

$$\dot{\eta} = \frac{1}{2} G^{\mathrm{T}} \omega^b \tag{3.30}$$

$$\omega^b = 2G\dot{\eta} = -2\dot{G}\eta \tag{3.31}$$

where ω^b is the body-fixed angular velocity.

Property 3.18. From Shivarama [81], Shivarama and Fahrenthold [82] we have that

$$S(\omega^b) = 2G\dot{G}^{\mathrm{T}} = -2\dot{G}G^{\mathrm{T}}. \tag{3.32}$$

Property 3.19. The quaternion representation can be computed from the angle-axis representation by [19]

$$\eta_r = \cos(\vartheta/2) \tag{3.33}$$

$$\eta_i = \bar{n}\sin(\vartheta/2). \tag{3.34}$$

Property 3.20. The unit quaternions η and $-\eta$ have the same physical interpretation.

Proof. This can most easily be derived from Property 3.19:

$$-\eta_r = -\cos(\vartheta/2) = \cos([\vartheta + 2\pi]/2) \tag{3.35}$$

$$-\eta_i = -\bar{n}\sin(\vartheta/2) = \bar{n}\sin([\vartheta + 2\pi]/2). \tag{3.36}$$

Since ϑ and $\vartheta + 2\pi$ are equivalent to the same rotation, $\eta = [\eta_r, \eta_i^{\mathrm{T}}]^{\mathrm{T}}$ and $-\eta = [-\eta_r, -\eta_i^{\mathrm{T}}]^{\mathrm{T}}$ have the same physical interpretation. Note that this does not mean that η and $-\eta$ have the same numerical value. □

We note that, unlike angle-axis representation, $\dot{\eta}$ is always well defined (Property 3.17). η is also well-defined for no rotation; $\eta = [1, 0_{1\times3}]^{\mathrm{T}}$ (and $\eta = [-1, 0_{1\times3}]^{\mathrm{T}}$, see Property 3.20) is equivalent to zero rotation.

However, like the angle-axis representation, the quaternion is not uniquely determined by R (which is why we have Property 3.20).

Euler angles

Euler angles are three-parameter parametrizations of the rotation matrix. The basic concept is to (conceptually) first rotate the body frame around a body axis, then around another of the (now rotated) body axes, and then finally around a third (rotated) body axis. There are several ways to do this, and they all share the same basic strengths and weaknesses. The method presented here is commonly known as roll–pitch–yaw, xyz and sometimes zyx.

For roll–pitch–yaw, the body frame is first rotated around the body x-axis (roll), then around the (rotated) body y-axis (pitch) and finally around the (rotated) body z-axis (yaw). The simple rotations around each of these axis are given by [19, 24]

$$R_x(\phi) = \begin{bmatrix} 1 & 0 & 0 \\ 0 & \cos(\phi) & -\sin(\phi) \\ 0 & \sin(\phi) & \cos(\phi) \end{bmatrix} \tag{3.37}$$

$$R_y(\theta) = \begin{bmatrix} \cos(\theta) & 0 & \sin(\theta) \\ 0 & 1 & 0 \\ -\sin(\phi) & 0 & \cos(\phi) \end{bmatrix} \tag{3.38}$$

$$R_z(\psi) = \begin{bmatrix} \cos(\psi) & -\sin(\psi) & 0 \\ \sin(\psi) & \cos(\psi) & 0 \\ 0 & 0 & 1 \end{bmatrix}. \tag{3.39}$$

We combine the three angles into the vector Θ defined by

$$\Theta \triangleq [\phi, \theta, \psi]^{\mathrm{T}} \tag{3.40}$$

The components of Θ is known as the Euler angles with roll is given by ϕ, pitch by θ and yaw by ψ.

Property 3.21. The rotation matrix is given by

$$R(\Theta) = \begin{bmatrix} \mathrm{c}\theta\mathrm{c}\psi & \mathrm{s}\phi\mathrm{s}\theta\mathrm{c}\psi - \mathrm{c}\phi\mathrm{s}\psi & \mathrm{c}\phi\mathrm{s}\theta\mathrm{c}\psi + \mathrm{s}\phi\mathrm{s}\psi \\ \mathrm{c}\theta\mathrm{s}\psi & \mathrm{s}\phi\mathrm{s}\theta\mathrm{s}\psi + \mathrm{c}\phi\mathrm{c}\psi & \mathrm{c}\phi\mathrm{s}\theta\mathrm{s}\psi - \mathrm{s}\phi\mathrm{c}\psi \\ -\mathrm{s}\theta & \mathrm{s}\phi\mathrm{c}\theta & \mathrm{c}\phi\mathrm{c}\theta \end{bmatrix} \tag{3.41}$$

where $\mathrm{s}\cdot = \sin(\cdot)$ and $\mathrm{c}\cdot = \cos(\cdot)$.

Proof. By Property 3.11, $R(\Theta) = R_z(\psi)R_y(\theta)R_x(\phi)$. Computing this product gives Equation (3.41). □

Property 3.22. The time derivative of Θ is given by [19, 24]

$$\dot{\Theta} = G_\Theta(\Theta)\omega^b. \tag{3.42}$$

where

$$G_\Theta(\Theta) = \begin{bmatrix} 1 & \sin(\phi)\tan(\theta) & \cos(\phi)\tan(\theta) \\ 0 & \cos(\phi) & -\sin(\phi) \\ 0 & \frac{\sin(\phi)}{\cos(\theta)} & \frac{\cos(\phi)}{\cos(\theta)} \end{bmatrix}, \quad \cos(\theta) \neq 0. \tag{3.43}$$

The inverse of G_Θ is given by

$$G_\Theta^{-1}(\Theta) = \begin{bmatrix} 1 & 0 & -\sin(\theta) \\ 0 & \cos(\phi) & \sin(\phi)\cos(\theta) \\ 0 & -\sin(\phi) & \cos(\phi)\cos(\theta) \end{bmatrix}. \tag{3.44}$$

Property 3.23. The matrix G_Θ is undefined for $\theta = \pi/2 + 2\pi k, k \in \{0, \pm 1, \pm 2, \ldots\}$. (This corresponds to the rigid body pointing nose up or nose down.) For the same values of θ, R becomes a function of a single parameter.

Proof. For the specified values of θ, $\cos(\theta) = 0$ and $\sin(\theta) = \pm 1$, and the divisors in the third row of G_Θ are zero. The $\tan(\theta)$ terms in the first row are also undefined.

At $\cos(\theta) = 0$, R becomes

$$\begin{aligned} R(\Theta) &= \begin{bmatrix} 0 & \pm \mathrm{s}\phi\mathrm{c}\psi - \mathrm{c}\phi\mathrm{s}\psi & \pm \mathrm{c}\phi\mathrm{c}\psi + \mathrm{s}\phi\mathrm{s}\psi \\ 0 & \pm \mathrm{s}\phi\mathrm{s}\psi + \mathrm{c}\phi\mathrm{c}\psi & \pm \mathrm{c}\phi\mathrm{s}\psi - \mathrm{s}\phi\mathrm{c}\psi \\ \mp 1 & 0 & 0 \end{bmatrix} \\ &= \begin{bmatrix} 0 & \pm \sin(\phi \mp \psi) & \pm \cos(\phi \mp \psi) \\ 0 & \cos(\phi \mp \psi) & -\sin(\psi \mp \psi) \\ \mp 1 & 0 & 0 \end{bmatrix} \\ &= \begin{bmatrix} 0 & \pm \sin(\bar{\vartheta}) & \pm \cos(\bar{\vartheta}) \\ 0 & \cos(\bar{\vartheta}) & -\sin(\bar{\vartheta}) \\ \mp 1 & 0 & 0 \end{bmatrix} \end{aligned}$$

with $\bar{\vartheta} \triangleq \phi \mp \psi$. □

The practical implications of this is that, for $\cos(\theta) = 0$, it is impossible to determine the rate of change of the Euler angles. It is also impossible to tell if the rigid body is rotating around the x- or z-axis (or some combination). This phenomenon is sometimes referred to as gimbal lock.

Property 3.24. Any Euler-angle representation will break down for some specific rotations, regardless of which simple rotations it comprises. In general, this holds true for *any* three-parameter parametrization of R [19].

Property 3.25. All $\Theta = [\phi + 2\pi k_1, \theta + 2\pi k_2, \psi + 2\pi k_3,]^{\mathrm{T}}$ have the same physical interpretation for all all $k_i \in \{0, \pm 1, \pm 2, \ldots\}$.

Proof. This follows trivially from the 2π-periodicity of trigonometric functions. □

Euler angles are simpler than quaternions or angle-axis representation, having one fewer degree of freedom. They also have a more intuitive physical interpretation.

The major drawback is the singularity (at $\theta = \pm\pi/2$ for roll–pitch–yaw). Like the other two representations listed in this chapter, Euler angles are also not uniquely determined by R, as an infinite number of Θ triples have the same physical interpretation (Property 3.25).

3.3 Choice of kinematics

Given the analysis of the previous section, we have decided to use unit quaternions as the default representation of the ship's orientation. This gives

$$\dot{\mathrm{x}}^n = R(\eta)v^b \tag{3.45}$$

$$\dot{\eta} = \frac{1}{2}G^{\mathrm{T}}(\eta)\omega^b \tag{3.46}$$

as the kinematic equations.

In some cases, we will use reduced-order models. In those cases, quaternions are not quite as applicable. We will therefore use Euler angles to derive reduced-order models. Temporarily, we will therefore use

$$\dot{\mathrm{x}}^n = R(\Theta)v^b \tag{3.47}$$

$$\dot{\eta} = G_\Theta(\Theta)\omega^b \tag{3.48}$$

as the kinematic equations where $R(\Theta)$ is here to be understood as (3.41).

Chapter 4

Equations of motion for a rigid body in $\mathbb{R}^3$

In this chapter, the equations of motion for a rigid body in $\mathbb{R}^3$ is developed using Hamiltonian mechanics. The results in this chapter are used as a foundation for the model in Chapter 5. The model in Chapter 7 expands upon the results in Chapter 4 to a 7-DOF non-rigid body (a ship with a u-tank).

Dynamics for a rigid body translating and rotating in $\mathbb{R}^3$ is presented in Egeland and Gravdahl [19], Fossen [24] among other places, but the equations of motion are presented without potential energy. Shivarama [81], Shivarama and Fahrenthold [82] presented the dynamics for a rigid body translating and rotating in $\mathbb{R}^3$, with the translational motion given in the inertial frame and the rotational motion given in the body frame.

This chapter presents the dynamics of a rigid body translating and rotating in $\mathbb{R}^3$ subject to potential (and kinetic) energy with both the translational and the rotational motion given in the body frame.

The dynamics can be written in singularity-free form using seven coordinates for generalized position and six coordinates for generalized momentum (or generalized velocity).

The results in this chapter have not been published by me, nor are they lifted from other authors' work.

4.1 Energy of the rigid body

As in the previous chapter, we let $x^n \in \mathbb{R}^3$ be the position of the body origin in the inertial frame. Then, the linear velocity $\vec{v}$ is given by

$$v^n = \dot{x}^n. \tag{4.1}$$

The velocities in the body and inertial frames (respectively v^b and v^n), satisfy

$$\dot{x}^n = Rv^b \quad \Leftrightarrow \quad v^b = R^{\mathrm{T}}\dot{x}^n. \tag{4.2}$$

The body frame (and the rigid body with it) is rotating with an angular velocity $\omega^b \in \mathbb{R}^3$ (given in the body frame) relative to the inertial frame.

We define

$$q \triangleq [x^{n\mathrm{T}}, \eta^{\mathrm{T}}]^{\mathrm{T}} \in \mathbb{R}^7 \tag{4.3}$$

$$\nu \triangleq [v^{b\mathrm{T}}, \omega^{b\mathrm{T}}]^{\mathrm{T}} \in \mathbb{R}^6 \tag{4.4}$$

and

$$P(\eta) \triangleq \begin{bmatrix} R^{\mathrm{T}}(\eta) & 0_{3\times 4} \\ 0_{3\times 3} & 2G(\eta) \end{bmatrix} \in \mathbb{R}^{6\times 7} \tag{4.5}$$

$$\mathcal{P}(\eta) \triangleq \begin{bmatrix} R^{\mathrm{T}}(\eta) & 0_{3\times 3} \\ 0_{4\times 3} & \frac{1}{2}G(\eta) \end{bmatrix} \in \mathbb{R}^{6\times 7} \tag{4.6}$$

so that

$$\dot{q} = \mathcal{P}^{\mathrm{T}}(\eta)\nu \tag{4.7}$$

$$\nu = P(\eta)\dot{q} \tag{4.8}$$

by (4.2) and Property 3.17. For brevity, we skip function arguments of P, $\mathcal{P}$, R and G for the rest of the chapter.

We assume that the potential energy of the system $U = U(q) \in \mathbb{R}$ has an (at least local) minimum $U_{\min} = U(q_{\min})$ for some $q = q_{\min}$.

The rigid body has mass $m > 0 \in \mathbb{R}$ and moment of inertia $J = J^{\mathrm{T}} > 0 \in \mathbb{R}^{3\times 3}$ about the body origin, in the body frame. The rigid body's center of gravity is located at r_g^b (in the body frame).

The inertia matrix M_{RB} of the system is given by [19, 24]

$$M_{\mathrm{RB}} = \begin{bmatrix} mI_3 & -mS(r_g^b) \\ mS(r_g^b) & J \end{bmatrix} = M_{\mathrm{RB}}^{\mathrm{T}} > 0 \in \mathbb{R}^{6\times 6}. \tag{4.9}$$

The complementary kinetic energy[1] T^* of the system is then given by [19, 24]

$$T^* = \frac{1}{2}\nu^{\mathrm{T}} M_{\mathrm{RB}} \nu = \frac{1}{2}\dot{q}^{\mathrm{T}} P^{\mathrm{T}} M_{\mathrm{RB}} P \dot{q} = \frac{1}{2}\dot{q}^{\mathrm{T}} \mathcal{M} \dot{q} \tag{4.10}$$

with

$$\mathcal{M} \triangleq P^{\mathrm{T}} M_{\mathrm{RB}} P = \mathcal{M}^{\mathrm{T}} \in \mathbb{R}^{7\times 7}. \tag{4.11}$$

We note that $\det(\mathcal{M}) = 0$. The matrix $\mathcal{M}$ is singular since the system is over-parametrized; $q \in \mathbb{R}^7$, while a freely translating and moving body in $\mathbb{R}^3$ only has six degrees of freedom [19, 24].

We define

$$\mathcal{W} \triangleq \mathcal{P}^{\mathrm{T}} M_{\mathrm{RB}}^{-1} \mathcal{P} = \mathcal{W}^{\mathrm{T}} \in \mathbb{R}^{7\times 7}. \tag{4.12}$$

$\mathcal{W}$ is also singular.

We note that the matrices P, $\mathcal{P}$, $\mathcal{M}$ and $\mathcal{W}$ satisfy several properties:

[1] Complementary kinetic energy is the kinetic energy as a function of the time derivative of the generalized coordinates.

Property 4.1. $\mathcal{M}$ is symmetric and positive semidefinite.

Proof. $\mathcal{M} = \mathcal{M}^{\mathrm{T}} \geq 0$ if it satisfies $w^{\mathrm{T}}\mathcal{M}w \geq 0 \; \forall \; w \in \mathbb{R}^7$. From the definition of $\mathcal{M}$, $w^{\mathrm{T}}\mathcal{M}w = w^{\mathrm{T}}P^{\mathrm{T}}M_{\mathrm{RB}}Pw = \tilde{w}^{\mathrm{T}}M_{\mathrm{RB}}\tilde{w} \geq 0$ with $\tilde{w} = Pw$ since $M_{\mathrm{RB}} = M_{\mathrm{RB}}^{\mathrm{T}} > 0$. Thus $\mathcal{M}$ is at least positive semidefinite. It is not positive definite, however, because $w = [0_{1\times 3}, \eta^{\mathrm{T}}]^{\mathrm{T}} \Rightarrow w^{\mathrm{T}}\mathcal{M}w = 0$ since $G\eta = 0$ (by Property 3.15). □

Property 4.2. $\mathcal{W}$ is symmetric and positive semidefinite.

Proof. $\mathcal{W} = \mathcal{W}^{\mathrm{T}} \geq 0$ if it satisfies $w^{\mathrm{T}}\mathcal{W}w \geq 0 \; \forall \; w \in \mathbb{R}^7$. From the definition of $\mathcal{W}$, $w^{\mathrm{T}}\mathcal{W}w = w^{\mathrm{T}}\mathcal{P}^{\mathrm{T}}M_{\mathrm{RB}}^{-1}\mathcal{P}w = \tilde{w}^{\mathrm{T}}M_{\mathrm{RB}}^{-1}\tilde{w} \geq 0$ with $\tilde{w} = \mathcal{P}w$ since $M_{\mathrm{RB}} = M_{\mathrm{RB}}^{\mathrm{T}} > 0$ implies $M_{\mathrm{RB}}^{-1} = M_{\mathrm{RB}}^{-\mathrm{T}} > 0$. Thus $\mathcal{W}$ is at least positive semidefinite. It is not positive definite, however, because $w = [0_{1\times 3}, \eta^{\mathrm{T}}]^{\mathrm{T}} \Rightarrow w^{\mathrm{T}}\mathcal{W}w = 0$ since $G\eta = 0$ (by Property 3.15). □

Property 4.3. $\mathcal{P}P^{\mathrm{T}} = I_6$.

Proof. We have

$$\mathcal{P}P^{\mathrm{T}} = \begin{bmatrix} R^{\mathrm{T}} & 0_{3\times 4} \\ 0_{3\times 3} & \frac{1}{2}G \end{bmatrix} \begin{bmatrix} R & 0_{3\times 3} \\ 0_{4\times 3} & 2G^{\mathrm{T}} \end{bmatrix} = \begin{bmatrix} R^{\mathrm{T}}R & 0_{3\times 3} \\ 0_{3\times 3} & GG^{\mathrm{T}} \end{bmatrix} = I_6$$

since $R^{\mathrm{T}} = R^{-1}$ and $GG^{\mathrm{T}} = I_3$. □

Property 4.4. $P\mathcal{P}^{\mathrm{T}} = I_6$.

Proof. We have

$$P\mathcal{P}^{\mathrm{T}} = \begin{bmatrix} R^{\mathrm{T}} & 0_{3\times 4} \\ 0_{3\times 3} & 2G \end{bmatrix} \begin{bmatrix} R & 0_{3\times 3} \\ 0_{4\times 3} & \frac{1}{2}G^{\mathrm{T}} \end{bmatrix} = \begin{bmatrix} R^{\mathrm{T}}R & 0_{3\times 3} \\ 0_{3\times 3} & GG^{\mathrm{T}} \end{bmatrix} = I_6$$

since $R^{\mathrm{T}} = R^{-1}$ and $GG^{\mathrm{T}} = I_3$. □

Property 4.5. $\mathcal{P}^{\mathrm{T}}P\mathcal{P}^{\mathrm{T}} = \mathcal{P}^{\mathrm{T}}$.

Proof. We have $\mathcal{P}^{\mathrm{T}}P\mathcal{P}^{\mathrm{T}} = \mathcal{P}^{\mathrm{T}}I_6 = \mathcal{P}^{\mathrm{T}}$. □

Property 4.6. $P^{\mathrm{T}}\mathcal{P}P^{\mathrm{T}} = P^{\mathrm{T}}$.

Proof. We have $P^{\mathrm{T}}\mathcal{P}P^{\mathrm{T}} = P^{\mathrm{T}}I_6 = P^{\mathrm{T}}$. □

Property 4.7. $\mathcal{W}\mathcal{M}\mathcal{W} = \mathcal{W}$.

Proof. We have

$$\mathcal{W}\mathcal{M}\mathcal{W} = \mathcal{P}^{\mathrm{T}}M_{\mathrm{RB}}^{-1}\mathcal{P}P^{\mathrm{T}}M_{\mathrm{RB}}P\mathcal{P}^{\mathrm{T}}M_{\mathrm{RB}}^{-1}\mathcal{P} = \mathcal{P}^{\mathrm{T}}P\mathcal{P}^{\mathrm{T}}M_{\mathrm{RB}}^{-1}\mathcal{P} = \mathcal{P}^{\mathrm{T}}M_{\mathrm{RB}}^{-1}\mathcal{P} = \mathcal{W}$$

where Properties 4.3 and 4.5 have been used. □

Property 4.8. $\mathcal{M}\mathcal{W}\mathcal{M} = \mathcal{M}$.

Proof. We have

$$\mathcal{M}\mathcal{W}\mathcal{M} = P^{\mathrm{T}}M_{\mathrm{RB}}P\mathcal{P}^{\mathrm{T}}M_{\mathrm{RB}}^{-1}\mathcal{P}P^{\mathrm{T}}M_{\mathrm{RB}}P = P^{\mathrm{T}}\mathcal{P}P^{\mathrm{T}}M_{\mathrm{RB}}P = P^{\mathrm{T}}M_{\mathrm{RB}}P = \mathcal{M}$$

where Properties 4.4 and 4.6 have been used. □

4.2 Virtual work

Following Shivarama [81], Shivarama and Fahrenthold [82], we define the quasi-coordinates q_ω associated with the co-rotating components of the angular velocity as

$$\dot{q}_\omega = \omega^b. \tag{4.13}$$

The virtual work done by imposed forces $\tau_f^n(t)$ and torques $\tau_t^b(t)$ is then given by

$$\delta W = \delta x^{n\mathrm{T}} \tau_f^n(t) + \delta q_\omega^{\mathrm{T}} \tau_t^b(t). \tag{4.14}$$

Since

$$\delta q_\omega = 2G\delta\eta, \tag{4.15}$$

(by Property 3.17) we get

$$\delta W = \delta x^{n\mathrm{T}} \tau_f^n(t) + 2\delta\eta^{\mathrm{T}} G^{\mathrm{T}} \tau_t^b(t) = \delta q^{\mathrm{T}} \begin{bmatrix} \tau_f^n \\ 2G^{\mathrm{T}}\tau_t^b \end{bmatrix}. \tag{4.16}$$

We therefore see that the vector of generalized forces associated with the virtual work δW is

$$\tau^n \triangleq \begin{bmatrix} \tau_f^n \\ 2G^{\mathrm{T}}\tau_t^b \end{bmatrix} \in \mathbb{R}^7 \tag{4.17}$$

with a slight abuse of notation. τ^n is strictly speaking not a vector in the inertial frame, as $\tau^n \in \mathbb{R}^7$, not $\mathbb{R}^3$. And while τ_f^n *is* the forces in the inertial frame, $2G^{\mathrm{T}}\tau_t^b$ is not the torque in the inertial frame.

4.3 Hamilton's equations

Using the kinetic and potential energies of Section 4.1, in addition to the virtual work defined in Section 4.2, we can derive the dynamics of the system. Initially, this will be given using a generalized momentum in $\mathbb{R}^7$. This is somewhat inconvenient, as the generalized momentum can be expressed in $\mathbb{R}^6$. However, we need to initially use the more complex form as a stepping stone to get the more compact representation.

4.3.1 Generalized momentum and Hamiltonian

The generalized momentum of the system is given by [36, 55]

$$p^n = \frac{\partial T^*}{\partial \dot{q}} = \mathcal{M}\dot{q} \in \mathbb{R}^7. \tag{4.18}$$

This is a slight abuse of notation, as p^n is not a vector in the inertial frame, as $p^n \in \mathbb{R}^7$, not $\mathbb{R}^3$.

We know that the value of T and T^* are the same [36, 55], giving

$$T(q,p^n) = T^*(q,\dot{q}) = \frac{1}{2}\dot{q}^{\mathrm{T}}\mathcal{M}\dot{q} = \frac{1}{2}\dot{q}^{\mathrm{T}}\mathcal{M}\mathcal{W}\mathcal{M}\dot{q} = \frac{1}{2}{p^n}^{\mathrm{T}}\mathcal{W}p^n \tag{4.19}$$

using Property 4.8.[2]

Due to the shape of T and U, the Hamiltonian H is simply equal to the sum of the energy in the system (see Appendix B), or

$$H(q,p^n) = T(q,p^n) + U(q) = \frac{1}{2}{p^n}^{\mathrm{T}}\mathcal{W}(q)p^n + U(q). \tag{4.20}$$

4.3.2 Using generalized momentum in $\mathbb{R}^7$

Since $\dim q = 7$, while there are only six degrees of freedom, the system has a single algebraic constraint to satisfy:

$$\xi(q,p^n) \triangleq \eta^{\mathrm{T}}\eta - 1 = 0 \tag{4.21}$$

since the quaternion η has to be a unit quaternion (see Chapter 3). We note that

$$\frac{\partial \xi}{\partial q} = \begin{bmatrix} 0_3 \\ 2\eta \end{bmatrix} \tag{4.22}$$

$$\frac{\partial \xi}{\partial p^n} = 0. \tag{4.23}$$

We find the system dynamics to be (see Appendix B)

$$\dot{q} = \frac{\partial H}{\partial p^n} + \lambda\frac{\partial \xi}{\partial p^n} = \frac{\partial T}{\partial p^n} = \mathcal{W}p^n \tag{4.24}$$

$$\begin{aligned}\dot{p}^n &= -\frac{\partial H}{\partial q} - \lambda\frac{\partial \xi}{\partial q} + \tau^n = -\frac{\partial T}{\partial q} - \frac{\partial U}{\partial q} - 2\lambda\begin{bmatrix} 0_3 \\ \eta \end{bmatrix} + \tau^n \\ &= \frac{\partial T^*}{\partial q} - \frac{\partial U}{\partial q} - 2\lambda\begin{bmatrix} 0_3 \\ \eta \end{bmatrix} + \tau^n \end{aligned} \tag{4.25}$$

by Property B.1, where λ is a Lagrangian multiplier to be determined. To find the dynamics, we need to expand (4.25).

Since $\mathcal{M}$ and thus T^* are not functions of x^n,

$$\frac{\partial T^*}{\partial x^n} = 0. \tag{4.26}$$

Since M_{RB} is not a function of η, we can use Lemma A.3 to find that

$$\begin{aligned}\frac{\partial T^*}{\partial \eta} &= \frac{1}{2}\frac{\partial \dot{q}^{\mathrm{T}}\mathcal{M}\dot{q}}{\partial \eta} = \frac{1}{2}\frac{\partial \dot{q}^{\mathrm{T}}P^{\mathrm{T}}M_{\mathrm{RB}}P\dot{q}}{\partial \eta} \\ &= \frac{1}{2}\frac{\partial f^{\mathrm{T}}(q,\dot{q})M_{\mathrm{RB}}f(q,\dot{q})}{\partial \eta} = \frac{\partial f}{\partial \eta}M_{\mathrm{RB}}f(q,\dot{q}) = \frac{\partial f}{\partial \eta}M_{\mathrm{RB}}P\dot{q}\end{aligned}$$

[2] We could also have found T via the Legendre transform (see Appendix B).

with

$$f(q,\dot{q}) \triangleq P\dot{q} = \begin{bmatrix} R^{\mathrm{T}}\dot{x}^n \\ 2G\dot{\eta} \end{bmatrix} = \begin{bmatrix} R^{\mathrm{T}}\dot{x}^n \\ -2\dot{G}\eta \end{bmatrix}$$

since $G\dot{\eta} = -\dot{G}\eta$ (by Property 3.16).

The partial derivative of f with respect to η is then given by

$$\begin{aligned}\frac{\partial f}{\partial \eta} &= \begin{bmatrix} \frac{\partial (R^{\mathrm{T}}\dot{x}^n)}{\partial \eta} & -2\frac{\partial (\dot{G}\eta)}{\partial \eta} \end{bmatrix} = \begin{bmatrix} \frac{\partial R^{\mathrm{T}}}{\partial \eta}(\dot{x}^n \otimes I_3) & -2\frac{\partial \eta}{\partial \eta}(1 \otimes \dot{G}^{\mathrm{T}}) \end{bmatrix} \\ &= \begin{bmatrix} \frac{\partial R^{\mathrm{T}}}{\partial \eta}(\dot{x}^n \otimes I_3) & -2\dot{G}^{\mathrm{T}} \end{bmatrix}\end{aligned}$$

where Lemma A.2 has been used and $\otimes$ is the Kronecker product.

Furthermore, $R^{\mathrm{T}} = I_3 - 2\eta_r S(\eta_i) + 2S^2(\eta_i)$, giving

$$\frac{\partial R^{\mathrm{T}}}{\partial \eta} = -2\frac{\partial}{\partial \eta}\left(\eta_r S(\eta_i)\right) + 2\frac{\partial}{\partial \eta}S^2(\eta_i)$$

with (by Lemma A.2)

$$\begin{aligned}\frac{\partial}{\partial \eta}\left(\eta_r S(\eta_i)\right) &= \frac{\partial \eta_r I_3}{\partial \eta}\left(S(\eta_i) \otimes I_3\right) + \frac{\partial S(\eta_i)}{\partial \eta}\left(I_3 \otimes n_r I_3\right) \\ &= \begin{bmatrix} (\operatorname{vec} S(\eta_i))^{\mathrm{T}} \\ 0_{3\times 9} \end{bmatrix} + \eta_r \frac{\partial S(\eta_i)}{\partial \eta} \\ \frac{\partial}{\partial \eta}S^2(\eta_i) &= \frac{\partial S(\eta_i)}{\partial \eta}\left(S(\eta_i) \otimes I_3\right) - \frac{\partial S(\eta_i)}{\partial \eta}\left(I_3 \otimes S(\eta_i)\right)\end{aligned}$$

where

$$\frac{\partial S(\eta_i)}{\partial \eta} = \begin{bmatrix} 0 & 0 & 0 & 0 & 0 & 0 & 0 & 0 & 0 \\ 0 & 0 & 0 & 0 & 0 & 1 & 0 & -1 & 0 \\ 0 & 0 & -1 & 0 & 0 & 0 & 1 & 0 & 0 \\ 0 & 1 & 0 & -1 & 0 & 0 & 0 & 0 & 0 \end{bmatrix}.$$

This gives

$$\begin{aligned}\frac{\partial R^{\mathrm{T}}}{\partial \eta}(\dot{x}^n \otimes I_3) &= -2\begin{bmatrix} (\operatorname{vec} S(\eta_i))^{\mathrm{T}} \\ 0_{3\times 9} \end{bmatrix}(\dot{x}^n \otimes I_3) \\ &\quad - 2\frac{\partial S(\eta_i)}{\partial \eta}\left[\eta_r I_9 - S(\eta_i) \otimes I_3 + I_3 \otimes S(\eta_i)\right](\dot{x}^n \otimes I_3) \\ &= -2\begin{bmatrix} [S(\eta_i)\dot{x}^n]^{\mathrm{T}} \\ \eta_r S(\dot{x}^n) - S(S(\eta_i)\dot{x}^n) + S(\dot{x}^n)S(\eta_i) \end{bmatrix} \\ &= -2\begin{bmatrix} \eta_i^{\mathrm{T}} S(\dot{x}^n) \\ \eta_r S(\dot{x}^n) - S(\eta_i)S(\dot{x}^n) + 2S(\dot{x}^n)S(\eta_i) \end{bmatrix}. \end{aligned} \tag{4.27}$$

Thus,

$$\frac{\partial T^*}{\partial \eta} = \begin{bmatrix} \frac{\partial R^{\mathrm{T}}}{\partial \eta}(\dot{x}^n \otimes I_3) & -2\dot{G}^{\mathrm{T}} \end{bmatrix} M_{\mathrm{RB}} P\dot{q}. \tag{4.28}$$

This expression could now be inserted into (4.25), but using a generalized momentum in $\mathbb{R}^7$ is needlessly complicated and is therefore only used as a stepping stone.

4.3.3 Using generalized momentum in $\mathbb{R}^6$

The body-fixed momentum vector p is given by

$$p = M_{\mathrm{RB}}\nu \in \mathbb{R}^6 \tag{4.29}$$

and note that

$$p^n = \mathcal{M}\dot{q} = P^{\mathrm{T}} M_{\mathrm{RB}} P\dot{q} = P^{\mathrm{T}} M_{\mathrm{RB}}\nu = P^{\mathrm{T}} p \tag{4.30}$$

which implies

$$p = \mathcal{P}p^n \tag{4.31}$$

since $\mathcal{P}P^{\mathrm{T}} = I_6$. Also worth noting is that

$$p = M_{\mathrm{RB}} P\dot{q} \tag{4.32}$$

$$\dot{q} = \mathcal{P}^{\mathrm{T}} M_{\mathrm{RB}}^{-1} p \tag{4.33}$$

since $P\mathcal{P}^{\mathrm{T}} = I_6$.

Therefore,

$$\begin{aligned}
\dot{p} &= \dot{\mathcal{P}}p^n + \mathcal{P}\dot{p}^n = \dot{\mathcal{P}}P^{\mathrm{T}}p + \mathcal{P}\dot{p}^n = \begin{bmatrix} \dot{R}^{\mathrm{T}} & 0_{3\times 4} \\ 0_{3\times 3} & \frac{1}{2}\dot{G} \end{bmatrix} p^n + \mathcal{P}\dot{p}^n \\
&= \begin{bmatrix} -S(\omega^b)R^{\mathrm{T}} & 0_{3\times 4} \\ 0_{3\times 3} & \frac{1}{2}\dot{G} \end{bmatrix} \begin{bmatrix} R & 0_{3\times 3} \\ 0_{4\times 3} & 2G^{\mathrm{T}} \end{bmatrix} p + \mathcal{P}\dot{p}^n \\
&= \begin{bmatrix} -S(\omega^b) & 0_{3\times 3} \\ 0_{3\times 3} & \dot{G}G^{\mathrm{T}} \end{bmatrix} p + \mathcal{P}\dot{p}^n \\
&= \begin{bmatrix} -S(\omega^b) & 0_{3\times 3} \\ 0_{3\times 3} & -\frac{1}{2}S(\omega^b) \end{bmatrix} p + \mathcal{P}\left(\frac{\partial T^*}{\partial q} - \frac{\partial U}{\partial q} - 2\lambda \begin{bmatrix} 0_3 \\ \eta \end{bmatrix} + \tau^n(t) \right) \\
&= -\begin{bmatrix} S(\omega^b) & 0_{3\times 3} \\ 0_{3\times 3} & \frac{1}{2}S(\omega^b) \end{bmatrix} p + \mathcal{P}\frac{\partial T^*}{\partial q} - \mathcal{P}\frac{\partial U}{\partial q} - 2\lambda\mathcal{P} \begin{bmatrix} 0_3 \\ \eta \end{bmatrix} + \mathcal{P}\tau^n(t)
\end{aligned} \tag{4.34}$$

since $2\dot{G}G^{\mathrm{T}} = -S(\omega^b)$ (by Property 3.18), $\dot{R} = RS(\omega^b)$ (by Property 3.12) and $R^{\mathrm{T}} = R^{-1}$ (by Property 3.9).

We see that

$$\begin{aligned}
\mathcal{P} \begin{bmatrix} 0_3 \\ \eta \end{bmatrix} &= \begin{bmatrix} 0_3 \\ \frac{1}{2}G\eta \end{bmatrix} = 0 \\
\mathcal{P}\tau^n(t) &= \begin{bmatrix} R^{\mathrm{T}}\tau_f^n(t) \\ GG^{\mathrm{T}}\tau_t^b(t) \end{bmatrix} = \begin{bmatrix} \tau_f^b(t) \\ \tau_t^b(t) \end{bmatrix} \triangleq \tau(t) \\
\mathcal{P}\frac{\partial T^*}{\partial q} &= \begin{bmatrix} R^{\mathrm{T}}\frac{\partial T^*}{\partial x^n} \\ \frac{1}{2}G\frac{\partial T^*}{\partial \eta} \end{bmatrix} = \begin{bmatrix} 0_{3\times 1} \\ \frac{1}{2}G\frac{\partial T^*}{\partial \eta} \end{bmatrix}.
\end{aligned}$$

This gives

$$\dot{p} = \begin{bmatrix} -S(\omega^b) & 0_{3\times 3} \\ 0_{3\times 3} & -\frac{1}{2}S(\omega^b) \end{bmatrix} p + \begin{bmatrix} 0_{3\times 1} \\ \frac{1}{2}G\frac{\partial T^*}{\partial \eta} \end{bmatrix} - \mathcal{P}\frac{\partial U}{\partial q} + \tau(t). \tag{4.35}$$

Note that the Lagrangian multiplier λ has completely disappeared from (4.35).

We define

$$p_l \triangleq \begin{bmatrix} I_3 & 0_{3\times 3} \end{bmatrix} p \tag{4.36}$$

$$p_t \triangleq \begin{bmatrix} 0_{3\times 3} & I_3 \end{bmatrix} p \tag{4.37}$$

as the translational and rotational momentum. By using (4.28), we find that

$$\begin{aligned} G\frac{\partial T^*}{\partial \eta} &= G\begin{bmatrix} \frac{\partial R^{\mathrm{T}}}{\partial \eta}(\dot{x}^n \otimes I_3) & -2\dot{G}^{\mathrm{T}} \end{bmatrix} M_{\mathrm{RB}} P\dot{q} = G\begin{bmatrix} \frac{\partial R^{\mathrm{T}}}{\partial \eta}(\dot{x}^n \otimes I_3) & -2\dot{G}^{\mathrm{T}} \end{bmatrix} p \\ &= G\begin{bmatrix} \frac{\partial R^{\mathrm{T}}}{\partial \eta}(\dot{x}^n \otimes I_3) & -2\dot{G}^{\mathrm{T}} \end{bmatrix} \begin{bmatrix} p_l \\ p_r \end{bmatrix} = G\left[\frac{\partial R^{\mathrm{T}}}{\partial \eta}(\dot{x}^n \otimes I_3)p_l - 2\dot{G}^{\mathrm{T}}p_r\right] \\ &= G\frac{\partial R^{\mathrm{T}}}{\partial \eta}(\dot{x}^n \otimes I_3)p_l - 2G\dot{G}^{\mathrm{T}}p_r = G\frac{\partial R^{\mathrm{T}}}{\partial \eta}(\dot{x}^n \otimes I_3)p_l - S(\omega^b)p_r. \end{aligned}$$

Furthermore, by using (3.20) and (4.27),

$$\begin{aligned} G\frac{\partial R^{\mathrm{T}}}{\partial \eta}(\dot{x}^n \otimes I_3)p_l &= -2\begin{bmatrix} -\eta_i & \eta_r I_3 - S(\eta_i) \end{bmatrix} \\ &\qquad \times \begin{bmatrix} \eta_i^{\mathrm{T}} S(\dot{x}^n) \\ \eta_r S(\dot{x}^n) - S(\eta_i)S(\dot{x}^n) + 2S(\dot{x}^n)S(\eta_i) \end{bmatrix} p_l \\ &= 2\left[\eta_i\eta_i^{\mathrm{T}} - S^2(\eta_i) - \eta_r^2 I_3 + 2\eta_r S(\eta_i)\right] S(\dot{x}^n)p_l \\ &\quad + 4\left[S(\eta_i) - \eta_r I_3\right] S(\dot{x}^n)S(\eta_i)p_l \\ &= 2\left[\left(\eta_i^{\mathrm{T}}\eta_i - \eta_r^2\right) I_3 + 2\eta_r S(\eta_i)\right] S(\dot{x}^n)p_l \\ &\quad + 4\left[S(\eta_i) - \eta_r I_3\right] S(\dot{x}^n)S(\eta_i)p_l \\ &= -2\big[S((\eta_r^2 - \eta_i^{\mathrm{T}}\eta_i)\dot{x}^n) + 2S(S^2(\eta_i)\dot{x}^n) \\ &\quad - S(2\eta_r S(\eta_i)\dot{x}^n) + S(2\eta_i^{\mathrm{T}}\eta_i\dot{x}^n)\big]p_l \\ &= -2S((I_3 - 2\eta_r S(\eta_i) + 2S^2(\eta_i))\dot{x}^n)p_l \\ &= -2S(R^{\mathrm{T}}\dot{x}^n)p_l = -2S(v^b)p_l \end{aligned}$$

giving

$$\frac{1}{2}G\frac{\partial T^*}{\partial \eta} = -S(v^b)p_l - \frac{1}{2}S(\omega^b)p_r = -\begin{bmatrix} S(v^b) & \frac{1}{2}S(\omega^b) \end{bmatrix} p. \tag{4.38}$$

Therefore,

$$\dot{p} = -\begin{bmatrix} S(\omega^b) & 0_{3\times 3} \\ S(v^b) & S(\omega^b) \end{bmatrix} p - \begin{bmatrix} R^{\mathrm{T}}\frac{\partial U}{\partial x^n} \\ \frac{1}{2}G\frac{\partial U}{\partial \eta} \end{bmatrix} + \tau(t) \tag{4.39}$$

Defining

$$k_c(q) \triangleq \begin{bmatrix} R^{\mathrm{T}}\frac{\partial U}{\partial x^n} \\ \frac{1}{2}G\frac{\partial U}{\partial \eta} \end{bmatrix} = \mathcal{P}\frac{\partial U}{\partial q} \in \mathbb{R}^6 \tag{4.40}$$

$$\mathcal{S}(\nu) \triangleq \begin{bmatrix} S(\omega^b) & 0_{3\times 3} \\ S(v^b) & S(\omega^b) \end{bmatrix} \in \mathbb{R}^{6\times 6} \tag{4.41}$$

we can write the kinetics as

$$\dot{p} = -\mathcal{S}(\nu)p - k_c(q) + \tau(t). \tag{4.42}$$

Since M_{RB} is a constant, $\dot{p} = M_{\mathrm{RB}}\dot{\nu}$. If $k_c(q) \equiv 0 \Rightarrow U(q) \equiv 0$, we recognize (4.42) as Kirchoff's equations for a system with (complementary) kinetic energy $T^*(\nu) = \frac{1}{2}\nu^{\mathrm{T}} M_{\mathrm{RB}}\nu$ (see Egeland and Gravdahl [19], Fossen [24]),

$$M_{\mathrm{RB}}\dot{\nu} + \mathcal{S}(\nu)M_{\mathrm{RB}}\nu = \tau(t) \quad \Leftrightarrow \quad \dot{p} + \mathcal{S}(\nu)p = \tau(t) \tag{4.43}$$

as we would expect.

We can rewrite (4.42) by noting that

$$\begin{aligned}
\mathcal{S}(\nu)p &= \mathcal{S}(\nu)M_{\mathrm{RB}}\nu \\
&= \begin{bmatrix} mS(\omega^b)v^b - mS(\omega^b)S(r_g^b) \\ mS(\omega^b)S(r_g^b)v^b - mS(v^b)S(r_g^b)\omega^b + S(\omega^b)J\omega^b \end{bmatrix} \\
&= \begin{bmatrix} mS(\omega^b)v^b - mS(\omega^b)S(r_g^b) \\ mS(r_g^b)S(\omega^b)v^b - S(J\omega^b)\omega^b \end{bmatrix} \\
&= \begin{bmatrix} mS(\omega^b) & -mS(\omega^b)S(r_g^b) \\ mS(r_g^b)S(\omega^b) & -S(J\omega^b) \end{bmatrix} \begin{bmatrix} v^b \\ \omega^b \end{bmatrix} \\
&= C_{\mathrm{RB}}(\omega^b)\nu = C_{\mathrm{RB}}(\omega^b)M_{\mathrm{RB}}^{-1}p
\end{aligned} \tag{4.44}$$

where

$$C_{\mathrm{RB}}(\omega^b) \triangleq \begin{bmatrix} mS(\omega^b) & -mS(\omega^b)S(r_g^b) \\ mS(r_g^b)S(\omega^b) & -S(J\omega^b) \end{bmatrix} = -C_{\mathrm{RB}}^{\mathrm{T}}(\omega^b). \tag{4.45}$$

We can write the kinematics as

$$\dot{q} = \mathcal{W}p^n = \mathcal{P}^{\mathrm{T}}M_{\mathrm{RB}}^{-1}\mathcal{P}P^{\mathrm{T}}p = \mathcal{P}^{\mathrm{T}}M_{\mathrm{RB}}^{-1}p \tag{4.46}$$

since $\mathcal{P}P^{\mathrm{T}} = I_6$. We note that $M_{\mathrm{RB}}^{-1}p = \nu$, that is, the vector of generalized velocities in the body frame. This matches the expected result [19, 24].

We are now ready to define the dynamics for a rigid body with a momentum vector in $\mathbb{R}^6$.

Model I (Momentum-based 6-DOF model of rigid bodies in $\mathbb{R}^3$)**.**

$$\dot{q} = \mathcal{P}^{\mathrm{T}}(q)M_{\mathrm{RB}}^{-1}p \tag{4.47}$$

$$\dot{p} = \tau(t) - C_{\mathrm{RB}}(\omega^b)M_{\mathrm{RB}}^{-1}p - k_c(q) \tag{4.48}$$

where $\mathcal{P}$ is defined in (4.6), M_{RB} in (4.9), C_{RB} in (4.45) and k_c in (4.40).

The dynamics satisfy two important properties:

Property 4.9. The function

$$E = \frac{1}{2}p^{\mathrm{T}}M_{\mathrm{RB}}^{-1}p + U(q - q_{\min}) - U_{\min} \tag{4.49}$$

is a positive definite energy function for the system.

Proof. We know that $p^{\mathrm{T}} M_{\mathrm{RB}}^{-1} p = \nu^{\mathrm{T}} M_{\mathrm{RB}} \nu$, so the first term is kinetic energy. The second term is potential energy in the inertial frame, which as been assumed to be positive definite in q around $q_{\min}$. Subtracting $U(q_{\min})$ is simply to make E zero in zero. □

Property 4.10. The system is passive, in fact lossless, with p as output and $M_{\mathrm{RB}}^{-1}\tau$ as input. The system is also lossless with $\nu = M_{\mathrm{RB}}^{-1} p$ as output and τ as input.

Proof. We take E of (4.49) as the storage function for our system.

$$\begin{aligned}
\dot{E} &= p^{\mathrm{T}} M_{\mathrm{RB}}^{-1} \dot{p} + \dot{q}^{\mathrm{T}} \frac{\partial U}{\partial q} \\
&= p^{\mathrm{T}} M_{\mathrm{RB}}^{-1} \left(\tau(t) - C_{\mathrm{RB}}(\omega^b) M_{\mathrm{RB}}^{-1} p - k_c(q) \right) + p^{\mathrm{T}} M_{\mathrm{RB}}^{-T} \mathcal{P} \frac{\partial U}{\partial q} \\
&= p^{\mathrm{T}} M_{\mathrm{RB}}^{-1} \left(\tau(t) + \mathcal{P} \frac{\partial U}{\partial q} - k_c(q) \right) - p^{\mathrm{T}} M_{\mathrm{RB}}^{-1} C(\omega^b) M_{\mathrm{RB}}^{-1} p \\
&= p^{\mathrm{T}} M_{\mathrm{RB}}^{-1} \tau(t) \\
&= \nu^{\mathrm{T}} \tau(t)
\end{aligned}$$

since $p^{\mathrm{T}} M_{\mathrm{RB}}^{-1} C_{\mathrm{RB}}(\omega^b) M_{\mathrm{RB}}^{-1} p = 0$ (since C_{RB} is skew-symmetric) and $k_c(q) \triangleq \mathcal{P} \frac{\partial U}{\partial q}$ (by (4.40)). Choosing $M_{\mathrm{RB}}^{-1}\tau$ as input and p as output the system is lossless by Khalil [52, Definition 6.3]. If we instead use τ as input and ν as output, the system is lossless by the same definition. □

Since the inertia matrix M_{RB} of a rigid body is constant, $\dot{p} = M_{\mathrm{RB}} \dot{\nu}$ and we can define an alternate model.

Model II (Velocity-based 6-DOF model of rigid bodies in $\mathbb{R}^3$)**.**

$$\dot{q} = \mathcal{P}^{\mathrm{T}}(\eta) \nu \tag{4.50}$$

$$M_{\mathrm{RB}} \dot{\nu} = \tau(t) - C_{\mathrm{RB}}(\omega^b) \nu - k_c(q) \tag{4.51}$$

where all the matrices are as in Model I.

The dynamics satisfy two important properties:

Property 4.11. The function

$$E = \frac{1}{2} \nu^{\mathrm{T}} M_{\mathrm{RB}} \nu + U(q - q_{\min}) - U_{\min} \tag{4.52}$$

is a positive definite energy function for the system.

Proof. We know that the first term is kinetic energy. The second term is potential energy in the inertial frame, which as been assumed to be positive definite in q around $q_{\min}$. Subtracting $U(q_{\min})$ is simply to make E zero in zero. □

Property 4.12. The system is passive, in fact lossless, with ν as output and τ as input.

Proof. We take E of (4.52) as the storage function for our system.

$$\begin{aligned}\dot{E} &= \nu^{\mathrm{T}} M_{\mathrm{RB}} \dot{\nu} + \dot{q}^{\mathrm{T}} \frac{\partial U}{\partial q} \\ &= \nu^{\mathrm{T}} \left(\tau(t) - C_{\mathrm{RB}}(\omega^b)\nu - k_c(q)\right) + \nu^{\mathrm{T}} \mathcal{P} \frac{\partial U}{\partial q} \\ &= \nu^{\mathrm{T}} \left(\tau(t) + \mathcal{P}\frac{\partial U}{\partial q} - k_c(q)\right) - \nu^{\mathrm{T}} C(\omega^b)\nu \\ &= \nu^{\mathrm{T}} \tau(t)\end{aligned}$$

since C_{RB} is skew-symmetric and $k_c(q) \triangleq \mathcal{P}\frac{\partial U}{\partial q}$ (by (4.40)). Choosing τ as input and ν as output the system is lossless by Khalil [52, Definition 6.3]. □

Chapter 5

Equations of motion for a ship in waves

The results of Chapter 4 describe the equations of motion for any rigid body freely moving and rotating in $\mathbb{R}^3$. This chapter extends that with the forces and moments known to be acting on a surface ship in waves, giving a 6-DOF ship model. In addition, this chapter presents a Matlab implementations of the equations of motion with simulation results.

Furthermore, this chapter presents a 1-DOF parametric roll model suitable for ships with non-constant velocity. This model is verified against the 6-DOF model. It is also shown that the commonly used Mathieu equation is not suitable when the velocity is not constant.

The material in this chapter is based on Chapter 4 and Breu et al. [8].

5.1 Conservative forces and moments on a ship

In this Chapter, we will use the velocity-based 6-DOF model of a rigid body (Model II) as basis for the equations of motion of a ship in waves:

$$\dot{q} = \mathcal{P}^{\mathrm{T}}(\eta)\nu \tag{5.1}$$

$$M_{\mathrm{RB}}\dot{\nu} = \tau(t) - C_{\mathrm{RB}}(\omega^b)\nu - k_c(q). \tag{5.2}$$

A ship floating on the surface of the ocean is affected by one potential force, gravity.[1] The ship's center of gravity is located at $r_g^b = [x_g^b, y_g^b, z_g^b]^{\mathrm{T}}$ in the body frame. This vector is constant, since the ship is a rigid body. If we assume that the ship has port–starboard symmetry, then by the definition of the body frame in Section 3.1, $y_g^b = 0$.

We need to find the potential energy of the ship. Any infinitesimal volume block $\mathrm{d}V$ of the ship at a position $\vec{r}$ has density $\rho_s(\vec{r})$ and is at a height $h(\vec{r})$ above some

[1] Technically, buoyancy (which affects any object submerged in a fluid) is also a potential force, but this is rendered quite complex in the presence of waves, especially for a moving ship. We will therefore add buoyancy later.

arbitrary zero point. We note that h is the zero level minus the inertial z-component of $\vec{r}$, i.e.,

$$h(\vec{r}) = h_0 - e_z^{\mathrm{T}} r^n = h_0 - e_z^{\mathrm{T}} R r^b \tag{5.3}$$

where $e_z^{\mathrm{T}} \triangleq [0, 0, 1]$. The negative signage is because the z-axis has the same direction as the gravity field.

The potential energy $\mathrm{d}U$ of $\mathrm{d}V$ is given by

$$\mathrm{d}U = g\rho_s(\vec{r})h(\vec{r})\mathrm{d}V, \tag{5.4}$$

which, in the body frame, can be written as

$$\mathrm{d}U = g\rho_s(r^b)h(r^b)\mathrm{d}V = g\rho_s(r^b)\left(h_0 - e_z^{\mathrm{T}} R r^b\right)\mathrm{d}V. \tag{5.5}$$

The total potential energy U of the ship is then given by

$$\begin{aligned} U &= \int_{\text{ship}} \mathrm{d}U = gmh_0 - ge_z^{\mathrm{T}} R \int_{\text{ship}} \rho_s(r^b) r^b \, \mathrm{d}V \\ &= gmh_0 - gme_z^{\mathrm{T}} R r_g^b \end{aligned} \tag{5.6}$$

since

$$r_g^b \triangleq \frac{1}{m} \int_{\text{ship}} \rho_s(r^b) r^b \, \mathrm{d}V \tag{5.7}$$

is the definition of the center of gravity.

A priori we know that $x^n = 0, R = I_3$ is an equilibrium point for the system. We therefore take U to be zero at this point. The value of U at the equilibrium point is therefore

$$U_0 = gmh_0 - gm[0, 0, 1]r_g^b = gmh_0 - gmz_g^b \triangleq 0.$$

Thus,

$$h_0 \triangleq z_g^b. \tag{5.8}$$

This gives the potential energy

$$U(q) = gm\left[z_g^b - e_z^{\mathrm{T}} R(\eta) r_g^b\right]. \tag{5.9}$$

The partial derivatives of U are given by

$$\begin{aligned} \frac{\partial U}{\partial x^n} &= 0 \\ \frac{\partial U}{\partial \eta} &= -mg \frac{\partial e_z^{\mathrm{T}} R}{\partial \eta} r_g^b. \end{aligned}$$

From (3.21), we have

$$e_z^{\mathrm{T}} R = \begin{bmatrix} 2(\eta_{i,1}\eta_{i,3} - \eta_{i,2}\eta_r) & 2(\eta_{i,2}\eta_{i,3} + \eta_{i,1}\eta_r) & 1 - 2(\eta_{i,1}^2 + \eta_{i,2}^2) \end{bmatrix},$$

so

$$\frac{\partial e_z^{\mathrm{T}} R}{\partial \eta} = 2 \begin{bmatrix} -\eta_{i,2} & \eta_{i,1} & 0 \\ \eta_{i,3} & \eta_r & -2\eta_{i,1} \\ -\eta_r & \eta_{i,3} & -2\eta_{i,2} \\ \eta_{i,1} & \eta_{i,2} & 0 \end{bmatrix} \in \mathbb{R}^{4\times 3}. \tag{5.10}$$

From (4.40), we have

$$k_c(q) = \begin{bmatrix} R^{\mathrm{T}} \frac{\partial U}{\partial x^n} \\ \frac{1}{2} G \frac{\partial U}{\partial \eta} \end{bmatrix} = -mg \begin{bmatrix} 0_{3\times 1} \\ \frac{1}{2} G \frac{\partial e_z^{\mathrm{T}} R}{\partial \eta} r_g^b \end{bmatrix} \tag{5.11}$$

From (3.20) and (5.10) we get

$$\begin{aligned} G\frac{\partial e_z^{\mathrm{T}} R}{\partial \eta} &= 2 \begin{bmatrix} -\eta_{i,1} & \eta_r & \eta_{i,3} & -\eta_{i,2} \\ -\eta_{i,2} & -\eta_{i,3} & \eta_r & \eta_{i,1} \\ -\eta_{i,3} & \eta_{i,2} & -\eta_{i,1} & \eta_r \end{bmatrix} \begin{bmatrix} -\eta_{i,2} & \eta_{i,1} & 0 \\ \eta_{i,3} & \eta_r & -2\eta_{i,1} \\ -\eta_r & \eta_{i,3} & -2\eta_{i,2} \\ \eta_{i,1} & \eta_{i,2} & 0 \end{bmatrix} \\ &= 2 \begin{bmatrix} 0 & 1 - 2\eta_{i,1}^2 - 2\eta_{i,2}^2 & -2\eta_r\eta_{i,1} - 2\eta_{i,2}\eta_{i,3} \\ -1 + 2\eta_{i,1}^2 + 2\eta_{i,2}^2 & 0 & -2\eta_r\eta_{i,2} + 2\eta_{i,1}\eta_{i,3} \\ 2\eta_r\eta_{i,1} + 2\eta_{i,2}\eta_{i,3} & 2\eta_r\eta_{i,2} - 2\eta_{1,2}\eta_{i,3} & 0 \end{bmatrix} \\ &= -2S(R^{\mathrm{T}}(\eta)e_z) \end{aligned} \tag{5.12}$$

where the relationship $\eta^{\mathrm{T}}\eta = 1$ has been used.

Thus,

$$k_c(q) = mg \begin{bmatrix} 0_{3\times 1} \\ S(R^{\mathrm{T}}(\eta)e_z) r_g^b \end{bmatrix}. \tag{5.13}$$

5.2 Hydrodynamic forces and moments on a ship

To derive the hydrodynamic forces and moments on a ship, we need to make certain assumptions:

Assumption 1. There is no current.

Assumption 2. The hull can be split into triangular and quadrangular panels that can be parametrized as two-dimensional surfaces embedded in $\mathbb{R}^3$.

Assumption 3. Following maneuvering theory [24], the frequency-dependent damping, added mass and Coriolis/centripetal matrices can be represented at a constant excitation frequency.

Assumption 4. The ocean is infinitely deep.

Assumption 5. The pressure field in the ocean is unchanged by the passage of the ship (in effect, waves are traveling "through" the ship's hull).

Assumption 6. Generalized forces associated with the virtual work defined in Section 4.2 obey the superposition principle.

The external generalized forces τ are largely a result of the the propulsion system, wind, gravity, the (dynamic and static) pressure exerted by the surrounding ocean and various dissipative forces. By assumption, we will neglect wind-induced forces.

We therefore write

$$\tau = \tau_g + \tau_p + \tau_d + \tau_c + \tau_e \in \mathbb{R}^6 \tag{5.14}$$

where τ_g is the weight of the ship, τ_p is the pressure-induced generalized force, τ_c are generalized forces due to the propulsion system, τ_d are generalized dissipative forces due to skin friction, vortex shedding, etc. and τ_e are umodeled generalized forces and disturbances (including any wind-induced forces).

At any given point r^n in the ocean (in the inertial frame), there will be a local pressure field $\Psi = \Psi(r^n, q, \nu, \dot{\nu}, t) \in \mathbb{R}$ [75, 91]. We assume (Assumption 2) that each section of the ship's hull can be parametrized with parameters u and v, so that the vector $r_i^b(u, v)$ gives the position of a point on the surface of panel i, in the body frame.

Defining

$$\Psi_i(u, v) \triangleq \Psi([Rr_i^b(u, v) + x^n], q, \nu, \dot{\nu}, t), \tag{5.15}$$

we can then take the generalized pressure-induced force on the ship as [18, 75, 91]

$$\tau_p = -\sum_i \begin{bmatrix} \int_{S_{w,i}} \Psi_i(u, v) \frac{\partial r_i^b}{\partial u}(u, v) \times \frac{\partial r_i^b}{\partial v}(u, v) \, \mathrm{d}u \, \mathrm{d}v \\ \int_{S_{w,i}} \Psi_i(u, v) r_i^b(u, v) \times \left(\frac{\partial r_i^b}{\partial u}(u, v) \times \frac{\partial r_i^b}{\partial v}(u, v) \right) \, \mathrm{d}u \, \mathrm{d}v \end{bmatrix} \tag{5.16}$$

where $S_{w,i}$ is the wetted (submerged) part of panel i and the ship is parametrized so that the normal vector $(\partial r_i^b / \partial u) \times (\partial r_i^b / \partial u)^2$ points out of the hull. The effects of current and waves can all be accounted for in the force τ_p [20, 75].

Unfortunately, computing the pressure field Ψ requires the solution to the Navier-Stokes equations, where some of the boundary conditions are the state of the ship [54]. In practice, this is unsolvable without resorting to computational fluid dynamics [91]. We therefore simplify Ψ to

$$\Psi(r^n, q, \nu, \dot{\nu}, t) \approx \Psi_d(r^n, \nu, t) + \Psi_a(r^n, \dot{\nu}, t) + \Psi_b(r^n, t), \tag{5.17}$$

take

$$\Psi_{d,i}(u, v) = \Psi_d(Rr_i^b(u, v) + x^n, R\nu, t) \tag{5.18}$$

$$\Psi_{a,i}(u, v) = \Psi_a(Rr_i^b(u, v) + x^n, R\dot{\nu}, t) \tag{5.19}$$

$$\Psi_{b,i}(u, v) = \Psi_b(Rr_i^b(u, v) + x^n, t) \tag{5.20}$$

[2] See Edwards and Penney [18] for proof that this is a normal vector.

and τ_p as

$$\begin{aligned}\tau_p \approx &-\sum_i \begin{bmatrix} \int_{S_{w,i}} \Psi_{d,i} \frac{\partial r_i^b}{\partial u} \times \frac{\partial r_i^b}{\partial v} \, \mathrm{d}u \, \mathrm{d}v \\ \int_{S_{w,i}} \Psi_{d,i} r_i^b \times \left(\frac{\partial r_i^b}{\partial u} \times \frac{\partial r_i^b}{\partial v} \right) \mathrm{d}u \, \mathrm{d}v \end{bmatrix} \\ &-\sum_i \begin{bmatrix} \int_{S_{w,i}} \Psi_{a,i} \frac{\partial r_i^b}{\partial u} \times \frac{\partial r_i^b}{\partial v} \, \mathrm{d}u \, \mathrm{d}v \\ \int_{S_{w,i}} \Psi_{a,i} r_i^b \times \left(\frac{\partial r_i^b}{\partial u} \times \frac{\partial r_i^b}{\partial v} \right) \mathrm{d}u \, \mathrm{d}v \end{bmatrix} \\ &-\sum_i \begin{bmatrix} \int_{S_{w,i}} \Psi_{b,i} \frac{\partial r_i^b}{\partial u} \times \frac{\partial r_i^b}{\partial v} \, \mathrm{d}u \, \mathrm{d}v \\ \int_{S_{w,i}} \Psi_{b,i} r_i^b \times \left(\frac{\partial r_i^b}{\partial u} \times \frac{\partial r_i^b}{\partial v} \right) \mathrm{d}u \, \mathrm{d}v \end{bmatrix} \\ \approx &-D_p \nu - C_A(\nu)\nu - M_A(\Omega)\dot{\nu} - k(q,t) \end{aligned} \tag{5.21}$$

and D_p, C_A and M_A are recognized as

$$D_p \nu + C_A(\nu)\nu \approx \sum_i \begin{bmatrix} \int_{S_{w,i}} \Psi_{d,i} \frac{\partial r_i^b}{\partial u} \times \frac{\partial r_i^b}{\partial v} \, \mathrm{d}u \, \mathrm{d}v \\ \int_{S_{w,i}} \Psi_{d,i} r_i^b \times \left(\frac{\partial r_i^b}{\partial u} \times \frac{\partial r_i^b}{\partial v} \right) \mathrm{d}u \, \mathrm{d}v \end{bmatrix} \tag{5.22}$$

$$M_A(\Omega)\dot{\nu} \approx \sum_i \begin{bmatrix} \int_{S_{w,i}} \Psi_{a,i} \frac{\partial r_i^b}{\partial u} \times \frac{\partial r_i^b}{\partial v} \, \mathrm{d}u \, \mathrm{d}v \\ \int_{S_{w,i}} \Psi_{a,i} r_i^b \times \left(\frac{\partial r_i^b}{\partial u} \times \frac{\partial r_i^b}{\partial v} \right) \mathrm{d}u \, \mathrm{d}v \end{bmatrix} \tag{5.23}$$

$$k_p(q,t) \approx \sum_i \begin{bmatrix} \int_{S_{w,i}} \Psi_{b,i} \frac{\partial r_i^b}{\partial u} \times \frac{\partial r_i^b}{\partial v} \, \mathrm{d}u \, \mathrm{d}v \\ \int_{S_{w,i}} \Psi_{b,i} r_i^b \times \left(\frac{\partial r_i^b}{\partial u} \times \frac{\partial r_i^b}{\partial v} \right) \mathrm{d}u \, \mathrm{d}v \end{bmatrix}. \tag{5.24}$$

Following Assumption 3, the frequency-dependence of D_p, C_A and M_A is omitted.

The matrices are assumed to satisfy

$$r^{\mathrm{T}} D_p r > 0 \; \forall \; r \neq 0 \in \mathbb{R}^6 \tag{5.25}$$

$$C_A^{\mathrm{T}}(\nu) = -C_A(\nu) \; \forall \; \nu \in \mathbb{R}^6 \tag{5.26}$$

$$M_A = M_A^{\mathrm{T}} > 0. \tag{5.27}$$

Note that the above simplifications are only valid if there is zero current; otherwise the velocities would have to be the velocities of the ship relative to the current.

The generalized force $-D_p\nu$ is a dissipative force, removing energy from the system. In addition to this pressure-induced damping, there are also other dissipative effects such as viscous damping and vortex shedding. We include all these other damping effects in the generalized force

$$\tau_d = -D_v(\nu)\nu \tag{5.28}$$

where D_v satisfies $r^{\mathrm{T}} D_v(\nu) r > 0 \; \forall \; r \neq 0 \in \mathbb{R}^6, \nu \in \mathbb{R}^6$.

Although it is perhaps not obvious, buoyancy is included in the term k_p, and the first three elements of k_p (pressure-induced forces) are non-zero even in calm water for a ship at rest. As the ship is floating, there needs to be a force counteracting

this. In fact, this is the weight of the ship. This was not included in the term k_c, as the potential energy of the ship and thus its weight does not depend on the ship's position, only its orientation. We therefore add this force manually as [24]

$$\tau_g(q) = mg \begin{bmatrix} R^{\mathrm{T}}(\eta) e_z \\ 0_{3\times 1} \end{bmatrix}. \tag{5.29}$$

Combining all the above, we can write the 6-DOF model for a ship in waves:

Model III (6-DOF model of a ship in waves)**.**

$$\dot{q} = \mathcal{P}^{\mathrm{T}}(\eta)\nu \tag{5.30}$$

$$M\dot{\nu} + D(\nu)\nu + C(\nu)\nu + k(q,t) = \tau_c(t) + \tau_e(t). \tag{5.31}$$

where

$$\begin{aligned} M &\triangleq M_{\mathrm{RB}} + M_A \\ D(\nu) &\triangleq D_p(\nu) + D_v(\nu) \\ C(\nu) &\triangleq C_{\mathrm{RB}}(\nu) + C_A(\nu) \\ k(q,t) &\triangleq k_p(q,t) - \tau_g(q) + k_c(q). \end{aligned}$$

By Fossen [24], the Coriolis/centripetal matrices C can be found from M. If

$$M = \begin{bmatrix} M_{11} & M_{12} \\ M_{21} & M_{22} \end{bmatrix} \in \mathbb{R}^{6\times 6}, \quad M_{11}, M_{12}, M_{21}, M_{22} \in \mathbb{R}^{3\times 3}$$

then

$$C(\nu) = \begin{bmatrix} 0_{3\times 3} & -S(M_{11}v^b + M_{12}\omega^b) \\ -S(M_{11}v^b + M_{12}\omega^b) & -S(M_{21}v^b + M_{22}\omega^b) \end{bmatrix}.$$

5.3 Computer implementation of (5.30)–(5.31)

To implement a computer version of the model (5.30)–(5.31), we use data from a specific, 280 m long container ship. The main characteristics of this vessel can be found in Table 5.1.

Table 5.1: Main characteristics of the container ship.

Quantity	Value
Length between perpendiculars	281 m
Beam amidships	32.3 m
Draught amidships	11.8 m
Displacement	76 468 m^3
Roll radius of gyration	12.23 m
Transverse metacentric height	1.84 m

While Model III can be used for other sea states, we have chosen to create an implementation suitable for parametric roll. As such, we assume that the waves are planar and sinusoidal.

5.3.1 Forces other than k_p

We computed the parameters for inertia M_{RB}, added mass M_A and damping D_p and D_v in VERES [23]. We set the unmodeled force vector τ_e to zero and the control force τ_c as

$$\tau_c = -\begin{bmatrix} k_p(v_1^b - v_{1,d}^b) + k_i \int_{t_0}^{t} (v_1^b(T) - v_{1,d}^b(T))\,\mathrm{d}T \\ 0 \\ 0 \\ 0 \\ 0 \\ \kappa_p(\psi - \psi_d) + \kappa_d(\dot{\psi} - \dot{\psi}_d) + \kappa_i \int_{t_0}^{t} (\psi(T) - \psi_d(T))\,\mathrm{d}T \end{bmatrix} \tag{5.32}$$

with $v_{1,d}^b$ the desired surge speed and ψ_d the desired heading. The rudimentary PID controllers in surge and yaw are there to keep the ship on course in the presence of the other forces. Without these controllers, the simulated ship tends to drift quite heavily off course.

The parameters used are

$$M_{\mathrm{RB}} = \begin{bmatrix} mI_3 & -mS(r_g^b) \\ mS(r_g^b) & J \end{bmatrix}$$

$$m = 7.7358\text{E}7$$

$$r_g^b = [-3.7486, 0, -1.120]^{\mathrm{T}}$$

$$g = 9.81$$

$$J = \begin{bmatrix} 1.41\text{E}10 & 0 & 0 \\ 0 & 3.70\text{E}11 & 0 \\ 0 & 0 & 3.70\text{E}11 \end{bmatrix}$$

$$M_A = \begin{bmatrix} 0 & 0 & 0 & 0 & 0 & 0 \\ 0 & 7.59\text{E}7 & 0 & 6.43\text{E}7 & 0 & -1.04\text{E}9 \\ 0 & 0 & 7.80\text{E}7 & 0 & -7.8\text{E}8 & 0 \\ 0 & 6.43\text{E}7 & 0 & 2.20\text{E}9 & 0 & -9.08\text{E}9 \\ 0 & 0 & -7.83\text{E}8 & 0 & 3.39\text{E}11 & 0 \\ 0 & -1.04\text{E}9 & 0 & -9.08\text{E}9 & 0 & 4.48\text{E}11 \end{bmatrix}$$

$$D(\nu) = \begin{bmatrix} 5.66\text{E}3 & 0 & 0 & 0 & 0 & 0 \\ 0 & 3.31\text{E}7 & 0 & 1.50\text{E}7 & 0 & 1.22\text{E}8 \\ 0 & 0 & 4.66\text{E}7 & 0 & -1.05\text{E}9 & 0 \\ 0 & 1.50\text{E}7 & 0 & 2.48\text{E}8 & 0 & -2.27\text{E}9 \\ 0 & 0 & -4.03\text{E}8 & 0 & 2.73\text{E}11 & 0 \\ 0 & -5.03\text{E}8 & 0 & -2.79\text{E}9 & 0 & 1.35\text{E}11 \end{bmatrix} + \begin{bmatrix} 2.83\text{E}4|v_1| & 0_{1\times 5} \\ 0_{5\times 1} & 0_{5\times 5} \end{bmatrix}$$

$$k_p = 7.7358\text{E}7$$

$$k_i = 7.7358\text{E}6$$

$$\kappa_p = 8.18\text{E}11$$

$$\kappa_d = \kappa_i = 0$$

with all values in base SI units (kg–m–s).

With these numbers, all forces and moments of (5.31) except for k_p can be computed.

5.3.2 Pressure-induced forces k_p

The final generalized force that needs to be computed is the pressure-induced spring term $k_p(q,t)$. This is computed directly from (5.24) with some further simplifications:

Assumption 7. The waves are a simple, planar, standing sinusoid.

Assumption 8. The "hydrostatic" part of the pressure extends from the instantaneous ocean surface and down.

Assumption 9. The "dynamic" part of the pressure extends from the mean ocean surface and down.

By Faltinsen [20], these approximations and the ones used in deriving (5.31) give a first-order approximation of the wave forces and moments.

Pressure field

From Faltinsen [20], we have that the ocean surface under these conditions is given by

$$\zeta(t, r^n) = \zeta_0 \cos(\omega_0 t - k_w r_1^n + \alpha_\zeta) \tag{5.33}$$

in the inertial frame, with ζ giving the wave height at a position $r^n = [r_1^n, r_2^n, r_3^n]^{\mathrm{T}}$. The ocean surface is then at $[r_1^n, r_2^n, \zeta(t, r^n)]^{\mathrm{T}}$.

The constant parameters are the wave amplitude ζ_0, the frequency of the waves as seen by an observer stationary in the inertial frame ω_0, and the wave number k_w. For waves traveling in negative x-direction, $k_w < 0$ and vice versa.

By Faltinsen [20], the pressure field Ψ_b is given by

$$\Psi_b(r^n, t) = g\rho\zeta_0 e^{-k_w \max(r_3^n, 0)} \cos(\omega_0 t - k_w r_1^n + \alpha_\zeta) + g\rho r_3^n. \tag{5.34}$$

The parameters are the acceleration of gravity g and the density of sea water ρ. The term $g\rho r_3^n$ is the "hydrostatic" pressure, and $g\rho\zeta_0 e^{-k_w \max(r_3^n, 0)} \cos(\omega_0 t - k_w r_1^n + \alpha_\zeta)$ the "dynamic" pressure.

The submerged part of the ship

The ship's hull, as previously mentioned, is split into panels, each forming a triangle or quadrangle. In the body frame, panel i has corners $p_{i,j}^b$, $j \in \{1,2,3,4\}$ for quadrangles and $j \in \{1,2,3\}$ for triangles. In the inertial frame,

$$p_{i,j}^n = R p_{i,j}^b + x^n. \tag{5.35}$$

As (5.33) gives the explicit wave surface (in the inertial frame) we can compute which points, at any given time and physical location, are above or below the wave surface by solving the equation

$$e_z^{\mathrm{T}} p_{i,j}^n = \zeta(t, p_{i,j}^n).$$

Rather than solving the equation explicitly, an approximation is used. First, the points are transformed using

$$\bar{p}_{i,j}^n = p_{i,j}^n - [0, 0, \zeta(t, p_{i,j}^n)]^{\mathrm{T}}. \tag{5.36}$$

Any point with a positive z-value is submerged. See Figures 5.1(a) and 5.1(b).

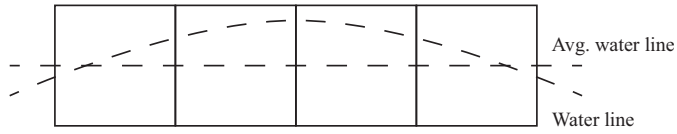

(a) Initial state.

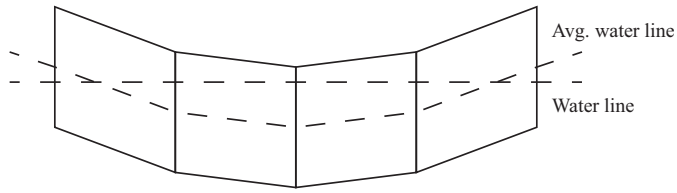

(b) Post-transformation.

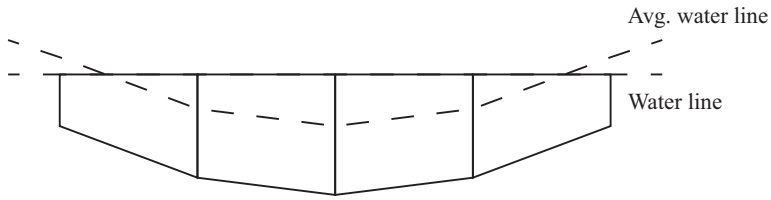

(c) Post-cutting.

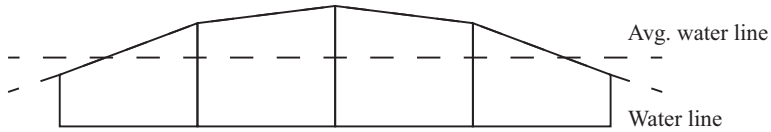

(d) Reverse transformation.

Figure 5.1: Transforming panels.

Each panel was individually parametrized with a bilinear interpolation, so that for each panel i,

$$\bar{p}_i^n = \bar{k}_0 + \bar{k}_u u + \bar{k}_v v + \bar{k}_{uv} uv \tag{5.37}$$

with $u, v \in [0, 1)$ defines all points on panel i.

For each partially submerged panel (one with at least one point underwater and at least one point above water), the parametrization is used to find where the edges of the panel intersect the water line, and to compute the coordinates of these points. The submerged points and the points in the waterline then make up (one or more) new panel(s). Note that the panels whose submerged part forms a pentagon are split into three triangular panels, whereas panels whose submerged part forms a triangle or a quadrangle are kept as such, see Figure 5.2.

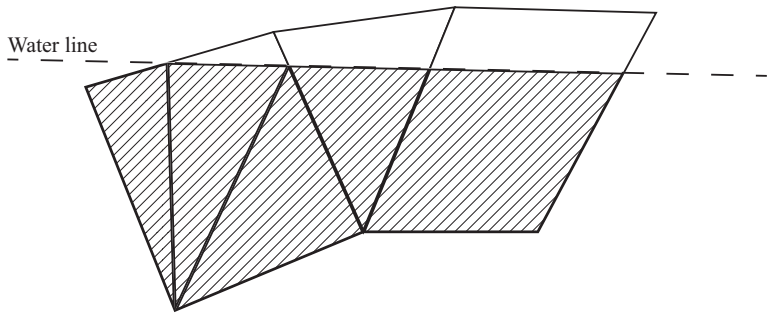

Figure 5.2: Cutting partially submerged panels into new fully submerged panels.

The partially submerged panels and the panels wholly above the waterline are discarded. The fully submerged panels based on the partially submerged panels and the original fully submerged panels are kept.

Before computing the forces and moments, the transformation (5.36) needs to be reversed so that the points are expressed in the inertial frame. We therefore take

$$p_{i,j}^n = \bar{p}_{i,j}^n + [0, 0, \zeta(t, p_{i,j}^n)]^{\mathrm{T}}. \tag{5.38}$$

The entire transformation–cutting–inverse transformation process can be seen in Figure 5.1.

The approximation to find the true intersection of the hull and the ocean surface is good if the average size of the panels is small relative to the wave length.

The generalized forces

We parametrize the submerged panels bilinearly so that

$$p_i^n = k_0 + k_u u + k_v v + k_{uv} uv \tag{5.39}$$

with $u, v \in [0, 1)$ define all points on panel i, in the inertial frame.

The partial derivatives of p_i^n with respect to u and v can be explicitly found as

$$\frac{\partial p_i^n}{\partial u} = k_u + k_{uv} v \tag{5.40}$$

$$\frac{\partial p_i^n}{\partial v} = k_v + k_{uv} u. \tag{5.41}$$

It is worth noting that for triangular panels, $k_{uv} = 0$.

For each panel, we can compute the pressure-induced force in the inertial frame as

$$f_i^n = \begin{cases} \int_0^1 \int_0^1 \Psi_b(p_i^n(u,v),t)\,[k_u + k_{uv}v] \times [k_v + k_{uv}u]\ \mathrm{d}u\,\mathrm{d}v & \text{quadrangles} \\ \int_0^1 \int_0^{1-v} \Psi_b(p_i^n(u,v),t) k_u \times k_v\ \mathrm{d}u\,\mathrm{d}v & \text{triangles} \end{cases}$$

The integration must be done numerically. Although more points could be used, for increased computational speed, only corner points were used in the calculation of the pressure forces. Thus,

$$f_i^n \approx \begin{cases} \frac{1}{4}\sum_{j=1}^4 \Psi_b(p_i^n(\bar{u}_j,\bar{v}_j),t)\,[k_u + k_{uv}\bar{v}_j] \times [k_v + k_{uv}\bar{u}_j] & \text{quadrangles} \\ \frac{1}{6}\sum_{j=1}^3 \Psi_b(p_i^n(\bar{u}_j,\bar{v}_j),t) k_u \times k_v & \text{triangles} \end{cases}$$

where

$$\begin{aligned} \bar{u}_1 &= 0, & \bar{v}_1 &= 0, \\ \bar{u}_2 &= 0, & \bar{v}_2 &= 1, \\ \bar{u}_3 &= 1, & \bar{v}_3 &= 0, \\ \bar{u}_4 &= 1, & \bar{v}_4 &= 1. \end{aligned}$$

Computations for the torque is similar. However, we need the torque relative to the body origin rather than the inertial origin. We therefore get

$$m_i^n = \begin{cases} \int_0^1 \int_0^1 \Psi_b(p_i^n(u,v),t)\,[p_i^n(u,v) - x^n] \\ \qquad \times ([k_u + k_{uv}v] \times [k_v + k_{uv}u])\ \mathrm{d}u\,\mathrm{d}v & \text{quadr.} \\ \int_0^1 \int_0^{1-v} \Psi_b(p_i^n(u,v),t)\,[p_i^n(u,v) - x^n] \times (k_u \times k_v)\ \mathrm{d}u\,\mathrm{d}v & \text{triangles} \end{cases}$$

This is approximated as

$$m_i^n \approx \begin{cases} \frac{1}{4}\sum_{j=1}^4 \Psi_b(p_i^n(\bar{u}_j,\bar{v}_j),t)\,[p_i^n(\bar{u}_j,\bar{v}_j) - x^n] \\ \qquad \times ([k_u + k_{uv}\bar{v}_j] \times [k_v + k_{uv}\bar{u}_j]) & \text{quadr.} \\ \frac{1}{6}\sum_{j=1}^3 \Psi_b(p_i^n(\bar{u}_j,\bar{v}_j),t)\,[p_i^n(\bar{u}_j,\bar{v}_j) - x^n] \times (k_u \times k_v) & \text{triangles} \end{cases}$$

Note that this torque is still in the inertial frame, but relative to the body origin.

If the set $\bar{S}$ consists of all i such that panel i is one of the original, fully submerged panels *or* one of the newly created (also fully submerged) panels, we can then take

$$k_p(q,t) \approx \begin{bmatrix} R^{\mathrm{T}} \sum_{i\in\bar{S}} f_i^n \\ R^{\mathrm{T}} \sum_{i\in\bar{S}} m_i^n \end{bmatrix} \tag{5.42}$$

to get the total pressure-induced force and moment in the body frame.

The system was simulated with a fixed time step, and for each time instant, the outlined procedure for computing k_p was performed.

It is worth noting that the procedure automatically handles such effects as (first-order) wave-induced forces and Doppler shift of these. The first by simple virtue of the pressure field including the dynamic pressure and the second by including x^n in (5.35).

5.4 The encounter frequency

To an observer standing in a fixed location on the ocean surface, waves will appear to have a specific frequency of oscillation (or a range of frequencies if the waves are irregular). We look at regular sinusoidal waves, described by (5.33).

To a stationary observer, r^n is constant. To a moving observer, the waves will appear to behave differently than to the stationary observer due to the Doppler effect. We take $r^n = x^n$ to be the location of the observer (i.e., the ship) in the inertial frame and assume, without loss of generality, that $x^n(t_0) = 0$. The observer's velocity in the inertial x-direction is then

$$\dot{x}^n \triangleq v_1^n \tag{5.43}$$

so that

$$\zeta(t, x^n) = \zeta_0 \cos\left(\omega_0 t - k_w \int_{t_0}^{t} v_1^n(\tau)\, \mathrm{d}\tau + \alpha_\zeta\right) . \tag{5.44}$$

Since the velocity in Model III is given in the body frame, we use

$$v_1^n = e_x^{\mathrm{T}} R v^b \tag{5.45}$$

where $e_x = [1, 0, 0]^{\mathrm{T}}$.

We can then define the encounter frequency between the observer and the wave – or the frequency seen by the observer – as

$$\begin{aligned} \omega_e &\triangleq \frac{\mathrm{d}}{\mathrm{d}t}\left(\omega_0 t - k_w \int_{t_0}^{t} v_1^n(\tau)\, \mathrm{d}\tau\right) && (5.46)\\ &= \omega_0 - k_w e_x^{\mathrm{T}} R v^b \approx \omega_0 - k_w e_x^{\mathrm{T}} R [v_1^b, 0, 0]^{\mathrm{T}} \\ &= \omega_0 - k_w \cos(\theta)\cos(\psi) v_1^b \approx \omega_0 - k_w v_1^b && (5.47) \end{aligned}$$

and rewrite (5.44) as

$$\zeta(t, x^n) = \zeta_0 \cos\left(\int_{t_0}^{t} \omega_e(\tau)\, \mathrm{d}\tau + \alpha_\zeta\right) . \tag{5.48}$$

We note that if v_1^n is a constant, then so is ω_e, and the above simply becomes

$$\zeta(t, x^n) = \zeta_0 \cos\left(\omega_e t + \alpha_\zeta\right) . \tag{5.49}$$

It is an important fact that whereas we cannot change ω_0, we can change ω_e by changing the velocity.

5.5 Simplified roll equation

The spring term in the full 6-DOF model is analytically unknown. To derive a 1-DOF roll model we will also make the following extra assumption:

Assumption 10. The ship is traveling directly into the waves.

Note that the ship is still allowed to change forward speed.

For ships in parametric resonance, it's well-known that the most important degrees of freedom are heave, roll and pitch [40, 64]. Heave and pitch are already coupled, and during parametric resonance these transfer energy to roll.

Setting all other degrees of freedom to zero, we define

$$q_{r_3} \triangleq [z^n, \phi, \theta]^{\mathrm{T}} \tag{5.50}$$

$$\nu_{r_3} \triangleq [v_3^b, \omega_1^b, \omega_2^b]^{\mathrm{T}} \tag{5.51}$$

and note that (from Properties 3.21 and 3.22)

$$\dot{q}_{r_3} = \begin{bmatrix} \cos(\phi)\cos(\theta) & 0 & 0 \\ 0 & 1 & \sin(\phi)\tan(\theta) \\ 0 & 0 & \cos(\phi) \end{bmatrix} \nu_{r_3} \approx \nu_{r_3} \ . \tag{5.52}$$

This 3-DOF model can be written as

$$M_{r_3}\dot{\nu}_{r_3} + C_{r_3}\left(\nu_{r_3}\right)\nu_{r_3} + D_{r_3}(\nu_{r_3})\nu_{r_3} + k_{r_3}\left(q_{r_3}, t\right) = \tau_{c,r_3} + \tau_{e,r_3} \ . \tag{5.53}$$

For simplicity, we will assume that the velocities in heave and pitch are low, and that the only coupling between these two degrees of freedom and roll exists in the spring term k_{r_3}. This allows us to write

$$M_{r_3} = \begin{bmatrix} m_{33} & 0 & m_{35} \\ 0 & m_{44} & 0 \\ m_{53} & 0 & m_{55} \end{bmatrix}$$

$$C_{r_3}\left(\nu_{r_3}\right) = 0_{3\times 3}$$

$$D_{r_3}\left(\nu_{r_3}\right) = \begin{bmatrix} d_{33} & 0 & d_{35} \\ 0 & d_{44} & 0 \\ d_{53} & 0 & d_{55} \end{bmatrix}$$

where m_{ij} and d_{ij} are the i,jth element of M and $D\left(0\right)$ from (5.31).

Furthermore, following Holden et al. [40] (see also Chapter 6 for derivation), we simplify k_{r_3} to

$$k_{r_3}\left(q_{r_3}, t\right) \approx \begin{bmatrix} k_{33} & 0 & k_{35} \\ 0 & k_{44} & 0 \\ k_{53} & 0 & k_{55} \end{bmatrix} q_{r_3} + \begin{bmatrix} 0 \\ k_{z\phi} z^n \phi + k_{\phi\theta}\phi\theta + k_{\phi^3}\phi^3 \\ 0 \end{bmatrix} + \bar{k}_{r_3}\left(t\right)$$

with

$$\bar{k}_{r_3}\left(t\right) = -\begin{bmatrix} a_z\zeta_0 \cos\left(\int_{t_0}^{t} \omega_e(\tau)\,\mathrm{d}\tau + \alpha_z\right) \\ 0 \\ a_\theta\zeta_0 \cos\left(\int_{t_0}^{t} \omega_e(\tau)\,\mathrm{d}\tau + \alpha_\theta\right) \end{bmatrix}$$

where a_z, α_z, a_θ, and α_θ are constant. We note that $\bar{k}_{r_3}\left(t\right)$ is merely ζ of (5.44) phase-shifted and scaled, effectively sent through a linear filter.

Neither heave nor roll nor pitch are likely to be directly actuated, so $\tau_{c,r_3} = 0$. The unmodeled disturbances τ_{e,r_3} are also assumed zero.

We can then rewrite (5.53) as

$$m_{44}\ddot{\phi} + d_{44}\dot{\phi} + k_{44}\phi + k_{\phi^3}\phi^3 = -[k_{z\phi}, k_{\phi\theta}]q_{\bar{r}_2}\phi \tag{5.54}$$

$$M_{\bar{r}_2}\ddot{q}_{\bar{r}_2} + D_{\bar{r}_2}\dot{q}_{\bar{r}_2} + K_{\bar{r}_2}q_{\bar{r}_2} = \bar{k}_{\bar{r}_2}\ . \tag{5.55}$$

with

$$\begin{aligned}
q_{\bar{r}_2} &= [z^n, \theta]^{\mathrm{T}} \\
M_{\bar{r}_2} &= \begin{bmatrix} m_{33} & m_{35} \\ m_{53} & m_{55} \end{bmatrix} \\
D_{\bar{r}_2} &= \begin{bmatrix} d_{33} & d_{35} \\ d_{53} & d_{55} \end{bmatrix} \\
K_{\bar{r}_2} &= \begin{bmatrix} k_{33} & k_{35} \\ k_{53} & k_{55} \end{bmatrix} \\
\bar{k}_{\bar{r}_2}(t) &= \begin{bmatrix} a_z\zeta_0 \cos\left(\int_{t_0}^{t} \omega_e(\tau)\ \mathrm{d}\tau + \alpha_z\right) \\ a_\theta\zeta_0 \cos\left(\int_{t_0}^{t} \omega_e(\tau)\ \mathrm{d}\tau + \alpha_\theta\right) \end{bmatrix}\ .
\end{aligned}$$

We note that the $q_{\bar{r}_2}$-subsystem (5.55) is completely decoupled from the roll-subsystem (5.54) and is merely a linear ordinary differential equation with constant coefficients and a sinusoidal input. If we assume that ω_e is constant, then the system will have as a steady-state solution

$$q_{\bar{r}_2}(t) = \begin{bmatrix} \bar{a}_z\zeta_0 \cos\left(\int_{t_0}^{t} \omega_e(\tau)\ \mathrm{d}\tau + \bar{\alpha}_z\right) \\ \bar{a}_\theta\zeta_0 \cos\left(\int_{t_0}^{t} \omega_e(\tau)\ \mathrm{d}\tau + \bar{\alpha}_\theta\right) \end{bmatrix} \tag{5.56}$$

where $\bar{a}_z$, $\bar{\alpha}_z$, $\bar{a}_\theta$ and $\bar{\alpha}_\theta$ are constant.

The main purpose of this chapter is to derive a roll model for changing ω_e, thus we consider the case when ω_e is not constant. Let us revisit the equation for ω_e, and note

$$\begin{aligned}
\dot{\omega}_e &= \frac{\mathrm{d}}{\mathrm{d}t}\left(\omega_0 - k_w e_x^{\mathrm{T}} R v^b\right) = -k_w e_x^{\mathrm{T}}\left(\dot{R}v^b + R\dot{v}^b\right) \\
&= -k_w e_x^{\mathrm{T}} R\left(S(\omega^b)v^b + \dot{v}^b\right)
\end{aligned} \tag{5.57}$$

giving

$$|\dot{\omega}_e| \leq |k_w|\,\|e_x\|\,\|R\|\left(\left\|S(\omega^b)v^b\right\| + \left\|\dot{v}^b\right\|\right) = |k_w|\left(\left\|S(\omega^b)v^b\right\| + \left\|\dot{v}^b\right\|\right) \tag{5.58}$$

since $\|e_x\| = \|R\| = 1$.

For large ships, neither the acceleration $\left\|\dot{v}^b\right\|$ nor the term $\left\|S(\omega^b)v^b\right\|$ is likely to be large. To cause parametric resonance, waves have to be approximately of the same length as the ship, and since k_w is inversely proportional to the wave length, k_w is likely to be quite low. Thus $|\dot{\omega}_e| \approx 0$ and a quasi-steady approach can be

used. We therefore take the solution to (5.55) to be given by (5.56) even when ω_e is non-constant.

We insert the solution (5.56) into the right-hand side of (5.54) and get

$$\begin{aligned}[k_{z\phi}, k_{\phi\theta}]q_{\bar{r}_2} &= k_{z\phi}\bar{a}_z\zeta_0 \cos\left(\int_{t_0}^{t} \omega_e(\tau)\,\mathrm{d}\tau + \bar{\alpha}_z\right) \\ &\quad + k_{\phi\theta}\bar{a}_\theta\zeta_0 \cos\left(\int_{t_0}^{t} \omega_e(\tau)\,\mathrm{d}\tau + \bar{\alpha}_\theta\right) \\ &= k_{\phi t} \cos\left(\int_{t_0}^{t} \omega_e(\tau)\,\mathrm{d}\tau + \alpha_\phi\right)\end{aligned}$$

where

$$\begin{aligned}k_{\phi t}^2 &= \zeta_0^2\left[k_{z\phi}^2\bar{a}_z^2 + k_{\phi\theta}^2\bar{a}_\theta^2 + 2k_{z\phi}k_{\phi\theta}\bar{a}_z\bar{a}_\theta\cos(\alpha_\theta - \alpha_z)\right] \\ \alpha_\phi &= \arctan\left(\frac{k_{z\phi}\bar{a}_z\sin(\alpha_z) + k_{\phi\theta}\bar{a}_\theta\sin(\alpha_\theta)}{k_{z\phi}\bar{a}_z\cos(\alpha_z) + k_{\phi\theta}\bar{a}_\theta\cos(\alpha_\theta)}\right).\end{aligned}$$

Thus, under the stated assumptions, we can formulate the 1-DOF parametric roll model:

Model IV (1-DOF parametric roll model)**.**

$$m_{44}\ddot{\phi} + d_{44}\dot{\phi} + \left[k_{44} + k_{\phi t}\cos\left(\int_{t_0}^{t}\omega_e(\tau)\,\mathrm{d}\tau + \alpha_\phi\right)\right]\phi + k_{\phi^3}\phi^3 = 0\,. \tag{5.59}$$

The natural roll frequency ω_ϕ is given by

$$\omega_\phi \triangleq \sqrt{\frac{k_{44}}{m_{44}}}. \tag{5.60}$$

We note that if we set $\dot{\omega}_e = 0$, then this is identical to the Mathieu equation with a cubic spring term:

Model V (Mathieu model)**.**

$$m_{44}\ddot{\phi} + d_{44}\dot{\phi} + \left[k_{44} + k_{\phi t}\cos(\omega_e t + \alpha_\phi)\right]\phi + k_{\phi^3}\phi^3 = 0\,. \tag{5.61}$$

5.6 Model verification

To determine the validity of the simplified roll model (5.59), we simulate it and compare it to simulations of the full 6-DOF model presented in Section 5.3. Since the Mathieu equation is commonly used to describe ships sailing with constant surge speed experiencing parametric roll resonance, we additionally investigate its ability to describe a dynamics of a ship for a non-constant encounter frequency.

As the main difference between the models is in the spring term, it is useful to compare these. Furthermore, the parameters of these are not known *a priori*, and need to be identified.

We define the spring torque for the 1-DOF roll Model IV and the Mathieu Model V as, respectively,

$$k_{\phi,c}(t;s) = \left[k_{44} + k_{\phi t}\cos\left(\int_{t_0}^{t}\omega_e(\tau)\ \mathrm{d}\tau + \alpha_\phi\right)\right]\phi_c(t) + k_{\phi^3}\phi_c^3(t) \tag{5.62}$$

$$k_{\phi,m}(t;s) = \left[k_{44} + k_{\phi t}\cos\left(\omega_e t + \alpha_\phi\right)\right]\phi_m(t) + k_{\phi^3}\phi_m^3(t) \tag{5.63}$$

where ϕ_c and ϕ_m indicate the values of ϕ computed based on the 1-DOF model and the Mathieu equation, respectively and the parameters are $s = [k_{44}, k_{\phi t}, \alpha_\phi, k_{\phi^3}]$.

To determine the parameters s in (5.62) and (5.63), we use nonlinear least-squares curve fitting:

$$s_c = \arg\min_s \sum_t |k_4(q(t),t) - k_{\phi,c}(t;s)|^2 \tag{5.64}$$

$$s_m = \arg\min_s \sum_t |k_4(q(t),t) - k_{\phi,m}(t;s)|^2 \tag{5.65}$$

where k_4 is the fourth element of k in the full 6-DOF Model III.

The instantaneous encounter frequency in the simplified roll equation is calculated from the simulation of the full 6-DOF model by (5.46). However, even when attempting to keep constant speed, the waves cause the ship's speed to oscillate. This is reflected in the 6-DOF model. Using the instantaneous values of ω_e, the Mathieu equation will not oscillate. Therefore, we use a low-pass filtered encounter frequency when simulating the Mathieu Model V. The 1-DOF Model IV uses the unfiltered values.

5.6.1 Constant forward speed

To compare the models when ω_e is kept approximately constant, we simulate the three models with constant speed (barring small variations due to wave-induced forces in surge).

In the following, the signals of the 6-DOF model is represented without subscript, while the subscripts c and m denote the simplified roll equation and the Mathieu equation, respectively. The simulation parameters and the model parameters are summarized in Table 5.2.

Figure 5.3 shows the simulation results for all three models. From Figure 5.3(a) it is evident that the ship is experiencing parametric roll resonance in this scenario. Figure 5.3(c) compares the spring torque divided by the roll angle of the the full 6-DOF model to the ones of the simplified roll equation and the Mathieu equation computed by (5.62), i.e., k_4/ϕ versus

$$\frac{k_{\phi,c}}{\phi_c} = k_{44} + k_{\phi t}\cos\left(\int_{t_0}^{t}\omega_e(\tau)\ \mathrm{d}\tau + \alpha_\phi\right) + k_{\phi^3}\phi_c^2$$

$$\frac{k_{\phi,m}}{\phi_m} = k_{44} + k_{\phi t}\cos\left(\omega_e t + \alpha_\phi\right) + k_{\phi^3}\phi_m^2.$$

Once steady-state is reached, there is good agreement between the 6-DOF Model III and the two 1-DOF Models IV and V.

Table 5.2: Simulation parameters, constant speed.

Quantity	Symbol	Value	
Mean forward speed	v_1^b	7.90	m/s
Mean encounter frequency	ω_e	0.645	rad/s
Wave amplitude	ζ_0	2.5	m
Wave length	λ	281	m
Wave number	k_w	−0.0224	–
Natural roll frequency	ω_ϕ	0.343	rad/s
Modal wave frequency	ω_0	0.4684	rad/s
Model parameters: Simplified roll equation	k_{44}	1.7646E9	$\mathrm{kg\,m^2/s^2}$
	$k_{\phi t}$	7.3224E8	$\mathrm{kg\,m^2/s^2}$
	α_ϕ	0.2295	rad
	k_{ϕ^3}	2.2741E9	$\mathrm{kg\,m^2/s^2}$
Model parameters: Mathieu equation	k_{44}	1.7685E9	$\mathrm{kg\,m^2/s^2}$
	$k_{\phi t}$	7.3369E8	$\mathrm{kg\,m^2/s^2}$
	α_ϕ	0.2118	rad
	k_{ϕ^3}	2.2691E9	$\mathrm{kg\,m^2/s^2}$

In this scenario, the 1-DOF Model IV and the Mathieu Model V behave almost identically. This is as expected, since with $\dot{\omega}_e = 0$ the two models are identical. The slight variations in ω_e in this scenario are not enough to cause any significant discrepancy.

Up until about 220 s, there is significant discrepancy between the 6-DOF Model III and the two 1-DOF Models IV and V. The two 1-DOF Models IV and V go to maximum roll angle much faster than the 6-DOF Model III. This is because the two 1-DOF Models IV and V are derived under the assumption that heave and pitch are in steady-state. For the first 200 s or so, that is not the case. Once steady-state heave and pitch are achieved, the 6-DOF Model III quickly catches up to the two Models IV and V.

5.6.2 Maximum roll angle

To compare the models under a wide range of scenarios, we simulate the three models for different (almost constant) forward speeds and different wave amplitudes and computed the maximum roll angle as a function of the encounter frequency and the wave amplitude. The simulation scenarios and parameters are identical for all three models. The spring torque constants for the simplified 1-DOF roll Model IV (s_c of (5.64)) and the Mathieu Model V (s_m of (5.65)) are re-estimated for each forward speed and each wave amplitude.

It is well-known that parametric resonance occurs at wave encounter frequencies approximately twice the natural roll frequency [27]. We therefore simulate the models for a nominal surge speed of 0.5 to 12.8 m/s, resulting in a frequency ratio ω_e/ω_ϕ of 1.4 to 2.2. The wave amplitude ζ_0 ranges from 0 to 6 meters.

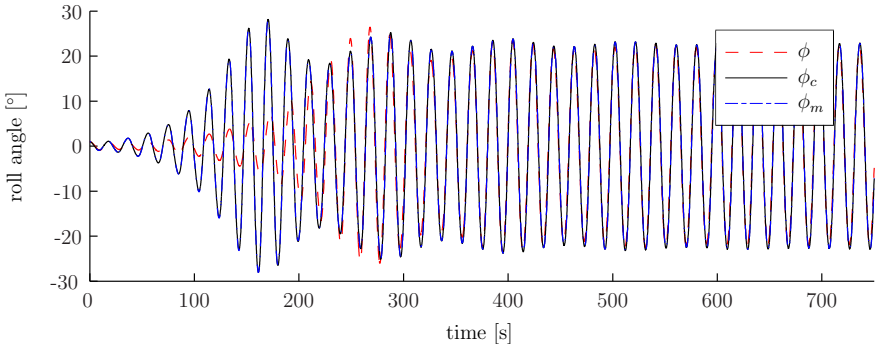

(a) Roll angle.

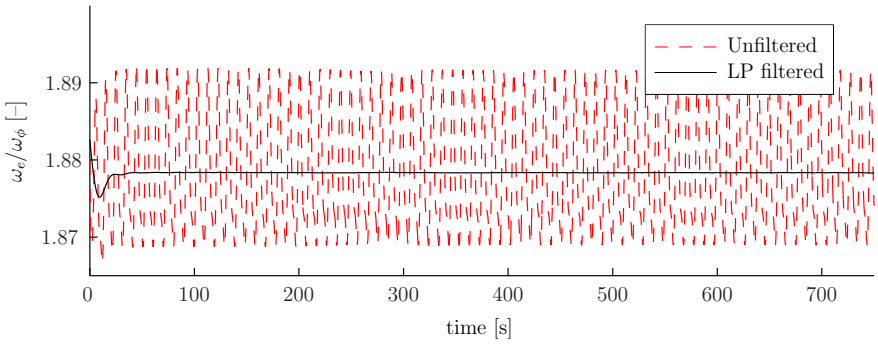

(b) Frequency ratio.

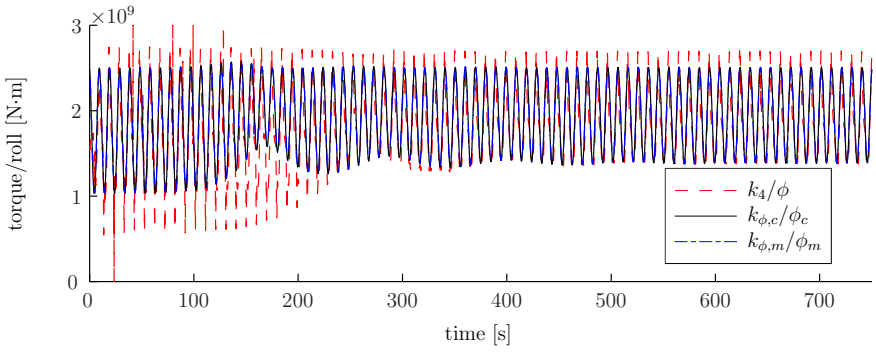

(c) Spring torque divided by roll angle.

Figure 5.3: Model comparison. ϕ, ϕ_c and ϕ_m are, respectively, roll angles from the 6-DOF Model III, 1-DOF Model IV and the Mathieu Model V.

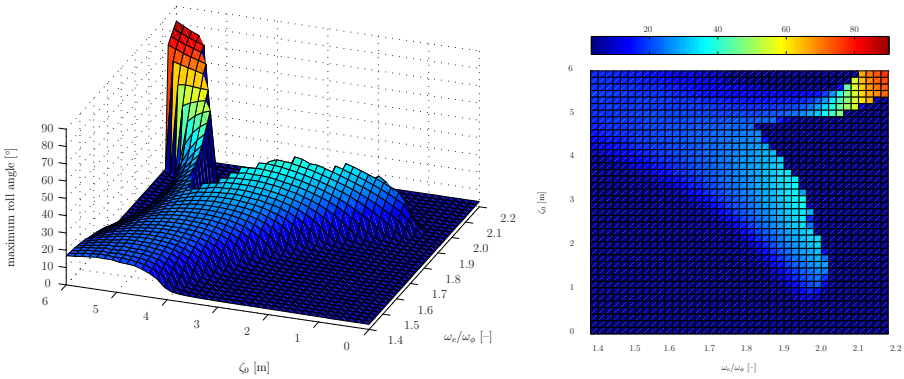

(a) Six-DOF Model III

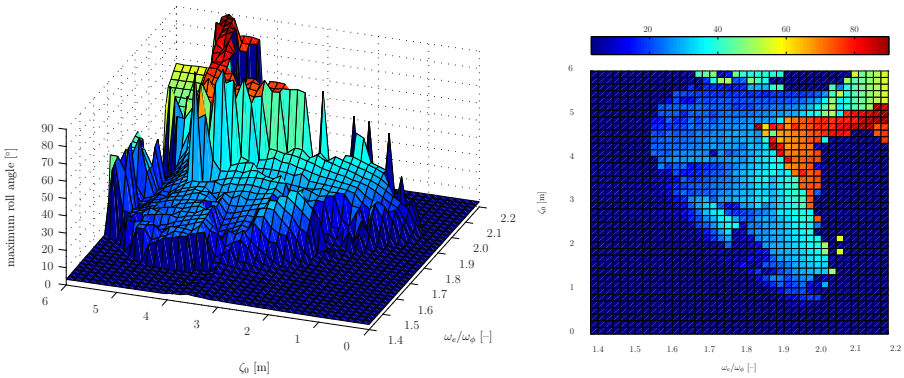

(b) One-DOF roll Model IV

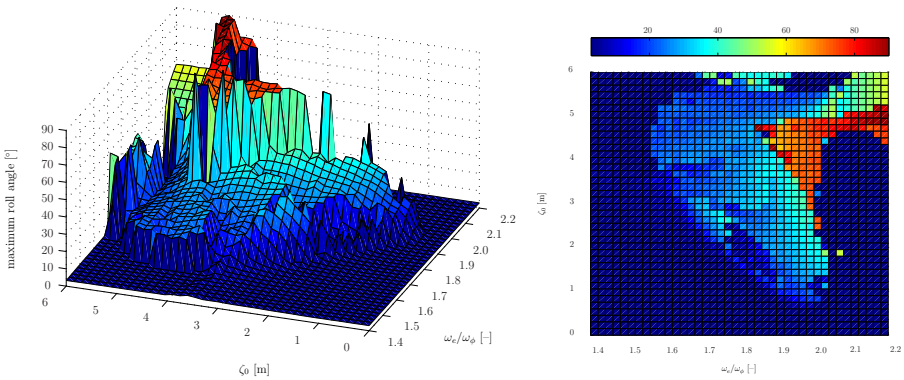

(c) Mathieu Model V

Figure 5.4: Maximum roll angle, model comparison.

Figure 5.4 depicts the maximum roll angle for the models of different complexity as a result of the simulations. The roll amplitude is limited to 90° in the plots for the simplified roll equation (Figure 5.4(b)) and the Mathieu equation (Figure 5.4(c)) for the sake of presentability. We note that qualitatively the simplified roll model (Figure 5.4(b)) is quite close to the 6-DOF model (Figure 5.4(a)), at least for low wave amplitudes.

The Mathieu equation (Figure 5.4(c)) simulated with the filtered wave encounter frequency also behaves reasonably well and is almost indistinguishable from the 1-DOF model. This is reasonable, as there are only very small variations in the value of ω_e.

5.6.3 Time-varying forward speed

Since the difference between the simplified roll model (5.59) and the Mathieu equation (5.61) only becomes apparent when the speed is non-constant, we simulate the system with non-constant forward speed. The scenario tested is a simple speed change, so that the desired surge speed $v^b_{1,d}$ is given by

$$v^b_{1,d}(t) = \begin{cases} v^b_{1,0} & \forall \quad t \in [t_0, t_1] \\ v^b_{1,0} + l(t - t_1) & \forall \quad t \in [t_1, t_2] \\ v^b_{1,1} & \forall \quad t \in [t_2, \infty) \end{cases}$$

where l is the desired acceleration and $v^b_{1,1} = v^b_{1,0} + l(t_2 - t_1)$. This gives an encounter frequency

$$\begin{aligned} \omega_e(t) &\approx \begin{cases} \omega_{e,0} & \forall \quad t \in [t_0, t_1] \\ \omega_{e,0} - k_w l(t - t_1) & \forall \quad t \in [t_1, t_2] \\ \omega_{e,1} & \forall \quad t \in [t_2, \infty) \end{cases} \\ &= \begin{cases} \omega_0 - k_w v^b_{1,0} & \forall \quad t \in [t_0, t_1] \\ \omega_0 - k_w \left[v^b_{1,0} + l(t - t_1) \right] & \forall \quad t \in [t_1, t_2] \\ \omega_0 - k_w v^b_{1,1} & \forall \quad t \in [t_2, \infty) \end{cases} . \end{aligned}$$

Due to small oscillations in surge, ω_e does not exactly match the desired value, as seen in Figure 5.5(b). The Mathieu Model V is once again fed the low-pass filtered values of ω_e, while the 1-DOF Model IV uses the unfiltered values.

The parameters used in the simulation are shown in Table 5.3.

Figure 5.5 depicts the results of the simulation. Again, the ship is in parametric roll resonance, as shown in Figure 5.5(a). The non-constant forward speed results in a non-constant encounter frequency and frequency ratio, see Figure 5.5(b). The spring torque divided by the roll angle is compared in Figure 5.5(c) for the three models. The simplified roll equation is able to estimate the roll motion well even for non-constant speed, whereas it is apparent that the Mathieu equation is not. It gradually becomes out of phase with the roll motion of the full 6-DOF model and never gets back in phase even when the steady-state is reached.

We conclude that the simulations indicate that the 1-DOF simplified roll Model IV is adequate to describe the ship's dynamics in parametric roll resonance when the wave encounter frequency is non-constant. The Mathieu Model V, on the other

hand, is not able to capture the dynamics to a sufficient extent unless the encounter frequency is very close to constant and only if the low-pass filtered value of ω_e is used.

Table 5.3: Simulation parameters, time-varying speed.

Quantity	Symbol	Value	
Initial mean forward speed	$v^b_{1,0}$	7.90	m/s
Desired acceleration	l	0.005	m/s^2
Final mean forward speed	$v^b_{1,1}$	9.43	m/s
Initial mean encounter frequency	$\omega_{e,0}$	0.645	rad/s
Final mean encounter frequency	$\omega_{e,1}$	0.680	rad/s
Simulation start time	t_0	0	s
Acceleration start time	t_1	300	s
Acceleration stop time	t_2	607	s
Wave amplitude	ζ_0	2.5	m
Wave length	λ	281	m
Wave number	k_w	−0.0224	–
Natural roll frequency	ω_ϕ	0.343	rad/s
Modal wave frequency	ω_0	0.4684	rad/s
	k_{44}	1.7646E9	$kg\,m^2/s^2$
Model parameters:	$k_{\phi t}$	7.3224E8	$kg\,m^2/s^2$
Simplified roll equation	α_ϕ	0.2295	rad
	k_{ϕ^3}	2.2741E9	$kg\,m^2/s^2$
	k_{44}	1.7676E9	$kg\,m^2/s^2$
Model parameters:	$k_{\phi t}$	7.3333E8	$kg\,m^2/s^2$
Mathieu equation	α_ϕ	0.2122	rad
	k_{ϕ^3}	2.2702E9	$kg\,m^2/s^2$

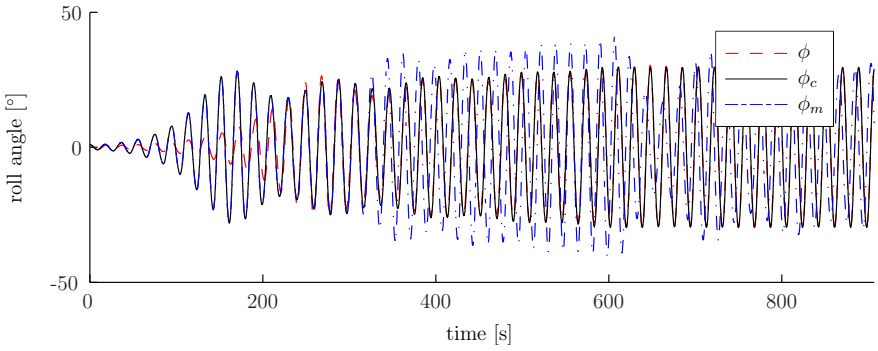

(a) Roll angle.

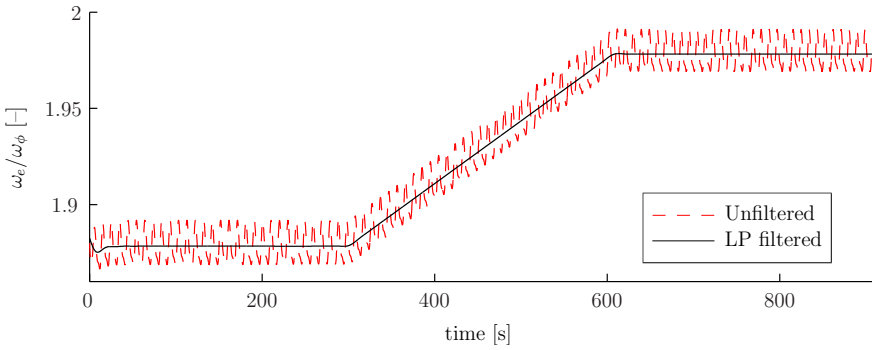

(b) Frequency ratio.

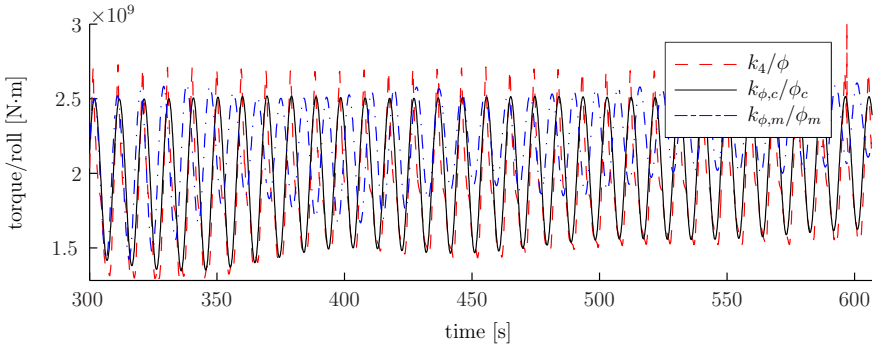

(c) Spring torque divided by roll angle.

Figure 5.5: Model comparison. ϕ, ϕ_c and ϕ_m are, respectively, roll angles from the 6-DOF Model III, 1-DOF Model IV and the Mathieu Model V.

Chapter 6

Reduced-order model of a ship in waves

The 6-DOF Model III and its computer implementation are quite powerful, and capable of describing a lot of complex ship behavior. However, it does have the disadvantage that the generalized pressure-induced force k_p is not analytically known; Matlab can give its value for any state at any time, but it cannot give the algebraic expression.

If we assume that the ship is not maneuvering or changing speed, the 6-DOF Model III can be dramatically simplified. This gives a third-order model, consisting of the heave, roll and pitch motions. To get an analytical model, k_p is approximated by a third-order Tayler expansion.

The reduced-order model has been experimentally verified, as detailed in this chapter.

The material in this chapter is largely based on Holden et al. [40], Rodriguez et al. [77].

6.1 Reduced-order equations of motion

In order to simplify the 6-DOF Model III, we need to rewrite the dynamics slightly.

Rather than use η to describe the orientation of the ship, we'll use the roll–pitch–yaw Euler angles described in Section 3.2.2. This is needed in order to reduce the order of the model.

We define

$$q_e \triangleq [x^{n\,\mathrm{T}}, \Theta^{\mathrm{T}}]^{\mathrm{T}} \in \mathbb{R}^6 \tag{6.1}$$

and rewrite (5.30) as

$$\dot{q}_e = F_e(\Theta)\nu \tag{6.2}$$

where

$$F_e(\Theta) \triangleq \begin{bmatrix} R(\Theta) & 0_{3\times 3} \\ 0_{3\times 3} & G_\Theta(\Theta) \end{bmatrix} \tag{6.3}$$

and $R(\Theta)$ and $G_\Theta(\Theta)$ are as in Properties 3.21 and 3.22, respectively. For the rest of this chapter, when writing R, it is to be understood that this is $R(\Theta)$.

Setting

$$\begin{aligned} x &\equiv x(t_0) \\ y &\equiv y(t_0) \\ \psi &\equiv \psi(t_0) \\ v_1^b &\equiv 0 \\ v_2^b &\equiv 0 \\ \omega_3^b &\equiv 0, \end{aligned}$$

we use $q_{r_3} = [z^n, \phi, \theta]^{\mathrm{T}}$ and $\nu_{r_3} = [v_3^b, \omega_1^b, \omega_2^b]^{\mathrm{T}}$ as in (5.50) and (5.51), with $\dot{q}_{r_3} \approx \nu_{r_3}$ as in (5.52). We can therefore use $\dot{q}_{r_3}$ as generalized velocities.

The forces other than k for the reduced-order system can easily be found by setting the other degrees of freedom to zero. Finding the spring forces k will, however, be done by a third-order Taylor series expansion of the terms and setting all other degrees of freedom to zero.

We will assume that the ship is sailing in head (or stern) seas, with the waves being planar and sinusoidal.

Setting surge, sway and yaw to zero, we can rewrite (5.31) and define a reduced-order model.

Model VI (3-DOF parametric roll model)**.**

$$M_{r_3}\ddot{q}_{r_3} + D_{r_3}(\dot{q}_{r_3})\dot{q}_{r_3} + k_{r_3}(q_{r_3}, t) = \tau_{e,r_3}(t) \tag{6.4}$$

where τ_{e,r_3} are directly wave-induced generalized forces and the restoring force vector k_{r_3} is the third, fourth and fifth elements of k of the 6-DOF Model III, with x, y and ψ set to zero. The reduced-order Coriolis/centripetal term is approximately zero. M_{r_3} and D_{r_3} are the relevant sub-matrices of M and D of the 6-DOF Model III.

Due to the port–starboard symmetry of the ship, we know that certain elements of the inertia and damping matrices are zero Fossen [24]. We also know that heave and pitch are likely to be fairly small, so we take the damping to be linear in these two degrees of freedom. However, in parametric resonance, roll might be large, so we use both linear and quadratic damping in roll. Therefore

$$M_{r_3} = \begin{bmatrix} m + m_{A,33} & 0 & m_{A,35} \\ 0 & J_{11} + m_{A,44} & 0 \\ m_{A,53} & 0 & J_{22} + m_{A,55} \end{bmatrix}$$

$$D_{r_3}(\dot{q}_{r_3}) = \begin{bmatrix} d_{33} & 0 & d_{35} \\ 0 & d_{44} + d_{44,n}|\dot{\phi}| & 0 \\ d_{53} & 0 & d_{55} \end{bmatrix}$$

where $m_{A,ij}$ is the i,jth element of the added mass matrix M_A, J_{ij} the i,jth element of J and d_{ij} is the i,jth element of $D(0)$ of the 6-DOF Model III, with the added assumption that $r_g^b = [0, 0, z_g^b]^{\mathrm{T}}$.

6.2 Generalized restoring forces

As mentioned, we desire an analytical expression for the restoring term k_{r_3}. This generalized force comes (see Chapter 5) from gravity and buoyancy. The gravity force on the ship is

$$f_g^n = mg \begin{bmatrix} 0 \\ 0 \\ 1 \end{bmatrix} \in \mathbb{R}^3 \tag{6.5}$$

where m is the mass of the ship and g is the acceleration of gravity. The buoyancy force on the ship is

$$f_g^n(q,\zeta) = -g\rho V_\nabla(q,\zeta) \begin{bmatrix} 0 \\ 0 \\ 1 \end{bmatrix} \in \mathbb{R}^3 \tag{6.6}$$

where ρ is the density of the ocean and $V_\nabla(q,\zeta)$ is the instantaneous displacement of the vessel [24].

If $r_b^b(q,\zeta) = [x_b^b(q,\zeta), y_b^b(q,\zeta), z_b^b(q,\zeta)]^{\mathrm{T}}$ is the instantaneous center of buoyancy, then the generalized restoring forces on the ship, in the body frame, is given by [24]

$$k(q,t) = \bar{k}(q,\zeta) = \begin{bmatrix} -R^{\mathrm{T}}\left(f_g^n + f_b^n\right) \\ \left(R^{\mathrm{T}}(\Theta) f_g^n\right) \times r_g^b + \left(R^{\mathrm{T}}(\Theta) f_b^n\right) \times r_b^b \end{bmatrix} \tag{6.7}$$

where it has been used that ζ is a function of q and t.

In a slight abuse of notation, we take $V_\nabla(q_{r_3},\zeta)$ and

$$r_b^b(q_{r_3},\zeta) = [x_b^b(q_{r_3},\zeta), y_b^b(q_{r_3},\zeta), z_b^b(q_{r_3},\zeta)]^{\mathrm{T}}$$

to mean the instantaneous displacement and center of buoyancy as a function of q_{r_3}, with the other degrees of freedom set to zero.

We then get

$$\bar{k}_{r_3}(q_{r_3},\zeta) = \begin{bmatrix} k_z(q_{r_3},\zeta) \\ k_\phi(q_{r_3},\zeta) \\ k_\theta(q_{r_3},\zeta) \end{bmatrix} \tag{6.8}$$

with

$$\begin{aligned} k_z(q_{r_3},\zeta) &= g[\rho V_\nabla(q_{r_3},\zeta) - m]\cos(\phi)\cos(\theta) \\ k_\phi(q_{r_3},\zeta) &= g\left[mz_g - \rho V_\nabla(q_{r_3},\zeta) z_b(q_{r_3},\zeta)\right]\sin(\phi)\cos(\theta) \\ &\quad + g\rho V_\nabla(q_{r_3},\zeta) y_b(q_{r_3},\zeta)\cos(\phi)\cos(\theta) \\ k_\theta(q_{r_3},\zeta) &= g\left[mz_g - \rho V_\nabla(q_{r_3},\zeta) z_b(q_{r_3},\zeta)\right]\sin(\theta) \\ &\quad - g\rho V_\nabla(q_{r_3},\zeta) x_b(q_{r_3},\zeta)\cos(\phi)\cos(\theta). \end{aligned}$$

Unfortunately, it is effectively impossible to compute $\bar{k}_{r_3}$ directly, because the exact analytical nature of V_∇ and r_b^b is quite complicated. To get analytical values,

the function $\bar{k}_{r_3}$ is Taylor-expanded around zero to the third order, and the coefficients numerically computed from hull data, loading conditions and knowledge of the sea state.

We then approximate $\bar{k}_{r_3}$ as

$$\begin{aligned}\bar{k}_{r_3}(q_{r_3},\zeta) = {} & k_z z + k_\phi \phi + k_\theta \theta + k_\zeta \zeta \\ & + k_{zz} z^2 + k_{z\phi} z\phi + k_{z\theta} z\theta + k_{z\zeta} z\zeta + k_{\phi\phi}\phi^2 \\ & + k_{\phi\theta}\phi\theta + k_{\phi\zeta}\phi\zeta + k_{\theta\theta}\theta^2 + k_{\theta\zeta}\theta\zeta + k_{\zeta\zeta}\zeta^2 \\ & + k_{zzz} z^3 + k_{\phi\phi\phi}\phi^3 + k_{\theta\theta\theta}\theta^3 + k_{zz\phi} z^2\phi + k_{zz\theta} z^2\theta \\ & + k_{z\phi\phi} z\phi^2 + k_{\phi\phi\theta}\phi^2\theta + k_{z\theta\theta} z\theta^2 + k_{\phi\theta\theta}\phi\theta^2 + k_{z\phi\theta} z\phi\theta \\ & + k_{zz\zeta} z^2\zeta + k_{\phi\phi\zeta}\phi^2\zeta + k_{\theta\theta\zeta}\theta^2\zeta + k_{z\phi\zeta} z\phi\zeta + k_{z\theta} z\theta\zeta \\ & + k_{z\zeta\zeta} z\zeta^2 + k_\phi \phi\zeta^2 + k_{\theta\zeta\zeta}\theta\zeta^2 + k_{\phi\theta\zeta}\phi\theta\zeta + k_{\zeta\zeta\zeta}\zeta^3\end{aligned} \tag{6.9}$$

where

$$\begin{aligned} k_\alpha &\triangleq \left.\frac{\partial \bar{k}_{r_3}}{\partial \alpha}\right|_{q_{r_3}=0,\zeta=0} \in \mathbb{R}^3 \\ k_{\alpha\beta} &\triangleq \left.\frac{\partial^2 \bar{k}_{r_3}}{\partial \alpha \partial \beta}\right|_{q_{r_3}=0,\zeta=0} \in \mathbb{R}^3 \\ k_{\alpha,\beta,\gamma} &\triangleq \left.\frac{\partial^3 \bar{k}_{r_3}}{\partial \alpha \partial \beta \partial \gamma}\right|_{q_{r_3}=0,\zeta=0} \in \mathbb{R}^3 \end{aligned}$$

with $\alpha, \beta, \gamma \in \{z, \phi, \theta, \zeta\}$.

It is worth noting that, due to the symmetry of the vessel and the nature of $\bar{k}_{r_3}$, not all the coefficients will be non-zero. Furthermore, the parameters that are related to hull–wave interactions (i.e, have subscript with at least one ζ) are functions of the wave frequency ω_0. The other parameters are constant.

Since three of the terms in (6.9) are purely a function of ζ, it makes sense to move them out of the spring term and incorporate them into the external forces.

6.3 External forces

The interaction between ship motion and wave passage is modeled as a variation of the geometry of the submerged hull defined by the instantaneous wave position. The external forcing vector τ_{e,r_3} includes only contributions independent of ship motions. For simplicity, we will only include first-order effects.

These forces are characterized by two contributions [20]: the first is due to Froude-Krylov forces, which are caused by incident waves considering the hull restrained from moving and under the assumption that the presence of the hull does not influence the wave field. The second contribution gives the diffraction forces, which provide the corrections necessary for the variation of the flow field produced by the hull.

The wave excitation forces are defined by the wave-force response amplitude operator (force RAO) for each degree of freedom. We can define the force RAOs

as complex-valued functions $F_z(\omega_e), F_\phi(\omega_e), F_\theta(\omega_e)$ so that

$$\tau_{e,r_3}(t) = \zeta_0 \begin{bmatrix} |F_z(\omega_e)| \cos(\omega_e t + \alpha_z(\omega_e)) \\ |F_\phi(\omega_e)| \cos(\omega_e t + \alpha_\phi(\omega_e)) \\ |F_\theta(\omega_e)| \cos(\omega_e t + \alpha_\theta(\omega_e)) \end{bmatrix} \tag{6.10}$$

where $\alpha_a(\omega_e) = \alpha_\zeta + \arg F_a(\omega_e), a \in \{z, \phi, \theta\}$ are the external forces for a simple sinusoidal wave ζ [75]. The force RAOs are technically also functions of the heading angle, but we are here assuming that the heading is constant, so this dependency is dropped. Effectively, the force RAO is a linear filter through which the wave function is sent to generate a force.

If the ship is sailing in head or stern seas, as assumed, then $F_\phi(\omega_e) \equiv 0$.

6.4 Generalized restoring forces, revisited

We use the relationships

$$\begin{aligned} \cos(\omega_e t + \alpha_\zeta) &= \cos(\alpha_\zeta)\cos(\omega_e t) - \sin(\alpha_\zeta)\sin(\omega_e t) \\ \cos^2(\omega_e t + \alpha_\zeta) &= \frac{1}{2}\left[1 + \cos(2\omega_e t + 2\alpha_\zeta)\right] \\ &= \frac{1}{2}\left[1 + \cos(2\alpha_\zeta)\cos(2\omega_e t) - \sin(2\alpha_\zeta)\sin(2\omega_e t)\right] \end{aligned}$$

so that

$$\begin{aligned} k_{\alpha\zeta}\alpha\zeta &= \zeta_0\left[k_{\alpha\zeta c}\cos(\omega_e t) + k_{\alpha\zeta s}\sin(\omega_e t)\right]\alpha \\ k_{\alpha\beta\zeta}\alpha\beta\zeta &= \zeta_0\left[k_{\alpha\beta\zeta c}\cos(\omega_e t) + k_{\alpha\beta\zeta s}\sin(\omega_e t)\right]\alpha\beta \\ k_{\alpha\zeta\zeta}\alpha\zeta^2 &= \zeta_0^2\left[k_{\alpha\zeta\zeta 0} + k_{\alpha\zeta\zeta c}\cos(2\omega_e t) + k_{\alpha\zeta\zeta s}\sin(2\omega_e t)\right]\alpha \end{aligned}$$

$\forall\ \alpha, \beta \in \{z, \phi, \theta\}$.

We let $k_\zeta\zeta = k_{\zeta\zeta}\zeta^2 = k_{\zeta\zeta\zeta}\zeta^3 = 0$ as forces induced directly by waves are already included in τ_{e,r_3}.

We recall (5.24):

$$k_p(q,t) \approx \sum_i \begin{bmatrix} \int_{S_{w,i}} \Psi_{b,i} \frac{\partial r_i^b}{\partial u} \times \frac{\partial r_i^b}{\partial v}\, \mathrm{d}u\, \mathrm{d}v \\ \int_{S_{w,i}} \Psi_{b,i} r_i^b \times \left(\frac{\partial r_i^b}{\partial u} \times \frac{\partial r_i^b}{\partial v}\right) \mathrm{d}u\, \mathrm{d}v \end{bmatrix}.$$

By integrating over the mean wetted surface and using the planar sinusoidal wave pressure field (5.34), we can numerically compute estimates of the parameters of (6.9).

Defining

$$k_\alpha \triangleq \begin{bmatrix} Z_\alpha \\ K_\alpha \\ M_\alpha \end{bmatrix}$$

$$k_{\alpha\beta} \triangleq \begin{bmatrix} Z_{\alpha\beta} \\ K_{\alpha\beta} \\ M_{\alpha\beta} \end{bmatrix}$$

$$k_{\alpha\beta\gamma} \triangleq \begin{bmatrix} Z_{\alpha\beta\gamma} \\ K_{\alpha\beta\gamma} \\ M_{\alpha\beta\gamma} \end{bmatrix}$$
$$k_{\alpha\zeta a} \triangleq \begin{bmatrix} Z_{\alpha\zeta a} \\ K_{\alpha\zeta a} \\ M_{\alpha\zeta a} \end{bmatrix}$$
$$k_{\alpha\beta\zeta a} \triangleq \begin{bmatrix} Z_{\alpha\beta\zeta a} \\ K_{\alpha\beta\zeta a} \\ M_{\alpha\beta\zeta a} \end{bmatrix}$$
$$k_{\alpha\zeta\zeta a} \triangleq \begin{bmatrix} Z_{\alpha\zeta\zeta a} \\ K_{\alpha\zeta\zeta a} \\ M_{\alpha\zeta\zeta a} \end{bmatrix}$$

$\forall\ \alpha, \beta \in \{z, \phi, \theta\}, a \in \{0, c, s\}$ and removing the parameters that equate to zero, we can rewrite (6.9) as

$$k_{r_3}(q_{r_3}, t) \approx \begin{bmatrix} Z(q_{r_3}, t) \\ K(q_{r_3}, t) \\ M(q_{r_3}, t) \end{bmatrix} \tag{6.11}$$

$$\begin{aligned}
Z(q_{r_3}, t) = {} & [Z_z + \zeta_0 Z_{z\zeta c} \cos(\omega_e t) + \zeta_0 Z_{z\zeta s} \sin(\omega_e t)]\, z \\
& + [Z_\theta + \zeta_0 Z_{\theta\zeta c} \cos(\omega_e t) + \zeta_0 Z_{\theta\zeta s} \sin(\omega_e t)]\, \theta \\
& + [Z_{\phi\phi} + \zeta_0 Z_{\phi\phi\zeta c} \cos(\omega_e t) + \zeta_0 Z_{\phi\phi\zeta s} \sin(\omega_e t)]\, \phi^2 \\
& + Z_{zz} z^2 + Z_{z\theta} z\theta + Z_{\theta\theta} \theta^2 + Z_{\theta\theta\theta} \theta^3 + Z_{\phi\phi z} \phi^2 z + Z_{\phi\phi\theta} \phi^2 \theta \\
K(q_{r_3}, t) = {} & [K_\phi + \zeta_0 K_{\phi\zeta c} \cos(\omega_e t) + \zeta_0 K_{\phi\zeta s} \sin(\omega_e t)]\, \phi \\
& + K_{z\phi} z\phi + K_{\phi\theta} \phi\theta + K_{\phi\phi\phi} \phi^3 + K_{zz\phi} z^2 \phi + K_{\phi\theta\theta} \phi\theta^2 \\
M(q_{r_3}, t) = {} & [M_z + \zeta_0 M_{z\zeta c} \cos(\omega_e t) + \zeta_0 M_{z\zeta s} \sin(\omega_e t)]\, z \\
& + [M_\theta + \zeta_0 M_{\theta\zeta c} \cos(\omega_e t) + \zeta_0 M_{\theta\zeta s} \sin(\omega_e t)]\, \theta \\
& + [M_{\phi\phi} + \zeta_0 M_{\phi\phi\zeta c} \cos(\omega_e t) + \zeta_0 M_{\phi\phi\zeta s} \sin(\omega_e t)]\, \phi^2 \\
& + M_{zz} z^2 + M_{z\theta} z\theta + M_{\theta\theta} \theta^2 + M_{\theta\theta\theta} \theta^3 + M_{\phi\phi z} \phi^2 z + M_{\phi\phi\theta} \phi^2 \theta.
\end{aligned}$$

We note that the natural roll frequency ω_ϕ is given by

$$\omega_\phi = \sqrt{\frac{K_\phi}{J_{11} + m_{A,44}}}. \tag{6.12}$$

The parameters in (6.11) that come from wave interaction (i.e., those with at least one ζ in the subscript) are functions of the wave frequency ω_0. The others, which can be derived from hydrostatics, are constant.

Parameters were computed for the experimental conditions. The parameters can be found in Appendix C.

It is worth noting that the model presented in this chapter has some strengths and some weaknesses relative to the 6-DOF Model III. The 3-DOF Model VI is analytical and reasonably manageable. It can be used for control design or analysis, and

is suitable for simulation. Unfortunately, it is only valid for a set of precomputed conditions, and conditions are not allowed to change during simulation because this invalidates the parameters and the model derivation.

The 6-DOF Model III of Chapter 5 on the other hand, is capable of handling almost any sea state, and conditions are allowed to change. Unfortunately, an analytical expression and parameters of such are not known. This model is highly suitable for simulation, but not for control design or analysis.

6.5 Experimental verification

Experiments were conducted with a 1:45 scale model of a container ship in the towing tank at SINTEF Marintek's facilities in Trondheim. In all experiments the ship was subjected to regular, sinusoidal waves in head seas condition.[1] For each experiment, different (but constant) wave heights, wave frequencies and encounter frequencies were used. A total of 22 different experiments were conducted. Dr Ingo Drummen performed the actual experiments. Details of the ship and other aspects of the experiments can be found in his PhD thesis (Drummen [17]).

The ship used in the experiments is the same that was used as the basis for the the computer implementation of Model III (Section 5.3). The main characteristics of the vessel (full scale) can be found in Table 5.1. A picture of the model ship can be seen in Figure 6.1.

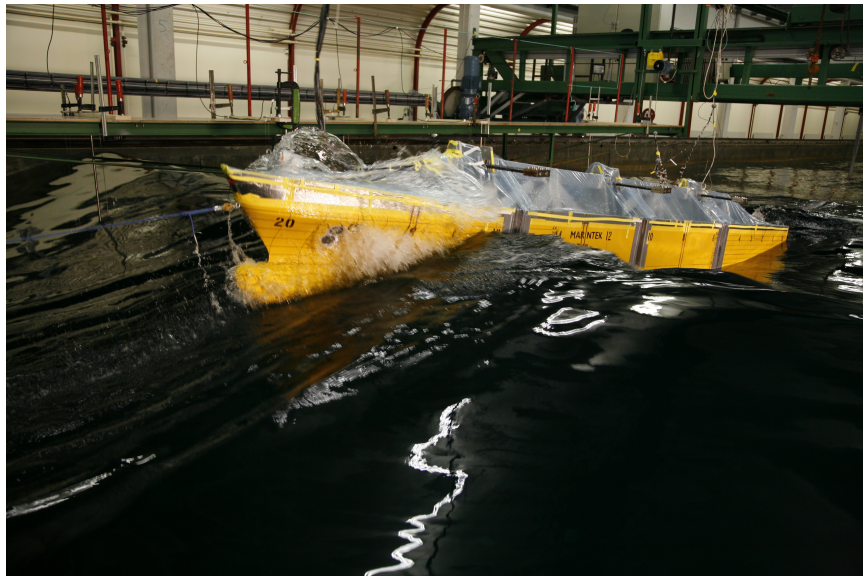

Figure 6.1: The ship used in the experiments. Photo courtesy of Dr Ingo Drummen.

[1] Some experiments were also conducted in irregular seas, but these are not listed. The model derived here is only valid or regular seas.

The experimental conditions (full scale equivalents) are summarized in Table 6.1, sorted by experiment number. The ship's forward speed v_1^b, the wave frequency ω_0, the wave amplitude ζ_0 and the computed encounter frequency ω_e are listed.

Table 6.1: Experimental conditions (full scale equivalents).

Exp.	v_1^b [m/s]	ω_0 [rad/s]	ζ_0 [m]	ω_e [rad/s]
1172	5.4806	0.4640	2.5	0.5844
1173	5.4806	0.4425	2.5	0.5519
1174	5.4806	0.4764	2.5	0.6031
1175	5.4806	0.4530	2.5	0.5677
1176	5.4806	0.4893	2.5	0.6231
1177	5.4806	0.4640	1.5	0.5844
1178	5.4806	0.4699	1.5	0.5933
1179	5.4806	0.4583	1.5	0.5756
1180	5.4806	0.4640	3.5	0.5844
1181	5.4806	0.4425	3.5	0.5519
1182	5.4806	0.4893	3.5	0.6231
1183	5.4806	0.4530	3.5	0.5677
1184	5.7556	0.4640	2.5	0.5904
1185	6.0240	0.4640	2.5	0.5963
1186	6.2990	0.4640	2.5	0.6023
1187	6.5740	0.4640	2.5	0.6084
1188	7.1241	0.4640	2.5	0.6204
1189	7.6675	0.4640	2.5	0.6324
1190	7.3991	0.4640	2.5	0.6265
1191	5.2056	0.4640	2.5	0.5783
1192	4.6555	0.4640	2.5	0.5662
1193	4.9305	0.4640	2.5	0.5723

The 3-DOF Model VI was simulated with the initial conditions of Table 6.2. During simulation, there was no feedback from the experimental data. Simulations started at $t = 0$ s and lasted to $t = 1000$ s.

A comparison of the simulation results with the experimental results can be seen in Table 6.3. The data in this table are sorted by wave amplitude ζ_0, then frequency ratio ω_e/ω_ϕ.

The data in the percentage error column, rounded to integer value, is given by

$$100\frac{\max|\phi_{\text{sim}}| - \max|\phi_{\text{exp}}|}{\max|\phi_{\text{exp}}|},$$

where $\max|\phi_{\text{sim}}|$ is the maximum simulated roll angle and $\max|\phi_{\text{exp}}|$ is the maximum experimentally measured roll angle. Note that most of the experiments were stopped before the final steady-state roll angle could be achieved due to fear of vessel capsizing. It is worth pointing out that the percentage errors in the cases with no parametric resonance are meaningless, as maximum simulated roll angle is merely the starting value, which was chosen arbitrarily.

The "Result" column indicates whether or not the model correctly predicted parametric roll. Entries marked "C" indicate a correct result (the simulations and experiments both showed parametric resonance, or both showed no parametric resonance), "FP" false positives (simulations show parametric resonance, but the

Table 6.2: Simulation initial conditions.

Exp.	$z(0)$ [m]	$\phi(0)$ [°]	$\theta(0)$ [°]	$\dot{z}(0)$ [m/s]	$\dot{\phi}(0)$ [°/s]	$\dot{\theta}(0)$ [°/s]
1172	0.025	0.2000	0	0	0	0
1173	0.050	2.0000	0	0	0	0
1174	0.050	0.0020	0	0	0	0
1175	0.050	1.0000	0	0	0	0
1176	0.050	0.0010	0	0	0	0
1177	0.050	2.4000	0	0	0	0
1178	0.050	0.5000	0	0	0	0
1179	0.050	2.0000	0	0	0	0
1180	0.050	0.0050	0	0	0	0
1181	0.050	2.0000	0	0	0	0
1182	0.050	0.0010	0	0	0	0
1183	0.050	0.0010	0	0	0	0
1184	0.050	0.1000	0	0	0	0
1185	0.050	0.0300	0	0	0	0
1186	0.050	0.0050	0	0	0	0
1187	0.050	0.0300	0	0	0	0
1188	0.050	0.0300	0	0	0	0
1189	0.050	0.1400	0	0	0	0
1190	0.050	0.0100	0	0	0	0
1191	0.050	0.2000	0	0	0	0
1192	0.050	2.0000	0	0	0	0
1193	0.050	0.1000	0	0	0	0

experiments don't) and "FN" (of which there are none) indicates false negatives (simulations show no parametric resonance, but the experiments do).

Figure 6.2 shows the maximum roll angle for a select number of the experiments (those with wave amplitude $\zeta_0 = 2.5$ m). Figures 6.3–6.24 show heave, roll and pitch as functions of time, both experimental and simulated.

6.6 Analysis of the model based on the verification results

In Figure 6.2, we can see the maximum roll angle achieved in the simulations and experiments for certain conditions, plotted against the ratio of encounter frequency to natural roll frequency (ω_e/ω_ϕ). The data in the figure is all for $\zeta_0 = 2.5$ m.

What is interesting is that the graph for the maximum simulated roll angle is quite similar to that of Figure 11.2. That figure is based on the model

$$\phi'' + 2\iota\gamma\phi' + [\kappa + 2\iota\cos(2\tilde{t})]\phi + \alpha\iota\phi^3 = 0$$

where prime indicates derivative with respect to the time $\tilde{t}$ and the parameters are constant. By comparing to the results of Chapter 11, it seems that the cubic term in the equations is causing the maximum roll angle to slant down for lower ω_e/ω_ϕ. To get a curve closer to the experimental one, it might be necessary to use a higher-order Taylor polynomial, or perhaps a trigonometric function for the roll nonlinearity. This was not further investigated during the thesis work due to time constraints.

The third-order Model VI developed for the 281 m long container ship shows high capabilities in reproducing the vertical and transversal dynamics of the vessel

Table 6.3: Simulation results.

Exp.	ζ_0 [m]	ω_0 [rad/s]	ω_e/ω_ϕ	$\max \phi_{\text{sim}}$ [°]	$\max \phi_{\text{exp}}$ [°]	Err [%]	Result
1179	1.5	0.4583	1.9337	2.0000	0.2791	617	C
1177	1.5	0.4640	1.9633	8.1666	16.9032	-52	C
1178	1.5	0.4699	1.9932	12.0995	22.2113	-46	C
1173	2.5	0.4425	1.8541	2.0000	0.6753	196	C
1192	2.5	0.4640	1.9021	9.7799	0.8459	1056	FP
1175	2.5	0.4530	1.9072	6.3508	0.6612	861	FP
1193	2.5	0.4640	1.9226	11.8080	1.8206	549	FP
1191	2.5	0.4640	1.9428	13.5465	21.5589	-37	C
1172	2.5	0.4640	1.9633	15.1622	23.6341	-36	C
1184	2.5	0.4640	1.9834	16.5792	22.5894	-27	C
1185	2.5	0.4640	2.0032	17.8812	20.6209	-13	C
1186	2.5	0.4640	2.0234	19.2712	21.3706	-10	C
1174	2.5	0.4764	2.0261	21.4924	26.2491	-18	C
1187	2.5	0.4640	2.0439	20.4611	20.2754	1	C
1188	2.5	0.4640	2.0842	22.4097	22.5976	-1	C
1176	2.5	0.4893	2.0933	26.7459	1.1659	2194	FP
1190	2.5	0.4640	2.1047	23.4472	1.3757	1604	FP
1189	2.5	0.4640	2.1245	24.2884	1.3689	1674	FP
1181	3.5	0.4425	1.8541	2.0000	1.9260	4	C
1183	3.5	0.4530	1.9072	11.0942	8.8094	26	C
1180	3.5	0.4640	1.9633	18.8898	23.8131	-21	C
1182	3.5	0.4893	2.0933	30.2110	24.6150	23	C

under parametric resonance conditions, as shown by the comparison of the experimental results (Figures 6.2–6.24).

Considering the 13 experiments where parametric resonance did occur, the implemented Model VI performs well: starting from similar initial conditions and being subjected to the same excitation forces used during the experiments, Model VI develops parametric resonance within the same time frame as the 1:45 scale model ship in most of the cases.

The most obvious differences between the simulation and the experimental results consists of the amplitude of the oscillations. In all the experiments where parametric resonance occurred, the peak value of the roll oscillations is higher than the saturation level at which Model VI settles. Although Model VI has a general tendency to underestimate the peak value of the roll motion, the gap is relatively small in most cases.

Considering the nine experiments where parametric roll did not occur, Model VI produced six false positives. In order to understand this disagreement between model behavior and experimental results, the tuning factor ω_e/ω_ϕ must be taken into consideration. All the five false-positive cases occur with a tuning factor close to the limits of the first instability region of the Mathieu equation ($\omega_e \approx 2\omega_\phi$), as shown in Figure 6.2. Looking at the peak value of the roll oscillations (Figure 6.2 and Table 6.3), it can be seen that the largest differences are in the region of high tunings ($\omega_e/\omega_\phi \geq 2.1$) for which Model VI predicts large roll motion whereas the experiments showed no amplification. It seems obvious that when the experimental conditions are close to the limits of stability Model VI does not match exactly the

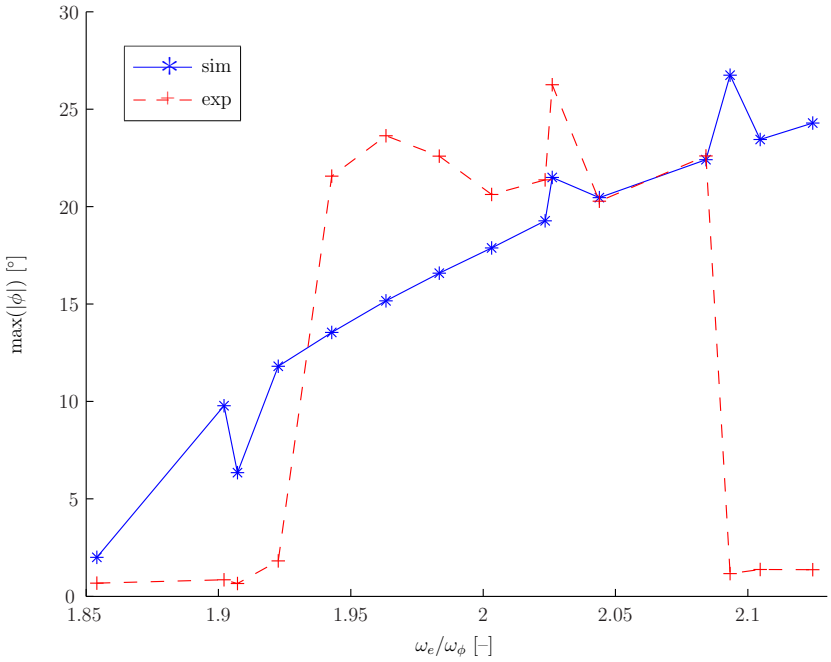

Figure 6.2: Maximum roll angle for $\zeta_0 = 2.5$ m.

frequency at which the abrupt variation in roll motion take place.

The errors indicated in experiments 1173, 1179 and 1181 have no real physical meaning, since the initial condition of 2° was chosen arbitrarily and high in order to indicate a decaying motion.

For all 22 experiments, heave and pitch dynamics have shown relatively good agreement with the experiments. In all the test runs the two modes oscillates at the excitation frequency, matching the experimental records. The amplitude of the oscillations is close to that of the experimental values.

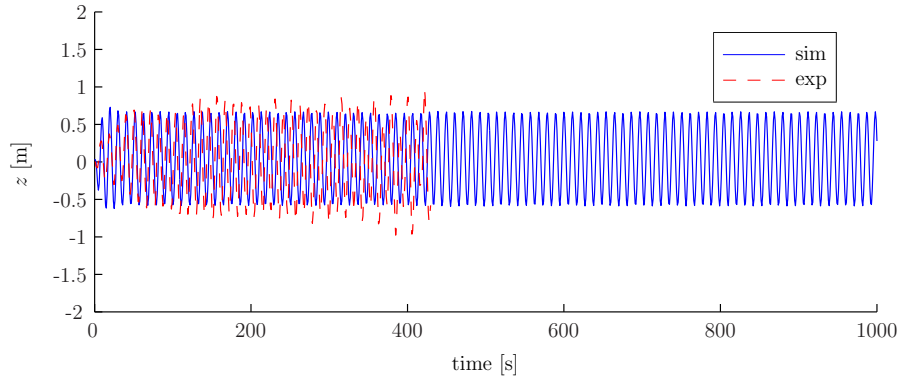

(a) Heave.

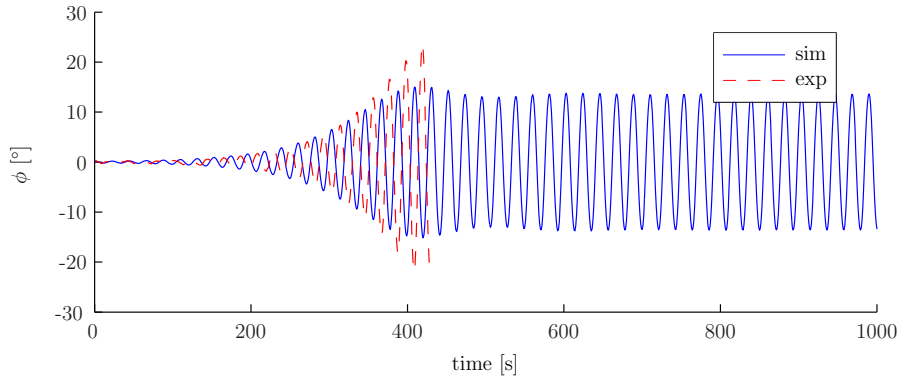

(b) Roll.

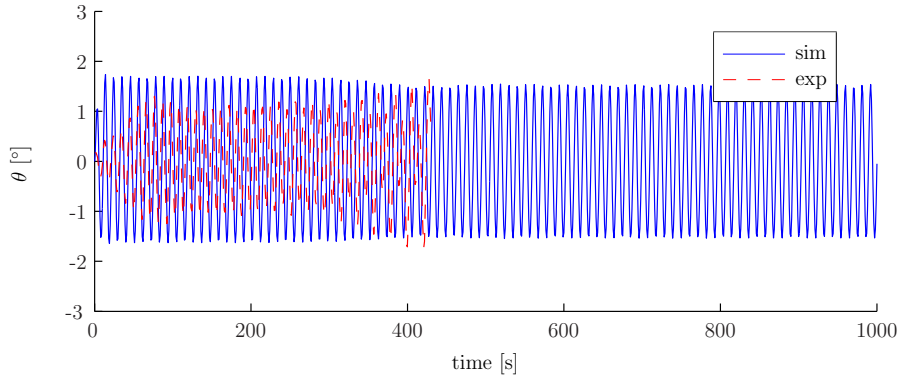

(c) Pitch.

Figure 6.3: Exp. 1172, simulation vs experiments (full scale).

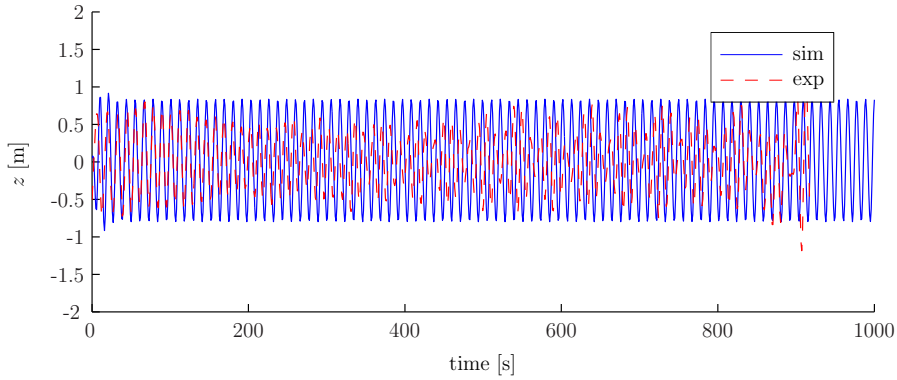

(a) Heave.

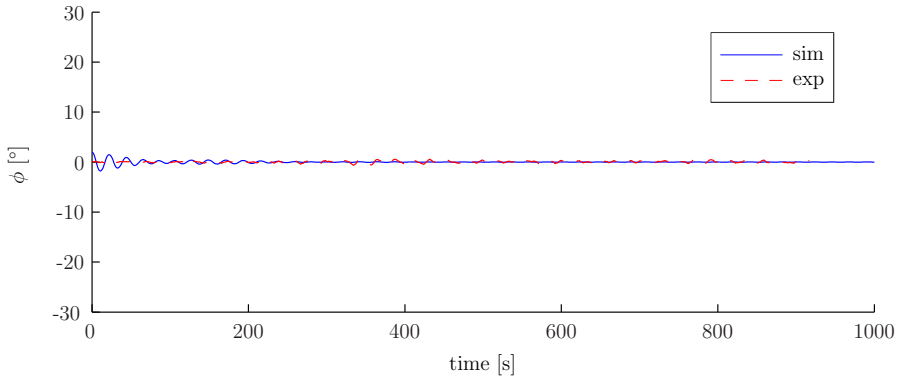

(b) Roll.

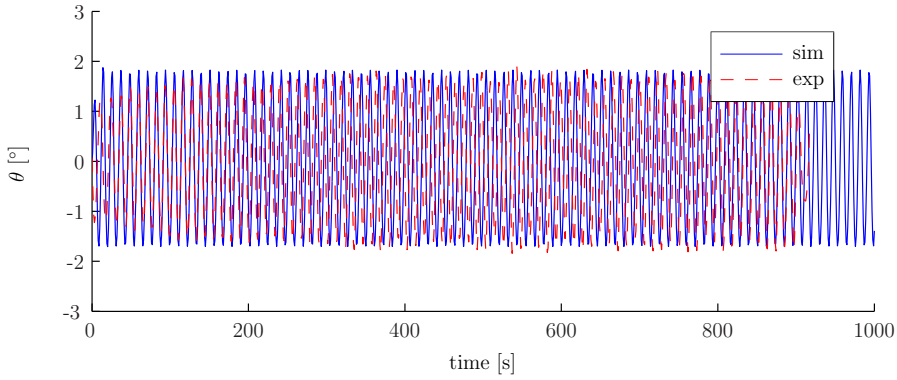

(c) Pitch.

Figure 6.4: Exp. 1173, simulation vs experiments (full scale).

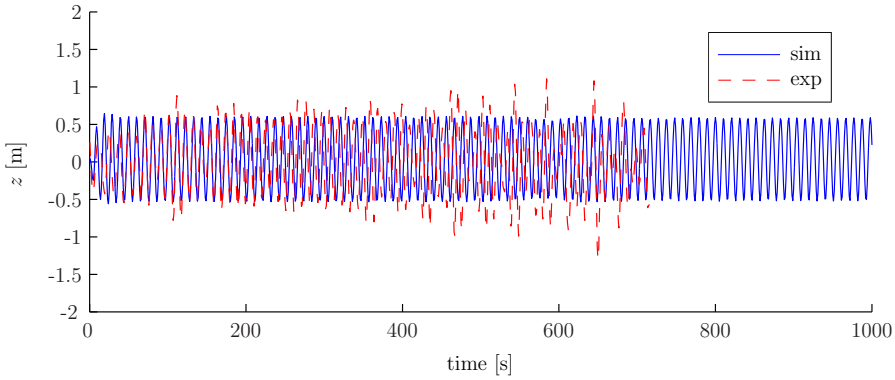

(a) Heave.

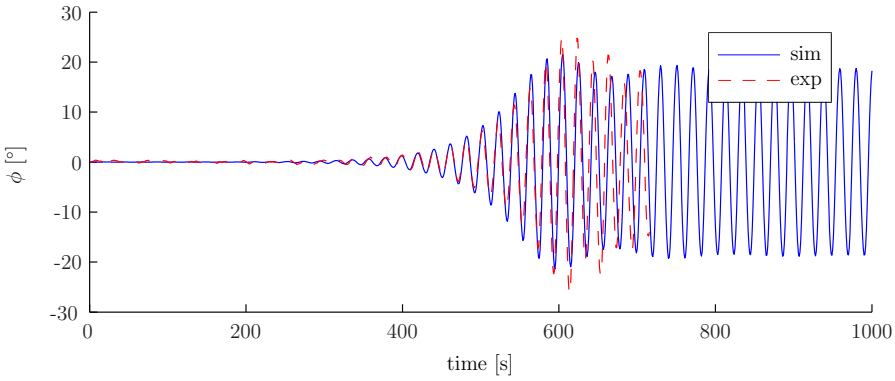

(b) Roll.

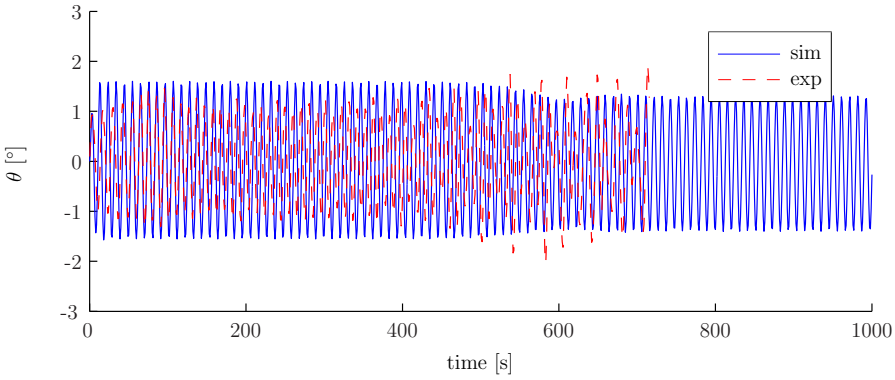

(c) Pitch.

Figure 6.5: Exp. 1174, simulation vs experiments (full scale).

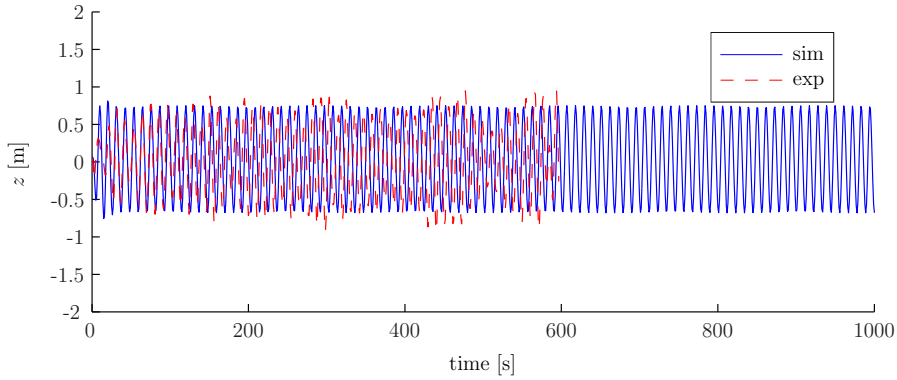

(a) Heave.

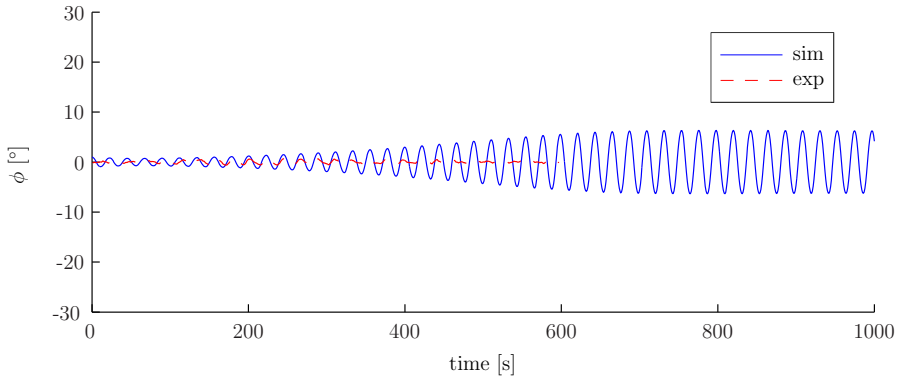

(b) Roll.

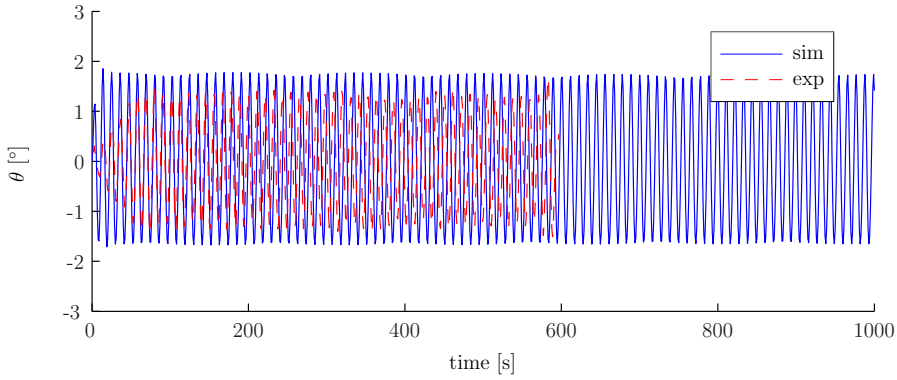

(c) Pitch.

Figure 6.6: Exp. 1175, simulation vs experiments (full scale).

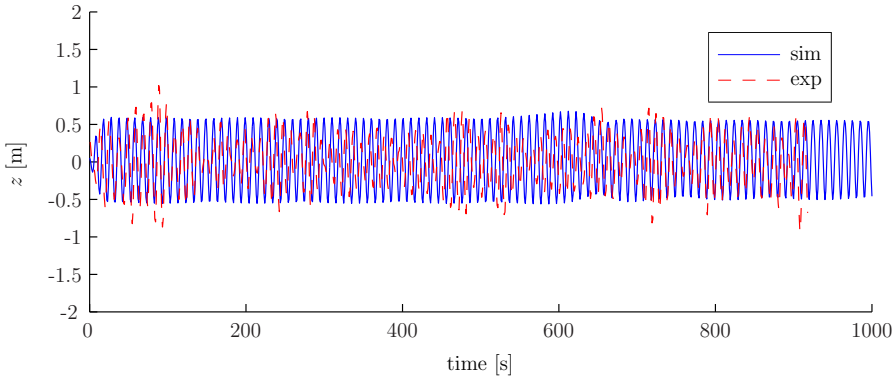

(a) Heave.

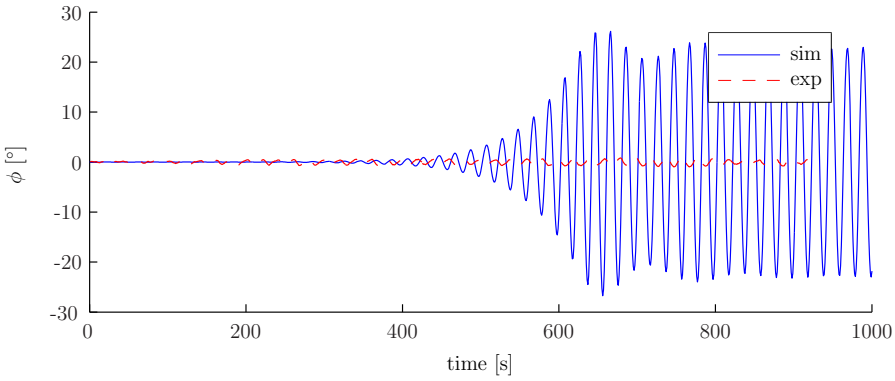

(b) Roll.

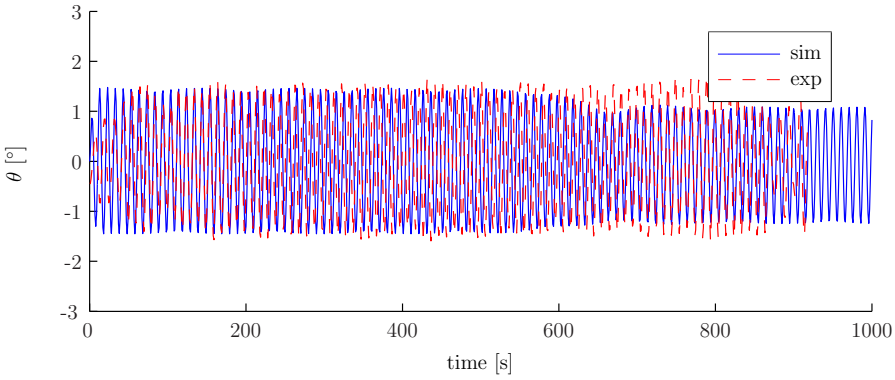

(c) Pitch.

Figure 6.7: Exp. 1176, simulation vs experiments (full scale).

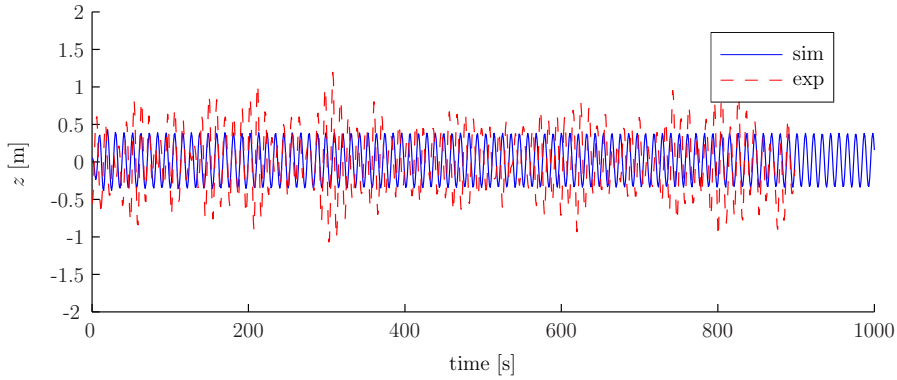

(a) Heave.

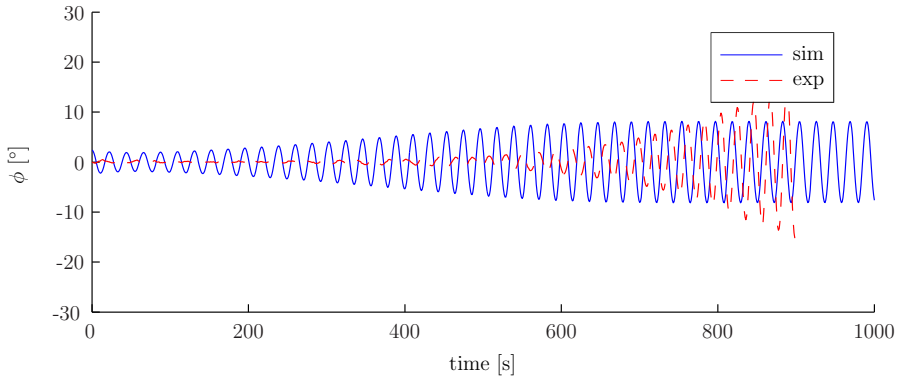

(b) Roll.

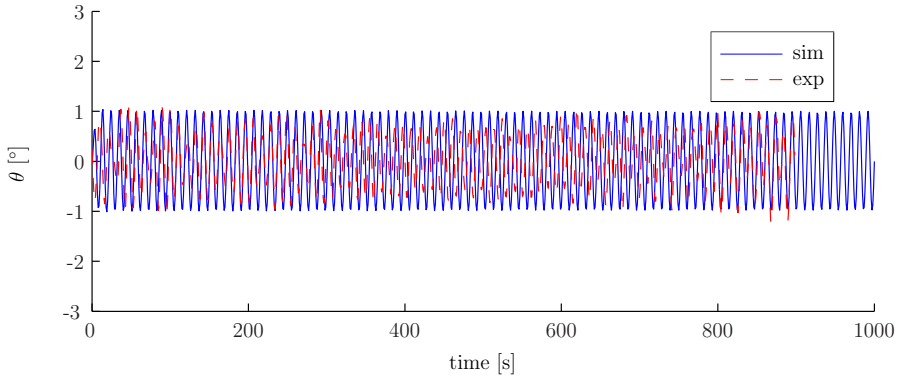

(c) Pitch.

Figure 6.8: Exp. 1177, simulation vs experiments (full scale).

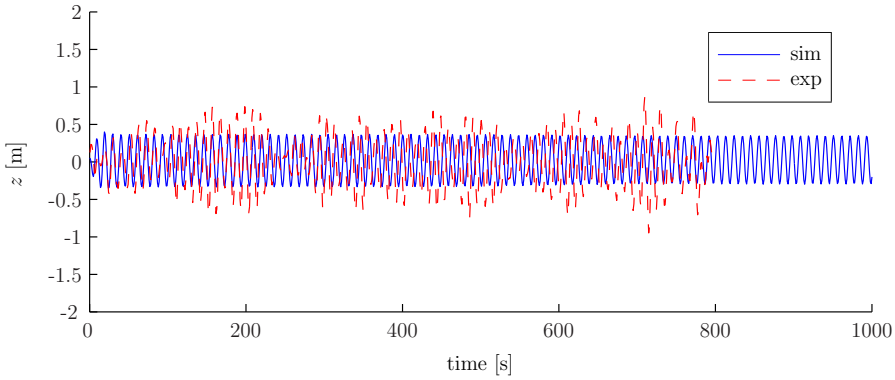

(a) Heave.

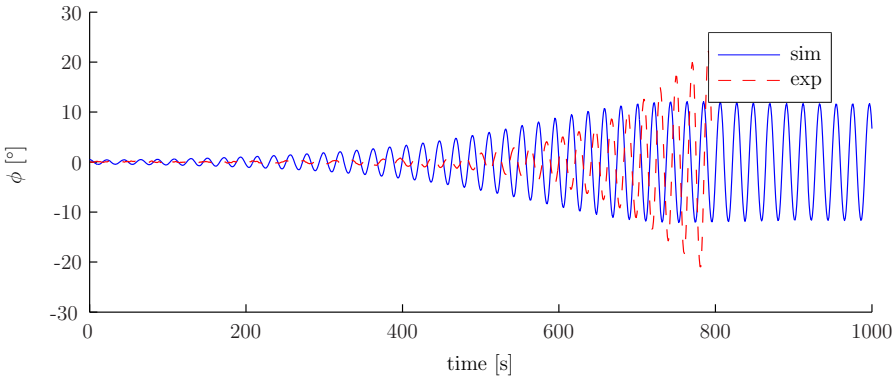

(b) Roll.

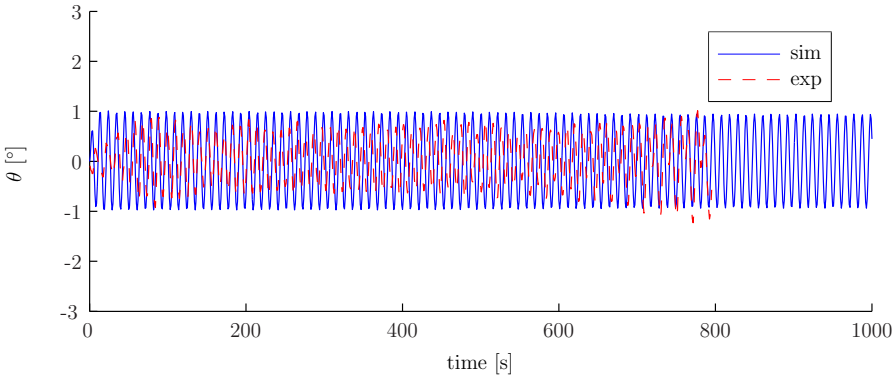

(c) Pitch.

Figure 6.9: Exp. 1178, simulation vs experiments (full scale).

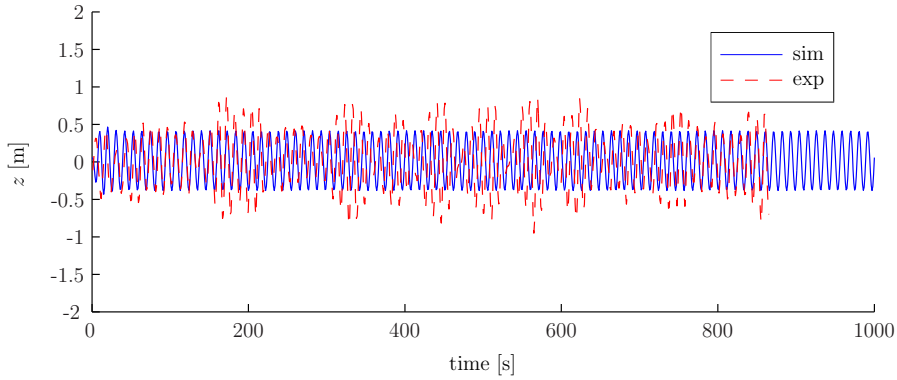

(a) Heave.

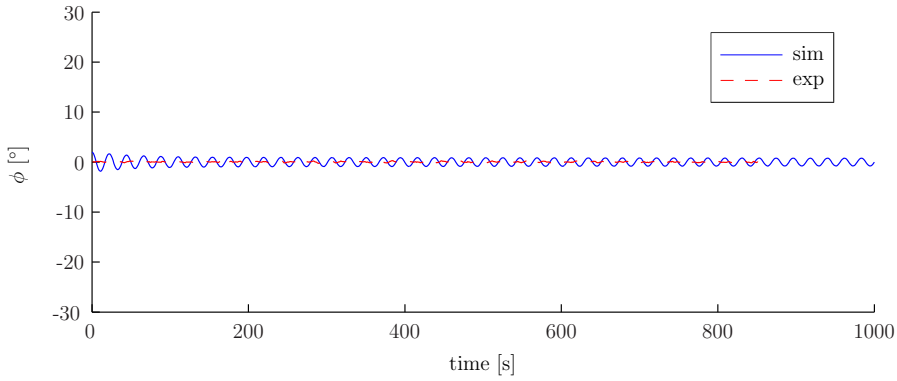

(b) Roll.

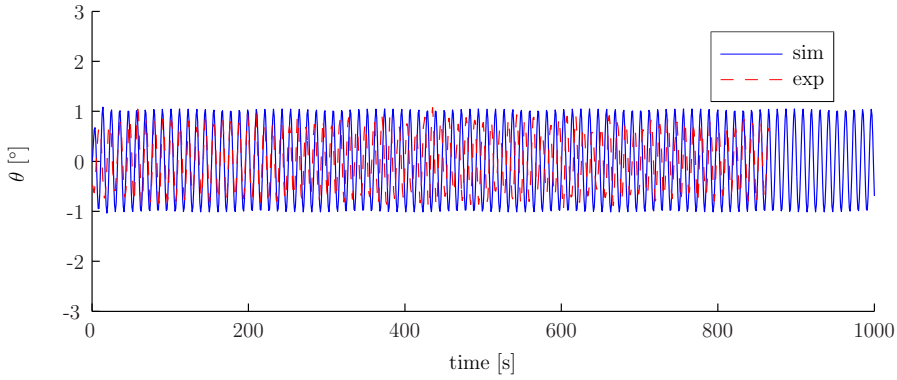

(c) Pitch.

Figure 6.10: Exp. 1179, simulation vs experiments (full scale).

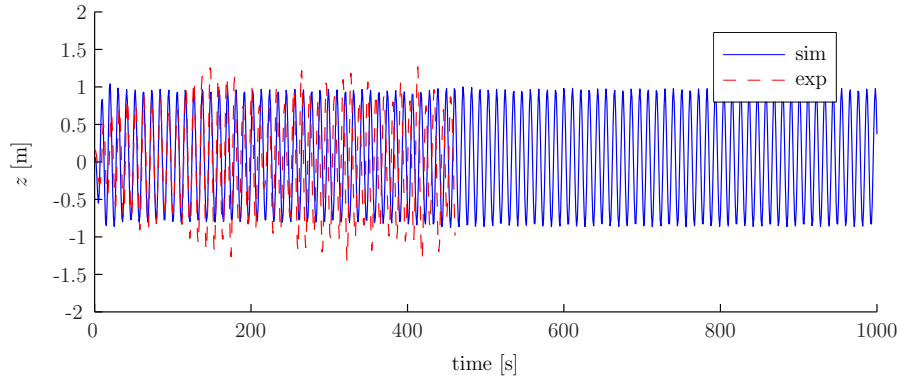

(a) Heave.

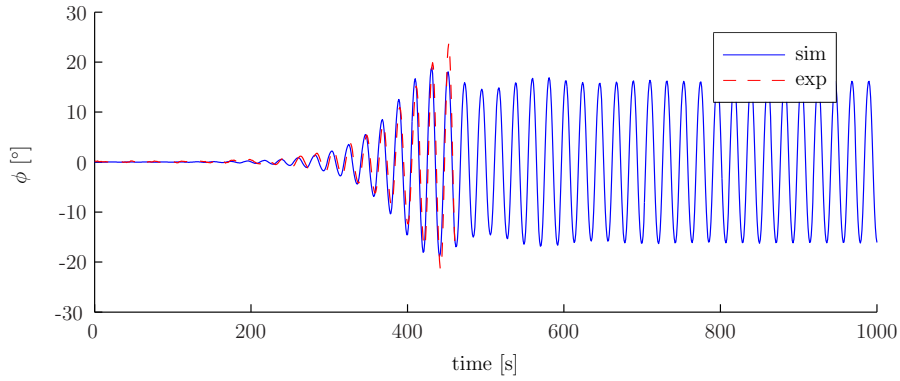

(b) Roll.

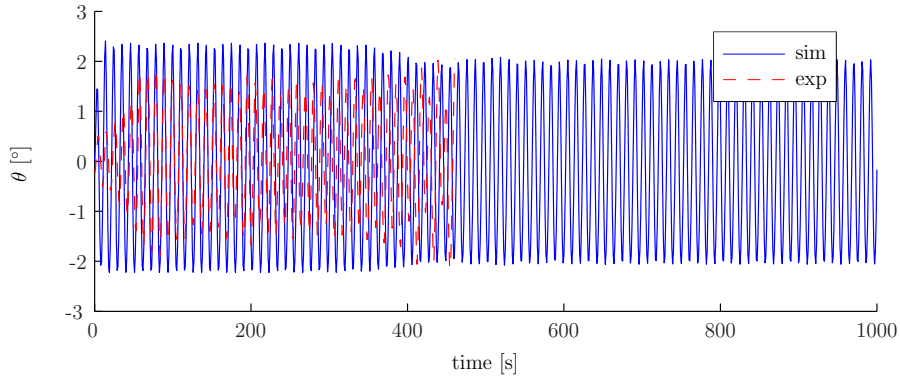

(c) Pitch.

Figure 6.11: Exp. 1180, simulation vs experiments (full scale).

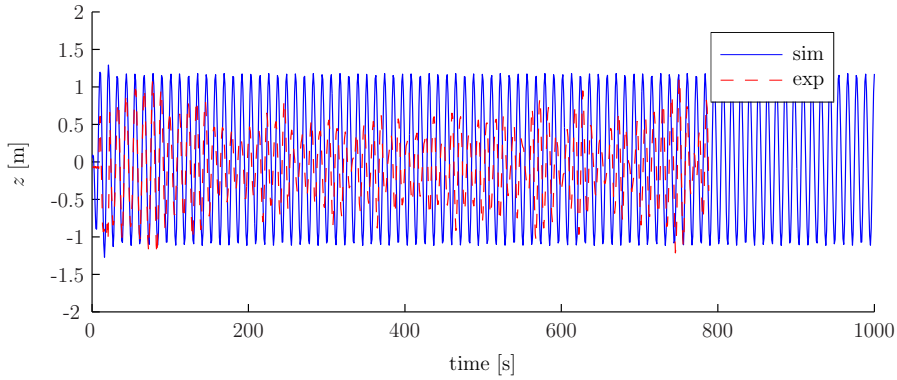

(a) Heave.

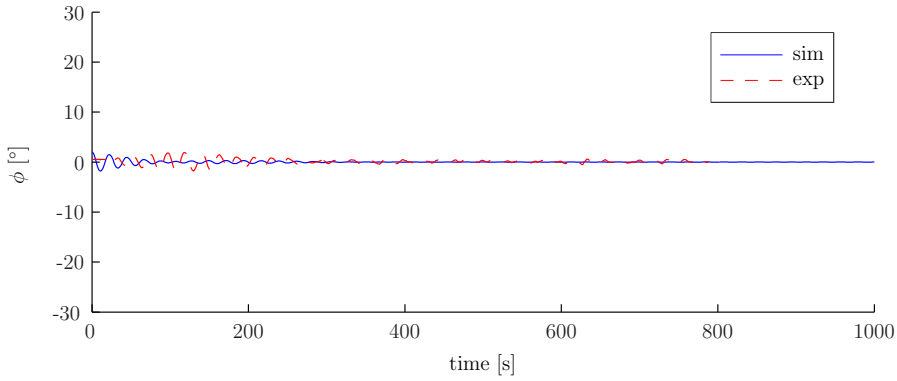

(b) Roll.

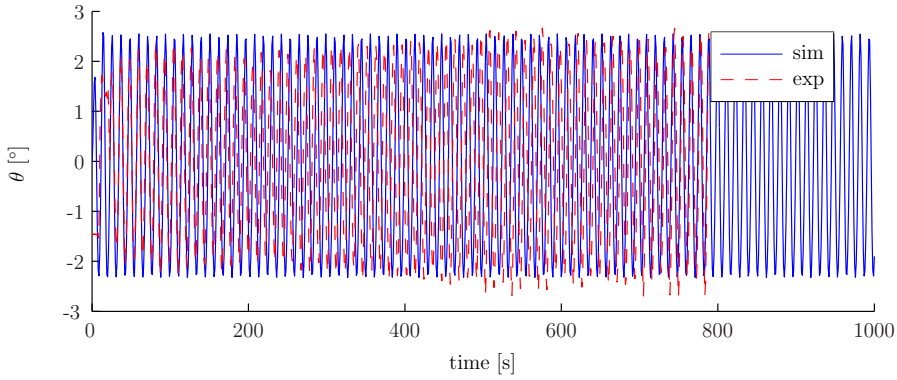

(c) Pitch.

Figure 6.12: Exp. 1181, simulation vs experiments (full scale).

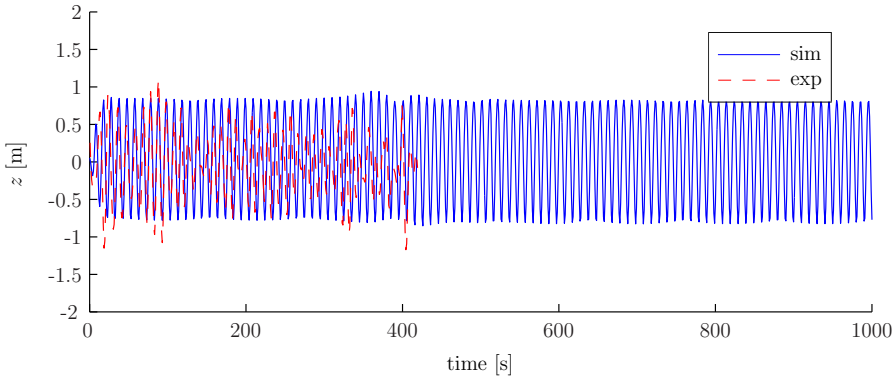

(a) Heave.

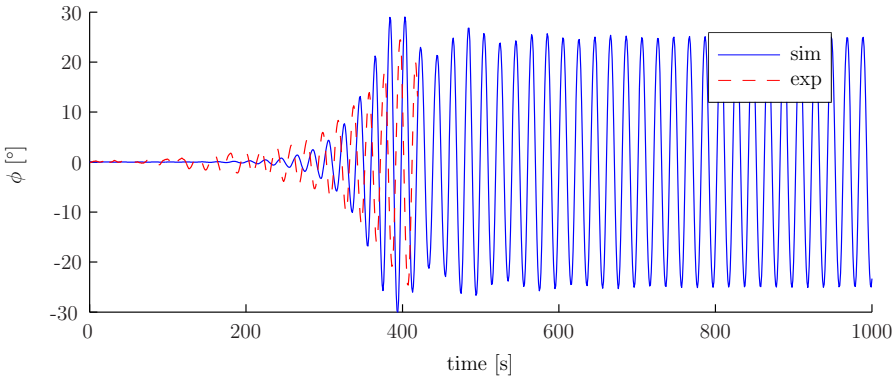

(b) Roll.

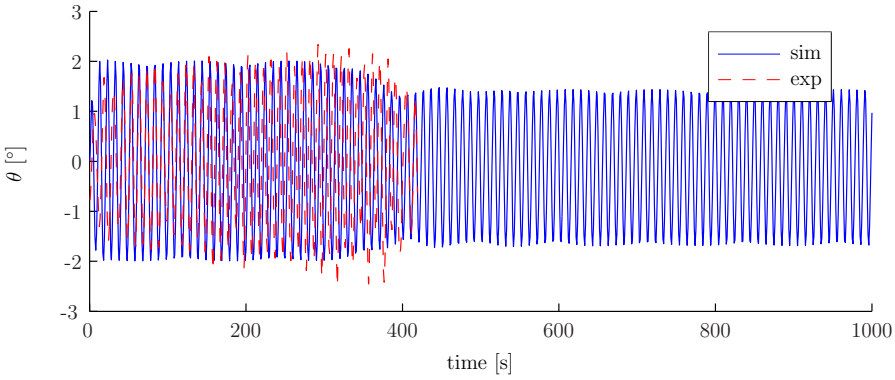

(c) Pitch.

Figure 6.13: Exp. 1182, simulation vs experiments (full scale).

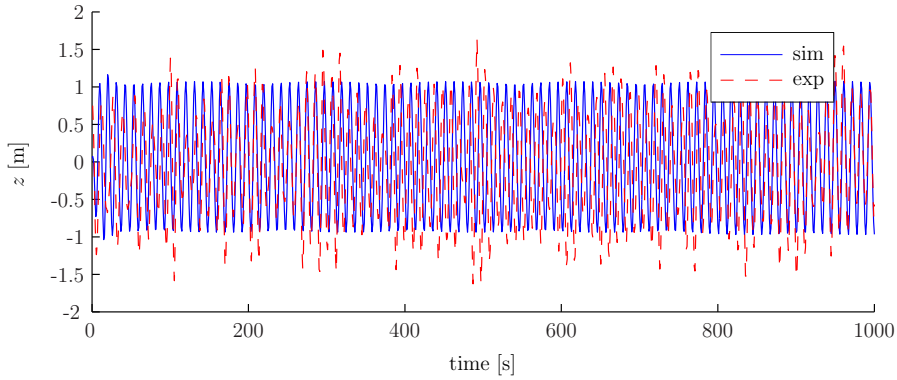

(a) Heave.

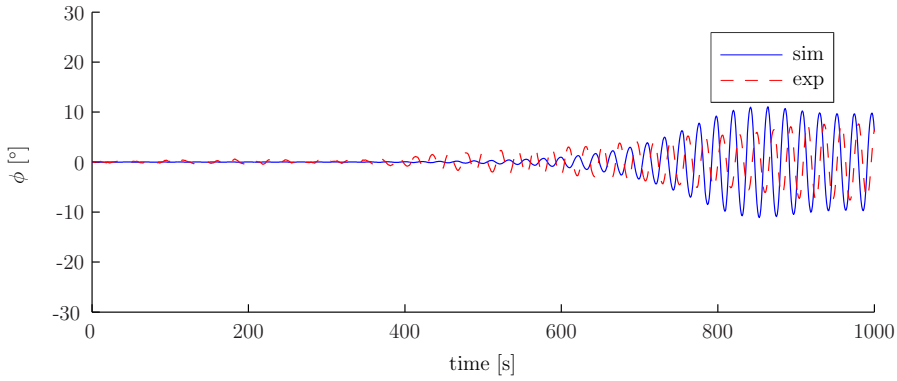

(b) Roll.

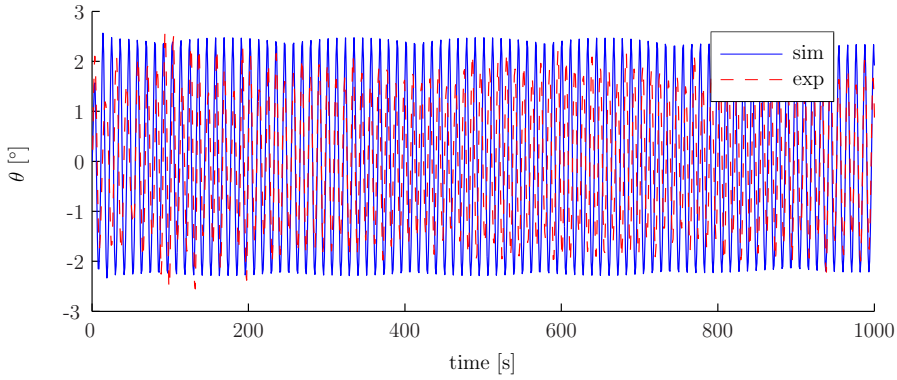

(c) Pitch.

Figure 6.14: Exp. 1183, simulation vs experiments (full scale).

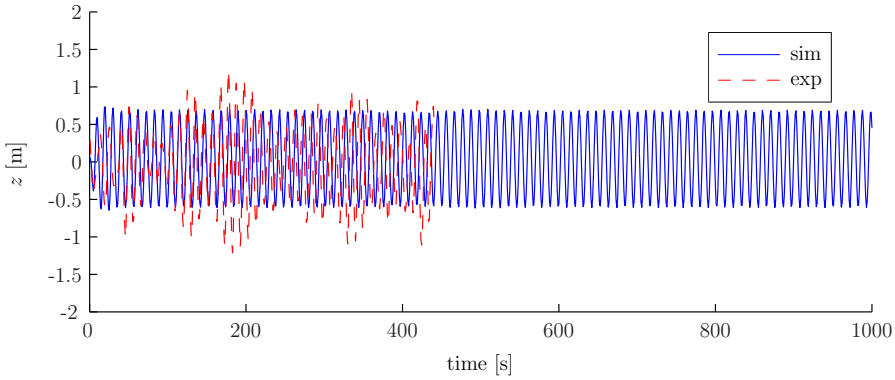

(a) Heave.

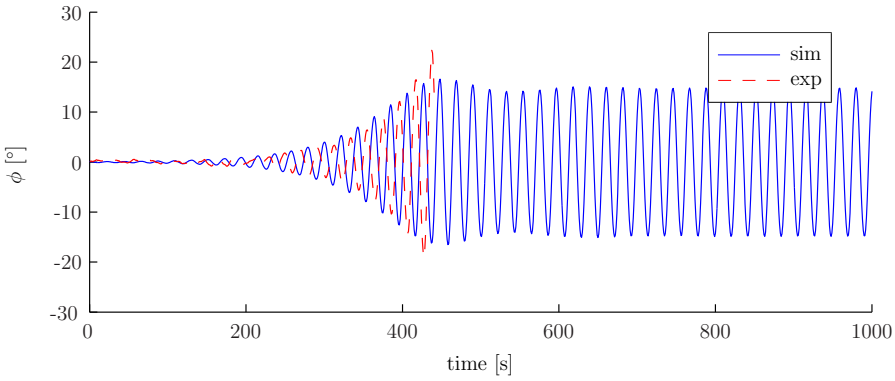

(b) Roll.

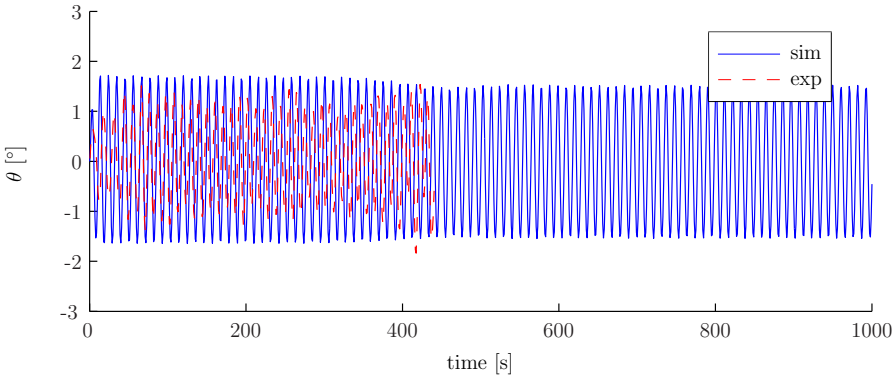

(c) Pitch.

Figure 6.15: Exp. 1184, simulation vs experiments (full scale).

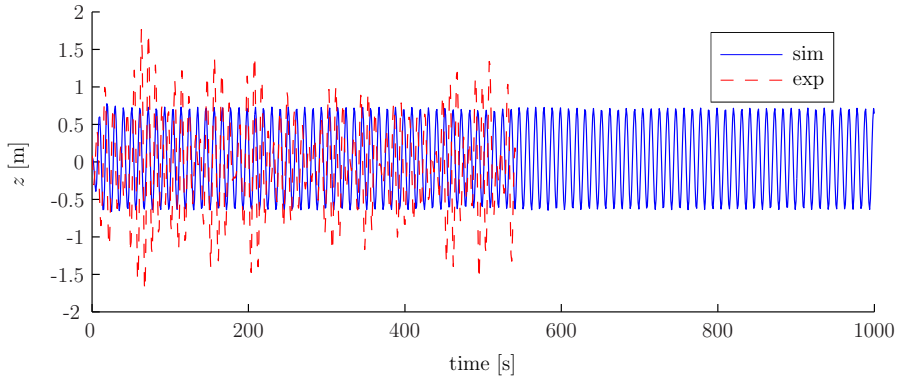

(a) Heave.

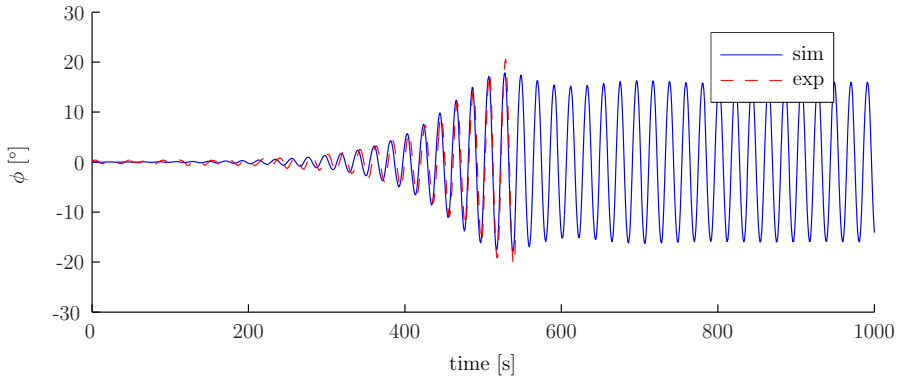

(b) Roll.

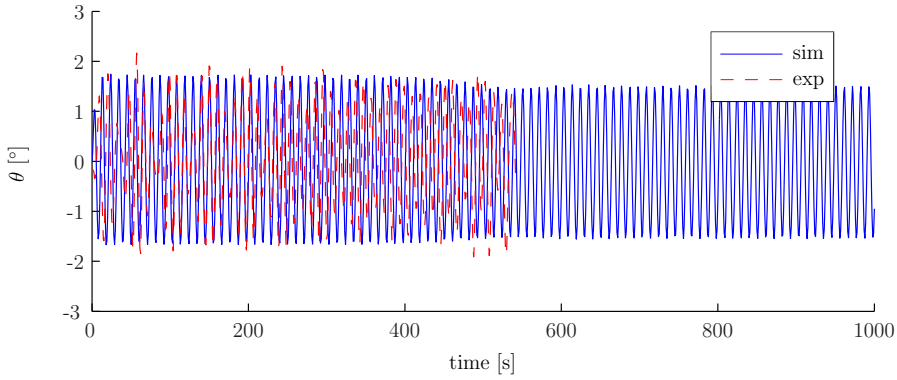

(c) Pitch.

Figure 6.16: Exp. 1185, simulation vs experiments (full scale).

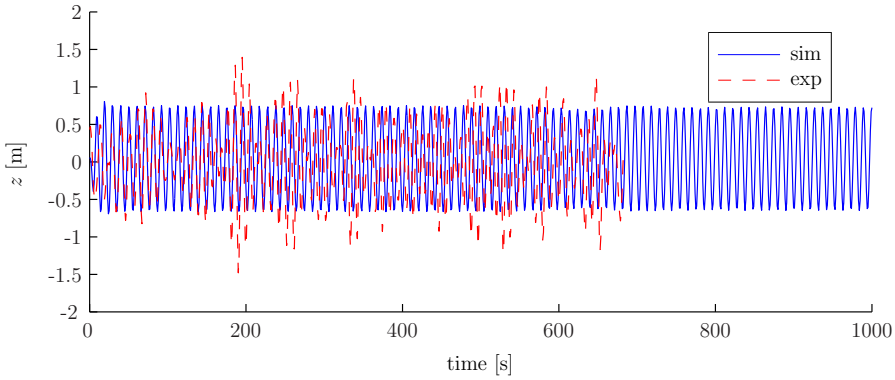

(a) Heave.

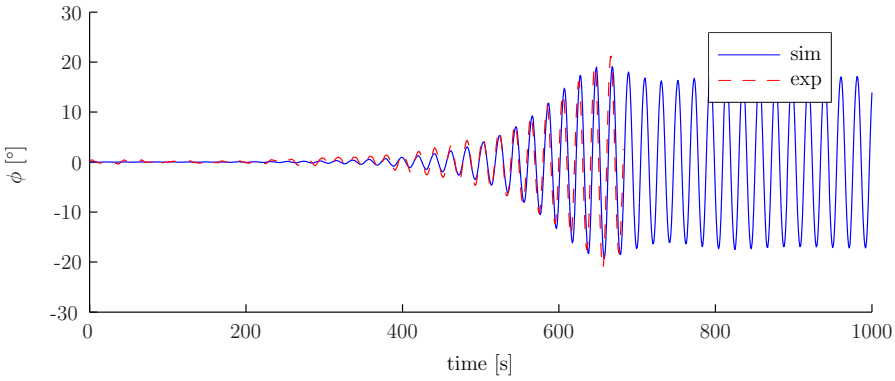

(b) Roll.

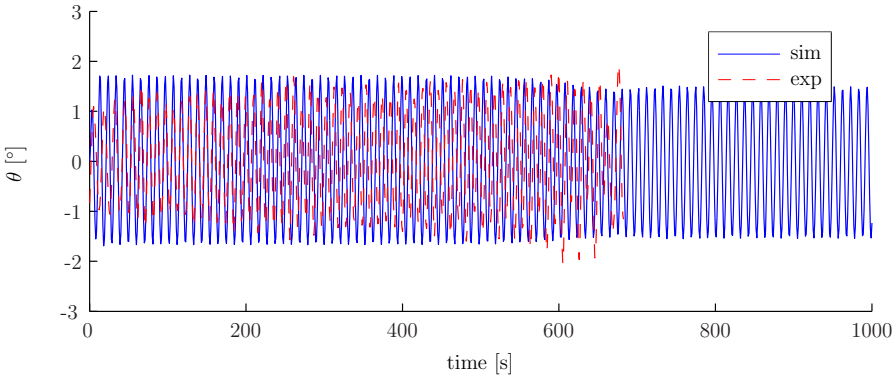

(c) Pitch.

Figure 6.17: Exp. 1186, simulation vs experiments (full scale).

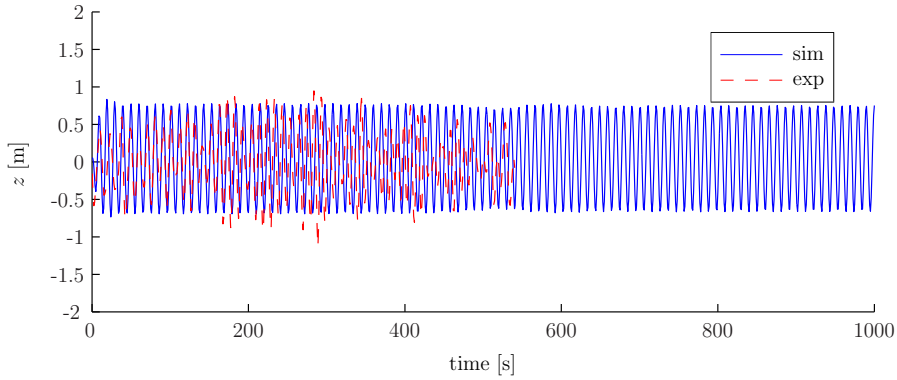

(a) Heave.

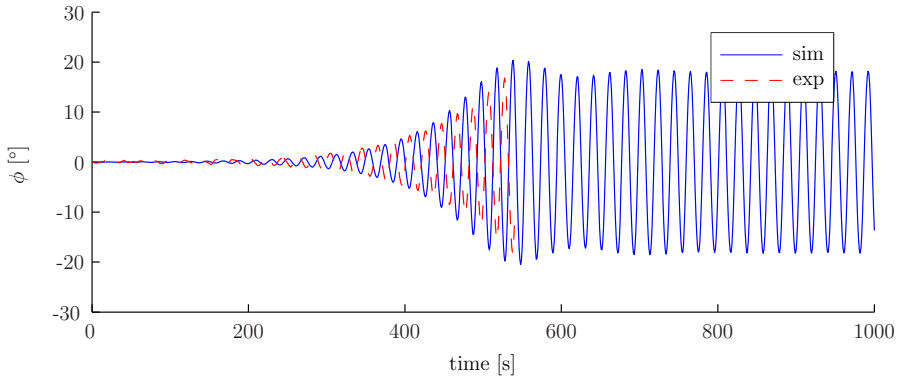

(b) Roll.

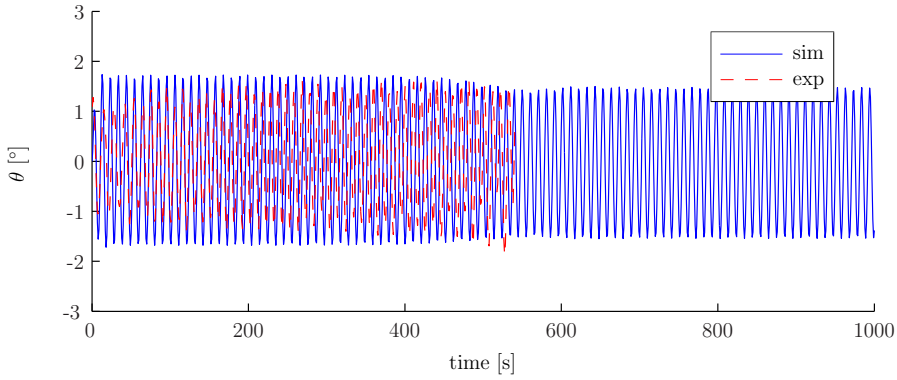

(c) Pitch.

Figure 6.18: Exp. 1187, simulation vs experiments (full scale).

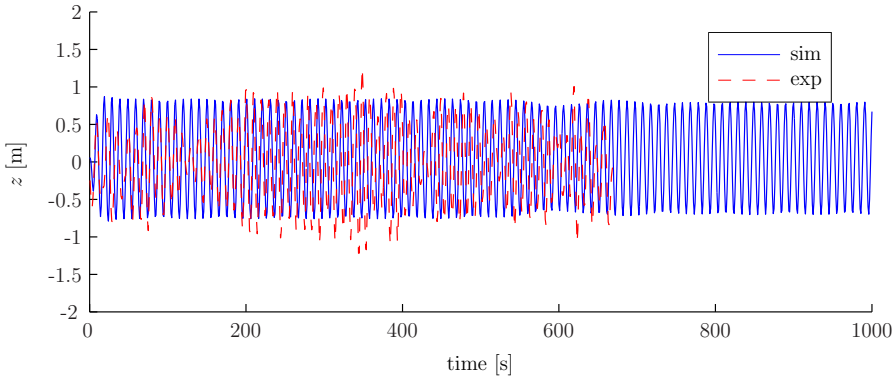

(a) Heave.

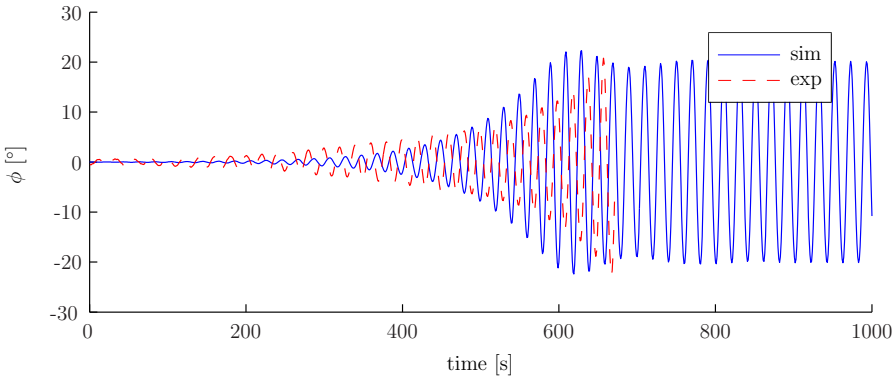

(b) Roll.

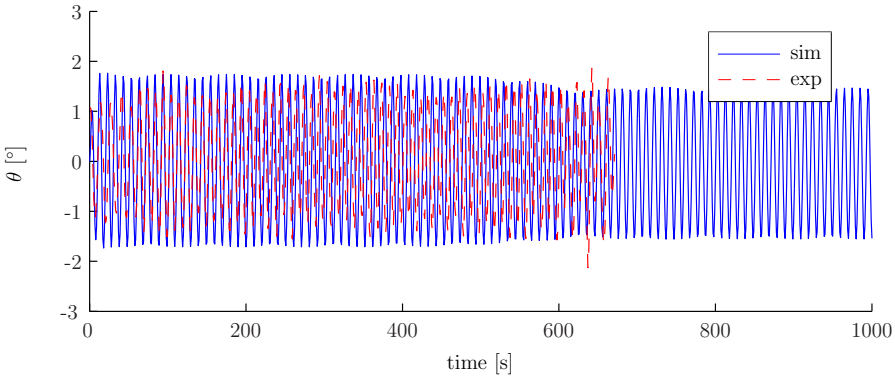

(c) Pitch.

Figure 6.19: Exp. 1188, simulation vs experiments (full scale).

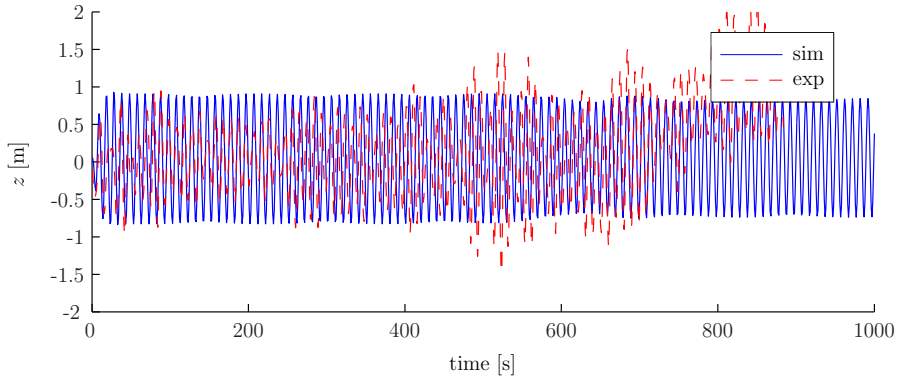

(a) Heave.

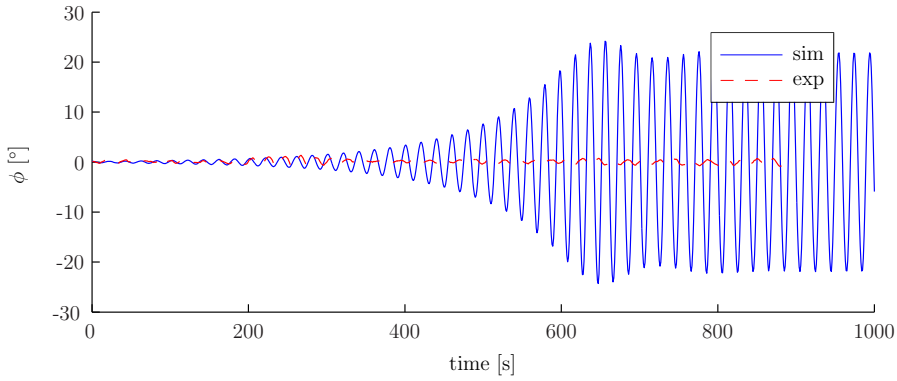

(b) Roll.

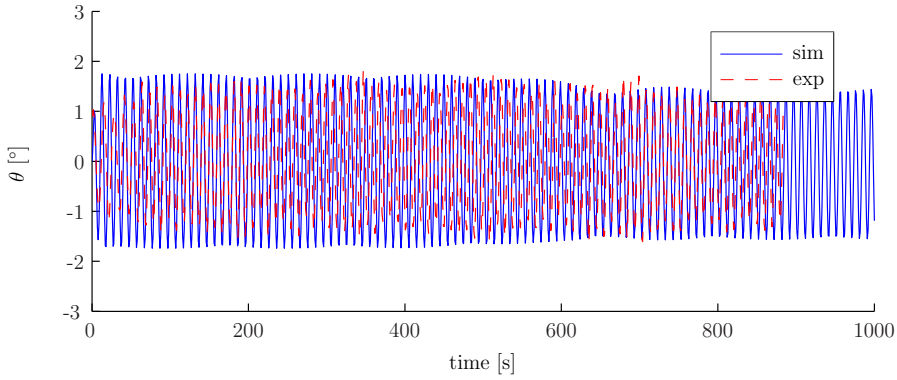

(c) Pitch.

Figure 6.20: Exp. 1189, simulation vs experiments (full scale).

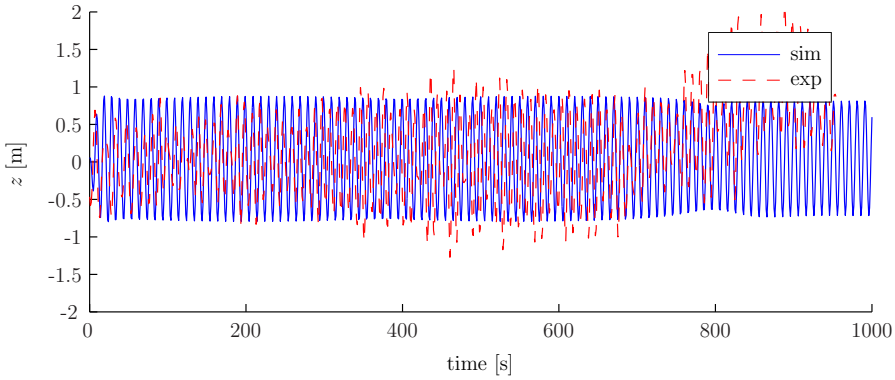

(a) Heave.

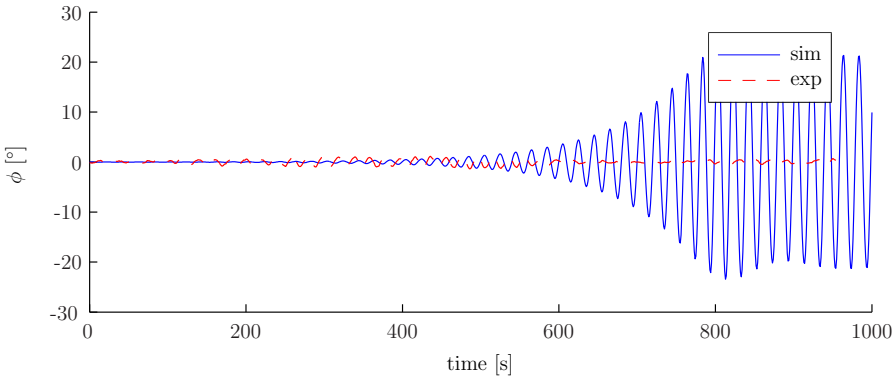

(b) Roll.

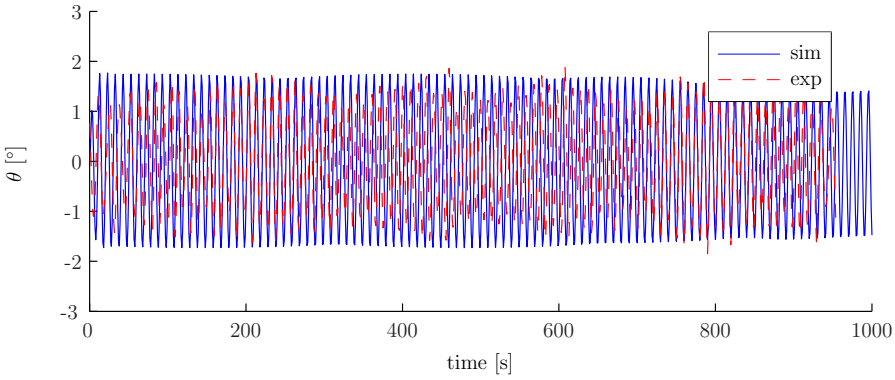

(c) Pitch.

Figure 6.21: Exp. 1190, simulation vs experiments (full scale).

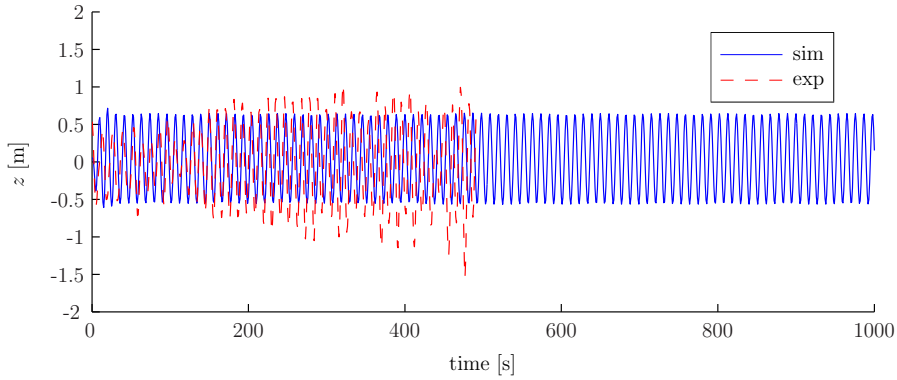

(a) Heave.

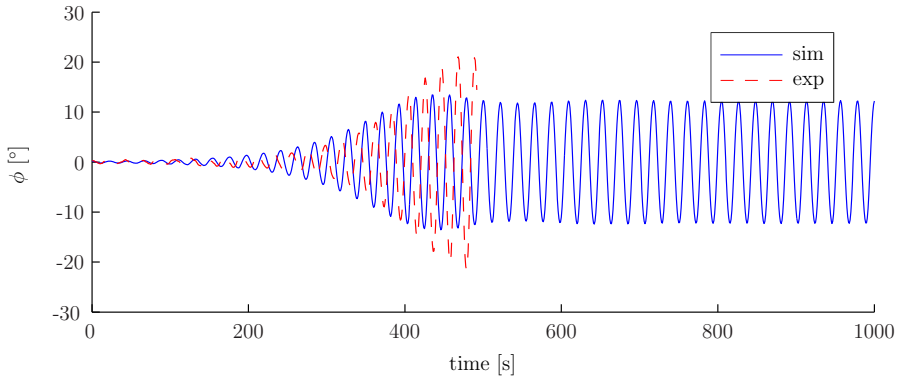

(b) Roll.

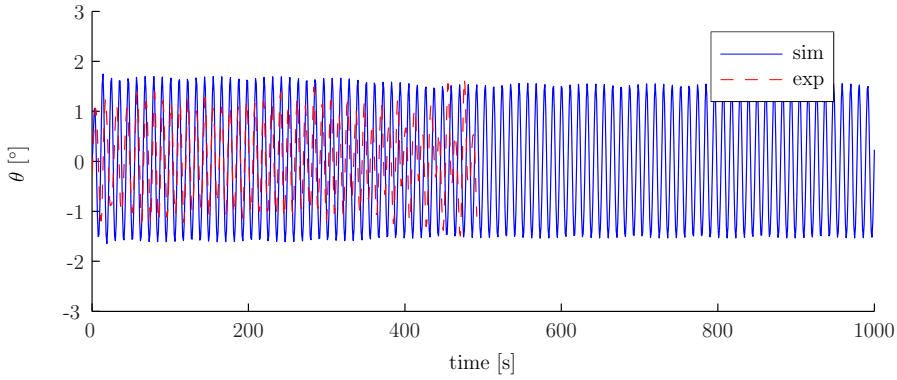

(c) Pitch.

Figure 6.22: Exp. 1191, simulation vs experiments (full scale).

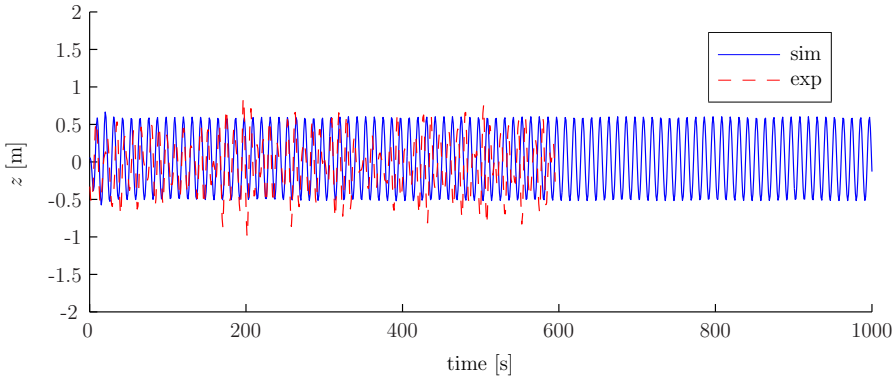

(a) Heave.

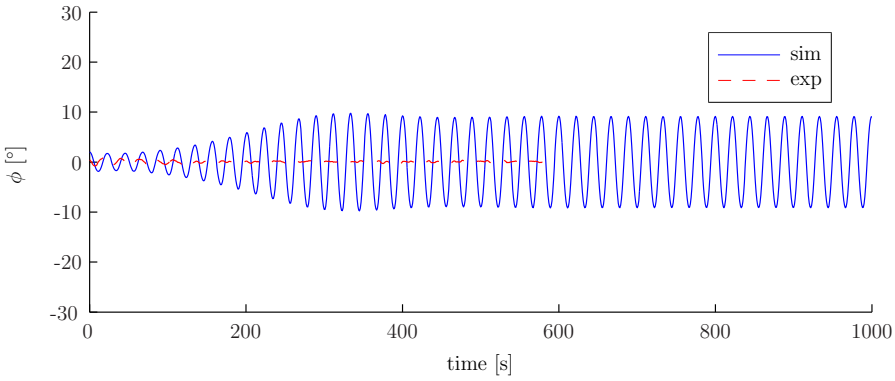

(b) Roll.

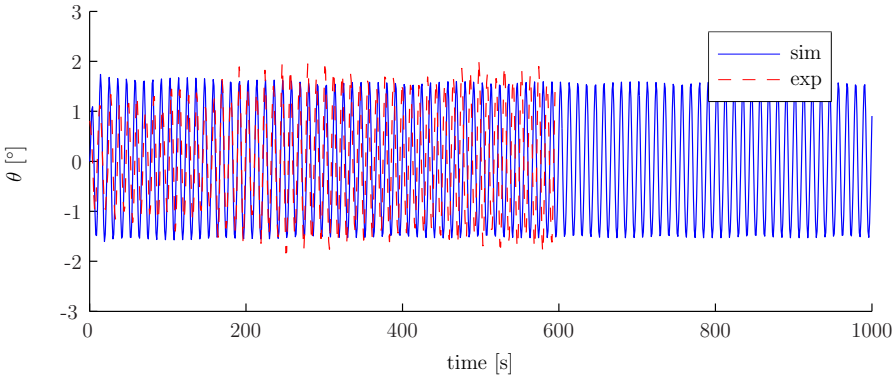

(c) Pitch.

Figure 6.23: Exp. 1192, simulation vs experiments (full scale).

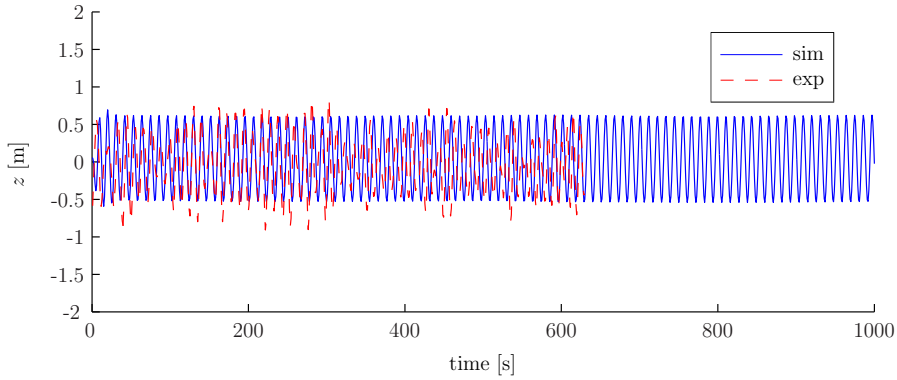

(a) Heave.

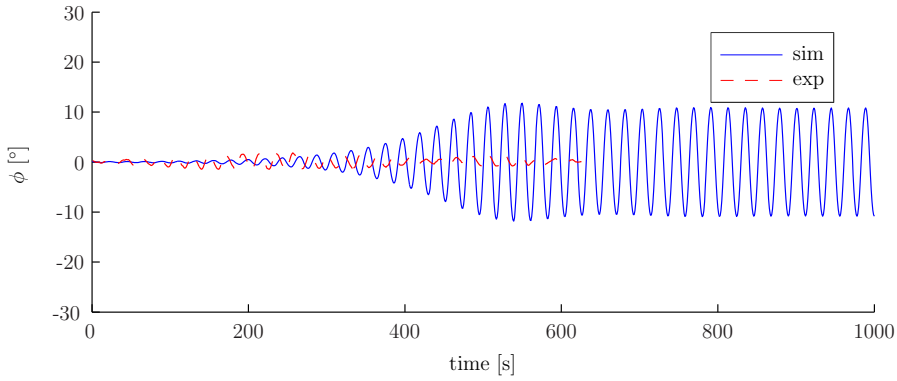

(b) Roll.

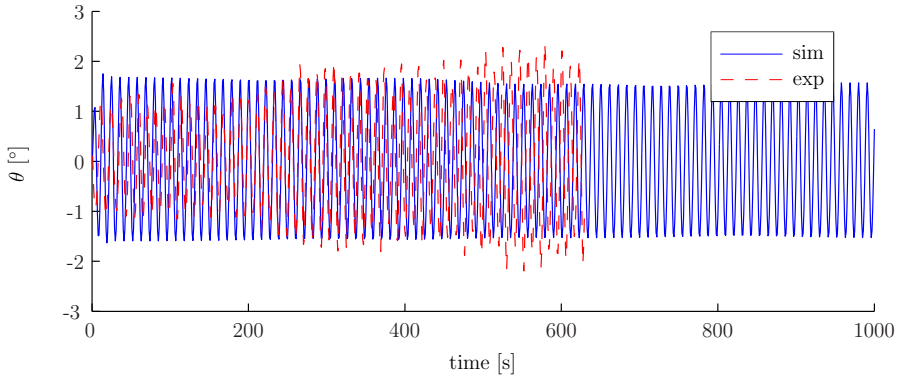

(c) Pitch.

Figure 6.24: Exp. 1193, simulation vs experiments (full scale).

Chapter 7

Equations of motion for a ship with a u-tank

As discussed in the introduction, u-tanks can be used to control parametric roll, but existing models have several drawbacks. This necessitated the derivation of a new model.

From Chapter 4 we have the dynamics of a rigid body in $\mathbb{R}^3$ and from Chapters 5 and 6 we have the equations of motion for a ship in a seaway. It is a not uncommon assumption that a ship is a rigid body [24], as was implicitly assumed in Chapter 5.[1] However, a ship equipped with a u-tank is not rigid. As the fluid in the tank moves, the distribution of mass in the ship changes, rendering the whole system non-rigid.

In general, one needs the full Navier-Stokes equations to describe the motion of both a ship in water and the water in the tank [54, 91]. However, the effects of the ocean on the ship can be greatly simplified as shown in Chapter 5, as can the motion of the fluid in that tank as will be shown in this chapter.

Here, a 7-DOF model for a ship and a u-tank is presented. The model is experimentally verified, as detailed in Chapter 9. In Chapter 8, it is compared to an existing model.

The model derivation presented in this chapter are unpublished results (the model is a generalization of the models of Holden and Fossen [39], Holden et al. [44]).

7.1 The tank fluid

A u-tank is simply two reservoirs of water or another liquid, one on the port side and the other at starboard, with a duct in between to allow the passage of liquid. To be able to model this intrinsically complicated behavior, some assumptions have to be made (these come in addition to the assumptions listed in previous chapters):

Assumption 11. The surface of the fluid in the tank is perpendicular to the centerline of the tank.

[1] A ship actually has more in common with a flexible beam (see, e.g., Drummen [17]), but this distinction is often not important.

Assumption 12. The fluid in the tank is incompressible.

Assumption 13. The flow of fluid in the tank is one-dimensional.

Assumption 14. Tank fluid memory effects are negligible.

Assumption 15. The u-tank is placed at the transversal geometrical center of the ship.

Assumption 16. The tank is symmetrical around the ship centerline.

Assumption 17. There are no air bubbles in the tank.

Assumption 18. The centerline of the tank is smooth.

Assumption 19. The centerline of the tank runs port–starboard.

Assumption 11 is clearly false for a ship in motion; the actual fluid surface in the tank is likely to behave in a complicated and chaotic fashion. Modeling this accurately without resorting to computational fluid dynamics is unfeasible. Assuming the fluid surface to be horizontal would not be much more accurate than Assumption 11.

Assumptions 11–19 imply that the tank fluid is parametrizable as a tube of varying cross-sectional area. Defining the centerline of the tube of fluid as $\vec{r}_t(\sigma)$ with parameter σ, $r_t^b(\sigma)$ can be written as

$$r_t^b(\sigma) = \begin{bmatrix} x_t^b \\ y_t^b(\sigma) \\ z_t^b(\sigma) \end{bmatrix}. \tag{7.1}$$

The parameter σ is defined to have zero point at the ship centerline and be positive to port. The fluid surfaces are located at $\sigma = -\varsigma_s \leq 0$ (starboard side) and $\sigma = \varsigma_p \geq 0$ (port side). Thus, $\sigma \in [-\varsigma_s, \varsigma_p] \subset \mathbb{R}$ defines the fluid-filled part of the tank. When the water level is equal in both starboard and port side reservoirs, $\varsigma_p = \varsigma_s = \varsigma_0$, and $\sigma \in [-\varsigma_0, \varsigma_0] \subset \mathbb{R}$ defines the fluid-filled part of the tank.

Property 7.1 (Properties of r_t^b)**.** r_t^b satisfies the following properties:

- x_t^b is a constant, per Assumption 19.
- The functions y_t^b and z_t^b are smooth (specifically, C^1 or greater), per Assumption 18.
- y_t^b is odd and lies in the second and fourth quadrant (i.e., $y_t^b(-\sigma) = -y_t^b(\sigma)$, $y_t^b(0) = 0$ and $y_t^b(\sigma) < 0 \; \forall \; \sigma > 0$), per Assumptions 15 and 16.
- z_t^b is even (i.e., $z_t^b(-\sigma) = z_t^b(\sigma)$), per Assumption 16.
- $\max z_t^b = z_t^b(0)$, per Assumptions 15 and 16.

To fully describe the tank fluid, the cross-sectional area $A(\sigma)$ is also needed.

Property 7.2 (Properties of A)**.** By Assumption 17, the fluid fills the entire area $A(\sigma) \, \forall \, \sigma \in [-\varsigma_s, \varsigma_p]$. Assumption 16 implies that $A(-\sigma) = A(\sigma) > 0$.

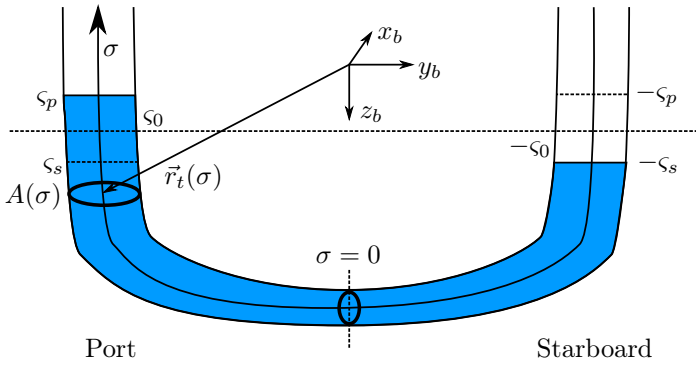

Figure 7.1: U-tank parameters.

See Figure 7.1 for an illustration of the u-tank and its parameters.

The chief physically measurable states of the system are the tank fluid levels ς_p, ς_s and the volumetric flow of the tank fluid Q (defined positive to port). ς_p and ς_s are related to the flow by

$$\dot{\varsigma}_p = \frac{Q}{A(\varsigma_p)}$$
$$\dot{\varsigma}_s = -\frac{Q}{A(\varsigma_s)}.$$

We define the generalized tank coordinate q_t as

$$q_t \triangleq \frac{1}{A_0} \int_{\varsigma_0}^{\varsigma_p} A(\sigma)\, \mathrm{d}\sigma \tag{7.2}$$

where A_0 is an arbitrary constant with unit m^2.

We note that the total fluid volume in the tank, V_t, is constant. Thus,

$$\begin{aligned} V_t &\triangleq \int_{-\varsigma_0}^{\varsigma_0} A(\sigma)\, \mathrm{d}\sigma = \int_{-\varsigma_s}^{\varsigma_p} A(\sigma)\, \mathrm{d}\sigma \\ &= \int_{-\varsigma_s}^{-\varsigma_0} A(\sigma)\, \mathrm{d}\sigma + \int_{-\varsigma_0}^{\varsigma_0} A(\sigma)\, \mathrm{d}\sigma + \int_{\varsigma_0}^{\varsigma_p} A(\sigma)\, \mathrm{d}\sigma \\ &= \int_{-\varsigma_s}^{-\varsigma_0} A(\sigma)\, \mathrm{d}\sigma + V_t + A_0 q_t, \end{aligned}$$

This gives

$$q_t = -\frac{1}{A_0} \int_{-\varsigma_s}^{-\varsigma_0} A(\sigma)\, \mathrm{d}\sigma. \tag{7.3}$$

The time derivative of q_t is given by

$$\dot{q}_t = \frac{1}{A_0} A(\varsigma_p) \frac{\mathrm{d}\varsigma_p}{\mathrm{d}t} = \frac{Q}{A_0}. \tag{7.4}$$

By differentiating on both sides of (7.2) and (7.3) with respect to q_t, we get

$$\frac{\mathrm{d}\varsigma_p}{\mathrm{d}q_t} = \frac{A_0}{A(\varsigma_p)} \tag{7.5}$$

$$\frac{\mathrm{d}\varsigma_s}{\mathrm{d}q_t} = -\frac{A_0}{A(\varsigma_s)}. \tag{7.6}$$

The speed of the tank fluid relative to the tank walls (i.e., the ship), at any point σ in the tank, is given by

$$\|\vec{v}_{t,r}(\sigma, \dot{q}_t)\| = \frac{Q}{A(\sigma)} = \frac{A_0 \dot{q}_t}{A(\sigma)}.$$

From calculus, we know that velocity is tangential to the path, giving

$$\vec{v}_{t,r}(\sigma, \dot{q}_t) = \frac{A_0 \dot{q}_t}{A(\sigma)} \frac{\mathrm{d}\bar{\vec{r}}_t}{\mathrm{d}\sigma}(\sigma), \tag{7.7}$$

where

$$\frac{\mathrm{d}\bar{\vec{r}}_t}{\mathrm{d}\sigma} \triangleq \frac{\frac{\mathrm{d}\vec{r}_t}{\mathrm{d}\sigma}}{\left\|\frac{\mathrm{d}\vec{r}_t}{\mathrm{d}\sigma}\right\|}. \tag{7.8}$$

Noting that $\mathrm{d}x_t^b/\mathrm{d}\sigma = 0$, we define

$$\frac{\mathrm{d}\bar{y}_t^b}{\mathrm{d}\sigma} \triangleq [0,1,0]\frac{\mathrm{d}\bar{r}_t^b}{\mathrm{d}\sigma} = \frac{\frac{\mathrm{d}y_t^b}{\mathrm{d}\sigma}}{\sqrt{\left(\frac{\mathrm{d}y_t^b}{\mathrm{d}\sigma}\right)^2 + \left(\frac{\mathrm{d}z_t^b}{\mathrm{d}\sigma}\right)^2}} \tag{7.9}$$

$$\frac{\mathrm{d}\bar{z}_t^b}{\mathrm{d}\sigma} \triangleq [0,0,1]\frac{\mathrm{d}\bar{r}_t^b}{\mathrm{d}\sigma} = \frac{\frac{\mathrm{d}z_t^b}{\mathrm{d}\sigma}}{\sqrt{\left(\frac{\mathrm{d}y_t^b}{\mathrm{d}\sigma}\right)^2 + \left(\frac{\mathrm{d}z_t^b}{\mathrm{d}\sigma}\right)^2}} \tag{7.10}$$

so that

$$\left(\frac{\mathrm{d}\bar{y}_t^b}{\mathrm{d}\sigma}\right)^2 + \left(\frac{\mathrm{d}\bar{z}_t^b}{\mathrm{d}\sigma}\right)^2 \equiv 1.$$

Of course, the ship (and the tank with it) is translating with velocity $\vec{v}$ and rotating with angular velocity $\vec{\omega}$ relative to the inertial frame. Thus, the velocity of the tank fluid relative to the inertial frame, at any point σ in the tank, is

$$\vec{v}_t(\sigma, \dot{q}_t, \vec{v}, \vec{\omega}) = \vec{v} + \vec{\omega} \times \vec{r}_t(\sigma) + \frac{A_0 \dot{q}_t}{A(\sigma)} \frac{\mathrm{d}\bar{\vec{r}}_t}{\mathrm{d}\sigma}(\sigma). \tag{7.11}$$

7.2 Energy of the ship–tank system

To use analytical mechanics, we need to know the potential and kinetic energies of the system. Here, we find the energy of the tank–ship system. The effects of the ocean are added later as in Chapters 4 and 5.

In the derivation of the model we will largely be following the path of Chapters 4 and 5, but now with the added complexity of having a non-rigid body and one more degree of freedom. Since the ship (without tank) has six degrees of freedom and the tank adds one extra degree of freedom, we now have seven degrees of freedom.

As generalized position, we choose

$$\tilde{q} \triangleq [x^{n\mathrm{T}}, \eta^{\mathrm{T}}, q_t] = [q^{\mathrm{T}}, q_t]^{\mathrm{T}} \in \mathbb{R}^8. \tag{7.12}$$

We note that again the dimension of the generalized position vector is greater than the number of degrees of freedom, so we will have to use Hamiltonian rather than Lagrangian mechanics [36, 55].

The time derivative of $\tilde{q}$ can be found from (4.7). We define $\tilde{\mathcal{P}}$ as

$$\tilde{\mathcal{P}}(\eta) \triangleq \begin{bmatrix} R^{\mathrm{T}}(\eta) & 0_{3\times 4} & 0_{3\times 1} \\ 0_{4\times 3} & \frac{1}{2}G(\eta) & 0_{4\times 1} \\ 0_{1\times 3} & 0_{1\times 4} & 1 \end{bmatrix} \in \mathbb{R}^{8\times 7} \tag{7.13}$$

and the generalized velocity vector $\tilde{\nu}$ as

$$\tilde{\nu} \triangleq \left[v^{b\mathrm{T}}, \omega^{b\mathrm{T}}, \dot{q}_t\right]^{\mathrm{T}} = \left[\nu^{\mathrm{T}}, \dot{q}_t\right]^{\mathrm{T}} \in \mathbb{R}^7 \tag{7.14}$$

so that

$$\dot{\tilde{q}} = \tilde{\mathcal{P}}^{\mathrm{T}}(\eta)\tilde{\nu}. \tag{7.15}$$

7.2.1 Potential energy

Any infinitesimal volume block $\mathrm{d}V$ of the tank or the ship at a position $\vec{r}$ has density $\bar{\rho}(\vec{r})$ given by

$$\bar{\rho}(\vec{r}) = \begin{cases} \rho_t & \text{in the tank} \\ \rho_s(\vec{r}) & \text{in the ship} \end{cases} \tag{7.16}$$

and is at a height $h(\vec{r})$ above some arbitrary zero point. We note that h is the zero level minus the inertial z-component of $\vec{r}$, i.e.,

$$h(\vec{r}) = h_0 - e_z^{\mathrm{T}} r^n = h_0 - e_z^{\mathrm{T}} R r^b \tag{7.17}$$

where $e_z^{\mathrm{T}} \triangleq [0, 0, 1]$. The negative signage is because the z-axis has the same direction as the gravity field.

The potential energy $\mathrm{d}\tilde{U}$ of $\mathrm{d}V$ is given by

$$\mathrm{d}\tilde{U} = g\bar{\rho}(\vec{r})h(\vec{r})\mathrm{d}V, \tag{7.18}$$

which, in the body frame, can be written

$$\mathrm{d}\tilde{U} = g\bar{\rho}(r^b)h(r^b)\mathrm{d}V = g\bar{\rho}(r^b)\left(h_0 - e_z^{\mathrm{T}} R r^b\right)\mathrm{d}V. \tag{7.19}$$

The total potential energy $\tilde{U}$ of the ship and the tank fluid is then given by

$$\begin{aligned}\tilde{U} &= \int_{\text{ship and tank}} \mathrm{d}\tilde{U} = gm_0h_0 - ge_z^{\mathrm{T}}R\left[\int_{\text{ship}} \rho_s(r^b)r^b \,\mathrm{d}V + \rho_t \int_{\text{tank}} r_t^b \,\mathrm{d}V\right] \\ &= gm_0h_0 - ge_z^{\mathrm{T}}R\left[mr_g^b + \rho_t \int_{-\varsigma_s(q_t)}^{\varsigma_p(q_t)} A(\sigma)r_t^b(\sigma)\,\mathrm{d}\sigma\right] \end{aligned} \tag{7.20}$$

where

$$m_0 \triangleq \int_{\text{ship and tank}} \bar{\rho}(r^b)\,\mathrm{d}V$$

is the combined mass of the ship and the tank fluid, since

$$r_g^b \triangleq \frac{1}{m}\int_{\text{ship}} \rho_s(r^b)r^b \,\mathrm{d}V \tag{7.21}$$

is the definition of the (ship's) center of gravity.

A priori we know that $x^n = 0, R = I_3, q_t = 0$ is an equilibrium point for the system. We therefore take $\tilde{U}$ to be zero at this point. We note that $q_t = 0 \Rightarrow \varsigma_p = \varsigma_s = \varsigma_0$. The value of $\tilde{U}$ at the equilibrium point is therefore

$$\begin{aligned}\tilde{U}_0 &= gm_0h_0 - gm[0,0,1]r_g^b - g\rho_t e_z^{\mathrm{T}} \int_{-\varsigma_0}^{\varsigma_0} r_t^b(\sigma)A(\sigma)\,\mathrm{d}\sigma \\ &= gm_0h_0 - gmz_g - g\rho_t \int_{-\varsigma_0}^{\varsigma_0} z_t^b(\sigma)A(\sigma)\,\mathrm{d}\sigma \\ &\triangleq 0.\end{aligned}$$

Thus,

$$m_0h_0 \triangleq gmz_g + g\rho_t \int_{-\varsigma_0}^{\varsigma_0} z_t^b(\sigma)A(\sigma)\,\mathrm{d}\sigma. \tag{7.22}$$

This gives potential energy

$$\begin{aligned}\tilde{U}(\tilde{q}) = {} & gmz_g + g\rho_t \int_{-\varsigma_0}^{\varsigma_0} z_t^b(\sigma)A(\sigma)\,\mathrm{d}\sigma \\ & - ge_z^{\mathrm{T}}R\left[mr_g^b + \rho_t \int_{-\varsigma_s(q_t)}^{\varsigma_p(q_t)} A(\sigma)r_t^b(\sigma)\,\mathrm{d}\sigma\right].\end{aligned} \tag{7.23}$$

7.2.2 Kinetic energy

An infinitesimal volume block $\mathrm{d}V$ of the tank or ship at a position $\vec{r}$ in the body frame has density $\bar{\rho}(\vec{r})$ given by (7.16) and velocity $\vec{v}_v(\vec{r})$ given by

$$\vec{v}_v(\vec{r}) = \begin{cases} \vec{v} + \vec{\omega} \times \vec{r} + \frac{A_0\dot{q}_t}{A(\sigma)}\frac{\mathrm{d}\bar{r}_t}{\mathrm{d}\sigma}(\sigma) & \text{in the tank} \\ \vec{v} + \vec{\omega} \times \vec{r} & \text{in the ship} \end{cases} \tag{7.24}$$

where $\vec{v}$ is the translational and $\vec{\omega}$ the angular velocity of the ship. The velocity of the tank fluid comes from (7.11).

The volume block has kinetic energy $\mathrm{d}\tilde{T}$ given by

$$\mathrm{d}\tilde{T} = \frac{1}{2}\bar{\rho}(\vec{r})\|\vec{v}_v(\vec{r})\|_2^2 \mathrm{d}V, \tag{7.25}$$

which, in the body frame, can be written

$$\mathrm{d}\tilde{T} = \frac{1}{2}\bar{\rho}(r^b)\|v_v^b(r^b)\|_2^2 \mathrm{d}V. \tag{7.26}$$

The total kinetic energy $\tilde{T}$ of the ship and the tank fluid is then given by

$$\begin{aligned}
\tilde{T}(\tilde{q},\tilde{\nu}) &= \frac{1}{2}\int_{\text{tank and ship}} \bar{\rho}(r^b)\|v_v^b(r^b)\|_2^2 \,\mathrm{d}V \\
&= \frac{1}{2}\int_{\text{ship}} \rho_s(r^b)\left\|v^b + \omega^b \times r^b\right\|_2^2 \,\mathrm{d}V \\
&\quad + \frac{1}{2}\rho_t \int_{-\varsigma_s(q_t)}^{\varsigma_p(q_t)} A(\sigma)\left\|v^b + \omega^b \times r_t^b(\sigma) + \frac{A_0\dot{q}_t}{A(\sigma)}\frac{\mathrm{d}\bar{r}_t^b}{\mathrm{d}\sigma}(\sigma)\right\|_2^2 \,\mathrm{d}\sigma \\
&= \frac{1}{2}\left[\int_{\text{ship}} \rho_s(r^b)\,\mathrm{d}V + \rho_t\int_{-\varsigma_s(q_t)}^{\varsigma_p(q_t)} A(\sigma)\,\mathrm{d}\sigma\right]\|v^b\|_2^2 \\
&\quad - \frac{1}{2}{\omega^b}^{\mathrm{T}}\left[\int_{\text{ship}} \rho_s(r^b)S^2(r^b)\,\mathrm{d}V + \rho_t\int_{-\varsigma_s(q_t)}^{\varsigma_p(q_t)} A(\sigma)S^2(r_t^b(\sigma))\,\mathrm{d}\sigma\right]\omega^b \\
&\quad + {\omega^b}^{\mathrm{T}}\left[\int_{\text{ship}} \rho_s(r^b)S(r^b)\,\mathrm{d}V + \rho_t\int_{-\varsigma_s(q_t)}^{\varsigma_p(q_t)} A(\sigma)S(r_t^b(\sigma))\,\mathrm{d}\sigma\right]v^b \\
&\quad + \rho_t A_0\dot{q}_t {v^b}^{\mathrm{T}}\left[\int_{-\varsigma_s(q_t)}^{\varsigma_p(q_t)} \frac{\mathrm{d}\bar{r}_t^b}{\mathrm{d}\sigma}(\sigma)\,\mathrm{d}\sigma\right] + \frac{\rho_t A_0^2\dot{q}_t^2}{2}\left[\int_{-\varsigma_s(q_t)}^{\varsigma_p(q_t)} \frac{1}{A(\sigma)}\,\mathrm{d}\sigma\right] \\
&\quad + \rho_t A_0\dot{q}_t {\omega^b}^{\mathrm{T}}\left[\int_{-\varsigma_s(q_t)}^{\varsigma_p(q_t)} S(r_t^b(\sigma))\frac{\mathrm{d}\bar{r}_t^b}{\mathrm{d}\sigma}(\sigma)\,\mathrm{d}\sigma\right] \\
&= \frac{1}{2}\tilde{\nu}^{\mathrm{T}} M_t(q_t)\tilde{\nu}
\end{aligned} \tag{7.27}$$

where

$$M_t(q_t) \triangleq \begin{bmatrix} (m_t+m)I_3 & -M_\nu(q_t) - mS(r_g^b) & m_{v,\dot{q}_t}(q_t) \\ M_\nu(q_t) + mS(r_g^b) & M_\omega(q_t) + J & m_{\omega,\dot{q}_t}(q_t) \\ m_{v,\dot{q}_t}^{\mathrm{T}}(q_t) & m_{\omega,\dot{q}_t}^{\mathrm{T}}(q_t) & \bar{m}_t(q_t) \end{bmatrix} \tag{7.28}$$

is the inertia matrix. We note that $M_t = M_t^{\mathrm{T}} \in \mathbb{R}^{7\times 7}$ is a positive definite matrix.

The components of the inertia matrix are:

$$m_t \triangleq \rho_t \int_{-\varsigma_s(q_t)}^{\varsigma_p(q_t)} A(\sigma)\,\mathrm{d}\sigma = \rho_t V_t > 0 \tag{7.29}$$

$$m = \int_{\text{ship}} \rho_s(r^b)\,\mathrm{d}V > 0 \tag{7.30}$$

are the mass of the tank fluid and the ship,

$$M_\nu(q_t) \triangleq \rho_t \int_{-\varsigma_s(q_t)}^{\varsigma_p(q_t)} A(\sigma) S(r_t^b(\sigma))\, \mathrm{d}\sigma = -M_\nu^{\mathrm{T}}(q_t) \in \mathbb{R}^{3\times 3} \tag{7.31}$$

$$mS(r_g^b) = \int_{\text{ship}} \rho_s(r^b) S(r^b)\, \mathrm{d}V = -mS^{\mathrm{T}}(r_g^b) \in \mathbb{R}^{3\times 3} \tag{7.32}$$

are the cross-couplings between the angular and translational accelerations,

$$M_\omega(q_t) \triangleq -\rho_t \int_{-\varsigma_s(q_t)}^{\varsigma_p(q_t)} A(\sigma) S^2(r_t^b(\sigma))\, \mathrm{d}\sigma = M_\omega^{\mathrm{T}}(q_t) > 0 \in \mathbb{R}^{3\times 3} \tag{7.33}$$

$$J = -\int_{\text{ship}} \rho_s(r^b) S^2(r^b)\, \mathrm{d}V = J^{\mathrm{T}} > 0 \in \mathbb{R}^{3\times 3} \tag{7.34}$$

are the moment of inertia of the tank fluid and the ship,

$$m_{v,\dot{q}_t}(q_t) \triangleq \rho_t A_0 \int_{-\varsigma_s(q_t)}^{\varsigma_p(q_t)} \frac{\mathrm{d}\bar{r}_t^b}{\mathrm{d}\sigma}(\sigma)\, \mathrm{d}\sigma \in \mathbb{R}^{3\times 1} \tag{7.35}$$

$$m_{\omega,\dot{q}_t}(q_t) \triangleq \rho_t A_0 \int_{-\varsigma_s(q_t)}^{\varsigma_p(q_t)} S(r_t^b(\sigma)) \frac{\mathrm{d}\bar{r}_t^b}{\mathrm{d}\sigma}(\sigma)\, \mathrm{d}\sigma \in \mathbb{R}^{3\times 1} \tag{7.36}$$

give the cross-coupling between the acceleration of the tank fluid and the rigid-body generalized velocities and

$$\bar{m}_t(q_t) \triangleq \rho_t \int_{-\varsigma_s(q_t)}^{\varsigma_p(q_t)} \frac{A_0^2}{A(\sigma)}\, \mathrm{d}\sigma > 0 \tag{7.37}$$

is the inertial mass of the tank fluid (which is distinct from the actual mass $m_t = \rho_t V_t$ of the tank fluid).

As in Chapter 4, we need to rewrite the kinetic energy as a function of the time derivative of the generalized position vector, $\dot{\tilde{q}}$. We note that

$$\tilde{\nu} = \begin{bmatrix} R^{\mathrm{T}}(\eta) & 0_{3\times 4} & 0_{3\times 1} \\ 0_{3\times 3} & 2G(\eta) & 0_{3\times 1} \\ 0_{1\times 3} & 0_{1\times 4} & 1 \end{bmatrix} \dot{\tilde{q}} = \tilde{P}(\eta)\dot{\tilde{q}}$$

with

$$\tilde{P}(\eta) \triangleq \begin{bmatrix} R^{\mathrm{T}}(\eta) & 0_{3\times 4} & 0_{3\times 1} \\ 0_{3\times 3} & 2G(\eta) & 0_{3\times 1} \\ 0_{1\times 3} & 0_{1\times 4} & 1 \end{bmatrix}. \tag{7.38}$$

Thus, the complimentary kinetic energy $\tilde{T}^*$ is given by

$$\tilde{T}^* = \frac{1}{2}\dot{\tilde{q}}^{\mathrm{T}} \tilde{\mathcal{M}}(\tilde{q}) \dot{\tilde{q}} \tag{7.39}$$

where

$$\tilde{\mathcal{M}}(\tilde{q}) \triangleq \tilde{P}^{\mathrm{T}}(\eta) M_t(q_t) \tilde{P}(\eta) = \tilde{\mathcal{M}}^{\mathrm{T}}(\tilde{q}) \in \mathbb{R}^{8\times 8}. \tag{7.40}$$

As was the case with $\mathcal{M}$ in Chapter 4, the matrix $\tilde{\mathcal{M}}$ is singular, so an inverse does not exist.

We define the matrix $\tilde{\mathcal{W}}$ as

$$\tilde{\mathcal{W}}(\tilde{q}) \triangleq \tilde{\mathcal{P}}^{\mathrm{T}}(\eta) M_t^{-1}(q_t) \tilde{\mathcal{P}}(\eta) = \tilde{\mathcal{W}}^{\mathrm{T}}(\tilde{q}). \tag{7.41}$$

The matrices $\tilde{P}$, $\tilde{\mathcal{P}}$, $\tilde{\mathcal{M}}$ and $\tilde{\mathcal{W}}$ satisfy several interesting properties:

Property 7.3. $\tilde{\mathcal{M}}$ is symmetric and positive semidefinite.

Proof. $\tilde{\mathcal{M}} = \tilde{\mathcal{M}}^{\mathrm{T}} \geq 0$ if it satisfies $w^{\mathrm{T}} \tilde{\mathcal{M}} w \geq 0 \; \forall \; w \in \mathbb{R}^7$. From the definition of $\tilde{\mathcal{M}}$, $w^{\mathrm{T}} \tilde{\mathcal{M}} w = w^{\mathrm{T}} P^{\mathrm{T}} M_t P w = \tilde{w}^{\mathrm{T}} M_t \tilde{w} \geq 0$ with $\tilde{w} = Pw$ since $M_t = M_t^{\mathrm{T}} > 0$. Thus $\tilde{\mathcal{M}}$ is at least positive semidefinite. It is not positive definite, however, because $w = [0_{1\times 3}, \eta^{\mathrm{T}}]^{\mathrm{T}} \Rightarrow w^{\mathrm{T}} \tilde{\mathcal{M}} w = 0$ since $G\eta = 0$ (by Property 3.15). □

Property 7.4. $\tilde{\mathcal{W}}$ is symmetric and positive semidefinite.

Proof. $\tilde{\mathcal{W}} = \tilde{\mathcal{W}}^{\mathrm{T}} \geq 0$ if it satisfies $w^{\mathrm{T}} \tilde{\mathcal{W}} w \geq 0 \; \forall \; w \in \mathbb{R}^7$. From the definition of $\tilde{\mathcal{W}}$, $w^{\mathrm{T}} \tilde{\mathcal{W}} w = w^{\mathrm{T}} \mathcal{P}^{\mathrm{T}} M_t^{-1} \mathcal{P} w = \tilde{w}^{\mathrm{T}} M_t^{-1} \tilde{w} \geq 0$ with $\tilde{w} = \mathcal{P} w$ since $M_t = M_t^{\mathrm{T}} > 0$ implies $M_t^{-1} = M_t^{-\mathrm{T}} > 0$. Thus $\tilde{\mathcal{W}}$ is at least positive semidefinite. It is not positive definite, however, because $w = [0_{1\times 3}, \eta^{\mathrm{T}}]^{\mathrm{T}} \Rightarrow w^{\mathrm{T}} \tilde{\mathcal{W}} w = 0$ since $G\eta = 0$ (by Property 3.15). □

Property 7.5. $\tilde{\mathcal{P}} \tilde{P}^{\mathrm{T}} = I_7$.

Proof. We have

$$\begin{aligned} \tilde{\mathcal{P}} \tilde{P}^{\mathrm{T}} &= \begin{bmatrix} R^{\mathrm{T}} & 0_{3\times 4} & 0_{3\times 1} \\ 0_{3\times 3} & \frac{1}{2} G & 0_{3\times 1} \\ 0_{1\times 3} & 0_{1\times 4} & 1 \end{bmatrix} \begin{bmatrix} R & 0_{3\times 3} & 0_{3\times 1} \\ 0_{4\times 3} & 2G^{\mathrm{T}} & 0_{4\times 1} \\ 0_{1\times 3} & 0_{1\times 3} & 1 \end{bmatrix} \\ &= \begin{bmatrix} R^{\mathrm{T}} R & 0_{3\times 3} & 0_{3\times 1} \\ 0_{3\times 3} & G G^{\mathrm{T}} & 0_{3\times 1} \\ 0_{1\times 3} & 0_{1\times 3} & 1 \end{bmatrix} = I_7 \end{aligned}$$

since $R^{\mathrm{T}} = R^{-1}$ and $G G^{\mathrm{T}} = I_3$. □

Property 7.6. $\tilde{P} \tilde{\mathcal{P}}^{\mathrm{T}} = I_7$.

Proof. We have

$$\begin{aligned} \tilde{P} \tilde{\mathcal{P}}^{\mathrm{T}} &= \begin{bmatrix} R^{\mathrm{T}} & 0_{3\times 4} & 0_{3\times 1} \\ 0_{3\times 3} & 2G & 0_{3\times 1} \\ 0_{1\times 3} & 0_{1\times 4} & 1 \end{bmatrix} \begin{bmatrix} R & 0_{3\times 3} & 0_{3\times 1} \\ 0_{4\times 3} & \frac{1}{2} G^{\mathrm{T}} & 0_{4\times 1} \\ 0_{1\times 3} & 0_{1\times 3} & 1 \end{bmatrix} \\ &= \begin{bmatrix} R^{\mathrm{T}} R & 0_{3\times 3} & 0_{3\times 1} \\ 0_{3\times 3} & G G^{\mathrm{T}} & 0_{3\times 1} \\ 0_{1\times 3} & 0_{1\times 3} & 1 \end{bmatrix} = I_7 \end{aligned}$$

since $R^{\mathrm{T}} = R^{-1}$ and $G G^{\mathrm{T}} = I_3$. □

Property 7.7. $\tilde{\mathcal{P}}^{\mathrm{T}} \tilde{P} \tilde{\mathcal{P}}^{\mathrm{T}} = \tilde{\mathcal{P}}^{\mathrm{T}}$.

Proof. We have $\tilde{\mathcal{P}}^{\mathrm{T}}\tilde{P}\tilde{\mathcal{P}}^{\mathrm{T}} = \tilde{\mathcal{P}}^{\mathrm{T}} I_7 = \tilde{\mathcal{P}}^{\mathrm{T}}$. □

Property 7.8. $\tilde{P}^{\mathrm{T}}\tilde{\mathcal{P}}\tilde{P}^{\mathrm{T}} = \tilde{P}^{\mathrm{T}}$.

Proof. We have $\tilde{P}^{\mathrm{T}}\tilde{\mathcal{P}}\tilde{P}^{\mathrm{T}} = \tilde{P}^{\mathrm{T}} I_7 = \tilde{P}^{\mathrm{T}}$. □

Property 7.9. $\tilde{\mathcal{W}}\tilde{\mathcal{M}}\tilde{\mathcal{W}} = \tilde{\mathcal{W}}$.

Proof. We have

$$\tilde{\mathcal{W}}\tilde{\mathcal{M}}\tilde{\mathcal{W}} = \tilde{\mathcal{P}}^{\mathrm{T}} M_t^{-1}\tilde{\mathcal{P}}\tilde{P}^{\mathrm{T}} M_t \tilde{P}\tilde{\mathcal{P}}^{\mathrm{T}} M_t^{-1}\tilde{\mathcal{P}} = \tilde{\mathcal{P}}^{\mathrm{T}}\tilde{P}\tilde{\mathcal{P}}^{\mathrm{T}} M_t^{-1}\tilde{\mathcal{P}} = \tilde{\mathcal{P}}^{\mathrm{T}} M_t^{-1}\tilde{\mathcal{P}} = \tilde{\mathcal{W}}$$

where Properties 7.5 and 7.7 have been used. □

Property 7.10. $\tilde{\mathcal{M}}\tilde{\mathcal{W}}\tilde{\mathcal{M}} = \tilde{\mathcal{M}}$.

Proof. We have

$$\tilde{\mathcal{M}}\tilde{\mathcal{W}}\tilde{\mathcal{M}} = \tilde{P}^{\mathrm{T}} M_t \tilde{P}\tilde{\mathcal{P}}^{\mathrm{T}} M_t^{-1}\tilde{\mathcal{P}}\tilde{P}^{\mathrm{T}} M_t \tilde{P} = \tilde{P}^{\mathrm{T}}\tilde{\mathcal{P}}\tilde{P}^{\mathrm{T}} M_t \tilde{P} = \tilde{P}^{\mathrm{T}} M_t \tilde{P} = \tilde{\mathcal{M}}$$

where Properties 7.6 and 7.8 have been used. □

7.3 Virtual work

Following Chapter 4, we define the quasi-coordinates q_ω associated with the co-rotating components of the angular velocity as

$$\dot{q}_\omega = \omega^b. \tag{7.42}$$

The virtual work done by imposed forces $\tau_f^n(t) \in \mathbb{R}^3$ and $\tau_t(t) \in \mathbb{R}$, and torques $\tau_t^b(t) \in \mathbb{R}^3$ is then given by

$$\delta W = \delta x^{n\mathrm{T}} \tau_f^n(t) + \delta q_\omega^{\mathrm{T}} \tau_t^b(t) + \delta q_t \tau_t(t). \tag{7.43}$$

Since

$$\delta q_\omega = 2G\delta\eta, \tag{7.44}$$

(by Property 3.17) we get

$$\delta W = \delta x^{n\mathrm{T}} \tau_f^n(t) + 2\delta\eta^{\mathrm{T}} G^{\mathrm{T}} \tau_t^b(t) + \delta q_t \tau_t(t) = \delta q^{\mathrm{T}} \begin{bmatrix} \tau_f^n \\ 2G^{\mathrm{T}}\tau_t^b \\ \tau_t \end{bmatrix}. \tag{7.45}$$

We therefore see that the vector of generalized forces associated with the virtual work δW is

$$\tilde{\tau}^n \triangleq \begin{bmatrix} \tau_f^n \\ 2G^{\mathrm{T}}\tau_t^b \\ \tau_t \end{bmatrix} \in \mathbb{R}^8 \tag{7.46}$$

with a slight abuse of notation. $\tilde{\tau}^n$ is strictly speaking not a vector in the inertial frame, as $\tilde{\tau}^n \in \mathbb{R}^8$, not $\mathbb{R}^3$. And while τ_f^n *is* the forces in the inertial frame, $2G^{\mathrm{T}}\tau_t^b$ is not the torque in the inertial frame and τ_t is a scalar.

7.4 Hamilton's equations

Using the kinetic and potential energies of Section 7.2, in addition to the virtual work defined in Section 7.3, we can derive the dynamics of the system. Initially, this will be given using a generalized momentum in $\mathbb{R}^8$. This is somewhat inconvenient, as the generalized momentum can be expressed in $\mathbb{R}^7$. However, we need to initially use the more complex form as a stepping stone to get the more compact representation.

7.4.1 Generalized momentum and Hamiltonian

As in Chapter 4, the generalized momentum $\tilde{p}^n \in \mathbb{R}^8$ can be found by

$$\tilde{p}^n = \frac{\partial \tilde{T}^*}{\partial \dot{\tilde{q}}} = \tilde{\mathcal{M}}\dot{\tilde{q}} \in \mathbb{R}^8. \tag{7.47}$$

This is a slight abuse of notation, as p^n is not a vector in the inertial frame, as $\tilde{p}^n \in \mathbb{R}^8$, not $\mathbb{R}^3$.

Due to Properties 7.9 and 7.10, we can take

$$\dot{\tilde{q}} = \tilde{\mathcal{W}}\tilde{p}^n. \tag{7.48}$$

By the Legendre transform,

$$\begin{aligned}\tilde{T} &= \tilde{p}^{n\mathrm{T}}\dot{\tilde{q}} - \tilde{T}^* = \tilde{p}^{n\mathrm{T}}\tilde{\mathcal{W}}\tilde{p}^n - \frac{1}{2}\dot{\tilde{q}}\tilde{\mathcal{M}}\dot{\tilde{q}} = \tilde{p}^{n\mathrm{T}}\tilde{\mathcal{W}}\tilde{p}^n - \frac{1}{2}\tilde{q}_t\tilde{\mathcal{W}}\tilde{\mathcal{M}}\tilde{\mathcal{W}}\tilde{p}^n \\ &= \tilde{p}^{n\mathrm{T}}\tilde{\mathcal{W}}\tilde{p}^n - \frac{1}{2}\tilde{q}_t\tilde{\mathcal{W}}\tilde{p}^n = \frac{1}{2}\tilde{p}^{n\mathrm{T}}\tilde{\mathcal{W}}\tilde{p}^n.\end{aligned} \tag{7.49}$$

Due to the shape of $\tilde{T}$ and $\tilde{U}$, the Hamiltonian $\tilde{H}$ is simply equal to the sum of the energy in the system (see Appendix B), or

$$\begin{aligned}\tilde{H}(\tilde{q}, \tilde{p}^n) &= \tilde{T}(\tilde{q}, \tilde{p}^n) + \tilde{U}(\tilde{q}) \\ &= \frac{1}{2}\tilde{p}^{n\mathrm{T}}\tilde{\mathcal{W}}\tilde{p}^n + gmz_g + g\rho_t \int_{-\varsigma_0}^{\varsigma_0} z_t^b(\sigma)A(\sigma)\,\mathrm{d}\sigma \\ &\quad - ge_z^{\mathrm{T}}R\left[mr_g^b + \rho_t \int_{-\varsigma_s(q_t)}^{\varsigma_p(q_t)} A(\sigma)r_t^b(\sigma)\,\mathrm{d}\sigma\right].\end{aligned} \tag{7.50}$$

7.4.2 Using generalized momentum in $\mathbb{R}^8$

Since $\dim \tilde{q} = 8$, while there are only seven degrees of freedom, the system has a single algebraic constraint to satisfy:

$$\tilde{\xi}(\tilde{q}, \tilde{p}^n) = \eta^{\mathrm{T}}\eta - 1 = 0. \tag{7.51}$$

By Appendix B, the dynamics (with $\tilde{q}, \tilde{p}^n \in \mathbb{R}^8$) are given by

$$\dot{\tilde{q}} = \tilde{\mathcal{W}}\tilde{p} \tag{7.52}$$

$$\dot{\tilde{p}}^n = \frac{\partial \tilde{T}^*}{\partial \tilde{q}} - \frac{\partial \tilde{U}}{\partial \tilde{q}} - 2\lambda \begin{bmatrix} 0_3 \\ \eta \\ 0 \end{bmatrix} + \tilde{\tau}^n(t). \tag{7.53}$$

Before we continue, we need to find $\partial\tilde{T}^*/\partial\tilde{q}$ and $\partial\tilde{U}/\partial\tilde{q}$.

From (7.39) we have that $\tilde{T}^*$ is not a function of x^n, but it is a function of η and q_t. Therefore,

$$\frac{\partial\tilde{T}^*}{\partial x^n} = 0. \tag{7.54}$$

Since M_t is not a function of η, we can use Lemma A.3 to find that

$$\frac{\partial\tilde{T}^*}{\partial\eta} = \frac{1}{2}\frac{\partial(\dot{\tilde{q}}^{\mathrm{T}}\tilde{P}^{\mathrm{T}}M_t\tilde{P}\dot{\tilde{q}})}{\partial\eta} = \frac{1}{2}\frac{\partial(f^{\mathrm{T}}(\tilde{q},\dot{\tilde{q}})M_t f(\tilde{q},\dot{\tilde{q}}))}{\partial\eta} = \frac{\partial f}{\partial\eta}M_t f(\tilde{q},\dot{\tilde{q}}) = \frac{\partial f}{\partial\eta}M_t\tilde{P}\dot{\tilde{q}}$$

with

$$f(\tilde{q},\dot{\tilde{q}}) \triangleq \tilde{P}\dot{\tilde{q}} = \begin{bmatrix} R^{\mathrm{T}}\dot{x}^n \\ 2G\dot{\eta} \\ q_t \end{bmatrix} = \begin{bmatrix} R^{\mathrm{T}}\dot{x}^n \\ -2\dot{G}\eta \\ q_t \end{bmatrix} \in \mathbb{R}^{7\times 1}.$$

since $G\dot{\eta} = -\dot{G}\eta$ (by Property 3.16). The partial derivative $\partial f/\partial\eta$ is then given by

$$\begin{aligned}\frac{\partial f}{\partial\eta} &= \begin{bmatrix} \frac{\partial(R^{\mathrm{T}}\dot{x}^n)}{\partial\eta} & -2\frac{\partial(G\dot{\eta})}{\partial\eta} & \frac{\partial q_t}{\partial\eta} \end{bmatrix} = \begin{bmatrix} \frac{\partial R^{\mathrm{T}}}{\partial\eta}(\dot{x}^n\otimes I_3) & -2\frac{\partial\eta}{\partial\eta}(1\otimes\dot{G}^{\mathrm{T}}) & 0_{4\times 1} \end{bmatrix} \\ &= \begin{bmatrix} \frac{\partial R^{\mathrm{T}}}{\partial\eta}(\dot{x}^n\otimes I_3) & -2\dot{G}^{\mathrm{T}} & 0_{4\times 1} \end{bmatrix}\end{aligned}$$

where Lemma A.2 has been used and $\otimes$ is the Kronecker product. From Chapter 4 we recall that

$$\frac{\partial R^{\mathrm{T}}}{\partial\eta}(\dot{x}^n\otimes I_3) = -2\begin{bmatrix} \eta_i^{\mathrm{T}}S(\dot{x}^n) \\ \eta_r S(\dot{x}^n) - S(\eta_i)S(\dot{x}^n) + 2S(\dot{x}^n)S(\eta_i) \end{bmatrix}.$$

Thus,

$$\frac{\partial\tilde{T}^*}{\partial\eta} = \begin{bmatrix} \frac{\partial R^{\mathrm{T}}}{\partial\eta}(\dot{x}^n\otimes I_3) & -2\dot{G}^{\mathrm{T}} & 0_{4\times 1} \end{bmatrix} M_t\tilde{P}\dot{\tilde{q}}. \tag{7.55}$$

The product $\tilde{P}\dot{\tilde{q}}$ is not a function of q_t, but M_t is. We therefore find (by Corollary A.4)

$$\begin{aligned}\frac{\partial\tilde{T}^*}{\partial q_t} &= \frac{1}{2}\dot{\tilde{q}}^{\mathrm{T}}\tilde{P}^{\mathrm{T}}\frac{\partial M_t}{\partial q_t}\tilde{P}\dot{\tilde{q}} = \frac{1}{2}\tilde{p}^{n\mathrm{T}}\tilde{\mathcal{P}}^{\mathrm{T}}M_t^{-1}\tilde{\mathcal{P}}\tilde{P}^{\mathrm{T}}\frac{\partial M_t}{\partial q_t}\tilde{P}\tilde{\mathcal{P}}^{\mathrm{T}}M_t^{-1}\tilde{\mathcal{P}}\tilde{p}^n \\ &= \frac{1}{2}\tilde{p}^{n\mathrm{T}}\tilde{\mathcal{P}}^{\mathrm{T}}M_t^{-1}\begin{bmatrix} 0_{3\times 3} & -\frac{\partial M_\nu}{\partial q_t} & \frac{\partial m_{v,\dot{q}_t}}{\partial q_t} \\ \frac{\partial M_\nu}{\partial q_t} & \frac{\partial M_\omega}{\partial q_t} & \frac{\partial m_{\omega,\dot{q}_t}}{\partial q_t} \\ \frac{\partial m_{v,\dot{q}_t}^{\mathrm{T}}}{\partial q_t} & \frac{\partial m_{\omega,\dot{q}_t}^{\mathrm{T}}}{\partial q_t} & \frac{\partial\bar{m}_t}{\partial q_t} \end{bmatrix} M_t^{-1}\tilde{\mathcal{P}}\tilde{p}^n\end{aligned}$$

since $\tilde{\mathcal{P}}\tilde{P}^{\mathrm{T}} = \tilde{P}\tilde{\mathcal{P}}^{\mathrm{T}} = I_7$.

From (7.31)–(7.37), we find that

$$\begin{aligned}\frac{\partial M_\nu}{\partial q_t} &= \rho_t A(\varsigma_p)\frac{\mathrm{d}\varsigma_p}{\mathrm{d}q_t}S(r_t^b(\varsigma_p)) + \rho_t A(\varsigma_s)\frac{\mathrm{d}\varsigma_s}{\mathrm{d}q_t}S(r_t^b(-\varsigma_s)) \\ &= \rho_t A_0 S(r_t^b(\varsigma_p) - r_t^b(-\varsigma_s)) \qquad (7.56)\\ \frac{\partial m_{v,\dot{q}_t}}{\partial q_t} &= \rho_t A_0 \frac{\mathrm{d}\varsigma_p}{\mathrm{d}q_t}\frac{\mathrm{d}\bar{r}_t^b}{\mathrm{d}\sigma}(\varsigma_p) + \rho_t A_0 \frac{\mathrm{d}\varsigma_s}{\mathrm{d}q_t}\frac{\mathrm{d}\bar{r}_t^b}{\mathrm{d}\sigma}(-\varsigma_s) \\ &= \rho_t A_0^2\left[\frac{1}{A(\varsigma_p)}\frac{\mathrm{d}\bar{r}_t^b}{\mathrm{d}\sigma}(\varsigma_p) - \frac{1}{A(\varsigma_s)}\frac{\mathrm{d}\bar{r}_t^b}{\mathrm{d}\sigma}(-\varsigma_s)\right] \qquad (7.57)\\ \frac{\partial M_\omega}{\partial q_t} &= -\rho_t \frac{\mathrm{d}\varsigma_p}{\mathrm{d}q_t}A(\varsigma_p)S^2(r_t^b(\varsigma_p)) - \rho_t \frac{\mathrm{d}\varsigma_s}{\mathrm{d}q_t}A(\varsigma_s)S^2(r_t^b(-\varsigma_s)) \\ &= -\rho_t A_0\left[S^2(r_t^b(\varsigma_0)) - S^2(r_t^b(-\varsigma_s))\right] \qquad (7.58)\\ \frac{\partial m_{\omega,\dot{q}_t}}{\partial q_t} &= \rho_t A_0 \frac{\mathrm{d}\varsigma_p}{\mathrm{d}q_t}S(r_t^b(\varsigma_p))\frac{\mathrm{d}\bar{r}_t^b}{\mathrm{d}\sigma}(\varsigma_p) + \rho_t A_0 \frac{\mathrm{d}\varsigma_s}{\mathrm{d}q_t}S(r_t^b(-\varsigma_s))\frac{\mathrm{d}\bar{r}_t^b}{\mathrm{d}\sigma}(-\varsigma_s) \\ &= \rho_t A_0^2\left[\frac{1}{A(\varsigma_p)}S(r_t^b(\varsigma_p))\frac{\mathrm{d}\bar{r}_t^b}{\mathrm{d}\sigma}(\varsigma_p) - \frac{1}{A(\varsigma_s)}S(r_t^b(-\varsigma_s))\frac{\mathrm{d}\bar{r}_t^b}{\mathrm{d}\sigma}(-\varsigma_s)\right] \qquad (7.59)\\ \frac{\partial \bar{m}_t}{\partial q_t} &= \rho_t \frac{A_0^2}{A(\varsigma_p)}\frac{\mathrm{d}\varsigma_p}{\mathrm{d}q_t} + \rho_t \frac{A_0^2}{A(\varsigma_s)}\frac{\mathrm{d}\varsigma_s}{\mathrm{d}q_t} \\ &= \rho_t A_0^3\left[\frac{1}{A^2(\varsigma_p)} - \frac{1}{A^2(\varsigma_s)}\right] \qquad (7.60)\end{aligned}$$

by differentiating under the integral sign. We note the partial derivatives of M_t are exclusively functions of q_t.

We can then write

$$\frac{\partial \tilde{T}^*}{\partial q_t} = \frac{1}{2}\tilde{p}^{n\mathrm{T}}\tilde{\mathcal{P}}^{\mathrm{T}}M_t^{-1}\frac{\partial M_t}{\partial q_t}M_t^{-1}\tilde{\mathcal{P}}\tilde{p}^n. \qquad (7.61)$$

We see that we can write $\partial\tilde{T}^*/\partial\tilde{q}$ as

$$\frac{\partial \tilde{T}^*}{\partial \tilde{q}} = \begin{bmatrix} 0_{3\times 7} \\ \begin{bmatrix} \frac{\partial R^{\mathrm{T}}}{\partial \eta}(\dot{x}^n \otimes I_3) & -2\dot{G}^{\mathrm{T}} & 0_{4\times 1} \end{bmatrix} \\ \frac{1}{2}\dot{\tilde{q}}^{\mathrm{T}}\tilde{P}^{\mathrm{T}}\frac{\partial M_t}{\partial q_t} \end{bmatrix} M_t\tilde{P}\dot{\tilde{q}}. \qquad (7.62)$$

The partial derivative of $\tilde{U}$ with respect to $\tilde{q}$ can be found by noting that it is not a function of x^n, but it is a function of η and q_t. We find

$$\begin{aligned}\frac{\partial \tilde{U}}{\partial x^n} &= 0_{3\times 1} \qquad (7.63)\\ \frac{\partial \tilde{U}}{\partial \eta} &= -g\frac{\partial (e_z^{\mathrm{T}}R)}{\partial \eta}\left[m r_g^b + \rho_t \int_{-\varsigma_s(q_t)}^{\varsigma_p(q_t)} r_t^b(\sigma)A(\sigma)\,\mathrm{d}\sigma\right] \qquad (7.64)\\ \frac{\partial \tilde{U}}{\partial q_t} &= -g\rho_t e_z^{\mathrm{T}}R\left[r_t^b(\varsigma_p)A(\varsigma_p)\frac{\mathrm{d}\varsigma_p}{\mathrm{d}q_t} + r_t^b(-\varsigma_s)A(\varsigma_s)\frac{\mathrm{d}\varsigma_s}{\mathrm{d}q_t}\right] \\ &= -g\rho_t A_0 e_z^{\mathrm{T}}R\left[r_t^b(\varsigma_p) - r_t^b(-\varsigma_s)\right] \qquad (7.65)\end{aligned}$$

using differentiation under the integral. From (5.10), we have

$$\frac{\partial(e_z^{\mathrm{T}} R)}{\partial \eta} = 2 \begin{bmatrix} -\eta_{i,2} & \eta_{i,1} & 0 \\ \eta_{i,3} & \eta_r & -2\eta_{i,1} \\ -\eta_r & \eta_{i,3} & -2\eta_{i,2} \\ \eta_{i,1} & \eta_{i,2} & 0 \end{bmatrix} \in \mathbb{R}^{4\times 3}.$$

Since we are not interested in the dynamical equations with a generalized momentum in $\mathbb{R}^8$ (except as an aid to find the dynamical equations with a generalized momentum in $\mathbb{R}^7$), we will not insert the expressions for $\partial \tilde{T}^*/\partial \tilde{q}$ and $\partial \tilde{U}/\partial \tilde{q}$ into (7.53).

7.4.3 Using generalized momentum in $\mathbb{R}^7$

We define the body-fixed momentum vector $\tilde{p}$ as

$$\tilde{p} \triangleq M_t \tilde{\nu} \in \mathbb{R}^7 \tag{7.66}$$

and note that

$$\tilde{p}^n = \tilde{P}^{\mathrm{T}} M_t \tilde{P} \dot{\tilde{q}} = \tilde{P}^{\mathrm{T}} M_t \tilde{\nu} = \tilde{P}^{\mathrm{T}} \tilde{p} \tag{7.67}$$

which implies

$$\tilde{p} = \tilde{\mathcal{P}} \tilde{p}^n \tag{7.68}$$

since $\tilde{\mathcal{P}} \tilde{P}^{\mathrm{T}} = I_7$. Also worth noting is that

$$\tilde{p} = M_t \tilde{P} \dot{\tilde{q}} \tag{7.69}$$

$$\dot{\tilde{q}} = \tilde{\mathcal{P}}^{\mathrm{T}} M_t^{-1} \tilde{p} \tag{7.70}$$

since $\tilde{P} \tilde{\mathcal{P}}^{\mathrm{T}} = I_7$.

Therefore,

$$\begin{aligned} \dot{\tilde{p}} &= \dot{\tilde{\mathcal{P}}} \tilde{p}^n + \tilde{\mathcal{P}} \dot{\tilde{p}}^n = \dot{\tilde{\mathcal{P}}} \tilde{P}^{\mathrm{T}} \tilde{p} + \tilde{\mathcal{P}} \dot{\tilde{p}}^n \\ &= \begin{bmatrix} -S(\omega^b) R^{\mathrm{T}} & 0_{3\times 4} & 0_{3\times 1} \\ 0_{3\times 3} & \frac{1}{2}\dot{G} & 0_{3\times 1} \\ 0_{1\times 3} & 0_{1\times 4} & 0 \end{bmatrix} \begin{bmatrix} R & 0_{3\times 3} & 0_{3\times 1} \\ 0_{4\times 3} & 2G^{\mathrm{T}} & 0_{4\times 1} \\ 0_{1\times 3} & 0_{1\times 3} & 1 \end{bmatrix} \tilde{p} + \tilde{\mathcal{P}} \dot{\tilde{p}}^n \\ &= \begin{bmatrix} -S(\omega^b) & 0_{3\times 3} & 0_{3\times 1} \\ 0_{3\times 3} & -\frac{1}{2} S(\omega^b) & 0_{3\times 1} \\ 0_{1\times 3} & 0_{1\times 3} & 0 \end{bmatrix} \tilde{p} + \tilde{\mathcal{P}} \dot{\tilde{p}}^n \end{aligned} \tag{7.71}$$

since $2\dot{G} G^{\mathrm{T}} = -S(\omega^b)$, $\dot{R} = R S(\omega^b)$ and $R^{\mathrm{T}} = R^{-1}$.

Inserting (7.53) into (7.71) gives

$$\begin{aligned}\dot{\tilde{p}} &= \begin{bmatrix} -S(\omega^b) & 0_{3\times3} & 0_{3\times1} \\ 0_{3\times3} & -\frac{1}{2}S(\omega^b) & 0_{3\times1} \\ 0_{1\times3} & 0_{1\times3} & 0 \end{bmatrix} p + \tilde{\mathcal{P}}\left(\frac{\partial \tilde{T}^*}{\partial \tilde{q}} - \frac{\partial \tilde{U}}{\partial \tilde{q}} - 2\lambda \begin{bmatrix} 0_{3\times1} \\ \eta \\ 0 \end{bmatrix} + \tilde{\tau}^n(t)\right) \\ &= \begin{bmatrix} -S(\omega^b) & 0_{3\times3} & 0_{3\times1} \\ 0_{3\times3} & -\frac{1}{2}S(\omega^b) & 0_{3\times1} \\ 0_{1\times3} & 0_{1\times3} & 0 \end{bmatrix} \tilde{p} \\ &\quad + \tilde{\mathcal{P}}\frac{\partial \tilde{T}^*}{\partial \tilde{q}} - \tilde{\mathcal{P}}\frac{\partial \tilde{U}}{\partial \tilde{q}} - 2\lambda\tilde{\mathcal{P}} \begin{bmatrix} 0_{3\times1} \\ \eta \\ 0 \end{bmatrix} + \tilde{\mathcal{P}}\tilde{\tau}^n(t).\end{aligned} \tag{7.72}$$

We se that

$$\tilde{\mathcal{P}} \begin{bmatrix} 0_{3\times1} \\ \eta \\ 0 \end{bmatrix} = \begin{bmatrix} 0_{3\times1} \\ \frac{1}{2}G\eta \\ 0 \end{bmatrix} = 0 \tag{7.73}$$

$$\tilde{\mathcal{P}}\tilde{\tau}^n(t) = \begin{bmatrix} R^{\mathrm{T}}\tau_f^n(t) \\ GG^{\mathrm{T}}\tau_t^b(t) \\ \tau_t(t) \end{bmatrix} = \begin{bmatrix} \tau_f^b(t) \\ \tau_t^b(t) \\ \tau_t(t) \end{bmatrix} \triangleq \tilde{\tau}(t) \tag{7.74}$$

$$\tilde{\mathcal{P}}\frac{\partial \tilde{U}}{\partial \tilde{q}} = \begin{bmatrix} R^{\mathrm{T}}\frac{\partial \tilde{U}}{\partial x^n} \\ \frac{1}{2}G\frac{\partial \tilde{U}}{\partial \eta} \\ \frac{\partial \tilde{U}}{\partial q_t} \end{bmatrix} = \begin{bmatrix} 0_{3\times1} \\ \frac{1}{2}G\frac{\partial \tilde{U}}{\partial \eta} \\ \frac{\partial \tilde{U}}{\partial q_t} \end{bmatrix} \tag{7.75}$$

$$\begin{aligned}\tilde{\mathcal{P}}\frac{\partial \tilde{T}^*}{\partial \tilde{q}} &= \begin{bmatrix} 0_{3\times7} \\ \frac{1}{2}G\begin{bmatrix} \frac{\partial R^{\mathrm{T}}}{\partial \eta}(\dot{x}^n \otimes I_3) & -2\dot{G}^{\mathrm{T}} & 0_{4\times1} \end{bmatrix} \\ \frac{1}{2}\tilde{q}^{\mathrm{T}}\tilde{P}^{\mathrm{T}}\frac{\partial M_t}{\partial q_t}M_t^{-1} \end{bmatrix} M_t\tilde{P}\dot{\tilde{q}} \\ &= \begin{bmatrix} 0_{3\times7} \\ \begin{bmatrix} \frac{1}{2}G\frac{\partial R^{\mathrm{T}}}{\partial \eta}(\dot{x}^n \otimes I_3) & -G\dot{G}^{\mathrm{T}} & 0_{4\times1} \end{bmatrix} \\ \frac{1}{2}\tilde{p}^{\mathrm{T}}M_t^{-1}\frac{\partial M_t}{\partial q_t}M_t^{-1} \end{bmatrix} \tilde{p}.\end{aligned} \tag{7.76}$$

From Chapter 4 we have that $G\frac{\partial R^{\mathrm{T}}}{\partial \eta}(\dot{x}^n \otimes I_3) = -2S(v^b)$ and from Chapter 3 that $2G\dot{G}^{\mathrm{T}} = S(\omega^b)$. From (7.64) we have

$$G\frac{\partial \tilde{U}}{\partial \eta} = -gG\frac{\partial e_z^{\mathrm{T}}R}{\partial \eta}\left[mr_g^b + \rho_t\int_{-\varsigma_s(q_t)}^{\varsigma_p(q_t)} r_t^b(\sigma)A(\sigma)\,\mathrm{d}\sigma\right]. \tag{7.77}$$

From (3.20) and (5.10) we get

$$G\frac{\partial e_z^{\mathrm{T}}R}{\partial \eta} = 2\begin{bmatrix} -\eta_{i,1} & \eta_r & \eta_{i,3} & -\eta_{i,2} \\ -\eta_{i,2} & -\eta_{i,3} & \eta_r & \eta_{i,1} \\ -\eta_{i,3} & \eta_{i,2} & -\eta_{i,1} & \eta_r \end{bmatrix} \begin{bmatrix} -\eta_{i,2} & \eta_{i,1} & 0 \\ \eta_{i,3} & \eta_r & -2\eta_{i,1} \\ -\eta_r & \eta_{i,3} & -2\eta_{i,2} \\ \eta_{i,1} & \eta_{i,2} & 0 \end{bmatrix}$$

$$
\begin{aligned}
&= 2\begin{bmatrix} 0 & 1-2\eta_{i,1}^2-2\eta_{i,2}^2 & -2\eta_r\eta_{i,1}-2\eta_{i,2}\eta_{i,3} \\ -1+2\eta_{i,1}^2+2\eta_{i,2}^2 & 0 & -2\eta_r\eta_{i,2}+2\eta_{i,1}\eta_{i,3} \\ 2\eta_r\eta_{i,1}+2\eta_{i,2}\eta_{i,3} & 2\eta_r\eta_{i,2}-2\eta_{1,2}\eta_{i,3} & 0 \end{bmatrix} \\
&= -2S(R^{\mathrm{T}}e_z) \qquad (7.78)
\end{aligned}
$$

where we have used that $\eta^{\mathrm{T}}\eta = 1$.

Inserting the above into (7.72), we get

$$
\begin{aligned}
\dot{\tilde{p}} &= -\begin{bmatrix} \begin{bmatrix} S(\omega^b) & 0_{3\times3} & 0_{3\times1} \\ S(v^b) & S(\omega^b) & 0_{3\times1} \end{bmatrix} \\ \frac{1}{2}\tilde{p}^{\mathrm{T}}M_t^{-1}\frac{\partial M_t}{\partial q_t}M_t^{-1} \end{bmatrix}\tilde{p} \\
&\quad -\begin{bmatrix} 0_{3\times1} \\ gS(R^{\mathrm{T}}e_z)\left[mr_g^b + \rho_t\int_{-\varsigma_s(q_t)}^{\varsigma_p(q_t)} r_t^b(\sigma)A(\sigma)\,\mathrm{d}\sigma\right] \\ g\rho_t A_0 e_z^{\mathrm{T}}R\left(r_t^b(\varsigma_p) - r_t^b(-\varsigma_s)\right) \end{bmatrix} + \tilde{\tau}(t) \\
&= \tilde{\tau}(t) - \begin{bmatrix} \begin{bmatrix} \mathcal{S}(\nu) & 0_{6\times1} \end{bmatrix} \\ -\frac{1}{2}\tilde{p}^{\mathrm{T}}M_t^{-1}\frac{\partial M_t}{\partial q_t}M_t^{-1} \end{bmatrix}\tilde{p} - \tilde{k}(\tilde{q}) \qquad (7.79)
\end{aligned}
$$

where

$$
\begin{aligned}
\mathcal{S}(\nu) &= \begin{bmatrix} S(\omega^b) & 0_{3\times3} \\ S(v^b) & S(\omega^b) \end{bmatrix} \\
k_t(\tilde{q}) &\triangleq g\begin{bmatrix} 0_{3\times1} \\ S(R^{\mathrm{T}}e_z)\left[mr_g^b + \rho_t\int_{-\varsigma_s(q_t)}^{\varsigma_p(q_t)} r_t^b(\sigma)A(\sigma)\,\mathrm{d}\sigma\right] \\ \rho_t A_0 e_z^{\mathrm{T}}R\left(r_t^b(\varsigma_p) - r_t^b(-\varsigma_s)\right) \end{bmatrix} = \tilde{\mathcal{P}}\frac{\partial\tilde{U}}{\partial q} \qquad (7.80)
\end{aligned}
$$

Similar to in Chapter 4, we define

$$
\tilde{p}_l \triangleq \begin{bmatrix} I_3 & 0_{3\times3} & 0_{3\times1} \end{bmatrix}\tilde{p} \in \mathbb{R}^3 \qquad (7.81)
$$

$$
\tilde{p}_r \triangleq \begin{bmatrix} 0_{3\times3} & I_3 & 0_{3\times1} \end{bmatrix}\tilde{p} \in \mathbb{R}^3 \qquad (7.82)
$$

$$
\tilde{p}_t \triangleq \begin{bmatrix} 0_{1\times3} & 0_{1\times3} & 1 \end{bmatrix}\tilde{p} \in \mathbb{R} \qquad (7.83)
$$

This allows us to rewrite the product $\begin{bmatrix} \mathcal{S}(\nu) & 0_{6\times1} \end{bmatrix}\tilde{p}$ in a more useful form:

$$
\begin{aligned}
\begin{bmatrix} \mathcal{S}(\nu) & 0_{6\times1} \end{bmatrix}\tilde{p} &= \begin{bmatrix} \begin{bmatrix} S(\omega^b) & 0_{3\times3} \\ S(v^b) & S(\omega^b) \end{bmatrix}\begin{bmatrix} \tilde{p}_l \\ \tilde{p}_r \end{bmatrix} \\ 0 \end{bmatrix} \\
&= \begin{bmatrix} -\begin{bmatrix} 0_{3\times3} & S(\tilde{p}_l) \\ S(\tilde{p}_l) & S(\tilde{p}_r) \end{bmatrix}\begin{bmatrix} v^b \\ \omega^b \end{bmatrix} \\ 0 \end{bmatrix} \\
&= \begin{bmatrix} C_s(\tilde{p}) & 0_{6\times1} \end{bmatrix}\tilde{\nu} = \begin{bmatrix} C_s(\tilde{p}) & 0_{6\times1} \end{bmatrix}M_t^{-1}\tilde{p} \qquad (7.84)
\end{aligned}
$$

where

$$
C_s(\tilde{p}) \triangleq -\begin{bmatrix} 0_{3\times3} & S(\tilde{p}_l) \\ S(\tilde{p}_l) & S(\tilde{p}_r) \end{bmatrix} = -C_s^{\mathrm{T}}(\tilde{p}). \qquad (7.85)
$$

Similarly, the product $\tilde{p}^{\mathrm{T}} M_t^{-1} \frac{\partial M_t}{\partial q_t} M_t^{-1} \tilde{p}$ can be rewritten in a more useful form:

$$\begin{aligned}
\begin{bmatrix} 0_{3\times 1} \\ 0_{3\times 1} \\ \frac{1}{2}\tilde{p}^{\mathrm{T}} M_t^{-1} \frac{\partial M_t}{\partial q_t} M_t^{-1} \tilde{p} \end{bmatrix} &= \dot{q}_t \begin{bmatrix} 0_{3\times 3} & -\frac{\partial M_\nu}{\partial q_t} & 0_{3\times 1} \\ 0_{3\times 3} & \frac{1}{2}\frac{\partial M_\omega}{\partial q_t} & 0_{3\times 1} \\ \frac{\partial m_{v,\dot{q}_t}^{\mathrm{T}}}{\partial q_t} & \frac{\partial m_{\omega,\dot{q}_t}^{\mathrm{T}}}{\partial q_t} & \frac{1}{2}\frac{\partial \bar{m}_t}{\partial q_t} \end{bmatrix} \tilde{\nu} \\
&\quad + \begin{bmatrix} 0_{3\times 3} & 0_{3\times 3} & \frac{\partial M_\nu}{\partial q_t}\omega^b \\ 0_{3\times 3} & 0_{3\times 3} & -\frac{1}{2}\frac{\partial M_\omega}{\partial q_t}\omega^b \\ \omega^{b\mathrm{T}} \frac{\partial M_\nu}{\partial q_t} & \frac{1}{2}\omega^{b\mathrm{T}} \frac{\partial M_\omega^{\mathrm{T}}}{\partial q_t} & 0 \end{bmatrix} \tilde{\nu} \\
&= \dot{q}_t \begin{bmatrix} 0_{3\times 3} & -\frac{\partial M_\nu}{\partial q_t} & 0_{3\times 1} \\ 0_{3\times 3} & \frac{1}{2}\frac{\partial M_\omega}{\partial q_t} & 0_{3\times 1} \\ \frac{\partial m_{v,\dot{q}_t}^{\mathrm{T}}}{\partial q_t} & \frac{\partial m_{\omega,\dot{q}_t}^{\mathrm{T}}}{\partial q_t} & \frac{1}{2}\frac{\partial \bar{m}_t}{\partial q_t} \end{bmatrix} M_t^{-1} \tilde{p} \\
&\quad + \begin{bmatrix} 0_{3\times 3} & 0_{3\times 3} & \frac{\partial M_\nu}{\partial q_t}\omega^b \\ 0_{3\times 3} & 0_{3\times 3} & -\frac{1}{2}\frac{\partial M_\omega}{\partial q_t}\omega^b \\ \omega^{b\mathrm{T}} \frac{\partial M_\nu}{\partial q_t} & \frac{1}{2}\omega^{b\mathrm{T}} \frac{\partial M_\omega^{\mathrm{T}}}{\partial q_t} & 0 \end{bmatrix} M_t^{-1} \tilde{p}.
\end{aligned} \tag{7.86}$$

We can rewrite the kinematics as

$$\dot{\tilde{q}} = \tilde{\mathcal{W}} \tilde{p}^n = \tilde{\mathcal{P}}^{\mathrm{T}} M_t^{-1} \tilde{\mathcal{P}} \tilde{P}^{\mathrm{T}} \tilde{p} = \tilde{\mathcal{P}}^{\mathrm{T}} M_t^{-1} \tilde{p} \tag{7.87}$$

since $\tilde{\mathcal{P}} \tilde{P}^{\mathrm{T}} = I_7$. Note that $M_t^{-1} \tilde{p} = \tilde{\nu}$, that is, the vector of generalized velocities in the body frame.

Noting that $\dot{q}_t = [0_{1\times 6}, 1] M_t^{-1} \tilde{p}$ and $\omega^b = [0_{3\times 3}, I_3, 0_{3\times 1}]\, M_t^{-1} \tilde{p}$, we define

$$\begin{aligned}
C_t(\tilde{q}, \tilde{p}) &\triangleq \begin{bmatrix} & C_s & & -\frac{\partial M_\nu}{\partial q_t}\omega^b \\ & & & \frac{1}{2}\frac{\partial M_\omega}{\partial q_t}\omega^b \\ -\ \omega^{b\mathrm{T}} \frac{\partial M_\nu}{\partial q_t} & & -\frac{1}{2}\omega^{b\mathrm{T}} \frac{\partial M_\omega^{\mathrm{T}}}{\partial q_t} & 0 \end{bmatrix} \\
&\quad - \dot{q}_t \begin{bmatrix} 0_{3\times 3} & -\frac{\partial M_\nu}{\partial q_t} & 0_{3\times 1} \\ 0_{3\times 3} & \frac{1}{2}\frac{\partial M_\omega}{\partial q_t} & 0_{3\times 1} \\ \frac{\partial m_{v,\dot{q}_t}^{\mathrm{T}}}{\partial q_t} & \frac{\partial m_{\omega,\dot{q}_t}^{\mathrm{T}}}{\partial q_t} & \frac{1}{2}\frac{\partial \bar{m}_t}{\partial q_t} \end{bmatrix} \\
&= C_w - \dot{q}_t C_m
\end{aligned} \tag{7.88}$$

were the function arguments have been omitted and

$$C_w \triangleq \begin{bmatrix} & C_s & & -\frac{\partial M_\nu}{\partial q_t}\omega^b \\ & & & \frac{1}{2}\frac{\partial M_\omega}{\partial q_t}\omega^b \\ -\ \omega^{b\mathrm{T}} \frac{\partial M_\nu^{\mathrm{T}}}{\partial q_t} & & -\frac{1}{2}\omega^{b\mathrm{T}} \frac{\partial M_\omega^{\mathrm{T}}}{\partial q_t} & 0 \end{bmatrix} = -C_w^{\mathrm{T}} \tag{7.89}$$

$$C_m \triangleq \begin{bmatrix} 0_{3\times 3} & -\frac{\partial M_\nu}{\partial q_t} & 0_{3\times 1} \\ 0_{3\times 3} & \frac{1}{2}\frac{\partial M_\omega}{\partial q_t} & 0_{3\times 1} \\ \frac{\partial m_{v,\dot{q}_t}^{\mathrm{T}}}{\partial q_t} & \frac{\partial m_{\omega,\dot{q}_t}^{\mathrm{T}}}{\partial q_t} & \frac{1}{2}\frac{\partial \bar{m}_t}{\partial q_t} \end{bmatrix} \tag{7.90}$$

We can then write the dynamics as

$$\dot{\tilde{q}} = \tilde{\mathcal{P}}^{\mathrm{T}}(\tilde{q}) M_t^{-1}(\tilde{q}) \tilde{p} \tag{7.91}$$

$$\dot{\tilde{p}} = \tilde{\tau}(t) - C_t(\tilde{q}, \tilde{p}) M_t^{-1}(\tilde{q}) \tilde{p} - k_t(\tilde{q}). \tag{7.92}$$

7.5 External forces

There are other, external, forces acting on the ship–tank system that were not included in the above analysis (other than through the virtual work principle). There are potential and viscous damping effects on the ship [24], damping effects on the tank fluid [26, 37, 44, 49, 50, 57, 58, 61, 62, 79], buoyancy on the ship [24], environmental forces [24], control forces and some gravity-induced forces. Hydrostatic buoyancy is actual a potential force, but buoyancy is rendered very complex in the presence of waves and was not included in the previous sections.

We write the external forces as

$$\tilde{\tau} = \tilde{\tau}_g + \begin{bmatrix} \tau_p \\ 0 \end{bmatrix} + \tilde{\tau}_d + \tilde{\tau}_c + \tilde{\tau}_e \tag{7.93}$$

where $\tilde{\tau}_g$ are gravity-induced forces not already included, τ_p are the pressure-induced forces calculated in Chapter 5, $\tilde{\tau}_d$ are damping forces, $\tilde{\tau}_c$ are control forces and $\tilde{\tau}_e$ are unmodeled forces. Most of the forces were computed in Chapter 5.

By the same argument as in Chapter 5, not all gravity-related terms were included in the analysis in this chapter. Specifically, the linear force was not included. By the same analysis as in Chapter 5,

$$\tilde{\tau}_g = - \begin{bmatrix} g(m + m_t) R^{\mathrm{T}} e_z \\ 0_{3\times 1} \\ 0 \end{bmatrix}. \tag{7.94}$$

The total mass of the ship–tank system $m + m_t$ is used, as both contribute to the weight of the ship–tank system.

The pressure forces act only on the ship (as the tank fluid is not in contact with the ocean). From Chapter 5, we get

$$\tau_p = -M_A \dot{\nu} + D_p \nu + C_A(\nu)\nu + k_p(q, t). \tag{7.95}$$

The damping term $D_p \nu$ only contains some generalized damping forces. There are also other dissipative effects, such as vortex shedding and viscous damping [20]. In addition, there is also the damping in the tank.

It is possible that the tank damping gives rise to a generalized force on the ship. When the fluid is moving in the tank, it is damped by (among other things) contact with the tank wall. By Newton's Third Law, this should give rise to an equal and opposite force on the tank (and thus, the ship). This effect is investigated in Chapter 9, but it is there found to be negligible and therefore not included in this chapter.

We therefore write the extra generalized damping force $\tilde{\tau}_d$ as

$$\tilde{\tau}_d = - \begin{bmatrix} D_v(\nu)\nu \\ d_t(\dot{q}_t)\dot{q}_t \end{bmatrix}. \tag{7.96}$$

We gather all damping terms in the matrix $\tilde{D}$ and let $\Omega \equiv \bar{\Omega}$ where $\bar{\Omega}$ is a constant, so that

$$\begin{bmatrix} D_p\nu + D_v(\nu)\nu \\ d_t(\dot{q}_t)\dot{q}_t \end{bmatrix} = \tilde{D}(\tilde{\nu})\tilde{\nu} \tag{7.97}$$

with

$$\tilde{D}(\tilde{\nu}) \triangleq \begin{bmatrix} D_p + D_v(\nu) & 0_{3\times 1} \\ 0_{1\times 3} & d_t(\dot{q}_t) \end{bmatrix}. \tag{7.98}$$

The control forces can be split into two: The forces acting directly on the ship, and the forces acting on the tank fluid. We let u be the control input to the ship, and u_t be the control input to the tank itself. Both of these can be multi-dimensional.

A surface ship will typically be directly actuated in surge, yaw and possibly sway, while not in the other degrees of freedom [24]. Typical actuators would be rudders and fixed or turnable propellers [75].

The tank can be actuated in several different ways. Placing pumps to pump the fluid around is a possibility. Sealing the two reservoirs and pumping in or releasing high-pressure air is another option. Valves could be used in the tank to control the cross-sectional area, but these would not be able to force the fluid to flow against the pull of gravity.

If the pump is located at $\sigma = 0$, and generates a pressure difference $u_t = \Delta P$ (starboard side pressure minus port side pressure), it will give a force of $\tau_{c,t}$ on the tank fluid given by

$$\tau_{c,t} = \frac{\Delta P}{A(0)} \tag{7.99}$$

positive to port.

If instead one uses air pumps giving the pressure p_s above the starboard reservoir and p_p over the port reservoir, then the force on the tank fluid will be

$$\tau_{c,t} = \frac{p_s}{A(\varsigma_s(q_t))} - \frac{p_p}{A(\varsigma_p(q_t))} \approx \frac{p_s - p_p}{A(\varsigma_0)} \tag{7.100}$$

positive to port. We can take $u_t = p_s - p_p$ or $u_t = [p_s, p_p]^{\mathrm{T}}$.

Combining all control forces into one vector $\tilde{\tau}_c$, we write

$$\tau_c = \begin{bmatrix} b_x & 0 \\ b_y & 0 \\ b_z & 0 \\ b_\phi & 0 \\ b_\theta & 0 \\ b_\psi & 0 \\ 0 & b_t \end{bmatrix} \begin{bmatrix} u \\ u_t \end{bmatrix} = \tilde{B}\tilde{u} \tag{7.101}$$

with

$$\tilde{B} \triangleq \begin{bmatrix} b_x & 0 \\ b_y & 0 \\ b_z & 0 \\ b_\phi & 0 \\ b_\theta & 0 \\ b_\psi & 0 \\ 0 & b_t \end{bmatrix}, \quad \tilde{u} \triangleq [u^{\mathrm{T}}, u_t^{\mathrm{T}}]^{\mathrm{T}}.$$

7.6 Total dynamical equations for the ship–tank–ocean system

We define the added mass in $\mathbb{R}^{7\times 7}$, $\tilde{M}_A$ as

$$\tilde{M}_A \triangleq \begin{bmatrix} M_A & 0_{3\times 1} \\ 0_{1\times 3} & 0 \end{bmatrix},$$

the added mass-induced Coriolis/centripetal matrix in $\mathbb{R}^{7\times 7}$, $\tilde{C}_A$ as

$$\tilde{C}_A(\tilde{\nu}) \triangleq \begin{bmatrix} C_A(\nu) & 0_{3\times 1} \\ 0_{1\times 3} & 0 \end{bmatrix} = -\tilde{C}_A^{\mathrm{T}}(\tilde{\nu}),$$

the total inertia matrix $\tilde{M}$ as

$$\tilde{M}(q_t) \triangleq M_t(q_t) + \tilde{M}_A \tag{7.102}$$

and the total generalized restoring force $\tilde{k}$ as

$$\begin{aligned} \tilde{k}(\tilde{q}, t) &\triangleq k_t(q) - \tilde{\tau}_g(\tilde{q}) + \begin{bmatrix} k_p(q,t) \\ 0 \end{bmatrix} \\ &= \begin{bmatrix} k_p(q,t) + k_g(\tilde{q}) \\ \rho_t A_0 e_z^{\mathrm{T}} R(\eta) \left[r_t^b(\varsigma_p(q_t)) - r_t^b(-\varsigma_s(q_t)) \right] \end{bmatrix}. \end{aligned} \tag{7.103}$$

with

$$k_g(\tilde{q}) \triangleq g \begin{bmatrix} (m + m_t) R^{\mathrm{T}}(\eta) e_z \\ S(R^{\mathrm{T}}(\eta) e_z) \left[m r_g^b + \rho_t \int_{-\varsigma_s(q_t)}^{\varsigma_p(q_t)} r_t^b(\sigma) A(\sigma) \, \mathrm{d}\sigma \right] \end{bmatrix} \in \mathbb{R}^6. \tag{7.104}$$

We can then write the total dynamics as

$$\dot{\tilde{q}} = \mathcal{P}^{\mathrm{T}} M^{-1} \tilde{p} \tag{7.105}$$

$$\dot{\tilde{p}} = \tilde{\tau}_e(t) + \tilde{B}\tilde{u} - \tilde{M}_A \dot{\tilde{\nu}} - \left[C_t(q_t, \tilde{p}) + \tilde{D}(\tilde{\nu}) + \tilde{C}_A(\tilde{\nu}) \right] M^{-1} \tilde{p} - \tilde{k}(\tilde{q}, t). \tag{7.106}$$

The presence of the added mass term (which gives a generalized force proportional to acceleration) makes it cumbersome to use generalized momentum as a state variable.

We find

$$\begin{aligned}\dot{\tilde{p}} &= M_t\dot{\tilde{\nu}} + \dot{M}_t\tilde{\nu} = M_t\dot{\tilde{\nu}} + \dot{q}_t\frac{\partial M_t}{\partial q_t}\tilde{\nu}\\ &= \tilde{\tau}_e(t) + \tilde{B}\tilde{u} - \tilde{M}_A\dot{\tilde{\nu}} - \left[C_t(q_t,\tilde{p}) + \tilde{D}(\tilde{\nu}) + \tilde{C}_A(\tilde{\nu})\right]M^{-1}\tilde{p} - \tilde{k}(\tilde{q},t)\\ &= \tilde{\tau}_e(t) + \tilde{B}\tilde{u} - \tilde{M}_A\dot{\tilde{\nu}} - \left[C_t(q_t,M_t\tilde{\nu}) + \tilde{D}(\tilde{\nu}) + \tilde{C}_A(\tilde{\nu})\right]\tilde{\nu} - \tilde{k}(\tilde{q},t).\end{aligned}$$

We rearrange the terms in the above equality and get

$$\tilde{M}(q_t)\dot{\tilde{\nu}} = \tilde{\tau}_e(t) + \tilde{B}\tilde{u} - \left[\tilde{C}(q_t,\tilde{\nu}) + \tilde{D}(\tilde{\nu})\right]\tilde{\nu} - \tilde{k}(\tilde{q},t) \tag{7.107}$$

where

$$\tilde{C}(q_t,\tilde{\nu}) \triangleq \dot{q}_t\frac{\partial M_t}{\partial q_t} + C_t(q_t,M_t\tilde{\nu}) + \tilde{C}_A(\tilde{\nu})$$

is the Coriolis/centripetal matrix.

Dropping function arguments for brevity, we can rewrite $\tilde{C}(q_t,\tilde{\nu})$ as

$$\begin{aligned}\tilde{C} &= \begin{bmatrix} C_s + C_A & -\frac{\partial M_\nu}{\partial q_t}\omega^b \\ -\ \omega^{b\mathrm{T}}\frac{\partial M_\nu}{\partial q_t} & \frac{1}{2}\frac{\partial M_\omega}{\partial q_t}\omega^b \\ & -\frac{1}{2}\omega^{b\mathrm{T}}\frac{\partial M_\omega^{\mathrm{T}}}{\partial q_t} \quad 0 \end{bmatrix}\\ &\quad - \dot{q}_t\begin{bmatrix} 0_{3\times3} & -\frac{\partial M_\nu}{\partial q_t} & 0_{3\times1} \\ 0_{3\times3} & \frac{1}{2}\frac{\partial M_\omega}{\partial q_t} & 0_{3\times1} \\ \frac{\partial m_{v,\dot{q}_t}^{\mathrm{T}}}{\partial q_t} & \frac{\partial m_{\omega,\dot{q}_t}^{\mathrm{T}}}{\partial q_t} & \frac{1}{2}\frac{\partial \bar{m}_t}{\partial q_t} \end{bmatrix} + \dot{q}_t\begin{bmatrix} 0_{3\times3} & -\frac{\partial M_\nu}{\partial q_t} & \frac{\partial m_{v,\dot{q}_t}}{\partial q_t} \\ \frac{\partial M_\nu}{\partial q_t} & \frac{\partial M_\omega}{\partial q_t} & \frac{\partial m_{\omega,\dot{q}_t}}{\partial q_t} \\ \frac{\partial m_{v,\dot{q}_t}^{\mathrm{T}}}{\partial q_t} & \frac{\partial m_{\omega,\dot{q}_t}^{\mathrm{T}}}{\partial q_t} & \frac{\partial \bar{m}_t}{\partial q_t} \end{bmatrix}\\ &= \begin{bmatrix} C_s + C_A & -\frac{\partial M_\nu}{\partial q_t}\omega^b \\ -\ \omega^{b\mathrm{T}}\frac{\partial M_\nu}{\partial q_t} & \frac{1}{2}\frac{\partial M_\omega}{\partial q_t}\omega^b \\ & -\frac{1}{2}\omega^{b\mathrm{T}}\frac{\partial M_\omega^{\mathrm{T}}}{\partial q_t} \quad 0 \end{bmatrix}\\ &\quad + \dot{q}_t\begin{bmatrix} 0_{3\times3} & 0_{3\times3} & \frac{\partial m_{v,\dot{q}_t}}{\partial q_t} \\ \frac{\partial M_\nu}{\partial q_t} & \frac{1}{2}\frac{\partial M_\omega}{\partial q_t} & \frac{\partial m_{\omega,\dot{q}_t}}{\partial q_t} \\ 0_{1\times3} & 0_{1\times3} & \frac{1}{2}\frac{\partial \bar{m}_t}{\partial q_t} \end{bmatrix}\\ &= \tilde{C}_w + \dot{q}_t C_m^{\mathrm{T}}\end{aligned} \tag{7.108}$$

with

$$\tilde{C}_w \triangleq \begin{bmatrix} C_s + C_A & -\frac{\partial M_\nu}{\partial q_t}\omega^b \\ -\ \omega^{b\mathrm{T}}\frac{\partial M_\nu}{\partial q_t} & \frac{1}{2}\frac{\partial M_\omega}{\partial q_t}\omega^b \\ & -\frac{1}{2}\omega^{b\mathrm{T}}\frac{\partial M_\omega^{\mathrm{T}}}{\partial q_t} \quad 0 \end{bmatrix} = -\tilde{C}_w^{\mathrm{T}}$$

$$C_m^{\mathrm{T}} = \begin{bmatrix} 0_{3\times3} & 0_{3\times3} & \frac{\partial m_{v,\dot{q}_t}}{\partial q_t} \\ \frac{\partial M_\nu}{\partial q_t} & \frac{1}{2}\frac{\partial M_\omega}{\partial q_t} & \frac{\partial m_{\omega,\dot{q}_t}}{\partial q_t} \\ 0_{1\times3} & 0_{1\times3} & \frac{1}{2}\frac{\partial \bar{m}_t}{\partial q_t} \end{bmatrix}$$

matching (7.90).

We note that $\tilde{M}$ and $\tilde{C}$ satisfy the following property:

Property 7.11. The matrix

$$\dot{\tilde{M}} - 2\tilde{C} \tag{7.109}$$

is skew-symmetric, that is

$$\dot{\tilde{M}} - 2\tilde{C} = -\left(\dot{\tilde{M}} - 2\tilde{C}\right)^{\mathrm{T}} \Leftrightarrow w^{\mathrm{T}}\left(\dot{\tilde{M}} - 2\tilde{C}\right) w = 0 \; \forall \; w \in \mathbb{R}^7. \tag{7.110}$$

Proof. We already know that $\tilde{C}_w$ is skew-symmetric, so the statement (7.110) is equivalent to the statement

$$\dot{\tilde{M}} - 2\dot{q}_t C_m^{\mathrm{T}} = -\left(\dot{\tilde{M}} - 2\dot{q}_t C_m^{\mathrm{T}}\right)^{\mathrm{T}}.$$

Since $\tilde{M}$ is only a function of q_t, we have

$$\begin{aligned}
\dot{\tilde{M}} - 2\dot{q}_t C_m^{\mathrm{T}} &= \dot{q}_t \frac{\partial \tilde{M}}{\partial q_t} - 2\dot{q}_t C_m^{\mathrm{T}} = \dot{q}_t \left(\frac{\partial M_t}{\partial q_t} - 2C_m^{\mathrm{T}} \right) \\
&= \dot{q}_t \begin{bmatrix} 0_{3\times 3} & -\frac{\partial M_\nu}{\partial q_t} & \frac{\partial m_{v,\dot{q}_t}}{\partial q_t} \\ \frac{\partial M_\nu}{\partial q_t} & \frac{\partial M_\omega}{\partial q_t} & \frac{\partial m_{\omega,\dot{q}_t}}{\partial q_t} \\ \frac{\partial m_{v,\dot{q}_t}^{\mathrm{T}}}{\partial q_t} & \frac{\partial m_{\omega,\dot{q}_t}^{\mathrm{T}}}{\partial q_t} & \frac{\partial \bar{m}_t}{\partial q_t} \end{bmatrix} - \dot{q}_t \begin{bmatrix} 0_{3\times 3} & 0_{3\times 3} & 2\frac{\partial m_{v,\dot{q}_t}}{\partial q_t} \\ 2\frac{\partial M_\nu}{\partial q_t} & \frac{\partial M_\omega}{\partial q_t} & 2\frac{\partial m_{\omega,\dot{q}_t}}{\partial q_t} \\ 0_{1\times 3} & 0_{1\times 3} & \frac{\partial \bar{m}_t}{\partial q_t} \end{bmatrix} \\
&= \dot{q}_t \begin{bmatrix} 0_{3\times 3} & -\frac{\partial M_\nu}{\partial q_t} & -\frac{\partial m_{v,\dot{q}_t}}{\partial q_t} \\ -\frac{\partial M_\nu}{\partial q_t} & 0_{3\times 3} & -\frac{\partial m_{\omega,\dot{q}_t}}{\partial q_t} \\ \frac{\partial m_{v,\dot{q}_t}^{\mathrm{T}}}{\partial q_t} & \frac{\partial m_{\omega,\dot{q}_t}^{\mathrm{T}}}{\partial q_t} & 0 \end{bmatrix} = -\left(\dot{\tilde{M}} - 2\dot{q}_t C_m^{\mathrm{T}}\right)^{\mathrm{T}}
\end{aligned}$$

since $M_\nu = -M_\nu^{\mathrm{T}}$ implies $\partial M_\nu / \partial q_t = -\partial M_\nu^{\mathrm{T}} / \partial q_t$. Proof of the equivalency of the two statements in (7.110) can be found in Kreyszig [53]. □

We can then write the dynamics for the full 7-DOF ship–tank–ocean system:

Model VII (7-DOF u-tank model)**.** The dynamics of the full 7-DOF u-tank model with a generic u-tank can be written as

$$\dot{\tilde{q}} = \tilde{\mathcal{P}}^{\mathrm{T}}(\eta)\tilde{\nu} \tag{7.111}$$

$$\tilde{M}(q_t)\dot{\tilde{\nu}} = \tilde{\tau}_e(t) + \tilde{B}\tilde{u} - \tilde{C}(q_t, \tilde{\nu})\tilde{\nu} - \tilde{D}(\tilde{\nu})\tilde{\nu} - \tilde{k}(\tilde{q}, t) \tag{7.112}$$

where $\tilde{\mathcal{P}}$ is defined in (7.13), $\tilde{M}$ in (7.102), $\tilde{B}$ in (7.101), $\tilde{C}$ in (7.108), $\tilde{D}$ in (7.98), $\tilde{k}$ in (7.103) and $\tilde{\tau}_e$ is the unmodeled disturbances.

Chapter 8

Rectangular-prism u-tanks and comparison to an existing model

Most existing models of u-tanks are for u-tanks that consist of three rectangular prisms; one for each reservoir and one for the duct (see Figure 8.1) [44, 50, 57, 58, 62, 79], so it makes sense to represent the generic-tank model of Chapter 7 for this special case.

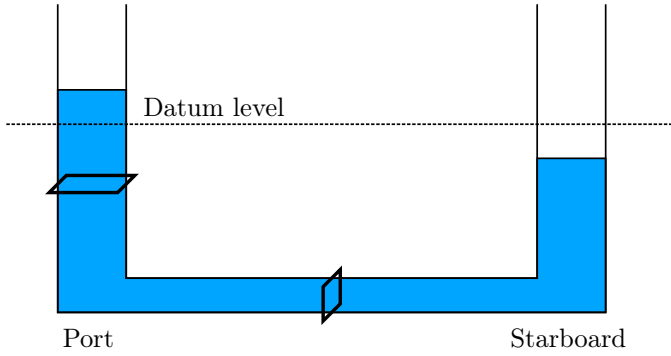

Figure 8.1: A rectangular-prism u-tank.

The results in this chapter are based on the results of Chapter 7 and Holden et al. [44].

8.1 Equations of motion for a rectangular-prism u-tank

A rectangular-prim u-tank does not fit into the framework developed in Chapter 7; the tank centerline function is not a C^1 function (the derivative doesn't exist at the reservoir–duct intersection since these are hard corners). The rectangular-prism u-tank can, however, be approximated to arbitrary precision by functions that are

C^1. We can use functions y_t^b, z_t^b and A given by

$$y_t^b(\sigma) = \begin{cases} \frac{w}{2} & \forall \quad \sigma \in (-\infty, -w/2 - \epsilon] \\ -a_0 - a_1\sigma - a_2\sigma^2 & \forall \quad \sigma \in [-w/2 - \epsilon, -w/2 + \epsilon] \\ -\sigma & \forall \quad \sigma \in [-w/2 + \epsilon, w/2 - \epsilon] \\ a_0 - a_1\sigma + a_2\sigma^2 & \forall \quad \sigma \in [w/2 - \epsilon, w/2 + \epsilon] \\ -\frac{w}{2} & \forall \quad \sigma \in [w/2 + \epsilon, \infty) \end{cases} \tag{8.1}$$

$$z_t^b(\sigma) = \begin{cases} r_d + \frac{w}{2} + \sigma & \forall \quad \sigma \in (-\infty, -w/2 - \epsilon] \\ -b_0 - b_1\sigma - b_2\sigma^2 & \forall \quad \sigma \in [-w/2 - \epsilon, -w/2 + \epsilon] \\ r_d & \forall \quad \sigma \in [-w/2 + \epsilon, w/2 - \epsilon] \\ -b_0 + b_1\sigma - b_2\sigma^2 & \forall \quad \sigma \in [w/2 - \epsilon, w/2 + \epsilon] \\ r_d + \frac{w}{2} - \sigma & \forall \quad \sigma \in [w/2 + \epsilon, \infty) \end{cases} \tag{8.2}$$

$$A(\sigma) = \begin{cases} A_r & \forall \quad \sigma \in (-\infty, -w/2 + \epsilon] \\ c_0 + c_1\sigma & \forall \quad \sigma \in [-w/2 - \epsilon, -w/2 + \epsilon] \\ A_d & \forall \quad \sigma \in [-w/2 + \epsilon, w/2 - \epsilon] \\ c_0 - c_1\sigma & \forall \quad \sigma \in [w/2 - \epsilon, w/2 + \epsilon] \\ A_r & \forall \quad \sigma \in [w/2 + \epsilon, \infty) \end{cases} \tag{8.3}$$

with $\epsilon \ll w/2$ and

$$\begin{aligned} a_0 &= \frac{\left(\epsilon - \frac{w}{2}\right)^2}{4\epsilon} \\ a_1 &= \frac{w + 2\epsilon}{4\epsilon} \\ a_2 = b_2 &= \frac{1}{4\epsilon} \\ b_0 &= \frac{\left(\epsilon - \frac{w}{2}\right)^2}{4\epsilon} - r_d \\ b_1 &= \frac{w - 2\epsilon}{4\epsilon} \\ c_0 &= \frac{2(A_d + A_r)\epsilon + w(A_d - A_r)}{4\epsilon} \\ c_1 &= \frac{A_d - A_r}{2\epsilon}. \end{aligned}$$

Since the tank has rectangular cross-section, we define

$$A_r \triangleq w_r l_r \tag{8.4}$$

$$A_d \triangleq h_d l_d. \tag{8.5}$$

Furthermore,

$$\varsigma_0 = h_t + \frac{w}{2}. \tag{8.6}$$

The value of A_0 is arbitrary. We choose

$$A_0 = A_r. \tag{8.7}$$

Note that this choice of a_i, b_i, c_i ensures that $y_t^b, z_t^b \in C^1$ and that $A \in C^0$. A tank described by these functions has a centerline function describing half a rounded rectangle. Letting $\epsilon \to 0$ gives a rectangular-prism u-tank. The parameters in (8.1)–(8.5) have the interpretation indicated in Figure 8.2.

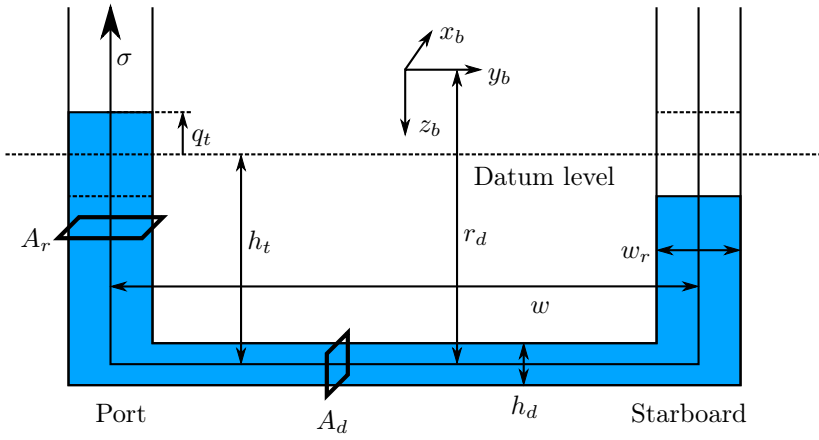

Figure 8.2: Measurements of the u-tank (8.1)–(8.5) with $\epsilon = 0$.

We could compute the integrals in the system equations before letting $\epsilon \to 0$, but it gives the same result as setting $\epsilon = 0$ first and then computing the integrals. The only caveat is that with $\epsilon = 0$, the model becomes invalid if the duct is not always full of fluid.

The functions for the u-tank is sufficiently simple such that it is possible to explicitly solve (7.2):

$$q_t = \frac{1}{A_0} \int_{\varsigma_0}^{\varsigma_p} A(\sigma) \, \mathrm{d}\sigma = \varsigma_p - h_t - \frac{w}{2} \tag{8.8}$$

$$q_t = \frac{-1}{A_0} \int_{-\varsigma_s}^{-\varsigma_0} A(\sigma) \, \mathrm{d}\sigma = h_t + \frac{w}{2} - \varsigma_s \tag{8.9}$$

from which we get the relationships

$$q_t = \varsigma_p - \varsigma_0 = \varsigma_0 - \varsigma_s \tag{8.10}$$

$$\varsigma_p + \varsigma_s \equiv 2h_t + w. \tag{8.11}$$

The integrals of M_t, C_t and k_t can also be solved explicitly. Recalling from (7.28) that

$$\tilde{M}(q_t) \triangleq \begin{bmatrix} (m_t + m) I_3 & -M_\nu(q_t) - mS(r_g^b) & m_{v,\dot{q}_t}(q_t) \\ M_\nu(q_t) + mS(r_g^b) & M_\omega(q_t) + J & m_{\omega,\dot{q}_t}(q_t) \\ m_{v,\dot{q}_t}^{\mathrm{T}}(q_t) & m_{\omega,\dot{q}_t}^{\mathrm{T}}(q_t) & \bar{m}_t(q_t) \end{bmatrix},$$

and dropping function arguments for brevity, we get

$$\begin{aligned} m_t &= \rho_t \int_{-\varsigma_0}^{\varsigma_0} A(\sigma)\,\mathrm{d}\sigma \\ &= \rho_t \int_{-h_t-w/2}^{-w/2} w_r l_r\,\mathrm{d}\sigma + \rho_t \int_{-w/2}^{w/2} h_d l_d\,\mathrm{d}\sigma + \rho_t \int_{w/2}^{h_t+w/2} w_r l_r\,\mathrm{d}\sigma \\ &= \left(2h_t w_r l_r + w h_d l_d\right)\rho_t \end{aligned} \tag{8.12}$$

as the mass of the tank fluid,

$$\begin{aligned} M_\nu &= \rho_t \int_{-\varsigma_s}^{\varsigma_p} A(\sigma) S(r_t^b(\sigma))\,\mathrm{d}\sigma = \rho_t \int_{-\varsigma_s}^{-w/2} w_r l_r S\left(\begin{bmatrix} x_t^b \\ w/2 \\ r_d + w/2 + \sigma \end{bmatrix}\right)\,\mathrm{d}\sigma \\ &\quad + \rho_t \int_{-w/2}^{w/2} h_d l_d S\left(\begin{bmatrix} x_t^b \\ -\sigma \\ r_d \end{bmatrix}\right)\,\mathrm{d}\sigma + \rho_t \int_{w/2}^{\varsigma_p} w_r l_r S\left(\begin{bmatrix} x_t^b \\ -w/2 \\ r_d + w/2 - \sigma \end{bmatrix}\right)\,\mathrm{d}\sigma \\ &= \rho_t S\left(\begin{bmatrix} x_t^b\left(2h_t w_r l_r + w h_d l_d\right) \\ -w w_r l_r q_t \\ 2x_r l_r r_d h_t + h_d l_d r_d w - w_r l_r h_t^2 - w_r l_r q_t^2 \end{bmatrix}\right) \end{aligned} \tag{8.13}$$

as the cross-coupling between angular and translational accelerations,

$$\begin{aligned} M_\omega &= -\rho_t \int_{-\varsigma_s}^{\varsigma_p} A(\sigma) S^2(r_t^b(\sigma))\,\mathrm{d}\sigma \\ &= -\rho_t \int_{-\varsigma_s}^{-w/2} w_r l_r S^2\left(\begin{bmatrix} x_t^b \\ w/2 \\ r_d + w/2 + \sigma \end{bmatrix}\right)\,\mathrm{d}\sigma \\ &\quad - \rho_t \int_{-w/2}^{w/2} h_d l_d S^2\left(\begin{bmatrix} x_t^b \\ -\sigma \\ r_d \end{bmatrix}\right)\,\mathrm{d}\sigma \\ &\quad - \rho_t \int_{w/2}^{\varsigma_p} w_r l_r S^2\left(\begin{bmatrix} x_t^b \\ -w/2 \\ r_d + w/2 - \sigma \end{bmatrix}\right)\,\mathrm{d}\sigma \\ &= \begin{bmatrix} M_{\omega,11} & M_{\omega,12} & M_{\omega,13} \\ M_{\omega,12} & M_{\omega,22} & M_{\omega,23} \\ M_{\omega,13} & M_{\omega,23} & M_{\omega,33} \end{bmatrix} \end{aligned} \tag{8.14}$$

$$\begin{aligned} M_{\omega,11} &= 2\rho_t w_r l_r (h_t - r_d) q_t^2 + \rho_t h_d l_d w \left(r d^2 - \frac{w^2}{12}\right) \\ &\quad + \rho_t \left(2r_d^2 + \frac{w^2}{2} + \frac{2}{3}h_t^2 - 2r_d h_t\right) w_r l_r h_t \\ M_{\omega,12} &= \rho_t w x_t^b w_r l_r q_t \\ M_{\omega,13} &= \rho_t x_t^b w_r l_r q_t^2 - 2\rho_t w_r l_r x_t^b r_d h_t - \rho_t h_d l_d r_d x_t^b w + \rho_t w_r l_r x_t^b h_t^2 \end{aligned}$$

$$
\begin{aligned}
M_{\omega,22} &= 2\rho_t w_r l_r (h_t - r_d) q_t^2 + \rho_t h_d l_d w \left(r_d^2 - (x_t^b)^2\right) \\
&\quad + \rho_t \left(2r_d^2 + 2(x_t^b)^2 + \frac{2}{3}h_t^2 - 2r_d h_t\right) w_r l_r h_t \\
M_{\omega,23} &= -\rho_t w w_r l_r (h_t - r_d) q_t \\
M_{\omega,33} &= \left(2(x_t^b)^2 + \frac{1}{2}w^2\right) \rho_t w_r l_r h_t + \left((x_t^b)^2 + \frac{1}{12}w^2\right) \rho_t h_d l_d w.
\end{aligned}
$$

as the moment of inertia of the tank fluid,

$$
\begin{aligned}
m_{v,\dot{q}_t} &= \rho_t A_0 \int_{-\varsigma_s}^{\varsigma_p} \frac{\mathrm{d}\bar{r}_t^b}{\mathrm{d}\sigma}\,\mathrm{d}\sigma = \rho_t w_r l_r \begin{bmatrix} 0 \\ -\int_{-w/2}^{w/2} \mathrm{d}\sigma \\ \int_{-\varsigma_s}^{-w/2} \mathrm{d}\sigma - \int_{w/2}^{\varsigma_p} \mathrm{d}\sigma \end{bmatrix} \\
&= -\rho_t w_r l_r \begin{bmatrix} 0 \\ w \\ 2q_t \end{bmatrix} \qquad (8.15) \\
m_{\omega,\dot{q}_t} &= \rho_t A_0 \int_{-\varsigma_s}^{\varsigma_p} S(r_t^b(q_t)) \frac{\mathrm{d}\bar{r}_t^b}{\mathrm{d}\sigma}(\sigma)\,\mathrm{d}\sigma \\
&= \rho_t w_r l_r \int_{-\varsigma_s}^{-w/2} S\left(\begin{bmatrix} x_t^b \\ w/2 \\ r_d + w/2 + \sigma \end{bmatrix}\right) \begin{bmatrix} 0 \\ 0 \\ 1 \end{bmatrix} \mathrm{d}\sigma \\
&\quad - \rho_t w_r l_r \int_{-w/2}^{w/2} S\left(\begin{bmatrix} x_t^b \\ -\sigma \\ r_d \end{bmatrix}\right) \begin{bmatrix} 0 \\ 1 \\ 0 \end{bmatrix} \mathrm{d}\sigma \\
&\quad - \rho_t h w_r l_r \int_{w/2}^{\varsigma_p} S\left(\begin{bmatrix} x_t^b \\ -w/2 \\ r_d + w/2 - \sigma \end{bmatrix}\right) \begin{bmatrix} 0 \\ 0 \\ 1 \end{bmatrix} \mathrm{d}\sigma \\
&= \rho_t w_r l_r \begin{bmatrix} (h_t + r_d) w \\ 2x_t^b q_t \\ -w x_t^b \end{bmatrix} \qquad (8.16)
\end{aligned}
$$

as the cross-couplings between the accelerations of the tank fluid and the rigid-body generalized velocities and

$$
\begin{aligned}
\bar{m}_t &= \rho_t A_0^2 \int_{-\varsigma_s}^{\varsigma_p} \frac{1}{A(\sigma)}\,\mathrm{d}\sigma \\
&= \rho_t \int_{-\varsigma_s}^{-w/2} w_r l_r\,\mathrm{d}\sigma + \rho_t \int_{-w/2}^{w/2} \frac{w_r^2 l_r^2}{h_d l_d}\,\mathrm{d}\sigma + \rho_t \int_{w/2}^{\varsigma_p} w_r l_r\,\mathrm{d}\sigma \\
&= \rho_t \left(2h_t w_r l_r + \frac{w_r^2 l_r^2 w}{h_d l_d}\right) \qquad (8.17)
\end{aligned}
$$

as the inertial mass of the tank fluid.

From (7.108), $\tilde{C}$ can be written as

$$\tilde{C} = \begin{bmatrix} C_s + C_A & -\frac{\partial M_\nu}{\partial q_t}\omega^b \\ -\omega^{b\mathrm{T}}\frac{\partial M_\nu}{\partial q_t} \quad -\frac{1}{2}\omega^{b\mathrm{T}}\frac{\partial M_\omega}{\partial q_t}^{\mathrm{T}} & \frac{1}{2}\frac{\partial M_\omega}{\partial q_t}\omega^b \\ & 0 \end{bmatrix} + \dot{q}_t \begin{bmatrix} 0_{3\times3} & 0_{3\times3} & \frac{\partial m_{v,\dot{q}_t}}{\partial q_t} \\ \frac{\partial M_\nu}{\partial q_t} & \frac{1}{2}\frac{\partial M_\omega}{\partial q_t} & \frac{\partial m_{\omega,\dot{q}_t}}{\partial q_t} \\ 0_{1\times3} & 0_{1\times3} & \frac{1}{2}\frac{\partial \bar{m}_t}{\partial q_t} \end{bmatrix}.$$

Using (8.12)–(8.17), we get

$$\frac{\partial M_\nu}{\partial q_t} = \rho_t S\left(\begin{bmatrix} 0 \\ -wh_d l_d \\ -2w_r l_r q_t \end{bmatrix}\right)$$

$$\frac{\partial M_\omega}{\partial q_t} = \rho_t \begin{bmatrix} 4w_r l_r (h_t - r_d)q_t & wx_t^b h_d l_d & 2x_t^b w_r l_r q_t \\ wx_t^b h_d l_d & 4w_r l_r (h_t - r_d)q_t & -wh_d l_d (h_t - r_d) \\ 2x_t^b w_r l_r q_t & -wh_d l_d (h_t - r_d) & 0 \end{bmatrix}$$

$$\frac{\partial m_{v,\dot{q}_t}}{\partial q_t} = -\rho_t h_d l_d \begin{bmatrix} 0 \\ 0 \\ 2\frac{h_d l_d}{w_r l_r} \end{bmatrix}$$

$$\frac{\partial m_{\omega,\dot{q}_t}}{\partial q_t} = \rho_t h_d l_d \begin{bmatrix} 0 \\ \frac{2x_t^b h_d l_d}{w_r l_r} \\ 0 \end{bmatrix}$$

$$\frac{\partial \bar{m}_t}{\partial q_t} = 0.$$

From (7.80) we have

$$k_t(q) = g\rho_t \begin{bmatrix} 0_3 \\ S(R^{\mathrm{T}} e_z) \int_{-\varsigma_s(q_t)}^{\varsigma_p(q_t)} r_t^b(\sigma) A(\sigma)\, \mathrm{d}\sigma \\ -A_0 e_z^{\mathrm{T}} R \left(r_t^b(\varsigma_p) - r_t^b(-\varsigma_s)\right) \end{bmatrix}.$$

We get

$$\begin{aligned} \int_{-\varsigma_s}^{\varsigma_p} r_t^b(\sigma) A(\sigma)\, \mathrm{d}\sigma = &\int_{-\varsigma_s}^{-w/2} w_r l_r \begin{bmatrix} x_t^b \\ w/2 \\ r_d + w/2 + \sigma \end{bmatrix} \mathrm{d}\sigma \\ &+ \int_{-w/2}^{w/2} h_d l_d \begin{bmatrix} x_t^b \\ -\sigma \\ r_d \end{bmatrix} \mathrm{d}\sigma \\ &+ \int_{w/2}^{\varsigma_p} w_r l_r \begin{bmatrix} x_t^b \\ -w/2 \\ r_d + w/2 - \sigma \end{bmatrix} \mathrm{d}\sigma \end{aligned}$$

$$= \begin{bmatrix} 2w_r l_r x_t^b h_t + h_d l_d w x_t^b \\ -w w_r l_r q_t \\ -w_r l_r q_t^2 + 2w_r l_r r_d h_t - w_r l_r h_t^2 + h_d l_d r_d w \end{bmatrix} \tag{8.18}$$

and

$$\begin{aligned} r_t^b(\varsigma_p) - r_t^b(-\varsigma_s) &= \begin{bmatrix} x_t^b \\ -w/2 \\ r_d + w/2 - \varsigma_p \end{bmatrix} - \begin{bmatrix} x_t^b \\ w/2 \\ r_d + w/2 - \varsigma_s \end{bmatrix} \\ &= \begin{bmatrix} 0 \\ -w \\ -2q_t \end{bmatrix}. \end{aligned} \tag{8.19}$$

8.2 Comparison to the model of Lloyd [57, 58]

Like most other u-tank models [21, 62, 79], the model of Lloyd [57, 58] has four degrees of freedom; namely sway, roll, yaw and a tank state. The model of Lloyd [57, 58] is also linear, and only valid for a rectangular-prism tank.

To reduce the order of the model to include only these four degrees of freedom, we need to rewrite the kinematics. We recall from Chapter 3 that the rigid-body kinematics can be written as

$$\begin{aligned} \dot{x}^n &= R(\Theta) v^b \\ \dot{\eta} &= \frac{1}{2} G_\Theta(\Theta) \omega^b \end{aligned}$$

where $\Theta = [\phi, \theta, \psi]^{\mathrm{T}}$ is a vector of Euler angles.

To get a four-degree-of-freedom model, we set all the other degrees of freedom to zero, i.e.,

$$x = z = \theta = v_1^b = v_3^b = \omega_2^b = 0 \tag{8.20}$$

and rewrite (7.111) and (7.112). We define

$$q_{r_4} \triangleq [y, \phi, \psi, q_t]^{\mathrm{T}} \tag{8.21}$$

$$\nu_{r_4} \triangleq [v_2^b, \omega_1^b, \omega_3^b, \dot{q}_t]^{\mathrm{T}} \tag{8.22}$$

and find that

$$\dot{q}_{r_4} = \begin{bmatrix} \cos(\phi)\cos(\psi) & 0 & 0 & 0 \\ 0 & 1 & 0 & 0 \\ 0 & 0 & \cos(\phi) & 0 \\ 0 & 0 & 0 & 1 \end{bmatrix} \nu_{r_4} \approx \nu_{r_4}$$

for small angles ϕ, ψ.

We define

$$M_{r_4} \triangleq \begin{bmatrix} m_{22} & m_{24} & m_{26} & m_{2t} \\ m_{24} & m_{44} & m_{46} & m_{4t} \\ m_{26} & m_{46} & m_{66} & m_{6t} \\ m_{2t} & m_{4t} & m_{6t} & \bar{m}_t \end{bmatrix} + \begin{bmatrix} m_{A,22} & m_{A,24} & m_{A,26} & 0 \\ m_{A,42} & m_{A,44} & m_{A,46} & 0 \\ m_{A,62} & m_{A,64} & m_{A,66} & 0 \\ 0 & 0 & 0 & 0 \end{bmatrix} \tag{8.23}$$

$$m_{22} = m + m_t = m + \rho_t \left(2h_t w_r l_r + w h_d l_d\right)$$

$$m_{24} = \rho_t \int_{-\varsigma_s}^{\varsigma_p} A z_t^b \, \mathrm{d}\sigma - m z_g = -\rho_t \left(2x_r l_r r_d h_t + h_d l_d r_d w - w_r l_r h_t^2\right) - m z_g$$

$$m_{26} = -\rho_t \int_{-\varsigma_s}^{\varsigma_p} A z_t^b \, \mathrm{d}\sigma + m x_g = \rho_t x_t^b \left(2h_t w_r l_r + w h_d l_d\right) + m x_g$$

$$m_{2t} = \rho_t A_0 \int_{-\varsigma_s}^{\varsigma_p} \frac{\mathrm{d}\bar{y}_t^b}{\mathrm{d}\sigma} \, \mathrm{d}\sigma = -\rho_t w_r l_r w$$

$$\begin{aligned} m_{44} &= J_{11} + \rho_t \int_{-\varsigma_s}^{\varsigma_p} A((y_t^b)^2 + (z_t^b)^2) \, \mathrm{d}\sigma \\ &= J_{11} + \rho_t h_d l_d w \left(r d^2 - \frac{w^2}{12}\right) + \rho_t \left(2r_d^2 + \frac{w^2}{2} + \frac{2}{3}h_t^2 - 2r_d h_t\right) w_r l_r h_t \end{aligned}$$

$$\begin{aligned} m_{46} &= J_{13} - \rho_t \int_{-\varsigma_s}^{\varsigma_p} A x_t^b z_t^b \, \mathrm{d}\sigma \\ &= J_{13} - 2\rho_t w_r l_r x_t^b r_d h_t - \rho_t h_d l_d r_d x_t^b w + \rho_t w_r l_r x_t^b h_t^2 \end{aligned}$$

$$m_{4t} = \rho_t A_0 \int_{-\varsigma_s}^{\varsigma_p} \left(y_t^b \frac{\mathrm{d}\bar{z}_t^b}{\mathrm{d}\sigma} - \frac{\mathrm{d}\bar{y}_t^b}{\mathrm{d}\sigma} z_t^b\right) \mathrm{d}\sigma = \rho_t w_r l_r w (h_t + r_d)$$

$$\begin{aligned} m_{66} &= J_{33} + \rho_t \int_{-\varsigma_s}^{\varsigma_p} A \left[(x_t^b)^2 + (y_t^b)^2\right] \, \mathrm{d}\sigma \\ &= J_{33} + \left(2(x_t^b)^2 + \frac{1}{2}w^2\right) \rho_t w_r l_r h_t + \left((x_t^b)^2 + \frac{1}{12}w^2\right) \rho_t h_d l_d w \end{aligned}$$

$$m_{6t} = \rho_t A_0 \int_{-\varsigma_s}^{\varsigma_p} \left(x_t^b \frac{\mathrm{d}\bar{y}_t^b}{\mathrm{d}\sigma} - \frac{\mathrm{d}\bar{x}_t^b}{\mathrm{d}\sigma} y_t^b\right) \mathrm{d}\sigma = \rho_t w_r l_r w x_t^b$$

$$\bar{m}_t = \rho_t \int_{-\varsigma_s}^{\varsigma_p} \frac{A_0^2}{A} \, \mathrm{d}\sigma = \rho_t \left(2h_t w_r l_r + \frac{w_r^2 l_r^2 w}{h_d l_d}\right).$$

as the inertia,

$$B_{r_4} = \begin{bmatrix} b_y & 0 \\ b_\phi & 0 \\ b_\psi & 0 \\ 0 & b_t \end{bmatrix} \tag{8.24}$$

defines the directly controlled states,

$$D_{r_4} = \begin{bmatrix} d_{22} & d_{24} & d_{26} & 0 \\ d_{42} & d_{44} & d_{46} & 0 \\ d_{62} & d_{64} & d_{66} & 0 \\ 0 & 0 & 0 & d_{tt} \end{bmatrix} \tag{8.25}$$

where d_{ij} is the i,jth element of $D(0)$ of Model III is the linear damping matrix and

$$\tau_{e,r_4}(t) = \begin{bmatrix} 0 & 1 & 0 & 0 & 0 & 0 & 0 \\ 0 & 0 & 0 & 1 & 0 & 0 & 0 \\ 0 & 0 & 0 & 0 & 0 & 1 & 0 \\ 0 & 0 & 0 & 0 & 0 & 0 & 1 \end{bmatrix} \tilde{\tau}(t) \tag{8.26}$$

are the unmodeled forces.

The restoring fore matrix K_{r_4} can be found from the reduced-order spring term k_{r_4} (the nonlinear restoring force for the four-degree-of-freedom model). If $k_{p,i}$ is the ith element of k_p of Model III, then k_{r_4} is given by

$$k_{r_4} = \begin{bmatrix} k_{p,2} \\ \Big(k_{p,4} + gmz_g \sin(\phi) + g\rho_t w w_r l_r q_t \cos(\phi) \\ \quad + g\rho_t \left[w_r l_r (2r_d h_t - h_t^2 - q_t^2) + h_d l_d r_d w\right] \sin(\phi)\Big) \\ k_{p,6} - g\left[x_t^b m_t + m x_g\right] \sin(\phi) \\ g\rho_t w_r l_r w \sin(\phi) + 2g\rho_t w_r l_r q_t \cos(\phi) \end{bmatrix},$$

so that

$$K_{r_4} = \left.\frac{\partial k_{r_4}}{\partial q_{r_4}}\right|_{\tilde{q}=0} \tag{8.27}$$

$$= \begin{bmatrix} k_{p,22} & k_{p,24} & k_{p,26} & 0 \\ k_{p,42} & \big(k_{p,44} + gmz_g \\ \quad + g\rho_t \left[w_r l_r h_t (2r_d - h_t) + h_d l_d r_d w\right]\big) & k_{p,46} & g\rho_t w_r l_r w \\ k_{p,62} & k_{p,64} - g\left[x_t^b m_t + m x_g\right] & k_{p,66} & 0 \\ 0 & g\rho_t w_r l_r w & 0 & 2g\rho_t w_r l_r \end{bmatrix}$$

where

$$k_{p,ij} = \left.\frac{\partial k_{p,i}}{\partial q_j}\right|_{\tilde{q}=0}$$

with q_j is the jth element of q are the partial derivatives of the pressure-induced restoring forces. These parameters may be time-varying.

From Fossen [24] we have that $k_{p,22} = k_{p,66} = 0$. If they are non-zero, it implies that uncontrolled ship will automatically keep its course and has a "preferred" position in the plane. This is clearly not true.

Model VIII (Linearized 4-DOF rectangular-prism u-tank model)**.**

$$M_{r_4}\ddot{q}_{r_4} + D_{r_4}\dot{q}_{r_4} + K_{r_4}(t)q_{r_4} = B_{r_4}\tilde{u} + \tau_{e,r_4}(t) \tag{8.28}$$

where M_{r_4} is defined in (8.23), D_{r_4} in (8.25), K_{r_4} in (8.27), B_{r_4} in (8.24) and τ_{e,r_4} in (8.26).

The model found in Lloyd [57, 58] is a linear, four-degree-of-freedom model, consisting of sway, roll, yaw and a tank state. The model is derived based on Newtonian mechanics. The model assumes a rectangular u-tank as in (8.1)–(8.3) with $\epsilon = 0$ and $l_r = l_d$.

We rewrite the model of Lloyd [57, 58] so that it has the same states as the model presented here.[1]

Model IX (The model of Lloyd [57, 58])**.**

$$M_L \ddot{q}_{r_4} + D_4 \dot{q}_{r_4} + K_L q_{r_4} = B_4 u + \tau_{e,4}(t) \tag{8.29}$$

where q_{r_4}, D_4, B_4 and $\tau_{e,4}$ are as in Model VIII, and

$$M_L = \begin{bmatrix} m + m_{A,22} & m_{A,24} & m_{A,26} & m_{2t} \\ m_{A,42} & J_{1,1} + m_{A,44} & m_{A,46} & m_{4t} \\ m_{A,62} & m_{A,64} & J_{3,3} + m_{A,66} & m_{6t} \\ m_{2t} & m_{4t} & m_{6t} & \bar{m}_t \end{bmatrix}$$

$$K_L = \begin{bmatrix} 0 & 0 & k_{p,26} & 0 \\ 0 & k_{p,44} + gmz_g & k_{p,46} & g\rho_t l_r w_r w \\ 0 & 0 & k_{p,66} & 0 \\ 0 & g\rho_t l_r w_r w & 0 & 2g\rho_t l_r w_r \end{bmatrix}$$

where matrix parameters are the same as in Model VIII.

This model is largely identical to the linear 4-DOF u-tank Model VIII. The main difference is in the mass matrix. In the model of Lloyd [57, 58], the only effect on the inertia matrix of the ship–tank system is adding the coupling terms (m_{2t}, m_{4t} and m_{6t}) and $\bar{m}_t$. In the calculations shown in this chapter and Chapter 7, the mass of the tank fluid will also change the other elements of the inertia matrix. Loading the tank with water will increase the ship's mass, and also changes its distribution. This changes the total mass of the ship, the center of gravity and the moment of inertia. This is not included in the model of Lloyd [57, 58]. However, the mass of the tank fluid is likely to be quite low compared to the mass of the ship (1–5 % [57, 58]), so this might not greatly affect the behavior of the model. The model of Lloyd [57, 58] also assumes that the body center of origin is the center of gravity, and that $J_{1,3} = 0$.

In addition, there are a few differences in the spring term. However, the only difference related to ship–tank interaction is the lack of the term $gx_t^b m_t$, which as been neglected in the model of Lloyd [57, 58].

[1] Note that in Lloyd [57, 58], the states called are x_2, x_4, x_6 and τ. These equal, respectively, y, ϕ, ψ and q_t/w. Also note that there are several signage errors in Lloyd [57, 58]:

Lloyd [58, Equation (12.53a) p. 265] reads $a_{\tau 2} = -Q_t$, but should read $a_{\tau 2} = Q_t$.

Lloyd [58, Equation (12.53d) p. 265] reads $a_{\tau 6} = -Q_t x_{B_1}$, but should read $a_{\tau 6} = Q_t x_{B_1}$.

Lloyd [58, Equation (12.54b) p. 266)] reads $a_{42}\ddot{x}_2 + b_{42}\dot{x}_2 + (I_{44} + a_{44})\ddot{x}_4 + b_{44}\dot{x}_4 + c_{44}x_4 + a_{46}\ddot{x}_6 + b_{46}\dot{x}_6 + c_{46}x_6 - [a_{4\tau}\ddot{\tau} + c_{4\tau}\tau] = F_{w40}\sin(\omega_e t + \gamma_4)$, but should read $a_{42}\ddot{x}_2 + b_{42}\dot{x}_2 + (I_{44} + a_{44})\ddot{x}_4 + b_{44}\dot{x}_4 + c_{44}x_4 + a_{46}\ddot{x}_6 + b_{46}\dot{x}_6 + c_{46}x_6 + [a_{4\tau}\ddot{\tau} + c_{4\tau}\tau] = F_{w40}\sin(\omega_e t + \gamma_4)$.

These errors are propagated throughout Lloyd [57, 58].

Of course, the main advantage of the 7-DOF u-tank Model VII over the model of Lloyd [57, 58] is that while that model assumes one very specific tank shape, is completely linear and only has four degrees of freedom, the new model can handle generic u-tank shapes, is as non-linear as is required, and has all seven degrees of freedom.

Chapter 9

Experimental verification of the u-tank model

In this chapter, the u-tank model of Chapter 7 is experimentally verified.

The results in this chapter are based on the results of Chapter 7 and Holden et al. [44].

9.1 Laboratory setup

To test the validity of the model of Chapter 7, we conducted 44 experiments at SINTEF Marintek's facilities in Trondheim. Since most u-tank models are of rectangular tanks, we decided to perform experimens on such a tank.

The purpose of the experiments was to verify the model of Chapter 7, and to determine the importance of the model nonlinearities.

9.1.1 The rig

The lab setup consists of a mechanized see-saw, powered by a computer-controlled electrical step motor. A rectangular tank of the type seen in Figure 8.2, described by (8.1)–(8.5) with $\epsilon = 0$, is placed on top of the movable part. The complete rig can be seen in Figure 9.1.

The motion of the see-saw is analogous to the rolling motion of the ship. The rig is also capable of moving sideways, analogous to sway, but this capability was not used in the experiments. The rig, excluding the tank, was borrowed from SINTEF Marintek.

The tank has dimensions

$$\begin{aligned} w_r &= 10 \text{ cm} \\ w &= 70 \text{ cm} \\ l_r &= l_d = 40 \text{ cm} \\ h_d &= 4 \text{ cm} \\ r_d &= 9.8 \text{ cm}. \end{aligned}$$

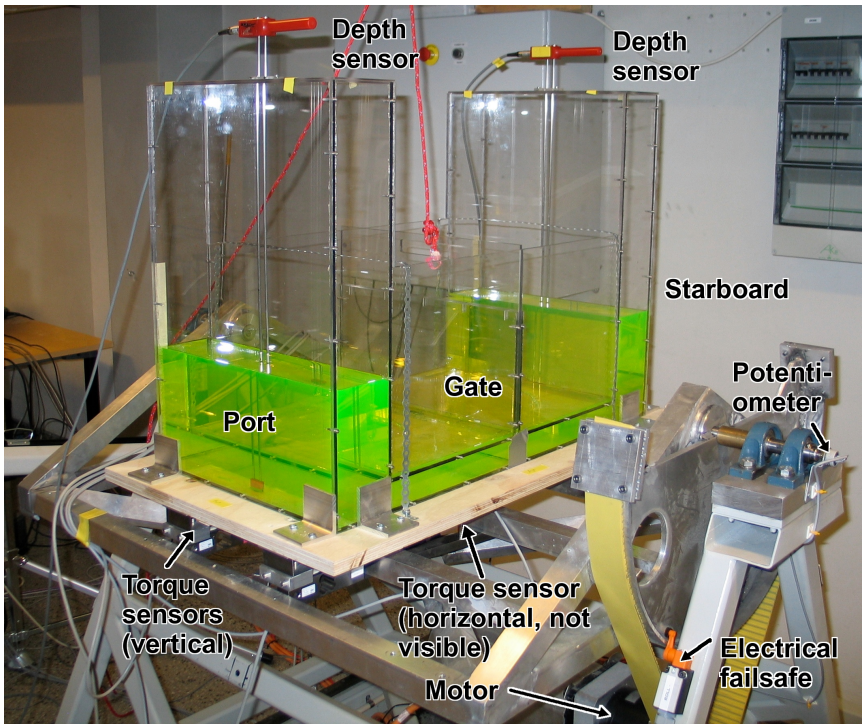

Figure 9.1: The laboratory setup at SINTEF Marintek.

All measurements are internal.

Due to the extremely elongated cross-section of the duct, it was impossible to fit an off-the-shelf valve on the tank. Instead, a gate mechanism was used: In the middle of the duct, an operator can lower or raise a gate to block the fluid or allow it to flow from one reservoir to the other. The gate is bigger than the duct cross section, and the interior of the duct is grooved to allow room for the gate. This design limits leakage. Despite this, the gate is not entirely water-tight. Also, when the gate is open, some fluid will flow up into the gate mechanism itself. These effects are small, and only measurable when the fluid is not in motion.

The tank was filled to a level of $h_t \approx 18$ cm with tap water. A few grams of the coloring agent "fluoresceinum natricum" was added for easier observation of the behavior of the fluid.

The parameters ρ_t and g were assumed to take the values

$$\rho_t = 1\,000 \text{ kg/m}^3$$
$$g = 9.81 \text{ m/s}^2.$$

9.1.2 Input

The rig is capable of running pre-programmed roll patterns, by use of the step motor, limited to a range of $\phi \in [-25, 25]^\circ$. The motor can handle speeds well in

excess of those needed in the experiments, even under full load.

9.1.3 Measurements

A potentiometer hooked up to the rotating axis was used to measure actual roll angle.

Three sets of sensors were used to measure the torque. The sensors all work by measuring the deformation of the beam upon which the tank is resting, which is proportional to the torques involved.

Two of the torque sensors measure the component of the torque normal to the beam upon which the tank is resting. The average of the two measurements is used. The final torque sensor measures the component of the torque parallel to the beam upon which the tank is resting. The total torque is then the sum of these two components, appropriately scaled.

The depth is measured with two separate resistive sensors, one on the port side and one on the starboard side. On each sensor, two straight, rigid, conductive rods are inserted into the fluid, which closes the circuit. The greater the depth of the fluid in the reservoir, the further up the rods the circuit is closed, giving a lower measured resistance. The port sensor measures q_t directly, and the starboard sensor measures $-q_t$. After sign-reversing the starboard measurement, the average of these two measurements is used.

9.1.4 Revised dynamics

The artificial laboratory setup has some key differences with the real-world system described in Chapter 7. The main differences are:

1. Motion is restricted to roll and the tank state.
2. Roll is the input into the system, not a state.
3. There are no pressure-induced forces.
4. There is no damping in roll.
5. The tank is a rectangular-prism tank as in Figure 8.1.

These differences necessitate some changes to the model.

Ignoring, for now, all points except for points 1 and 5, we can define several different models based on Chapter 7, even limited to two degrees of freedom (roll and the tank state).

We define the state $q_{r_2} \triangleq [\phi, q_t]^{\mathrm{T}}$ and define:

Model X (Model $\mathcal{L}$)**.** The model is given by

$$\mathcal{L}: \begin{cases} M_{r_2}(q_t)\ddot{q}_{r_2} + C_{r_2}(q_t, \dot{q}_{r_2})\dot{q}_{r_2} + D_{r_2}(\dot{q}_{r_2})\dot{q}_{r_2} \\ \quad +k_{r_2}(q_{r_2}, t) = \tau_{e,r_2}(t) + B_{r_2}u_t \end{cases} \tag{9.1}$$

with

$$M_{r_2}(q_t) = \begin{bmatrix} J_{11} + m_{A,44} + M_{\omega,11}(q_t) & \rho_t w_r l_r w(h_t + r_d) \\ \rho_t w_r l_r w(h_t + r_d) & \rho_t \left(2h_t w_r l_r + \frac{w_r^2 l_r^2 w}{h_d l_d}\right) \end{bmatrix}$$

$$M_{\omega,11}(q_t) = 2\rho_t w_r l_r (h_t - r_d) q_t^2 + \rho_t h_d l_d w \left(r d^2 - \frac{w^2}{12}\right) + \rho_t \left(2r_d^2 + \frac{w^2}{2} + \frac{2}{3}h_t^2 - 2r_d h_t\right) w_r l_r h_t$$

$$C_{r_2}(q_{r_2}, \dot{q}_{r_2}) = 2\rho_t x_t^b w_r (h_t - r_d) q_t \begin{bmatrix} \dot{q}_t & \dot{\phi} \\ -\dot{\phi} & 0 \end{bmatrix}$$

$$D_{r_2}(\dot{q}_{r_2}) = \begin{bmatrix} d_{44} + d_{44,n}|\dot{\phi}| & 0 \\ 0 & d_{tt} + d_{tt,n}|\dot{q}_t| \end{bmatrix}$$

$$k_{r_2}(q_{r_2}, t) = \begin{bmatrix} \Big(k_{p,4}(\phi, t) + gmz_g \sin(\phi) + g\rho_t w w_r l_r q_t \cos(\phi) \\ \quad + g\rho_t \left[w_r l_r (2r_d h_t - h_t^2 - q_t^2) + h_d l_d r_d w\right] \sin(\phi)\Big) \\ g\rho_t w_r l_r w \sin(\phi) + 2g\rho_t w_r l_r q_t \cos(\phi) \end{bmatrix}$$

$$\tau_{e,r_2}(t) = \begin{bmatrix} 0 & 0 & 0 & 1 & 0 & 0 & 0 \\ 0 & 0 & 0 & 0 & 0 & 0 & 1 \end{bmatrix} \tilde{\tau}(t)$$

$$B_{r_2} = \left[0, b_t^{\mathrm{T}}\right]^{\mathrm{T}}$$

where $k_{p,4}$ is the fourth element of k_p of the 6-DOF Model III with the non-roll, non-tank states set to zero.

Model XI (Linearized model $\mathcal{L}_l$)**.** Linearizing the model $\mathcal{L}$ about $q_{r_2} = 0$ gives the model

$$\mathcal{L}_l : \; M_{r_2}(0)\ddot{q}_{r_2} + D_{r_2}(0)\dot{q}_{r_2} + K_{r_2}(t) q_{r_2} = \tau_{e,r_2}(t) + B_{r_2} u_t \tag{9.2}$$

where

$$K_{r_2}(t) = \begin{bmatrix} k_{p,44}(t) + gmz_g + g\rho_t \left[w_r l_r h_t (2r_d - h_t) + h_d l_d r_d w\right] & g\rho_t w_r l_r w \\ g\rho_t w_r l_r w & 2g\rho_t w_r l_r \end{bmatrix}$$

where $k_{p,44} = \left.\frac{\partial k_{p,4}}{\partial \phi}\right|_{\phi=0}$ and the other matrices are as defined in Model X.

Model XII (Extended model e$\mathcal{L}$)**.** The model takes the form

$$\mathrm{e}\mathcal{L} : \; \begin{cases} M_{r_2}(q_t)\ddot{q}_{r_2} + C_{r_2}(q_t, \dot{q}_{r_2})\dot{q}_{r_2} + \bar{D}_{r_2}(\dot{q}_{r_2})\dot{q}_{r_2} \\ \quad + k_{r_2}(q_{r_2}, t) = \tau_{e,r_2}(t) + B_{r_2} u_t \end{cases} \tag{9.3}$$

where

$$\bar{D}_{r_2}(\dot{q}_{r_2}) = \begin{bmatrix} d_{44} + d_{44,n}|\dot{\phi}| & d_{4t} + d_{4t,n}|\dot{q}_t| \\ 0 & d_{tt} + d_{tt,n}|\dot{q}_t| \end{bmatrix}$$

and the other matrices are as defined in Model X.

Model XIII (Linearized extended model e$\mathcal{L}_l$)**.** Linearizing the extended model e$\mathcal{L}$ about $q_{r_2} = 0$ gives the model

$$\mathrm{e}\mathcal{L}_l: \; M_{r_2}(0)\ddot{q}_{r_2} + \bar{D}_{r_2}(0)\dot{q}_{r_2} + K_{r_2}(t)q_{r_2} = \tau_{e,r_2}(t) + B_{r_2}u_t \tag{9.4}$$

where the system matrices are as defined in Models X–XII.

Apart from the extra tank-induced torque in roll, the extended models are identical to their regular counterparts.

The creation of the two extended models e$\mathcal{L}$ and e$\mathcal{L}_l$ was prompted by Newton's Third Law. As the fluid is moving through the u-tank, a damping force is exerted upon it by contact with the tank walls. By the Third Law, an equal and opposite force is acting on the tank walls and thus the ship itself. This generates a moment in roll. On the other hand, roll experiences damping from the surrounding ocean, not from the tank fluid, so roll gives rise to no similar force on the tank fluid.

The question, of course, is whether or not this extra tank-induced moment in roll is significant.

Roll dynamics

During the experiments, roll is the input, not a state. As such, the actual roll angle ϕ is assumed to perfectly follow the commanded roll angle ϕ_d. The rolling motion is still governed by a differential equation. If we assume the model $\mathcal{L}$ of Model X to be correct, by Euler's second axiom

$$J_{11}\ddot{\phi} = -gmz_g\sin(\phi) + \tau_c + \tau_{\mathcal{L}}(q_{r_2}, \dot{q}_{r_2}, \ddot{q}_{r_2}) \tag{9.5}$$

where τ_c is the control input and

$$\begin{aligned}\tau_{\mathcal{L}}(q_{r_2}, \dot{q}_{r_2}, \ddot{q}_{r_2}) = &-M_{\omega,11}(q_t)\ddot{\phi} - \rho_t w_r l_r w(h_t + r_d)\ddot{q}_t \\ &- g\rho_t\left[w_r l_r(2h_t r_d - h_t^2 - q_t^2) + h_d l_d r_d w\right]\sin(\phi) \\ &- g\rho_t w w_r l_r q_t\cos(\phi) - 4\rho_t x_t^b w_r(h_t - r_d)q_t\dot{\phi}\dot{q}_t.\end{aligned} \tag{9.6}$$

$\tau_{\mathcal{L}}$ is the moment in roll that would be zero if $\rho_t = 0$. In the case where there is no fluid in the tank, $\tau_{\mathcal{L}} \equiv 0$. There is no surrounding water, and thus no pressure-induced forces.

The measured moment $\tau_m = -\tau_c$, giving

$$\tau_m = \tau_{\mathcal{L}}(q_{r_2}, \dot{q}_{r_2}, \ddot{q}_{r_2}) - J_{11}\ddot{\phi} - gmz_g\sin(\phi).$$

As $\phi(t) \equiv \phi_d(t)$ by assumption, the measured moment is then

$$\tau_m = \tau_{\mathcal{L}}([\phi_d, q_t]^{\mathrm{T}}, [\dot{\phi}_d, \dot{q}_t]^{\mathrm{T}}, [\ddot{\phi}_d, \ddot{q}_t]^{\mathrm{T}}) - J_{11}\ddot{\phi}_d - gmz_g\sin(\phi_d). \tag{9.7}$$

With no fluid in the tank, the measured roll moment is $\tau_{m,0} = -J_{11}\ddot{\phi}_d - gmz_g\sin(\phi_d)$.

Taking the difference $\tau_m - \tau_{m,0}$ yields

$$\tau_m - \tau_{m,0} = \tau_{\mathcal{L}}([\phi_d, q_t]^{\mathrm{T}}, [\dot{\phi}_d, \dot{q}_t]^{\mathrm{T}}, [\ddot{\phi}_d, \ddot{q}_t]^{\mathrm{T}}).$$

All experiments are therefore done both with and without fluid in the tank. The difference of the two measurements yields the total tank-induced moment in roll.

Doing similar analysis for the other models, we get

$$\begin{aligned}\tau_{\mathcal{L}} = &-M_{\omega,11}(q_t)\ddot{\phi}_d - \rho_t w_r l_r w(h_t + r_d)\ddot{q}_t \\ &- g\rho_t \left[w_r l_r(2h_t r_d - h_t^2 - q_t^2) + h_d l_d r_d w\right]\sin(\phi_d) \\ &- g\rho_t w w_r l_r q_t \cos(\phi_d) - 4\rho_t x_t^b w_r (h_t - r_d) q_t \dot{\phi}_d \dot{q}_t\end{aligned} \tag{9.8}$$

$$\begin{aligned}\tau_{\mathcal{L}_l} = &-M_{\omega,11}(0)\ddot{\phi}_d - \rho_t w_r l_r w(h_t + r_d)\ddot{q}_t \\ &- g\rho_t \left[w_r l_r h_t(2r_d - h_t) + h_d l_d r_d w\right]\phi_d - g\rho_t w w_r l_r q_t\end{aligned} \tag{9.9}$$

$$\begin{aligned}\tau_{e\mathcal{L}} = &-M_{\omega,11}(q_t)\ddot{\phi}_d - \rho_t w_r l_r w(h_t + r_d)\ddot{q}_t - (d_{4t} + d_{4t,n}|\dot{q}_t|)\,\dot{q}_t \\ &- g\rho_t \left[w_r l_r(2h_t r_d - h_t^2 - q_t^2) + h_d l_d r_d w\right]\sin(\phi_d) \\ &- g\rho_t w w_r l_r q_t \cos(\phi_d) - 4\rho_t x_t^b w_r (h_t - r_d) q_t \dot{\phi}_d \dot{q}_t\end{aligned} \tag{9.10}$$

$$\begin{aligned}\tau_{e\mathcal{L}_l} = &-M_{\omega,11}(0)\ddot{\phi}_d - \rho_t w_r l_r w(h_t + r_d)\ddot{q}_t - d_{4t}\dot{q}_t \\ &- g\rho_t \left[w_r l_r h_t(2r_d - h_t) + h_d l_d r_d w\right]\phi_d - g\rho_t w w_r l_r q_t\end{aligned} \tag{9.11}$$

as the total tank-induced torque in roll for, respectively, the model $\mathcal{L}$, the linearized model $\mathcal{L}_l$, the extended model e$\mathcal{L}$ and the extended linearized model e$\mathcal{L}_l$.

Tank dynamics

The nonlinear dynamics of (9.1) and (9.3) (models $\mathcal{L}$ and e$\mathcal{L}$) simplify down to

$$\begin{aligned}&\bar{m}_t\ddot{q}_t + (d_{tt} + d_{tt,n}|\dot{q}_t|)\,\dot{q}_t + 2g\rho_t w_r l_r q_t \cos(\phi_d) \\ &\quad + g\rho_t w_r l_r w \sin(\phi_d) + \rho_t w_r l_r w(h_t + r_d)\ddot{\phi}_d = 0.\end{aligned} \tag{9.12}$$

This is a second-order non-homogenous ordinary differential equation with ϕ_d as input.

The linear dynamics of (9.2) and (9.4) (models $\mathcal{L}_l$ and e$\mathcal{L}_l$) simplify down to

$$\bar{m}_t\ddot{q}_t + d_{tt}\dot{q}_t + 2g\rho_t w_r l_r q_t + g\rho_t w_r l_r w\phi_d + \rho_t w_r l_r w(h_t + r_d)\ddot{\phi}_d = 0. \tag{9.13}$$

This is a linear, second-order nonhomogenous ordinary differential equation with ϕ_d as input.

9.2 Tank free-decay tests

The purpose of these experiments was to determine the damping parameters in the tank, parameters that cannot be determined theoretically.

9.2.1 Experiment

To determine the damping in the tank, four experiments of two types were performed. They can be classified as follows:

Type A ($\phi_d(t) \equiv 0$, $q_t(0) \neq 0$) With the gate open, the tank was inclined to a non-zero roll angle. When the fluid level had stabilized, the gate was closed, and the tank returned to zero angle. When the fluid surface was calm, the gate was opened and the behavior of the fluid recorded.

Type B ($\phi_d(t) \equiv \phi_d(0) \neq 0$, $q_t(0) \approx 0$) With the gate closed and the tank fluid in the equilibrium position, the tank was inclined to a non-zero roll angle. When the fluid surface was calm, the gate was opened and the behavior of the fluid recorded.

There were two experiments of each type:

A1 $\phi_d(t) \equiv 0$, $q_t(0) = -3.65$ cm, $\dot{q}_t(0) = 0.62$ cm/s.

A2 $\phi_d(t) \equiv 0$, $q_t(0) = 2.95$ cm, $\dot{q}_t(0) = -0.20$ cm/s.

B1 $\phi_d(t) \equiv 6.78°$, $q_t(0) = -0.57$ cm, $\dot{q}_t(0) = -0.29$ cm/s.

B2 $\phi_d(t) \equiv -6.89°$, $q_t(0) = 0.53$ cm, $\dot{q}_t(0) = 0.24$ cm/s.

As the derivatives of the states were not directly measured, the values for $\dot{q}_t(0)$ are estimates calculated by taking the numerical derivative of q_t, which is directly measured, at $t = 0$.

9.2.2 Data processing

The data series gathered from tank free decay tests were processed with the following procedure (each step is performed on the output of the previous step):

1. Zero-phase lowpass-filtering with cut-off frequency of 3.0 Hz.
2. Downsampling from 200 Hz to 50 Hz.
3. Re-calibration.
4. Averaging the two depth measurements to get the final depth measurement.

9.2.3 Results

To determine the unknown parameters, least-squares curve fitting was used to fit the model to the experimental data.

For the nonlinear models $\mathcal{L}$, e$\mathcal{L}$,

$$(d_{tt}, d_{tt,n}, \bar{m}_t) = \arg \min_{d_{tt}, d_{tt,n}, \bar{m}_t} \sum_t \|q_t(t) - \bar{q}_t(t; d_{tt}, d_{tt,}, \bar{m}_t)\|_2^2$$

where $q_t(t)$ is the measured value of q_t and $\bar{q}_t(t; d_{tt}, d_{tt,n}, \bar{m}_t)$ is the simulated value of q_t using the specific parameters and (9.12).

For the linear models,

$$(d_{tt}, \bar{m}_t) = \arg \min_{d_{tt}, \bar{m}_t} \sum_t \|q_t(t) - \bar{q}_t(t; d_{tt}, \bar{m}_t)\|_2^2$$

where $q_t(t)$ is the measured value of q_t and $\bar{q}_t(t; d_{tt}, \bar{m}_t)$ is the simulated value of q_t using the specific parameters and (9.13).

Each of the minimization problems were solved for the four time series, each truncated so that they were of equal length. The simulations were started with the

same initial conditions as the real system, and then simulated without input from the measured data.

The results of the curve fitting can be seen in Tables 9.1 and 9.2. As an example, the results of experiment A1 can be seen in Figure 9.2.

Table 9.1: Tank decay tests, linear models ($\mathcal{L}_l$ and e$\mathcal{L}_l$).

	A1	A2	B1	B2	Avg.	Unit
d_{tt}	18.70	16.51	19.18	19.61	18.50	kg/s
$\bar{m}_t$	79.3	79.5	80.4	80.2	79.9	kg
MSE	1.28	0.98	1.36	1.26	1.22	10^{-2}cm^2

Table 9.2: Tank decay tests, nonlinear models ($\mathcal{L}$ and e$\mathcal{L}$).

	A1	A2	B1	B2	Avg.	Unit
d_{tt}	5.34	5.26	6.83	7.48	6.24	kg/s
$d_{tt,n}$	279.7	293.5	264.3	251.2	272.2	kg/m
$\bar{m}_t$	79.1	79.3	79.5	79.3	79.3	kg
MSE	0.13	0.24	0.52	0.46	0.34	10^{-2}cm^2

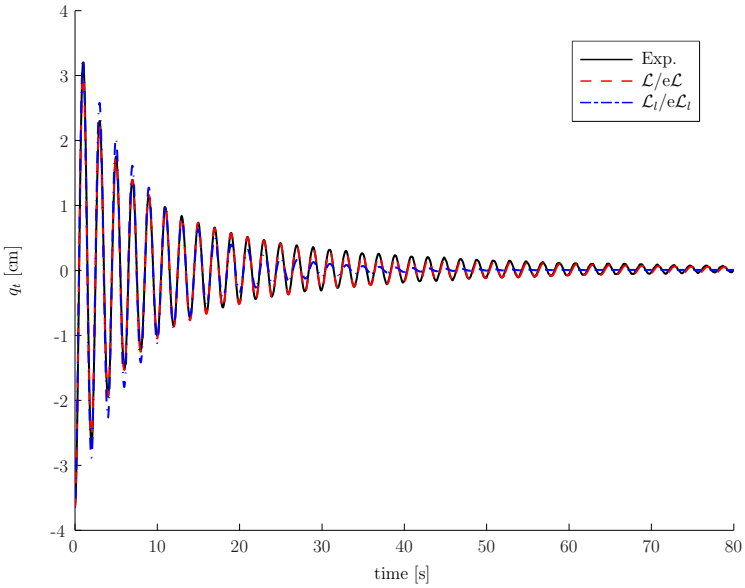

Figure 9.2: Tank decay test experiment A1.

As can be seen from Tables 9.1 and 9.2, the error of the nonlinear models is less than a third (27.9 %) of the error of the linear models. Changing the nonlin-

ear damping function to a higher-order polynomial did not significantly increase accuracy.

For use in the linear models, the average parameters in Table 9.1 will be used, while in the nonlinear models the average parameters in Table 9.2 will be used.

9.2.4 Analysis

The inertial tank fluid mass $\bar{m}_t$, which is distinct from the actual tank fluid mass m_t, can be computed from (8.12). However, for a tank with a non-smooth midline function, the velocity of the tank fluid becomes poorly defined at the points at which the spatial derivative of the midline function doesn't exist. In this case, the intersection between the duct and the reservoirs. One should therefore expect inaccuracies in the model parameters, most notably in the inertial tank fluid mass $\bar{m}_t$, which is based on the kinetic energy of the fluid. This is why the optimization algorithm was free to choose this parameter.

If we look at the theoretical value of $\bar{m}_t$, it should take the value $\bar{m}_t = \rho_t w_r l_r \left[2h_t + (ww_r)/h_d\right]$ (since $l_r = l_d$). For the tank used in the experiments, this gives $\bar{m}_t = 84.4$ kg. The algorithm gives a value of $\bar{m}_t$ of approximately 79.3 kg, a discrepancy of about 6 % from the numbers estimated by the optimization algorithm.

Is this difference significant? Instead of letting the curve fitting algorithm choose $\bar{m}_t$, we could use the theoretical value and just let the algorithm choose the damping parameters. This gives results as in Tables 9.3 and 9.4.

Table 9.3: Tank decay tests, linear models ($\mathcal{L}_l$ and e$\mathcal{L}_l$). Theoretical value of $\bar{m}_t$.

	A1	A2	B1	B2	Avg.	Unit
d_{tt}	30.7	28.3	27.2	28.2	28.6	kg/s
MSE	8.59	6.71	5.97	6.27	6.89	10^{-2}cm^2

Table 9.4: Tank decay tests, nonlinear models ($\mathcal{L}$ and e$\mathcal{L}$). Theoretical value of $\bar{m}_t$.

	A1	A2	B1	B2	Avg.	Unit
d_{tt}	43.3	42.3	38.5	38.9	40.7	kg/s
$d_{tt,n}$	-232	-321	-186	-170	-227	kg/m
MSE	8.34	6.44	6.68	7.00	7.11	10^{-2}cm^2

In the linear case, the mean square error has increased by 560 %, while in the nonlinear case, the mean square error has increased by 2 000 %.

This huge discrepancy is because $\bar{m}_t$ determines the natural frequency of the tank fluid, and even a small discrepancy here causes the simulations to be completely out of sync with the experimental data.

The areas of the tank where the model does not accurately reflect real behavior are the places where the spatial derivative of the tank midline function is discontin-

uous, i.e., the corners of the tank used in the experiments. Keeping the dimensions of the tank constant, the uncertain region increases in size with the ratio of duct height to fluid depth, h_d/h_t. One would expect that the discrepancy between actual values and theoretical values will increase as the ratio h_d/h_t increases. At any values $h_d/h_t \geq 2$, the model loses all validity as the duct will no longer be filled with fluid. (In the experiments, $h_d/h_t \approx 0.22$.)

This suggests that, for maximum accuracy, the value of $\bar{m}_t$ should be computed based on experimental data, rather than computed from theory, especially for high values of h_d/h_t.

9.3 Sinusoidal input tests

To determine the validity of the theoretical models, and determine the value of the parameters d_{4t} and $d_{4t,n}$, a series of experiments with sinusoidal inputs were performed.

9.3.1 Experiment

To get a smoother transient behavior of the system, an increasing sinusoid was used instead of a pure sinusoid. The input took the form

$$\phi_d(t) = \begin{cases} 0 & \forall \quad t \in [0,5] \\ r_u(t;5,5)\mathcal{A}\sin(\varpi(t-5)) & \forall \quad t \in (5,330] \\ r_d(t;5,330)\mathcal{A}\sin(\varpi(t-5)) & \forall \quad t \in (330,380] \\ 0 & \forall \quad t \in (380,\infty) \end{cases} \tag{9.14}$$

with

$$r_u(t;T,\Delta) = \frac{T-(T+t-\Delta)e^{-(t-\Delta)/T}}{T} \tag{9.15}$$

$$r_d(t;T,\Delta) = \frac{(T+t-\Delta)e^{-(t-\Delta)/T}}{T}. \tag{9.16}$$

An example input signal can be seen in Figure 9.3.

All inputs had amplitude $\mathcal{A} = 7°$, while the input frequencies ϖ were (in rad/s, to three decimals precision) $\varpi \in \{0.500, 1.000, 2.199, 2.387, 2.576, 2.764, 2.858, 2.953, 3.047, 3.141, 3.330, 3.518, 3.707, 3.895, 4.500, 5.000\}$.

For each ϖ, experiments were performed twice. Once with the gate open (where the tank fluid is free to move) and once without tank fluid, giving a total of 32 experiments.

9.3.2 Data processing

The data series gathered from experiments with sinusoidal input were processed with the following procedure (each step is performed on the output of the previous step):

1. Zero-phase bandpass-filtering with pass band between 0.05 Hz and 3.0 Hz.
2. Downsampling from 200 Hz to 50 Hz.

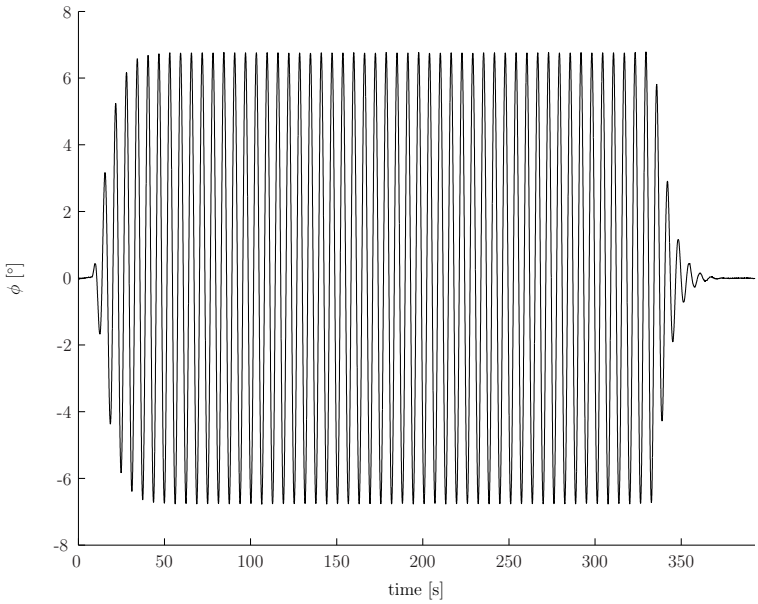

Figure 9.3: Example input signal. $\mathcal{A} = 7°$, $\varpi = 1$ rad/s.

3. Re-calibration.
4. a) Averaging the two depth measurements to get the final depth measurement.
   b) Calculating the roll moment based on the normal and parallel components.

9.3.3 Results

Tank fluid

For the motion of the tank fluid (see (9.12) and (9.13)) it was deemed advantageous to create a Bode diagram to summarize the data. However, the system (9.12) is nonlinear, and a standard Bode diagram is only applicable for linear systems. Instead, the following procedure was used:

For any single-input single-output system with input $\bar{u}$ and output $\bar{y}$ we define the functions amp and ph as

$$\operatorname{amp}(\bar{y}, \bar{u}; t_1, t_2) = \frac{\max\limits_{t\in[t_1,t_2]} |\bar{y}(t)|}{\max\limits_{t\in[t_1,t_2]} |\bar{u}(t)|}$$

$$\operatorname{ph}(\bar{y}, \bar{u}; t_1, t_2) = \arccos\left(\frac{2}{t_2 - t_1} \int_{t_1}^{t_2} \frac{\bar{y}(t)}{\max\limits_{t\in[t_1,t_2]} |\bar{y}(t)|} \frac{\bar{u}(t)}{\max\limits_{t\in[t_1,t_2]} |\bar{u}(t)|} \, \mathrm{d}t \right).$$

Assuming that $\bar{u}$ and $\bar{y}$ both are sinusoidal signals, the two functions amp and ph approximate the amplitude and phase difference between $\bar{u}$ and $\bar{y}$. For a linear system, with t_2 and t_1 given wide enough range, amp and ph are equal to the amplitude and phase difference.

Considering the roll angle $\phi = \phi_d$ as input and the tank state q_t as the output, the functions $\text{amp}(q_t, \phi_d; t_1, t_2)$ and $\text{ph}(q_t, \phi_d; t_1, t_2)$ (or rather, their discrete equivalents) were therefore used as a measure of the "amplitude" and the "phase" of the tank state. The time interval was chosen to be $t_1 = 100$ s to $t_2 = 300$ s, where the system is in steady-state.

The simulations were initialized with the same initial conditions as the real system, and then simulated without input from the measured data. The tank damping parameters found in Section 9.2.3 were used in the simulation. A comparison of the simulation and the measurements can be seen in Figure 9.4, showing amp in dB (using $20\log_{10}(\text{amp})$) and ph in degrees. The mean square errors are in Table 9.5. More detailed example figures can be seen in Figures 9.5 and 9.6.

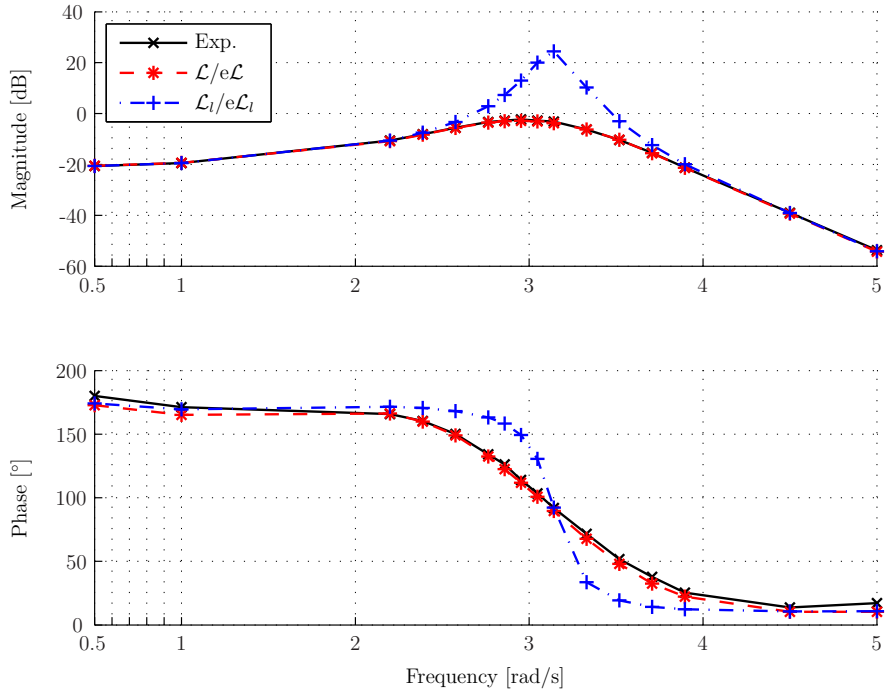

Figure 9.4: "Bode" diagram: Roll [rad] to depth [m].

The nonlinear models $\mathcal{L}$ and e$\mathcal{L}$ are significantly better fits to the experimental results than the linear models $\mathcal{L}_l$ and e$\mathcal{L}_l$, having only 0.14 % of the mean square error, a reduction by three orders of magnitude. However, it can be shown that this is almost entirely due to the presence of the nonlinear damping terms. Using linear damping terms in the (still) nonlinear models causes the accuracy of the linear and

Table 9.5: Mean square errors in q_{r_2}, sinusoidal input.

ϖ [rad/s]	MSE [cm^2] $\mathcal{L}_l$/e$\mathcal{L}_l$	$\mathcal{L}$/e$\mathcal{L}$
0.5000	0.0052	0.0038
1.0000	0.0024	0.0036
2.1991	0.2740	0.0068
2.3876	1.0679	0.0222
2.5761	4.6073	0.0918
2.7646	22.8388	0.1261
2.8588	46.8886	0.3873
2.9531	111.7322	0.2022
3.0473	265.9854	0.1768
3.1416	438.5790	0.1409
3.3301	93.7724	0.1183
3.5186	15.1579	0.0550
3.7071	3.0985	0.0764
3.8956	0.4164	0.0028
4.5000	0.0010	0.0006
5.0000	0.0003	0.0005
Avg.	62.7767	0.0884

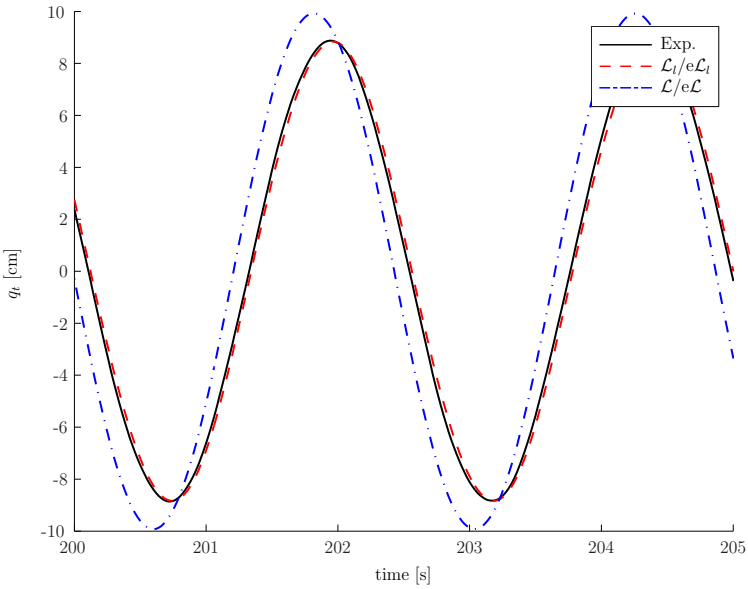

Figure 9.5: Depth measurements, sinusoidal inputs, $\varpi \approx 2.576$ rad/s.

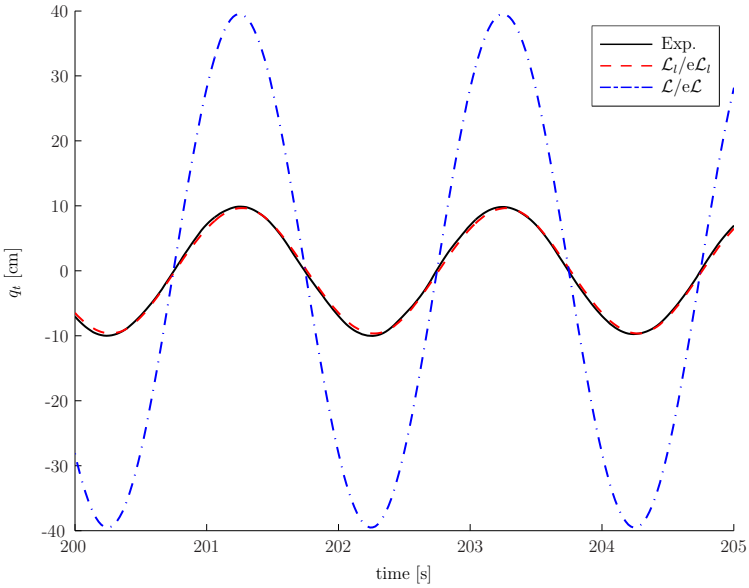

Figure 9.6: Depth measurements, sinusoidal inputs, $\varpi \approx 3.141$ rad/s.

nonlinear models to be almost identical.

Roll moment

The tank-induced moment in roll is merely an analytical function of the states and their derivatives, not a dynamical equation. As such, a Bode diagram is not applicable for this data. Instead, a direct comparison between the calculated torque and the measured torque is performed, and the mean square error computed.

To accurately reflect the differences in the models, the measured tank state was not used in these calculations. Instead, the tank simulations from Section 9.3.3 were used. The linear models $\mathcal{L}_l$ and e$\mathcal{L}_l$ were fed the linear simulation results, and the nonlinear models $\mathcal{L}$ and e$\mathcal{L}$ were fed the nonlinear simulation results.

For the extended models e$\mathcal{L}$ and e$\mathcal{L}_l$ there is the additional problem that the damping terms d_{4t} and $d_{4t,n}$ are unknown. To estimate them, we took the time interval $t \in [60, 315]$ s for all experiments (that is, the steady-state response) and used least squares curve fitting on the entire data set to find the parameters that best fitted the total data set. That is,

$$(d_{4t}, d_{4t,n}) = \arg \min_{d_{4t}, d_{4t,n}} \sum_t \|\tau_m(t) - \bar{\tau}_{e\mathcal{L}}(t; d_{4t}, d_{4t,n})\|^2$$

where

$$\bar{\tau}_{e\mathcal{L}}(t; d_{4t}, d_{4t,n}) = \tau_{e\mathcal{L}}([\phi_d(t), q_t(t)]^{\mathrm{T}}, [\dot{\phi}_d(t), \dot{q}_t(t)]^{\mathrm{T}}, [\ddot{\phi}_d(t), \ddot{q}_t(t)]^{\mathrm{T}}; d_{4t}, d_{4t,n})$$

for e$\mathcal{L}$ and

$$d_{4t} = \arg\min_{d_{4t}} \sum_t \|\tau_m(t) - \bar{\tau}_{e\mathcal{L}_l}(t; d_{4t})\|^2$$

where

$$\bar{\tau}_{e\mathcal{L}_l}(t; d_{4t}) = \tau_{e\mathcal{L}_l}([\phi_d(t), q_t(t)]^T, [\dot{\phi}_d(t), \dot{q}_t(t)]^T, [\ddot{\phi}_d(t), \ddot{q}_t(t)]^T; d_{4t})$$

for e$\mathcal{L}_l$, where τ_m is the combined measured moment for all experiments, and $\tau_{e\mathcal{L}}$ and $\tau_{e\mathcal{L}_l}$ are as in Equations (9.10) and (9.11). Note that the measured value of q_t was used for the purpose of finding the parameters. This means that different data sets were used for estimation and verification, as the verification was done using the simulated values of q_t.

For the nonlinear model e$\mathcal{L}$, the parameters found were

$$d_{4t} = 0.0578 \text{ kg·m/s}$$
$$d_{4t,n} = 4.3390 \text{ kg}.$$

For the linear model e$\mathcal{L}_l$, the parameter found was

$$d_{4t} = 1.3872 \text{ kg·m/s}.$$

The experimental results are summarized in Table 9.6. More detailed example figures can be seen in Figures 9.7 and 9.8.

Table 9.6: Mean square errors in roll moment, sinusoidal input.

ϖ	Mean square error $[(\text{N} \cdot \text{m})^2]$			
[rad/s]	e$\mathcal{L}_l$	$\mathcal{L}_l$	$\mathcal{L}$	e$\mathcal{L}$
0.50	0.12	0.12	0.12	0.12
1.00	0.05	0.05	0.05	0.05
2.20	1.60	1.29	0.09	0.07
2.39	5.09	4.37	0.23	0.17
2.58	18.68	16.95	0.70	0.52
2.76	82.65	78.33	1.20	0.89
2.86	168.31	162.21	2.42	1.87
2.95	376.90	367.71	1.90	1.44
3.05	870.74	860.27	1.42	1.01
3.14	1352.17	1351.37	1.10	0.82
3.33	276.25	283.29	0.62	0.37
3.52	39.56	42.15	0.31	0.19
3.71	6.16	6.98	0.19	0.14
3.90	1.04	1.32	0.17	0.14
4.50	0.48	0.54	0.49	0.48
5.00	0.53	0.55	0.54	0.54
Avg.	200.02	198.59	0.72	0.55

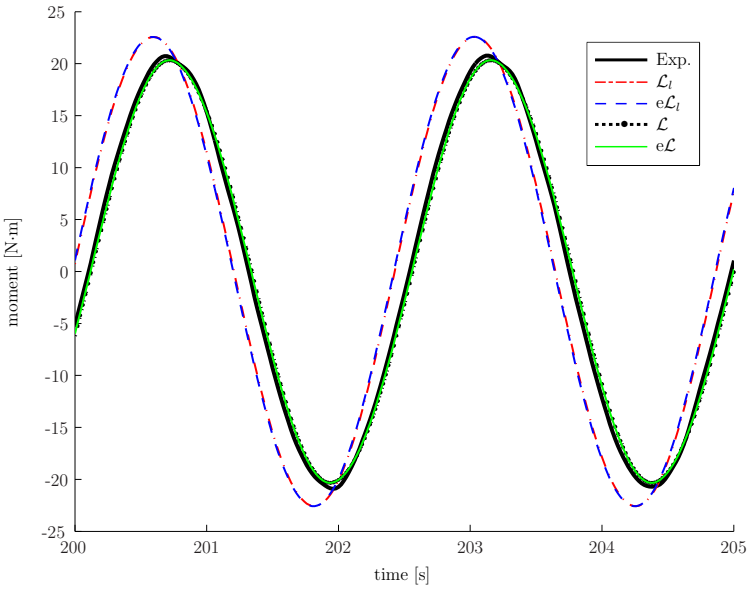

Figure 9.7: Torque measurements, sinusoidal inputs, $\varpi \approx 2.576$ rad/s.

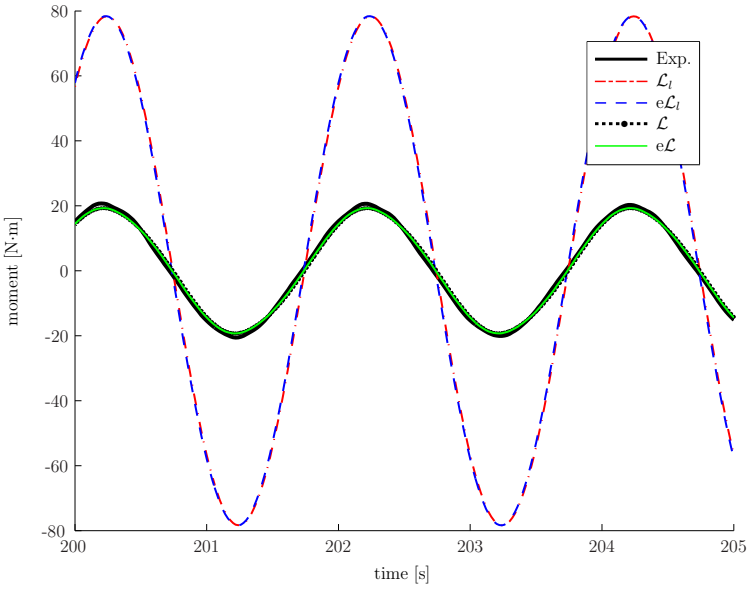

Figure 9.8: Torque measurements, sinusoidal inputs, $\varpi \approx 3.141$ rad/s.

As can be seen from the data, there is significant differences between the models. The nonlinear models $\mathcal{L}$ and e$\mathcal{L}$ had three orders of magnitude lower mean square error relative to the experimental data than the linear models $\mathcal{L}_l$ and e$\mathcal{L}_l$. The extended model e$\mathcal{L}$ also outperformed the model $\mathcal{L}$, having on average 24 % lower mean square error and 41 % lower at the most. The difference is greatest around the peak frequency (3.14 rad/s), as that is when the velocity of the tank fluid is greatest. However, the mean square errors are so low for the nonlinear models, that this difference is almost invisible to the naked eye.

The two linear models $\mathcal{L}_l$ and e$\mathcal{L}_l$ perform, for all practical purposes, identically. The extended model, in fact, performs marginally worse and is slightly more complicated. It is therefore reasonable to conclude that extending the linear model is not worthwhile.

9.4 Pseudorandom input tests

The purpose of these experiments was to verify he model using a pseudorandom desired roll angle ϕ_d.

9.4.1 Experiment

To approximate bandwidth-limited zero-mean Gaussian white noise, a sum of sinusoids with pseudorandomly selected frequencies and phases were used.

The pseudorandom input signals were generated as

$$\phi_d(t) = \sum_{n=1}^{N} \varphi_n(t)$$

$$\varphi_n(t) = \begin{cases} 0 & \forall \quad t \in [0, 5] \\ r_u(t; 2, 5)\mathcal{A}\sin(\varpi_n t + \theta_n) & \forall \quad t \in (5, 385] \\ r_d(t; 2, 385)\mathcal{A}\sin(\varpi_n t + \theta_n) & \forall \quad t \in (385, 405] \\ 0 & \forall \quad t \in (405, 410] \end{cases}$$

with r_u and r_d as in (9.15) and (9.16).

The number of sinusoids $N = 100$. The amplitude of each sinusoid $\mathcal{A} = 7°$ in all experiments. The phases θ_n were uniformly distributed in the range $[0, 2\pi)$. The frequencies ϖ_n were taken to lie in the range $[0.7\pi, 1.2\pi)$ rad/s $= [0.35, 0.6)$ Hz. The frequency range was split into N evenly distributed frequencies $\bar{\varpi}_i$, and ϖ_n uniformly randomly selected from the range $[\bar{\varpi}_n, \bar{\varpi}_{n+1})$.

Example input series and their power spectral density can be seen in Figures 9.9 and 9.10.

9.4.2 Data processing

The data series gathered from experiments with pseudorandom input were processed with the following procedure (each step is performed on the output of the previous step):

1. Zero-phase bandpass-filtering with pass band between 0.05 Hz and 3.0 Hz.

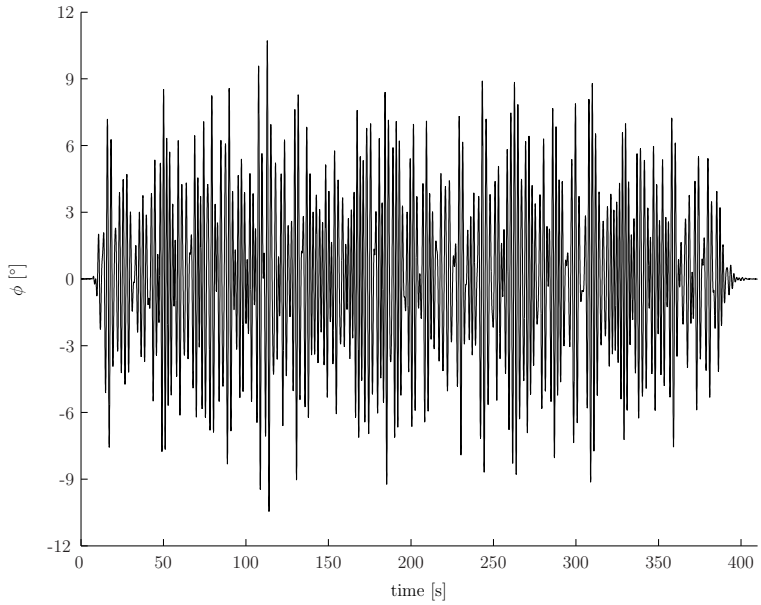

(a) Time domain.

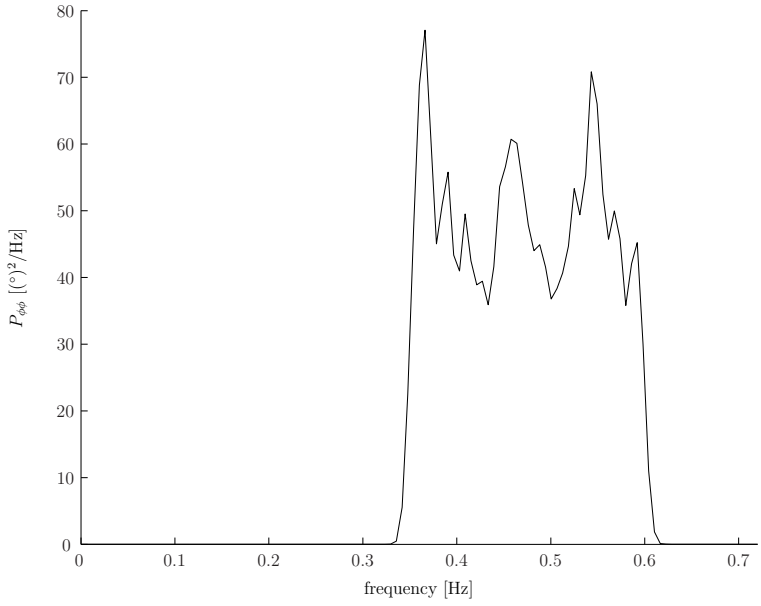

(b) Power spectral density (estimate).

Figure 9.9: Pseudorandom input 1.

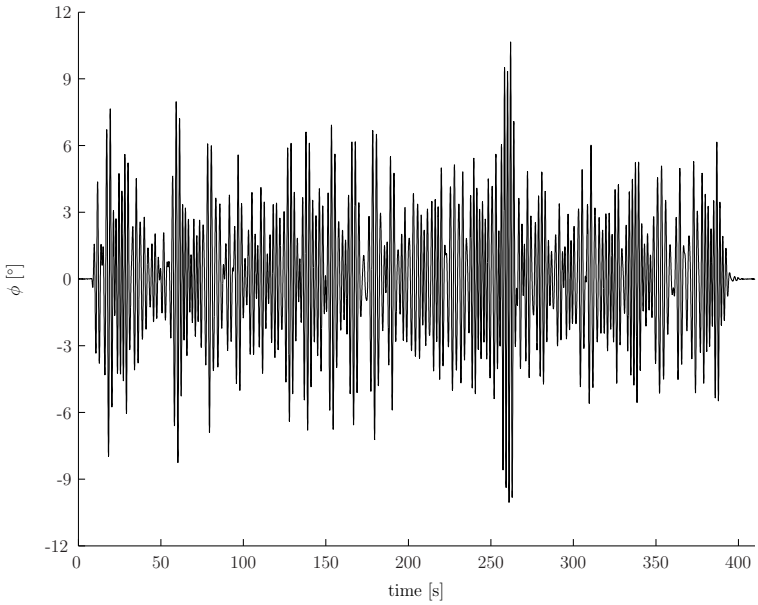

(a) Time domain.

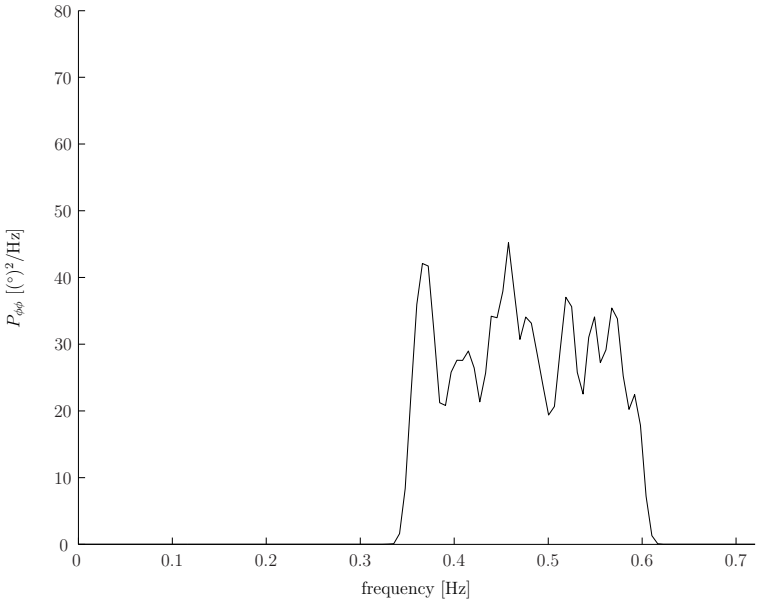

(b) Power spectral density (estimate).

Figure 9.10: Pseudorandom input 4.

2. Downsampling from 200 Hz to 50 Hz.
3. Re-calibration.
4. a) Averaging the two depth measurements to get the final depth measurement.
   b) Calculating the roll moment based on the normal and parallel components.

9.4.3 Results

Tank fluid

As before, the simulations were initialized with the same initial conditions as the real system, and then simulated without input from the measured data. The tank damping parameters found in Section 9.2.3 were used in the simulation. A Bode diagram is no longer suitable, so direct comparison between the experimental data and the models was performed. The results are summarized in Table 9.7. Example time series can be seen in Figures 9.11 and 9.12.

Table 9.7: Mean square errors in q_{r_2}, pseudorandom input.

Exp. no.	MSE [cm^2] $\mathcal{L}_l$/e$\mathcal{L}_l$	$\mathcal{L}$/e$\mathcal{L}$
1	31.4629	0.0380
2	40.1877	0.0541
3	23.1057	0.0536
4	17.7036	0.0679
Avg.	28.1150	0.0534

As can be seen from the data, the error is significantly lower with the nonlinear models than with the linear models, having a mean square error of only 0.19 % of the linear models. Once again, however, this difference is almost entirely due to the presence of the nonlinear damping terms in the nonlinear models. Using linear damping terms in the (still) nonlinear models causes the mean square error of the linear and nonlinear models to be almost identical.

Roll moment

As before, the estimated torques are directly compared to the measured torques. For the extended models, the parameters $d_{4t}, d_{4t,n}$ found in Section 9.3.3 were used. To accurately reflect the differences in the model, the simulated tank responses from Section 9.4.3 rather than the measured values were used to compute the estimated torques. The linear models $\mathcal{L}_l$ and e$\mathcal{L}_l$ were fed the linear simulation results, and the nonlinear models $\mathcal{L}$ and e$\mathcal{L}$ were fed the nonlinear simulation results. The details are summarized in Table 9.8. Example time series can be seen in Figures 9.13 and 9.14.

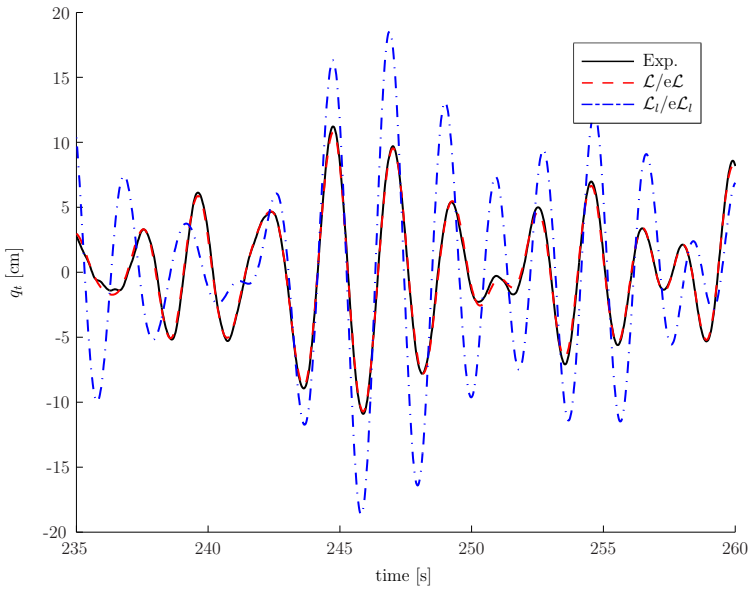

Figure 9.11: Depth with pseudorandom input, experiment number 1.

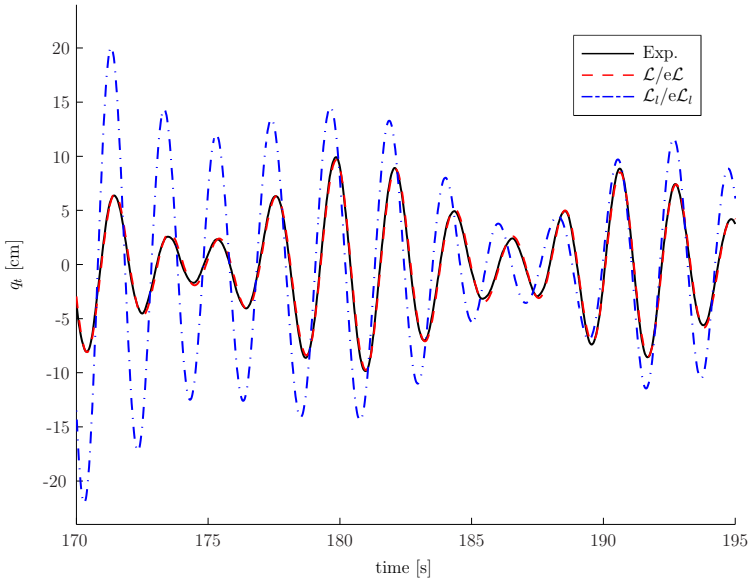

Figure 9.12: Depth with pseudorandom input, experiment number 4.

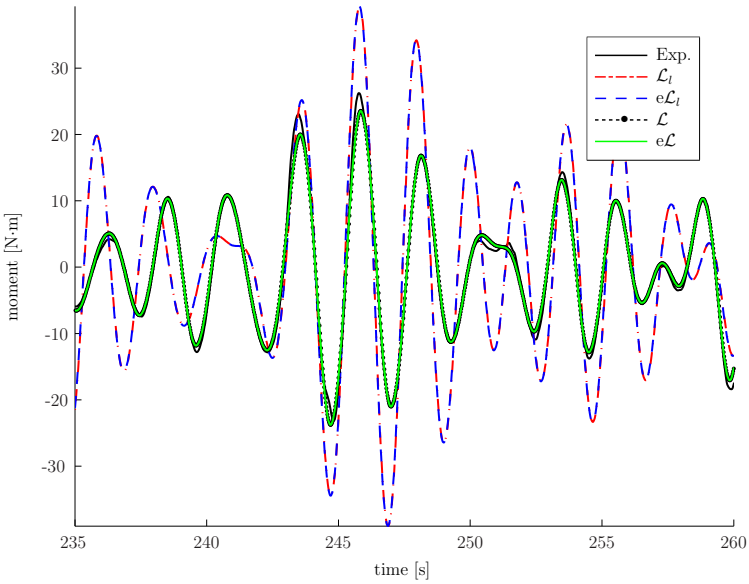

Figure 9.13: Torque measurements, pseudorandom input, experiment number 1.

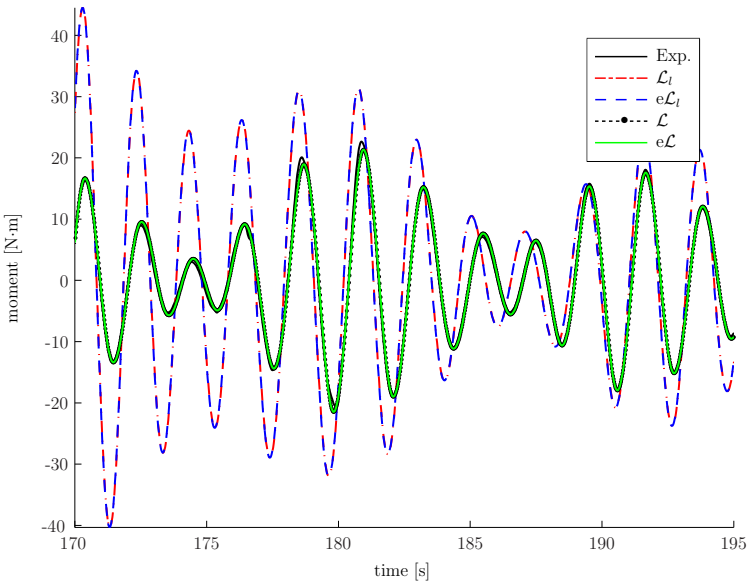

Figure 9.14: Torque measurements, pseudorandom input, experiment number 4.

Table 9.8: Mean square errors in roll moment, pseudorandom input.

Exp. no.	Mean square error $[(\mathrm{N{\cdot}m})^2]$			
	$e\mathcal{L}_l$	$\mathcal{L}_l$	$\mathcal{L}$	$e\mathcal{L}$
1	122.068	121.463	0.604	0.576
2	156.355	155.888	0.969	0.837
3	89.966	89.659	0.587	0.494
4	68.591	68.445	0.415	0.326
Avg.	109.245	108.864	0.644	0.559

The data is largely consistent with the results presented in Section 9.3.3. The nonlinear models $\mathcal{L}$ and $e\mathcal{L}$ had three orders of magnitude lower mean square error relative to experimental data than the linear models $\mathcal{L}_l$ and $e\mathcal{L}_l$. The extended model $e\mathcal{L}$ outperformed the model $\mathcal{L}$, having 13 % lower mean square error, on average. The pseudorandom experiments showed a lower reduction in mean square error than the sinusoidal experiments because the tank fluid moves at a lower velocity, on average, in the pseudorandom experiments. As before, the mean square error of the nonlinear models is so low that the difference between $\mathcal{L}$ and $e\mathcal{L}$ is almost invisible to the naked eye.

The two linear models $\mathcal{L}_l$ and $e\mathcal{L}_l$ are again almost indistinguishable in quality, and again the extended model is marginally worse.

9.5 Modeling revisited

From Sections 9.2–9.4, the extended model $e\mathcal{L}$ has the best fit with the experimental data. However, the model is fairly complex, highly nonlinear and only marginally better than the non-extended model $\mathcal{L}$ (which is also complex). Unfortunately, the linear models $e\mathcal{L}_l$ and $\mathcal{L}_l$ have significantly higher error relative to experimental data. But, as was noted in Sections 9.2–9.4, the most important nonlinearities are the damping terms. This suggests a simplified model.[1]

Model XIV (Simplified model $\mathcal{L}_r$)**.**

$$\mathcal{L}_r: \; M_{r_2}(0)\ddot{q}_{r_2} + D_{r_2}(\dot{q}_{r_2})\dot{q}_{r_2} + K_{r_2}(t)q_{r_2} = \tau_{e,r_2}(t) + B_{r_2}u_t \tag{9.17}$$

where M_{r_2}, D_{r_2} and K_{r_2} are as in Models X and XI.

Note that the linearization of $\mathcal{L}_r$ about $q_{r_2} = 0$ is identical to $\mathcal{L}_l$.

To test the model $\mathcal{L}_r$, it and the models $e\mathcal{L}$ and $\mathcal{L}_l$ were simulated and compared. For the pressure-induced torque, we used

$$k_{p,4}(\phi, t) = \frac{g(m + m_t)}{24L_d}\left[L_b^2 - 12L_d^2 + \frac{L_b^2}{\cos^2(\phi)}\right]\sin(\phi).$$

[1] Note that this model is slightly different from the model $e\mathcal{L}_r$ presented in Holden et al. [44].

This corresponds to the hydrostatic pressure of a barge (box-shaped ship) of length L_l, drought L_d and breadth L_b.

The following (arbitrary but consistent) parameters were used:

$$\begin{aligned} J_{11} &= 237.13 \text{ kg·m}^2 \\ m &= 2475 \text{ kg} \\ L_l &= 7.37 \text{ m} \\ L_b &= 0.9 \text{ m} \\ L_d &= 0.3731 \text{ m} \\ z_g &= 0.1119 \text{ m} \\ m_{A,44} &= 23.713 \text{ kg·m}^2 \\ d_{44} &= 25 \text{ kg·m}^2/\text{s} \end{aligned}$$

These parameters are not based on any real ship. The tank parameters were the same as those used (and found) in Sections 9.2–9.4. The mass of the tank fluid m_t is slightly more than 1 % of this ship's mass m.

The system was excited by a generalized force $\tau_{e,r_2}(t)$ given by

$$\tau_{e,r_2}(t) = \begin{bmatrix} A_\tau \sin(\omega_\tau t) \\ 0 \end{bmatrix}$$

with frequency $\omega_\tau = 3.1524$ rad/s, equal to the ship's – and the tank's – natural frequency. Ten simulations were performed, all with initial conditions $q_{r_2}(0) = \dot{q}_{r_2}(0) = 0$, and $A_\tau \in \{5, 10, 15, 20, 25, 30, 35, 40, 45, 50\}$ N·m. The tank state q_t was limited to the range $|q_t| \leq h_t$, so as not to violate the condition that the duct is always full of fluid.

The results are summarized in Tables 9.9 and 9.10. The mean square errors in Table 9.9 are based on steady-state data from $t = 30$ s to $t = 100$ s. An example time series can be seen in Figure 9.15. For comparison the linear model $\mathcal{L}_l$ has also been simulated.

The reduced model $\mathcal{L}_r$ is very accurate in predicting the correct amplitude for both ϕ and q_t, but is slightly off in phase. The phase error of the linear model $\mathcal{L}_l$ varies depending on the simulation, and can be both greater and smaller than the phase error of $\mathcal{L}_r$. However, the linear model $\mathcal{L}_l$ is highly inaccurate in amplitude for both states across all time series.

It is also worth noting that the linear model $\mathcal{L}_l$ overestimates the effectiveness of the tank, mostly due to overestimating the response of the tank fluid. The linear model estimates that the difference in fluid level between the port and starboard reservoirs will be much greater than the nonlinear models estimate, which gives an unreasonably high weight difference between port and starboard, and thus a greater torque. As can be seen in Table 9.9, the most accurate model e$\mathcal{L}$ predicts a reduction of, on average, 54 %, while the linear model $\mathcal{L}_l$ predicts a reduction of 67 % on average. The reduced model $\mathcal{L}_r$ predicts 54 % reduction.

If one uses a model with the nonlinear spring term $k_{r_2}(q_{r_2})$ rather than its linearization about $q_{r_2} = 0$, $K_{r_2} q_{r_2}$ (i.e., a model identical to $\mathcal{L}$ except with $C_{r_2} \equiv 0$

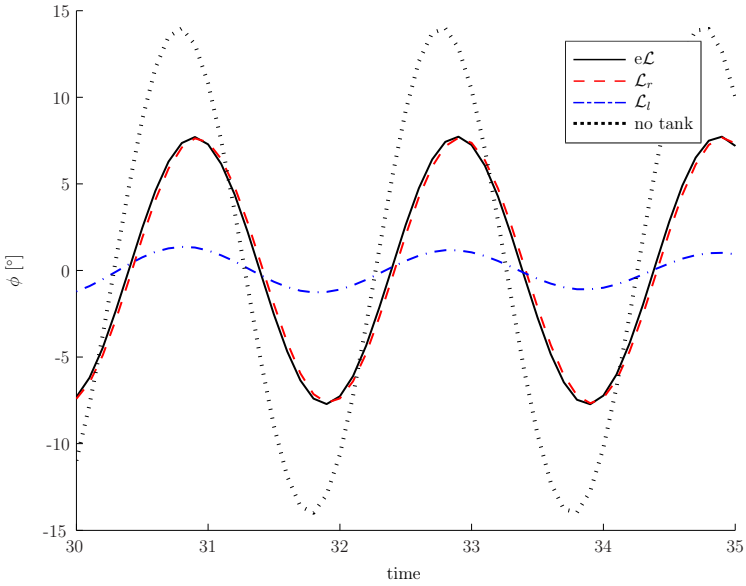

(a) Roll angle.

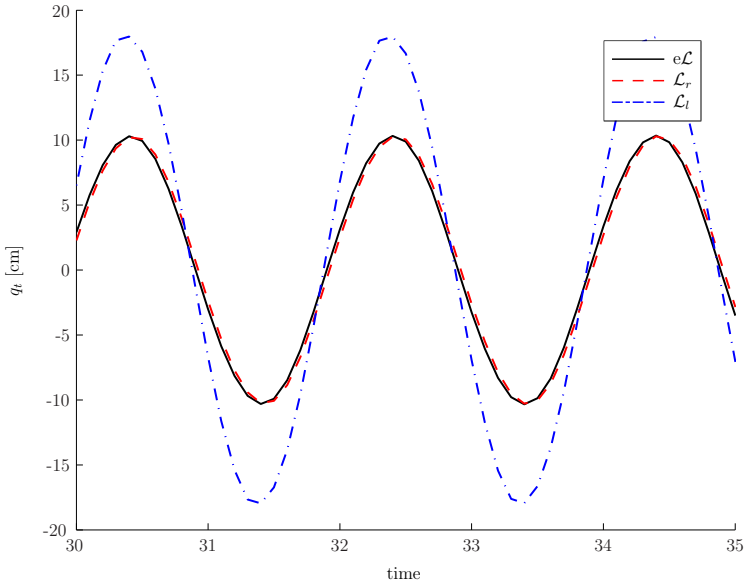

(b) Tank state.

Figure 9.15: Simulation results, $A_\tau = 35$ N·m.

and $M_{r_2} \equiv M_{r_2}(0)$), the reduced model performs almost identically to the full models $\mathcal{L}$ and e$\mathcal{L}$. However, this comes at a high cost in complexity. The reduced model $\mathcal{L}_r$ can therefore probably serve as a useful design tool, especially for feedback control, combining simplicity with reasonable accuracy. This is further investigated in Chapter 12.

Table 9.9: Mean square errors, simulations.

A_τ	e$\mathcal{L}$ to $\mathcal{L}_r$		e$\mathcal{L}$ to $\mathcal{L}_l$	
[N·m]	ϕ [(°)^2]	q_t [cm^2]	q_1 [(°)^2]	q_{r_2} [cm^2]
5	0.0000	0.0000	0.0340	0.0305
10	0.0000	0.0000	0.3893	0.2902
15	0.0001	0.0003	1.4595	1.1038
20	0.0017	0.0040	3.4996	2.8073
25	0.0125	0.0239	6.6244	5.6715
30	0.0573	0.0928	10.9539	9.6846
35	0.1941	0.2718	16.2193	16.3562
40	0.5272	0.6515	12.8853	18.8573
45	1.2102	1.3423	6.3290	20.2132
50	2.4334	2.4544	1.8136	24.1079
Avg.	0.4436	0.4841	6.0208	9.9122

Table 9.10: Estimated roll reduction tank vs. no tank, simulations.

A_τ	Reduction [%]		
[N·m]	e$\mathcal{L}$	$\mathcal{L}_r$	$\mathcal{L}_l$
5	77.0107	77.0111	77.7064
10	73.6133	73.6168	75.4787
15	68.7077	68.7540	73.3612
20	61.7126	61.8314	71.2425
25	55.3550	55.5995	69.1165
30	49.6062	50.0072	67.0226
35	44.4629	45.0067	64.9957
40	39.9191	40.5362	63.0462
45	35.9665	36.5259	61.1726
50	32.5646	32.9052	44.5092
Avg.	53.8919	54.1794	66.7652

Take control of the input and you
shall become master of the output.

Chairman Sheng-ji Yang,
"Essays on Mind and Matter",
Sid Meier's Alpha Centauri

Part III

Control

Chapter 10

The many ways of controlling parametric roll

Control strategies for parametric roll resonance can roughly be categorized as *direct* or *indirect* methods.

The direct methods are aimed at directly controlling the roll motion by generating an opposing roll moment, as seen in Holden and Fossen [39], Holden et al. [42], Umeda et al. [90]. Direct methods can further be categorized as *active* or *passive*. Active control uses actuators and feedback or feedforward, while with a passive system that is not the case. For instance, u-tanks with a control system are active, but they can also be used passive, letting the tank fluid moves on its owen accord through the system.

Indirect strategies attempt to violate the empirical conditions necessary for the onset of parametric roll resonance, as seen in Breu and Fossen [7], Jensen et al. [47, 48], Ribeiro e Silva et al. [76].

A hybrid approach, doing both at the same time, is also possible, as seen in Galeazzi [32], Galeazzi and Blanke [33], Galeazzi et al. [34].

A simple model of parametric roll resonance is the Mathieu equation [88]

$$m_{44}\ddot{\phi} + d_{44}\dot{\phi} + [k_{44} + k_{\phi t}\cos(\omega_e t + \alpha_\phi)]\,\phi = u_c$$

where m_{44} is the sum of the rigid-body moment of inertia and the added moment of inertia in roll, d_{44} is the linear hydrodynamic damping coefficient, k_{44} is the linear restoring moment coefficient, $k_{\phi t}$ gives the amplitude of the change in the linear restoring coefficient and ω_e is the encounter frequency. All the parameters are considered constant. The control input is u_c.

Direct methods use u_c as control input, while indirect methods change ω_e.

It is known [63] that the Mathieu equation parametrically resonates at $\omega_e \approx 2\sqrt{k_{44}/m_{44}}$. The encounter frequency ω_e is the Doppler-shifted frequency of the waves as seen from the ship. As the frequency is Doppler-shifted, it can be changed by changing the speed of the ship, as seen in Chapters 5 and 11.

In this thesis, both direct and indirect control schemes are considered.

In Chapter 11, we present a controller that is capable of stopping parametric resonance based on changing the encounter frequency. The main purpose of that

chapter is to show that it is feasible to control parametric roll resonance by changing the encounter frequency to violate the condition $\omega_e \approx 2\sqrt{k_{44}/m_{44}}$. We refer to this frequency detuning control.

Based on the 1-DOF roll Model IV of Chapter 5, we present a simple controller based on a linear change of the encounter frequency achieved by variation of the ship's forward speed. We then prove mathematically that the proposed controller is able to drive the ship out of parametric resonance, driving the roll motion to zero. It is worth noting that the controller is in fact simple enough that a human helmsman can perform the necessary control action, rendering a speed controller unnecessary.

However, in practice, the usefulness of the controller depends on the ability of the ship to rapidly perform a speed change. If the ship has high inertia or is at rest with the engines turned off, it is unlikely that the ship will be able to change its speed fast enough to avoid large roll angles.

There are also some disadvantages associated with direct control. Ships are often not actuated in roll [24], as such systems are not necessary for propulsion. Possible actuators include fins, tanks and gyro stabilizers [75]. During my PhD work, we have focused on the use of u-tanks as actuators. These have the advantage that they can be used even if the ship is at rest [58]. As they are internal, they do not increase drag. Unfortunately, they do take up space inside the hull, potentially decreasing the available space for other machinery, cargo or passengers.

The basic principle behind u-tank control is to use the weight and motion of the fluid to give a direct moment in roll, which can be used to counteract parametric resonance or other unwanted motion.

A disadvantage of u-tanks compared to other potential actuators, is that the roll and tank modes are tightly coupled, and only indirectly give a control moment in roll. Output stabilization (with roll angle as output and the tank state as an internal state) tends to not leave the tank in its equilibrium position as seen in Holden et al. [42].

In Chapter 12, we present a controller using a reduced-order (2-DOF) version of 7-DOF u-tank Model VII of Chapter 7 that is capable of driving the roll angle to zero in the presence of parametric roll resonance. The validity of the controller is mathematically proven, and tested in simulation.

Chapter 11

Frequency detuning control

As has been discussed in the previous chapters, ships can parametrically resonate when the encounter frequency is about twice the natural roll frequency. From Chapter 5, we have seen that the encounter frequency can be changed by changing the velocity of the vessel. In this chapter, we present a controller that is capable of stopping parametric roll by detuning the encounter frequency so that $\omega_e \neq 2\omega_\phi$.

The results in this chapter are based on the results Holden et al. [43].

11.1 The model used

We assume, in this chapter, that the ship is not equipped with actuators in roll. Instead, we change ω_e (by changing the forward speed) to detune the encounter frequency and thus violate a necessary condition for the existence of parametric roll resonance.

To analyze the effects of speed changes, we need to use a model that is valid under non-constant speed. As discussed in Chapter 5, the commonly used Mathieu equation is not adequate for time-varying speed.

We will use the simplified 1-DOF Model IV of Chapter 5, given by

$$m_{44}\ddot{\phi} + d_{44}\dot{\phi} + \left[k_{44} + k_{\phi t}\cos\left(\int_{t_0}^{t} \omega_e(t)\,\mathrm{d}\tau + \alpha_\phi\right)\right]\phi + k_{\phi^3}\phi^3 = 0 \tag{11.1}$$

where ϕ is the roll angle, m_{44} is the sum of the rigid-body moment of inertia about the x-axis and the added mass in roll, d_{44} is linear hydrodynamic damping, k_{44} is the linear restoring moment coefficient, $k_{\phi t}$ gives the amplitude of the change in the linear restoring coefficient and k_{ϕ^3} is the cubic restoring moment coefficient. These parameters are constant.

From Chapter 5, we have that the encounter frequency ω_e is given by

$$\omega_e = \omega_0 - k_w v_1^n = \omega_0 - k_w[1,0,0]Rv^b \tag{11.2}$$

and that, if the ship is not rotating (i.e., $\omega^b \equiv 0$), then

$$\begin{aligned}\dot{\omega}_e &= -k_w[1,0,0]R\dot{v}^b \approx -k_w e_x^{\mathrm{T}} R[\dot{v}_1^b, 0, 0]^{\mathrm{T}} \\ &\approx -k_w \dot{v}_1^b \cos(\theta)\cos(\psi) \approx -k_w \dot{v}_1^b \cos(\psi)\end{aligned} \tag{11.3}$$

by the assumption that $|v_2^b|, |v_3^b| \ll |v_1^b|$ (i.e., the ship's velocity is primarily due to surge) and that $\theta \approx 0$. The ship is assumed to be sailing in head or stern seas, that is $\cos(\psi) = 1$ (head seas) or $\cos(\psi) = -1$ (stern seas).

We can set $\dot{v}_1^b$ directly; this is the forward acceleration and can be changed by increasing or decreasing throttle. It will, however, be limited, so we take it to satisfy $|\dot{v}_1^b| \leq \dot{v}_{1,\max}^b$. Thus, we take $\dot{\omega}_e \triangleq u_c$ to be the control input, satisfying

$$|\dot{\omega}_e| = |u_c| \leq u_{\max} = |k_w| \dot{v}_{1,\max}^b \,. \tag{11.4}$$

Note that the assumption that the forward speed changes only slowly implies that $v_{1,\max}^b$ is quite small. The assumption of slow speed change is a necessity to derive the Model IV by a quasi-steady approach, as detailed in Chapter 5.

As we can see from the above equation, $u_{\max}$ depends on the size of $\dot{v}_{1,\max}^b$ and k_w. For the type of large, slow vessels that are susceptible to parametric resonance, $\dot{v}_{1,\max}^b$ is indeed likely to have quite a low value. For ships to parametrically resonate, the wave length has to be rather long, otherwise $k_{\phi t}$ will be too small [40]. A long wave length implies a small k_w, since $k_w = 2\pi/\lambda$ if λ is the wave length. Thus $u_{\max}$ is quite small.

11.2 Control design

The control objective is to design u_c such that the origin of the (unforced) roll subsystem (11.1) is (at least) asymptotically stable. Choosing a $\dot{v}_1^b$ so that $\dot{\omega}_e$ is equal to the desired u_c is a control allocation problem.[1]

11.2.1 Control principle

The basic control principle is to (slowly) change the encounter frequency from an undesired value $\omega_{e,0}$ to a desired value $\omega_{e,1}$.

We tentatively choose the controller

$$u_c(t) = \begin{cases} 0 & \forall \quad t \in [t_0, t_1] \\ \varepsilon & \forall \quad t \in [t_1, t_2] \\ 0 & \forall \quad t \in [t_2, \infty) \end{cases} \tag{11.5}$$

for some small constant ε, with $t_2 \geq t_1 \geq t_0$. The initial time is t_0.

If $\omega_e(t_0) = \omega_{e,0}$, then

$$\omega_e(t) = \int_{t_0}^{t} u(\tau)\, \mathrm{d}\tau + \omega_{e,0} = \begin{cases} \omega_{e,0} & \forall \quad t \in [t_0, t_1] \\ \omega_{e,0} + \varepsilon(t - t_1) & \forall \quad t \in [t_1, t_2] \\ \omega_{e,1} & \forall \quad t \in [t_2, \infty) \end{cases} \tag{11.6}$$

[1] It is also possible to change ω_e by changing course (i.e., changing ψ). This will have the unwanted side effect that the ship will now be directly excited by waves, which may also result in relatively large roll amplitude in the type of seas that give parametric resonance. Due to time constraints, changing ψ to change the encounter frequency was not investigated during my PhD work.

where $\omega_{e,1} = \omega_{e,0} + \varepsilon(t_2 - t_1)$. This gives

$$\int_{t_0}^{t} \omega_e(\tau)\, \mathrm{d}\tau = \begin{cases} \omega_{e,0}(t - t_0) & \forall \quad t \in [t_0, t_1] \\ \omega_{e,0}(t - t_0) + \frac{1}{2}\varepsilon(t - t_1)^2 & \forall \quad t \in [t_1, t_2] \\ \omega_{e,1}(t - t_2) + \omega_{e,0}(t_2 - t_0) + \frac{1}{2}\varepsilon(t_2 - t_1)^2 & \forall \quad t \in [t_2, \infty) \end{cases} .$$

If $\cos(\psi) \equiv \pm 1$ and $v_2^b = v_3^b = \theta = 0$, then

$$\omega_e(t) = \omega_0 - k_w v_1^b \cos(\psi) \tag{11.7}$$

and the encounter frequency of (11.6) can then be achieved with a surge velocity of

$$\begin{aligned} v_1^b &= \frac{\omega_0 - \omega_e(t)}{k_w \cos(\psi)} \\ &= \frac{1}{k_w \cos(\psi)} \begin{cases} \omega_0 - \omega_{e,0} & \forall \quad t \in [t_0, t_1] \\ \omega_0 - \omega_{e,0} - \varepsilon(t - t_1) & \forall \quad t \in [t_1, t_2] \\ \omega_0 - \omega_{e,1} & \forall \quad t \in [t_2, \infty) \end{cases} . \end{aligned} \tag{11.8}$$

Proving that the controller (11.5) works is done in two steps: First, ensuring that there exists a (unique finite) solution of (11.1) at $t = t_2$. This step is done in Appendix D.

Secondly, we need to prove that if $\omega_e(t) \equiv \omega_{e,1}\ \forall\ t \geq t_2$, then the solution to the initial value problem

$$\begin{aligned} m_{44}\ddot{\phi} + d_{44}\dot{\phi} + \left[k_{44} + k_{\phi t}\cos\left(\omega_{e,1}t + \bar{\alpha}_\phi\right)\right]\phi + k_{\phi^3}\phi^3 = 0\ , \\ \phi(t_2) = \phi_2, \dot{\phi}(t_2) = \dot{\phi}_2\ , \end{aligned} \tag{11.9}$$

where

$$\bar{\alpha}_\phi \triangleq \alpha_\phi - \omega_{e,1}t_2 + \omega_{e,0}(t_2 - t_0) + \frac{1}{2}\varepsilon(t_2 - t_1)^2$$

is a constant, goes to zero for all ϕ_2, $\dot{\phi}_2$.

11.2.2 The system (11.9) in the time interval $t \in [t_2, \infty)$

From the results in Appendix D, we know that there exists a finite solution to (11.1), valid at $t = t_2$. From $t \geq t_2$, the trajectories of the system will be the solution to the initial value problem (11.9).

From Nayfeh and Mook [63], we know that there are parameter values of $\omega_{e,1}$ which ensure that the trajectories of the system (11.9) go to zero. If we assume that $\omega_{e,0} \approx 2\omega_\phi$ (where parametric resonance of (11.1) is known to occur), we can find theoretical values for the regions of stability from the approximate methods of Nayfeh and Mook [63].

Theorem 11.1 (Frequency detuning control)**.** *The behavior of (11.9) can be categorized into three different categories, depending on the value of $\omega_{e,1}$:*

- *If $0 \leq \omega_{e,1} \leq \underline{\omega}_e$, then the origin of (11.9) is globally attractive.*

- *If $\underline{\omega}_e < \omega_{e,1} \leq \overline{\omega}_e$, then the origin of (11.9) is unstable, and there exists a high-amplitude, stable limit cycle. All trajectories of (11.9) converge to this limit cycle, with the exception of those starting in the origin.*
- *If $\omega_{e,1} > \overline{\omega}_e$, then the origin of (11.9) is locally asymptotically stable, there exists a high-amplitude, asymptotically stable limit cycle and a slightly lower-amplitude, asymptotically unstable limit cycle.*

$\underline{\omega}_e$ and $\overline{\omega}_e$ are the solutions to the equations

$$\sqrt{1 - \frac{d_{44}^2 \underline{\omega}_e^2}{k_{\phi t}^2}} - \frac{m_{44}\underline{\omega}_e^2}{k_{\phi t}} \left(2\sqrt{\frac{k_{44}}{m_{44}\underline{\omega}_e}} - 1 \right) = 0 \tag{11.10}$$

$$\sqrt{1 - \frac{d_{44}^2 \overline{\omega}_e^2}{k_{\phi t}^2}} + \frac{m_{44}\overline{\omega}_e^2}{k_{\phi t}} \left(2\sqrt{\frac{k_{44}}{m_{44}\overline{\omega}_e}} - 1 \right) = 0 \,. \tag{11.11}$$

In this theorem, asymptotic stability of limit cycles follows the definition of Khalil [52, Definition 8.1].

Proof. To simplify the analysis, we define the alternative dimensionless time scale

$$\tilde{t} \triangleq \frac{1}{2}\omega_{e,1} t + \bar{\alpha}_\phi \tag{11.12}$$

giving

$$\frac{\mathrm{d}}{\mathrm{d}t} = \frac{1}{2}\omega_{e,1}\frac{\mathrm{d}}{\mathrm{d}\tilde{t}}$$
$$\frac{\mathrm{d}^2}{\mathrm{d}t^2} = \frac{1}{4}\omega_{e,1}^2\frac{\mathrm{d}}{\mathrm{d}\tilde{t}^2} \,.$$

Using primes to indicate derivative with respect to $\tilde{t}$, we rewrite the system (11.9) as

$$\phi'' + 2\iota\gamma\phi' + \left[\kappa + 2\iota\cos(2\tilde{t})\right]\phi + \alpha\iota\phi^3 = 0 \tag{11.13}$$

where

$$\iota = \frac{2k_{\phi t}}{m_{44}\omega_{e,1}^2}$$
$$\gamma = \frac{d_{44}\omega_{e,1}}{2k_{\phi t}}$$
$$\kappa = \frac{4k_{44}}{m_{44}\omega_{e,1}}$$
$$\alpha = \frac{2k_{\phi^3}}{k_{\phi t}}$$

are all positive dimensionless parameters. It is assumed that ι is small.

Equation (11.13) is known to parametrically resonate if $\kappa \approx 1$ (i.e., $\omega_{e,0}^2 \approx 4k_{44}/m_{44} = 4\omega_\phi^2$; the encounter frequency is twice the natural roll frequency).

Using an $O(\iota)$ (big O notation) approximation to the solution of (11.13), Nayfeh and Mook [63] derives a solution using the method of multiple scales (see Nayfeh and Mook [63]) given by

$$\phi = a\cos(\tilde{t} - \beta/2) + O(\iota) \tag{11.14}$$

where a and β are slowly time-varying functions.

Defining the alternative (also dimensionless) time scale

$$\bar{t} = \iota\tilde{t} \tag{11.15}$$

(which is slowly varying) and letting

$$\sqrt{\kappa} = 1 - \iota\varsigma \tag{11.16}$$

(with ς representing the nearness of κ to unity, and thus the system to parametric resonance), a and β satisfy the (nonlinear homogenous ordinary) differential equations

$$\frac{\partial a}{\partial \bar{t}} = -\frac{a}{2\sqrt{\kappa}}\sin(\beta) - \gamma a \tag{11.17}$$

$$a\frac{\partial \beta}{\partial \bar{t}} = 2\varsigma a - \frac{a}{\sqrt{\kappa}}\cos(\beta) - \frac{3\alpha}{4\sqrt{\kappa}}a^3 \,. \tag{11.18}$$

The a–β system has equilibrium points (corresponding to a steady-state periodic motion of ϕ, i.e., a limit cycle) given by

$$a = 0, \qquad \beta \text{ arbitrary} \tag{11.19}$$

(the trivial solution) and

$$\sin(\beta) = -2\sqrt{\kappa}\gamma, \qquad \cos(\beta) = 2\varsigma\sqrt{\kappa} - \frac{3\alpha}{4}a^2 \,. \tag{11.20}$$

Since $\sqrt{\kappa} = 1 - \iota\varsigma$, the non-trivial steady-state solution of ϕ has the amplitude

$$a^2 = \frac{8\varsigma}{3\alpha} \pm \frac{4}{3\alpha}\sqrt{1 - 4\gamma^2} \tag{11.21}$$

where only the positive root is relevant.

If $2\gamma > 1$, then (11.21) has no real roots and only the trivial steady-state solution exists. As this is equivalent to high damping, if $2\gamma > 1$, parametric resonance will not occur. (The origin of (11.13) is then globally attractive for all $\omega_{e,1}$).

If $2\gamma \leq 1$, then there is one real root of (11.21) if $2|\varsigma| < \sqrt{1 - 4\gamma^2}$, and two if $2|\varsigma| > \sqrt{1 - 4\gamma^2}$. The condition $2\varsigma = -\sqrt{1 - 4\gamma^2}$ corresponds to (11.10) (giving $\underline{\omega}_e$) and $2\varsigma = \sqrt{1 - 4\gamma^2}$ to (11.11) (giving $\overline{\omega}_e$).

Figure 11.1 illustrates the stability properties of (11.13) for the different cases. Dashed lines represent unstable equilibrium values of a for different values of ς, and solid lines stable equilibrium values.[2]

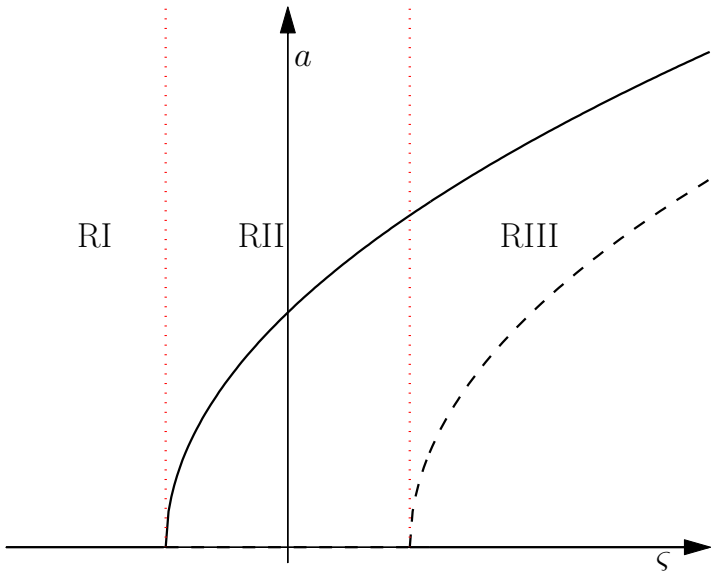

Figure 11.1: Stability regions of (11.13), theoretical.

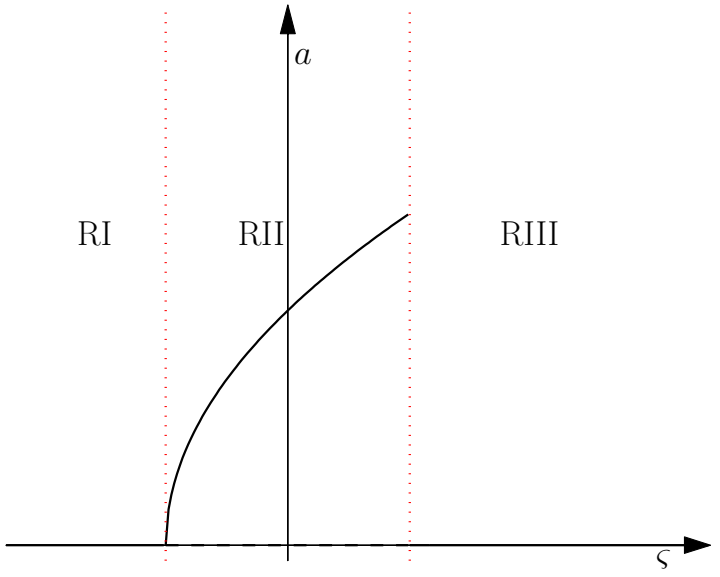

Figure 11.2: Stability regions of the 6-DOF Model III of Chapter 5, simulation.

In Region I, there is only the trivial solution. From Nayfeh and Mook [63], this is globally attractive.

In Region II (where we have parametric resonance), the trivial solution is unstable, and there exists a large-amplitude steady-state solution, a limit cycle. Apart from the case where $\phi(t_2) = \dot{\phi}(t_2) = 0$, this limit cycle is globally attractive [63] (this behavior is what has been referred to as being in parametric resonance previously in this thesis).

Region III has three equilibrium values, and is somewhat more complicated. The value $a = 0$ (equivalent to $\phi = 0$) is once again (locally) asymptotically stable. However, there exist two limit cycles, one high-amplitude and one low-amplitude. The high-amplitude one is (locally) asymptotically stable, whereas the low-amplitude one is unstable. □

Based on the proof of Theorem 11.1, we conclude that it is possible that, if one increases ω_e so that $\omega_{e,1} \gg 2\omega_\phi$ (i.e., $\varsigma \gg 0$), ϕ does not go to zero but instead to the high-amplitude limit cycle. If one instead decreases ω_e so that $\omega_{e,1} \ll 2\omega_\phi$ (i.e., $\varsigma \ll 0$), ϕ will go to zero no matter how large $\phi(t_2)$ is. This is illustrated Figure 11.3.

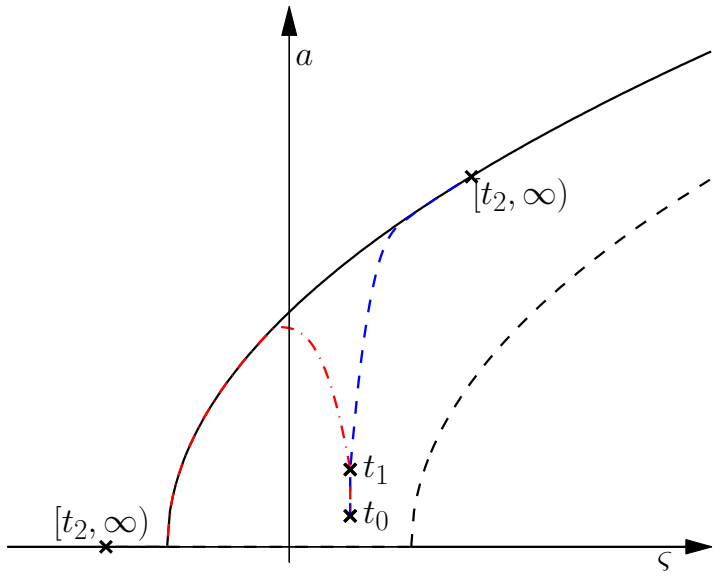

Figure 11.3: Control of parametric roll resonance: Increasing vs decreasing the encounter frequency.

This suggests that reducing the encounter frequency is the most sensible choice, and, in fact, the only option that can be guaranteed to work.

[2]It is worth noting that Figure 11.1 bears strong similarity to a cross-section with the wave height kept constant of the simulation of the full 6-DOF Model III of Chapter 5, except that with that model there was no evidence of the high-amplitude solutions of (11.13) in Region III. The stability regions indicated from simulating the 6-DOF model are shown in Figure 11.2.

It is, however, worth noting that the analysis is based on a simplification of the dynamics. The high-amplitude limit cycle has not been observed in the simulations with the more physically accurate 6-DOF ship Model III of Chapter 5. However, Galeazzi and Blanke [33], Ribeiro e Silva et al. [76] came to the opposite conclusion regarding speeding up versus slowing down. But bear in mind that in Galeazzi and Blanke [33], the conclusion was largely predicated on the need to have sufficient speed for fins (which were used in addition to speed change) to be effective.

None the less, decreasing the encounter frequency has another benefit: If we assume that ς starts at zero and slowly increases, trajectories will tend to go to a higher-amplitude limit cycle as the steady-state value of a increases with increasing ς in Region II. However, if we instead decrease ς, trajectories will tend to go to a lower-amplitude limit cycle *even if we are still in parametric resonance*. This phenomenon has been observed in the simulations with the 6-DOF Model III of Chapter 5, so there is reason to suspect that this holds true for real-world cases.

11.3 Simulation results

To test the validity of the controller (11.5), we simulated the closed-loop system using both the simplified model (11.1) (Model IV) and the full 6-DOF Model III of Chapter 5, in three different simulation scenarios. In all scenarios, we chose the initial conditions such that the ship was experiencing parametric roll resonance.

In accordance with the open-loop simulations in Chapter 5, a reduction of the frequency ratio to $\omega_{e,1}/\omega_\phi < 1.7$ will lead the ship out of the region where the ship is susceptible to parametric roll resonance.

We simulated three different scenarios:

1. *Slow* deceleration. The controller is turned on *after* parametric roll has already fully developed.
2. *Slow* deceleration. The controller is turned on *before* parametric roll has fully developed.
3. *Fast* deceleration. The controller is turned on *before* parametric roll has fully developed.

The simulation parameters are listed in Table 11.1. The control parameters are found in Tables 11.2–11.4. The simulation results are summarized in Tables 11.5–11.6, and can be seen in Figures 11.4–11.6.

Figure 11.4 shows the simulation results for the controlled system in comparison with the uncontrolled system for the first scenario. It is obvious from Figure 11.4(a) that the ship is experiencing large roll amplitudes caused by parametric resonance. The frequency ratio is gradually decreased after 300 s (Figure 11.4(c)) which causes the expected gradual reduction of the roll motion to zero.

The simulation results with the full 6-DOF Model III of Chapter 5 is shown in Figure 11.4(b). The controller works equally well with the more complex model.

Of course, since the controller is turned on only after parametric roll has fully developed, the maximum roll angle in Scenario 1 is the same for controlled and uncontrolled cases. (The steady-state roll angle is zero, as predicted.)

The simulation results of the second scenario is shown in Figure 11.5. In this scenario, we reduce the encounter frequency when the roll angle is much lower

Table 11.1: Simulation parameters.

Quantity	Symbol	Value	
Wave amplitude	ζ_0	2.5	m
Wave length	λ	281	m
Wave number	k_w	−0.0224	–
Natural roll frequency	ω_ϕ	0.343	rad/s
Modal wave frequency	ω_0	0.4684	rad/s
Simulation start time	t_0	0	s
Model parameters (simplified roll equation)	k_{44}	1.7533E9	$\mathrm{kg\,m^2/s^2}$
	$k_{\phi t}$	7.1373E8	$\mathrm{kg\,m^2/s^2}$
	α_ϕ	0.2741	rad
	k_{ϕ^3}	2.2627E9	$\mathrm{kg\,m^2/s^2}$

Table 11.2: Control parameters, Scenario 1.

Quantity	Symbol	Value	
Control action	ε	−1.7889E−4	$\mathrm{rad/s^2}$
Maximum deceleration	$\dot{v}^b_{1,\max}$	0.008	$\mathrm{m/s^2}$
Initial forward speed	$v^b_1(t_0)$	7.44	m/s
Initial encounter frequency	$\omega_{e,0}$	0.6346	rad/s
Final encounter frequency	$\omega_{e,1}$	0.5831	rad/s
Final forward speed	$v^b_1(t_2)$	5.14	m/s
Controller turned on	t_1	300	s
Controller turned off	t_2	588	s

Table 11.3: Control parameters, Scenario 2.

Quantity	Symbol	Value	
Control action	ε	−1.7889E−4	$\mathrm{rad/s^2}$
Maximum deceleration	$\dot{v}^b_{1,\max}$	0.008	$\mathrm{m/s^2}$
Initial forward speed	$v^b_1(t_0)$	7.44	m/s
Initial encounter frequency	$\omega_{e,0}$	0.6346	rad/s
Final encounter frequency	$\omega_{e,1}$	0.5831	rad/s
Final forward speed	$v^b_1(t_2)$	5.14	m/s
Controller turned on	t_1	93	s
Controller turned off	t_2	381	s

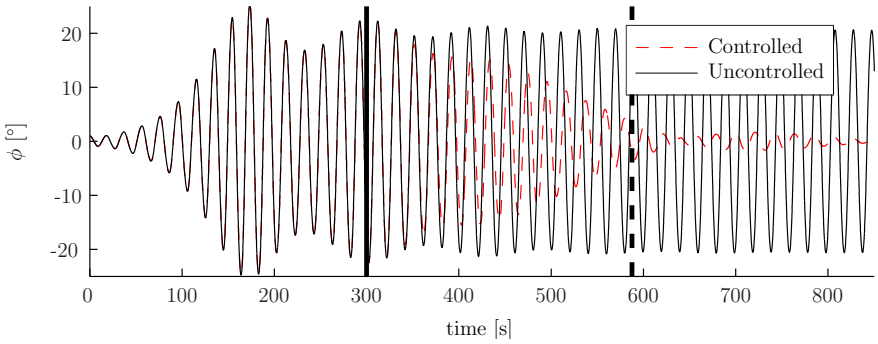

(a) 1-DOF Model IV.

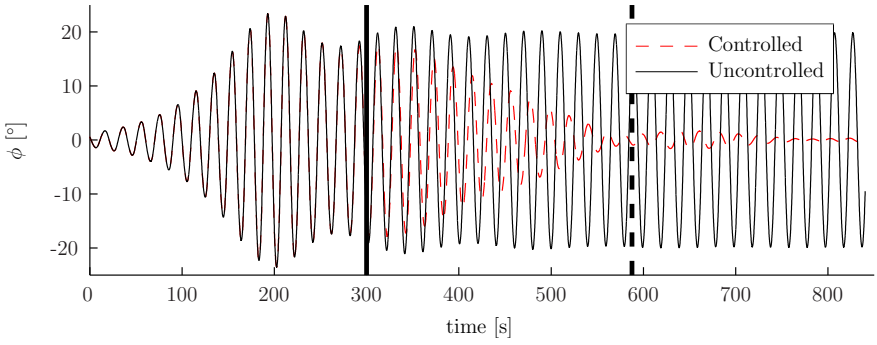

(b) 6-DOF Model III.

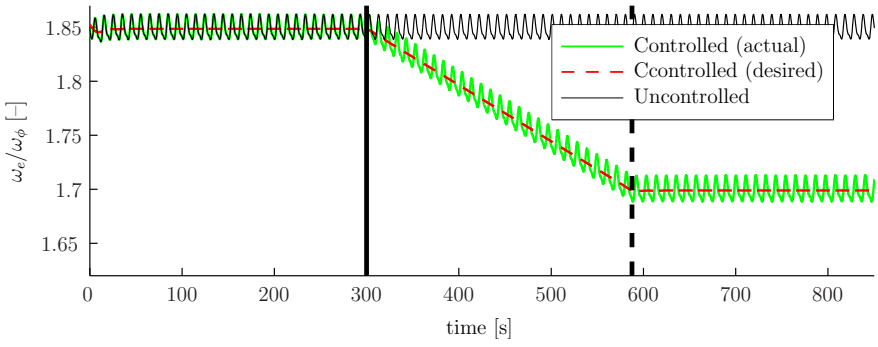

(c) Frequency ratio.

Figure 11.4: Simulation results, Scenario 1.

Table 11.4: Control parameters, Scenario 3.

Quantity	Symbol	Value	
Control action	ε	$-3.5778\text{E}{-4}$	rad/s^2
Maximum deceleration	$\dot{v}_{1,\max}^b$	0.016	m/s^2
Initial forward speed	$v_1^b(t_0)$	6.67	m/s
Initial encounter frequency	$\omega_{e,0}$	0.6174	rad/s
Final encounter frequency	$\omega_{e,1}$	0.5660	rad/s
Final forward speed	$v_1^b(t_2)$	4.37	m/s
Controller turned on	t_1	55	s
Controller turned off	t_2	199	s

Table 11.5: Simulation results, maximum roll angles, 1-DOF Model IV.

Scen.	Uncontrolled	Controlled	Reduction
1	25.34°	25.34°	0%
2	25.34°	22.40°	11.6%
3	23.57°	13.71°	41.8%

Table 11.6: Simulation results, maximum roll angles, 6-DOF Model III.

Scen.	Uncontrolled	Controlled	Reduction
1	23.34°	23.34°	0%
2	23.34°	20.33°	9.0%
3	17.99°	4.83°	73.2%

than in the first scenario, early enough that parametric rolling has not yet fully developed (specifically, when the roll angle is about 5°). Figure 11.5 shows that both the simplified 1-DOF Model IV and the full 6-DOF Model III behave similarly.

However, despite the controller being turned on when roll is only at 5°, the maximum roll angle is not greatly reduced compared to the uncontrolled case. This is simply because the ship is moving very slowly out of resonant condition. Steady-state roll angle is none the less zero, as predicted.

To get the ship to move out of resonant condition before the roll angle has reached dangerous levels requires, as it turned out, significantly faster deceleration than in Scenarios 1 and 1, even if the controller was turned on at a lower roll angle.

To this effect, we simulated Scenario 3. The controller is turned on early, at a time when the roll angle is about 2°. The ship is decelerating at twice the rate of Scenarios 1 and 2. Also, both the initial and final encounter frequencies are lower in Scenario 3 than in the two others. The results are plotted in Figure 11.6.

From Figure 11.6, we see that the controller is capable of reducing the roll angle sufficiently fast such that the maximum roll angle is only 1/2 (1-DOF) to 1/4 (6-DOF) of that of the uncontrolled case. Interestingly, from Figure 11.6(b) we see that the controller works significantly better for the full 6-DOF Model III than the

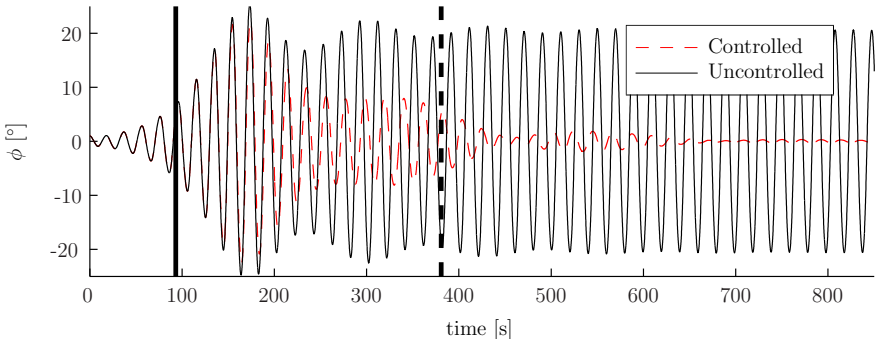

(a) 1-DOF Model IV.

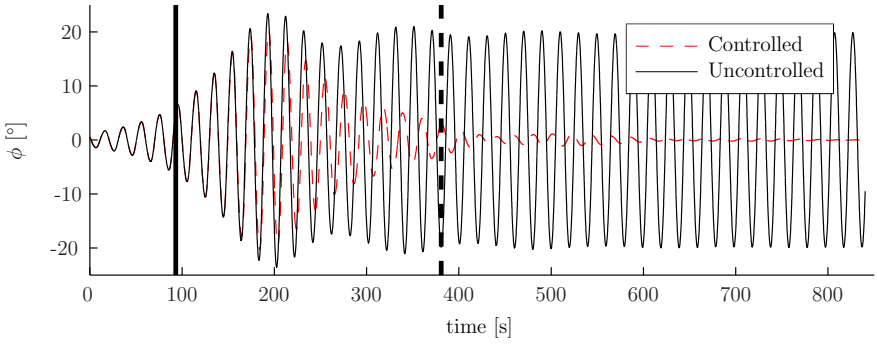

(b) 6-DOF Model III.

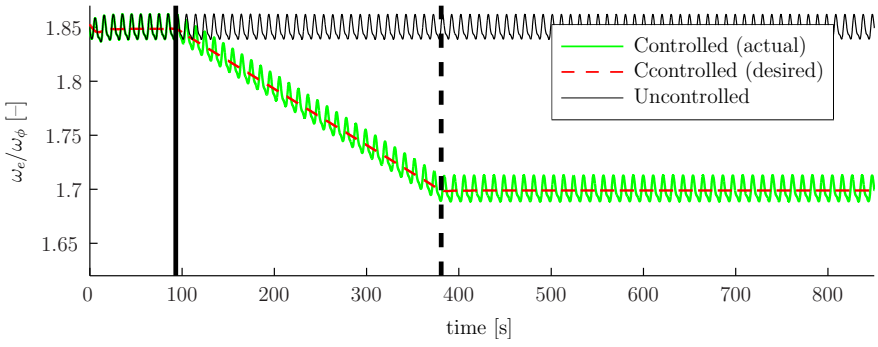

(c) Frequency ratio.

Figure 11.5: Simulation results, Scenario 2.

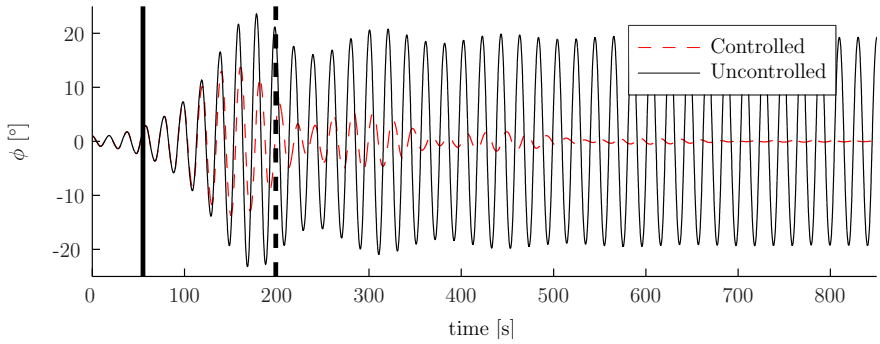

(a) 1-DOF model.

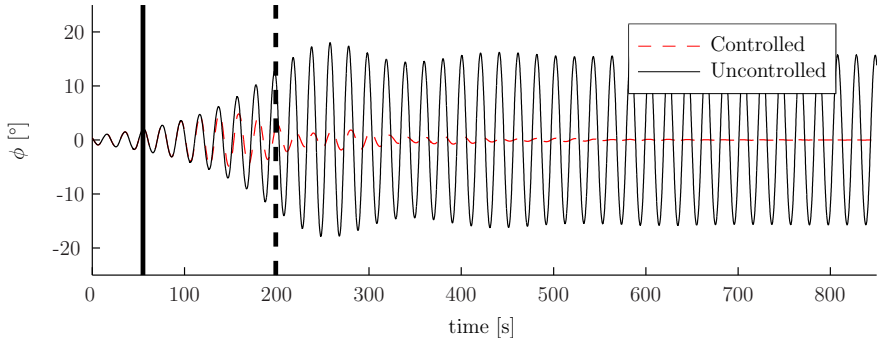

(b) 6-DOF model.

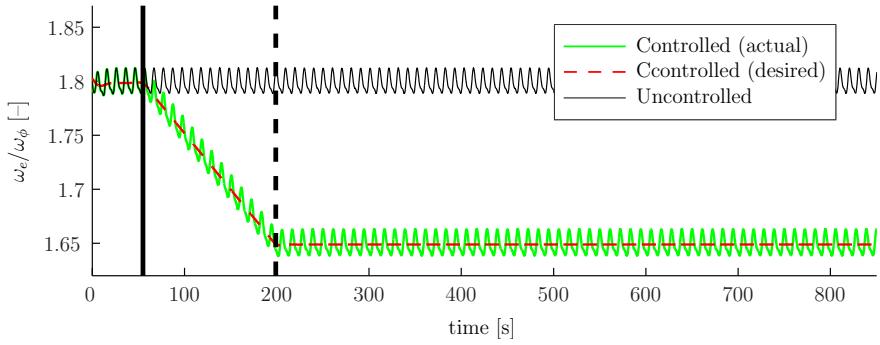

(c) Frequency ratio.

Figure 11.6: Simulation results, Scenario 3.

simplified 1-DOF Model IV. Steady-state, the roll angle is zero, as expected.

From the simulation results, we see that the controller is capable of bringing the controller out of parametric resonance and – assuming sufficient deceleration capability – reduce the maximum roll angle significantly. It is also vital to turn on the controller as early as possible. The simulations confirm the theoretical derivations presented in Section 11.2.

How practical the controller is in a real-world scenario depends almost entirely on the ability of the captain (or automated systems) to detect parametric resonance early, and the ability of the ship to rapidly decelerate. If these capabilities are present, then the controller could prove useful. In the absence of one or both of these abilities, the practicality of the controller is limited, at least on its own. However, it might be possible to pair it with another control scheme such as fins (as done in Galeazzi [32], Galeazzi et al. [34]), u-tanks (investigated used alone in Chapter 12), gyro stabilizers or other direct controllers.

Chapter 12

Direct control with u-tanks

In this chapter, an active, direct controller for parametric roll resonance using u-tanks as actuating system is developed.

This chapter is based on the model from Chapter 7, the results of Chapter 9 and Holden and Fossen [39].

12.1 U-tank model

The u-tank model presented in Chapter 7 is quite accurate. Unfortunately, it is quite complex.

The minimum number of degrees of freedom to describe the u-tank's effect on roll is two: roll, and the tank state. We therefore simplify the 7-DOF Model VII to a 2-DOF model.

We let $q_{r_2} = [\phi, q_t]^{\mathrm{T}}$ and $\nu_{r_2} = [\omega_1^b, \dot{q}_t]^{\mathrm{T}}$ as in Chapter 9, and note that $\dot{q}_{r_2} = \nu_{r_2}$.

We approximate the pressure-induced restoring moment in roll $k_{p,4}$ as

$$k_{p,4} \approx k_{44}\phi + k_{\phi t}\cos(\omega_e t + \alpha_\phi)\phi + k_{\phi^3}\phi^3 \tag{12.1}$$

as in Holden and Fossen [39], Holden et al. [40] and Chapters 6 and 11.

We can then define a reduced-order model.

Model XV (2-DOF generic u-tank model)**.** The dynamics of the reduced-order 2-DOF u-tank model with a generic u-tank can be written as

$$\begin{aligned} M_{r_2}(q_t)\ddot{q}_{r_2} + C_{r_2}(\dot{q}_{r_2})\dot{q}_{r_2} + D_{r_2}(\dot{q}_{r_2})\dot{q}_{r_2} + k_{r_2}(q_{r_2}) \\ + K_{r_2}q_{r_2} + K_{r_2,t}(t)q_{r_2} = \tau_{e,r_2}(t) + B_{r_2}u_t \end{aligned} \tag{12.2}$$

where

$$M_{r_2}(q_t) = \begin{bmatrix} J_{11} + m_{A,44} + M_{\omega,11}(q_t) & m_{\omega,\dot{q}_t,1} \\ m_{\omega,\dot{q}_t,1} & \bar{m}_t \end{bmatrix} = M_{r_2}^{\mathrm{T}}(q_t) > 0 \in \mathbb{R}^{2\times 2} \tag{12.3}$$

with

$$\begin{aligned} M_{\omega,11}(q_t) &= -\rho_t e_x^{\mathrm{T}} \left[\int_{-\varsigma_s(q_t)}^{\varsigma_p(q_t)} A(\sigma) S^2(r_g^b) \, \mathrm{d}\sigma \right] e_x \\ &= \rho_t \int_{-\varsigma_s(q_t)}^{\varsigma_p(q_t)} A(\sigma) \left[y_t^{b2}(\sigma) + z_t^{b2}(\sigma) \right] \, \mathrm{d}\sigma \\ m_{\omega,\dot{q}_t,1} &= \rho_t A_0 e_x^{\mathrm{T}} \int_{-\varsigma_s(q_t)}^{\varsigma_p(q_t)} S(r_t^b(\sigma)) \frac{\mathrm{d}\bar{r}_t^b}{\mathrm{d}\sigma}(\sigma) \, \mathrm{d}\sigma \\ &= \rho_t A_0 \int_{-\varsigma_s(q_t)}^{\varsigma_p(q_t)} y_t^b(\sigma) \frac{\mathrm{d}\bar{z}_t^b}{\mathrm{d}\sigma}(\sigma) - z_t^b(\sigma) \frac{\mathrm{d}\bar{y}_t^b}{\mathrm{d}\sigma}(\sigma) \, \mathrm{d}\sigma \end{aligned}$$

and $\bar{m}_t$ is as in (7.37). The damping matrix is given by

$$\begin{aligned} D_{r_2}(\nu_{r_2}) &\triangleq \begin{bmatrix} d_{44} & 0 \\ 0 & d_{tt} + d_{tt,n}|\dot{q}_t| \end{bmatrix} = D_0 + D_n(\dot{q}_t) \\ D_0 &\triangleq \begin{bmatrix} d_{44} & 0 \\ 0 & d_{tt} \end{bmatrix} \\ D_n(\dot{q}_t) &\triangleq \begin{bmatrix} 0 & 0 \\ 0 & d_{tt,n}|\dot{q}_t| \end{bmatrix} \end{aligned} \tag{12.4}$$

as in Chapter 9. We're only using linear damping in roll, as nonlinear damping in roll is known to be quite small [20]. Furthermore,

$$\begin{aligned} C_{r_2}(\dot{q}_t, \nu_{r_2}) \triangleq \frac{\dot{\phi}}{2} &\begin{bmatrix} 0 & \frac{\mathrm{d}M_{\omega,11}}{\mathrm{d}q_t}(q_t) \\ -\frac{\mathrm{d}M_{\omega,11}}{\mathrm{d}q_t}(q_t) & 0 \end{bmatrix} \\ + \frac{\dot{q}_t}{2} &\begin{bmatrix} \frac{\mathrm{d}M_{\omega,11}}{\mathrm{d}q_t}(q_t) & 2\frac{\mathrm{d}m_{\omega,\dot{q}_t,1}}{\mathrm{d}q_t}(q_t) \\ 0 & \frac{\mathrm{d}\bar{m}_t}{\mathrm{d}q_t}(q_t) \end{bmatrix} \end{aligned} \tag{12.5}$$

where

$$\begin{aligned} \frac{\mathrm{d}M_{\omega,11}}{\mathrm{d}q_t} &= \rho_t A_0 \left[y_t^{b2}(\varsigma_p) + z_t^{b2}(\varsigma_p) - y_t^{b2}(\varsigma_p) - z_t^{b2}(\varsigma_p) \right] \\ \frac{\mathrm{d}m_{\omega,\dot{q}_t,1}}{\mathrm{d}q_t} &= \rho_t A_0 \left[y_t^b(\varsigma_p) \frac{\mathrm{d}\bar{z}_t^b}{\mathrm{d}\sigma}(\varsigma_p) - z_t^b(\varsigma_p) \frac{\mathrm{d}\bar{y}_t^b}{\mathrm{d}\sigma}(\varsigma_p) \right] \\ &\quad - \rho_t A_0 \left[y_t^b(\varsigma_s) \frac{\mathrm{d}\bar{z}_t^b}{\mathrm{d}\sigma}(\varsigma_s) - z_t^b(\varsigma_s) \frac{\mathrm{d}\bar{y}_t^b}{\mathrm{d}\sigma}(\varsigma_s) \right] \\ \frac{\mathrm{d}\bar{m}_t}{\mathrm{d}q_t} &= \rho_t A_0^3 \left[\frac{1}{A^2(\varsigma_p)} - \frac{1}{A^2(\varsigma_s)} \right] \end{aligned}$$

and

$$K_{r_2} \triangleq \begin{bmatrix} k_{44} & 0 \\ 0 & 0 \end{bmatrix} \tag{12.6}$$

$$K_{r_2,t}(t) \triangleq \begin{bmatrix} k_{\phi t} \cos(\omega_e t + \alpha_\phi) & 0 \\ 0 & 0 \end{bmatrix} \tag{12.7}$$

$$k_{r_2}(q_{r_2}) \triangleq \begin{bmatrix} \left(mgz_g^b + g\rho_t \int_{-\varsigma_s}^{\varsigma_p} z_t^b A \,\mathrm{d}\sigma\right)\sin(\phi) \\ -g\rho_t A_0 \left[y_t^b(\varsigma_p) + y_t^b(\varsigma_s)\right]\sin(\phi) \end{bmatrix} + \begin{bmatrix} -g\rho_t \int_{-\varsigma_s}^{\varsigma_p} y_t^b A \,\mathrm{d}\sigma \cos(\phi) + k_{\phi^3}\phi^3 \\ -g\rho_t A_0 \left[z_t^b(\varsigma_p) - z_t^b(\varsigma_s)\right]\cos(\phi) \end{bmatrix} \tag{12.8}$$

$$B_{r_2} \triangleq \begin{bmatrix} 0 \\ b_t \end{bmatrix} = \begin{bmatrix} 0 \\ 1 \end{bmatrix} \tag{12.9}$$

$$\tau_{e,r_2}(t) \triangleq \begin{bmatrix} 0 & 0 & 0 & 1 & 0 & 0 & 0 \\ 0 & 0 & 0 & 0 & 0 & 0 & 1 \end{bmatrix} \tilde{\tau}_e(t). \tag{12.10}$$

This model structure follows quite readily from Model VII if the pressure-induced moment in roll is given by (12.1).

12.2 Control design

As investigated in Chapter 9, with the exception of the nonlinear damping, the nonlinearities of Model XV have very little effect on the behavior of the system. We therefore define a simplified model, which we will use for control design (we will use Model XV to verify the controller).

Model XVI (Simplified 2-DOF generic u-tank model)**.** The dynamics of the simplified reduced-order 2-DOF u-tank model with a generic u-tank can be written as

$$M_0\ddot{q}_{r_2} + D_{r_2}(\dot{q}_{r_2})\dot{q}_{r_2} + K_l q_{r_2} + K_{r_2,t}(t)q_{r_2} = \tau_{e,r_2}(t) + B_{r_2}u_t \tag{12.11}$$

where

$$M_0 \triangleq M_{r_2}(0) \triangleq \begin{bmatrix} m_{44} & m_{4t} \\ m_{4t} & \bar{m}_t \end{bmatrix} \tag{12.12}$$

$$K_l \triangleq K_{r_2} + \left.\frac{\partial k_{r_2}}{\partial q_{r_2}}\right|_{q_{r_2}=0} = \begin{bmatrix} \bar{k}_{44} & k_{4t} \\ k_{4t} & k_{tt} \end{bmatrix} \tag{12.13}$$

with

$$\bar{k}_{44} \triangleq k_{44} + mgz_g^b + 2g\rho_t \int_0^{\varsigma_0} A(\sigma) z_t^b(\sigma)\,\mathrm{d}\sigma$$
$$k_{4t} \triangleq -2g\rho_t A_0 y_t^b(\varsigma_0)$$
$$k_{tt} \triangleq -2g\rho_t \frac{A_0}{A(\varsigma_0)} \frac{\mathrm{d}z_t^b}{\mathrm{d}\sigma}(\varsigma_0)$$

and the system matrices are as in Model XV. We note that $y_t^b(\varsigma_0), \frac{\mathrm{d}z_t^b}{\mathrm{d}\sigma}(\varsigma_0) > 0$.

We take Model XV as the plant model.
We define

$$x_t \triangleq [q_{r_2}^{\mathrm{T}}, \dot{q}_{r_2}^{\mathrm{T}}]^{\mathrm{T}} \in \mathbb{R}^4 \tag{12.14}$$

and rewrite the dynamics as

$$\dot{x}_t = A_t x + B_t u_t + G_t(t)x_t + g_t(\dot{q}_{r_2}) \tag{12.15}$$

where

$$\begin{aligned}
A_t &\triangleq \begin{bmatrix} 0_{2\times 2} & I_2 \\ -M_0^{-1}K_l & -M_0^{-1}D_0 \end{bmatrix} \in \mathbb{R}^{4\times 4} \\
B_t &\triangleq \begin{bmatrix} 0_{2\times 1} \\ M_0^{-1}B_{r_2} \end{bmatrix} \in \mathbb{R}^{4\times 1} \\
G_t(t) &\triangleq \begin{bmatrix} 0_{2\times 2} & 0_{2\times 2} \\ -M_0^{-1}K_{r_2,t}(t) & 0_{2\times 2} \end{bmatrix} \in \mathbb{R}^{4\times 4} \\
g_t(\dot{q}_{r_2}) &\triangleq \begin{bmatrix} 0_{2\times 1} \\ -M_0^{-1}D_n(\dot{q}_t)\dot{q}_{r_2} \end{bmatrix} \in \mathbb{R}^{4\times 1}.
\end{aligned}$$

Theorem 12.1 (U-tank control)**.** *The origin of the system (12.15) is globally (uniformly) exponentially stabilized (following Khalil [52, Definition 4.5][1]) by the controller*

$$u_t = d_{tt,n}|\dot{q}_t|\dot{q}_t - K_p x_t, \tag{12.16}$$

where $K_p = [K_{p,1}, K_{p,2}, K_{p,3}, K_{p,4}] \in \mathbb{R}^{1\times 4}$ is a matrix such that $A_t - B_t K_p$ is Hurwitz and the eigenvalues of $A_t - B_t K_p$ chosen such that

$$\lambda_{\max}(P_t) < \frac{1}{2k_{\phi t}\|M_0^{-1}\|_2} \tag{12.17}$$

where P_t is the solution to the Lyapunov equation

$$P_t(A_t - B_t K_p) + (A_t - B_t K_p)^{\mathrm{T}} P_t = -I_4$$

and $\lambda_{\max}(P_t)$ is the maximum eigenvalue of P_t. Moreover, a K_p such that (12.17) is satisfied can always be found.

Proof. We immediately note that by choosing $u_t = d_{tt,n}|\dot{q}_t|\dot{q}_t + v_t$, we can transform the dynamics of the system (12.15) into the linear system

$$\dot{x}_t = A_t x_t + B_t v_t + G_t(t)x_t. \tag{12.18}$$

The term $G_t(t)x_t$ can be viewed as a time-varying disturbance to the system. We cannot directly cancel it, both because the parameters are unlikely to be known and because roll is not directly actuated.

The unperturbed system has the dynamics

$$\dot{x}_t = A_t x_t + B_t v_t. \tag{12.19}$$

[1] By this definition, exponential stability is stronger than uniform asymptotic stability, and thus the uniformity is implied.

This system is controllable if its controllability matrix

$$\mathcal{C} = \begin{bmatrix} B_t & A_t B_t & A_t^2 B_t & A_t^3 B_t \end{bmatrix} \tag{12.20}$$

has full rank (i.e., is nonsingular) [13].

The controllability matrix is given by

$$\mathcal{C} = \begin{bmatrix} M_0^{-1} & 0_{2\times 2} \\ 0_{2\times 2} & M_0^{-1} \end{bmatrix} \bar{\mathcal{C}}\,, \quad \bar{\mathcal{C}} \triangleq \begin{bmatrix} 0 & 0 & \bar{a}_1 & \bar{b}_1 \\ 0 & 1 & \bar{a}_2 & \bar{b}_2 \\ 0 & \bar{a}_1 & \bar{b}_1 & \bar{c}_1 \\ 1 & \bar{a}_2 & \bar{b}_2 & \bar{c}_2 \end{bmatrix}$$

where the parameters are given by

$$\begin{aligned} \begin{bmatrix} \bar{a}_1 \\ \bar{a}_2 \end{bmatrix} &= -D_0 M_0^{-1} B_{r_2} \\ \begin{bmatrix} \bar{b}_1 \\ \bar{b}_2 \end{bmatrix} &= (D_0 M_0^{-1} D_0 - K_l) M_0^{-1} B_{r_2} \\ \begin{bmatrix} \bar{c}_1 \\ \bar{c}_2 \end{bmatrix} &= (K_l M_0^{-1} D_0 + D_0 M_0^{-1} K_l - D_0 M_0^{-1} D_0 M_0^{-1} D_0) M_0^{-1} B_{r_2}. \end{aligned}$$

From Chen [13], we have that $\text{rank}(\mathcal{C}) = \text{rank}(\bar{\mathcal{C}})$ since the matrix

$$\begin{bmatrix} M_0^{-1} & 0_{2\times 2} \\ 0_{2\times 2} & M_0^{-1} \end{bmatrix} \in \mathbb{R}^{4\times 4}$$

is nonsingular.

$\bar{\mathcal{C}}$ has full rank if its determinant is nonzero [13]. Since

$$\det(\bar{\mathcal{C}}) = -\frac{1}{\det^2(M_0)} \left(\left[\bar{k}_{44} m_{4t} - k_{4t} m_{44} \right]^2 + d_{44}^2 k_{4t} m_{4t} \right)\,, \tag{12.21}$$

this gives the condition

$$\left[\bar{k}_{44} m_{4t} - k_{4t} m_{44} \right]^2 + d_{44}^2 k_{4t} m_{4t} \neq 0\,. \tag{12.22}$$

As long as this condition is satisfied, (12.19) is controllable. Since all the parameters in (12.22) are strictly positive, this condition is always satisfied.

As (12.19) is controllable, we can select a $v_t = -K_p x_t$, $K_p \in \mathbb{R}^{1\times 4}$, such that $A_t - B_t K_p$ is Hurwitz, and can place the poles arbitrarily far into the left half-plane [13]. The closed-loop system is then given by

$$\dot{x}_t = (A_t - B_t K_p) x_t + G_t(t) x\,. \tag{12.23}$$

From Khalil [52], we know that for any positive definite symmetric matrix N_t, there exists a positive definite symmetric matrix P_t such that

$$P_t (A_t - B_t K_p) + (A_t - B_t K_p)^{\mathrm{T}} P_t = -N_t\,. \tag{12.24}$$

We choose Lyapunov function candidate

$$\mathcal{V}(x_t) = x_t^{\mathrm{T}} P_t x_t \tag{12.25}$$

with P as the solution to (12.24). We note that $\mathcal{V}$ is positive definite and decrescent. Specifically,

$$\lambda_{\min}(P_t)\|x_t\|_2^2 \leq \mathcal{V}(x_t) \leq \lambda_{\max}(P_t)\|x_t\|_2^2 \tag{12.26}$$

where $\lambda_{\min}(P_t)$ and $\lambda_{\max}(P_t)$ are the minimum and maximum eigenvalues of P_t.

The time derivative of $\mathcal{V}$ along the trajectories of the closed-loop system (12.23) is given by

$$\begin{aligned}
\dot{\mathcal{V}}(x_t) &= x_t^{\mathrm{T}} P_t \dot{x}_t + \dot{x}_t^{\mathrm{T}} P_t x_t \\
&= x_t^{\mathrm{T}} \left[P_t(A_t - B_t K_p) + (A_t - B_t K_p)^{\mathrm{T}} P_t \right] x_t + x_t^{\mathrm{T}} \left[P_t G_t(t) + G_t^{\mathrm{T}}(t) P_t \right] x_t \\
&= -x_t^{\mathrm{T}} N_t x_t + x_t^{\mathrm{T}} \left[P_t G_t(t) + G_t^{\mathrm{T}}(t) P_t \right] x_t \\
&\leq -\lambda_{\min}(N_t)\|x_t\|_2^2 + 2\lambda_{\max}(P_t) \max_t \|G_t(t)\|_2 \|x_t\|_2^2 \\
&\leq -\lambda_{\min}(N_t)\|x_t\|_2^2 + 2k_{\phi t}\lambda_{\max}(P_t)\|M_0^{-1}\|_2\|x_t\|_2^2 \\
&= -\left[\lambda_{\min}(N_t) - 2k_{\phi t}\lambda_{\max}(P_t)\|M_0^{-1}\|_2 \right] \|x_t\|_2^2
\end{aligned} \tag{12.27}$$

where we have used that

$$\max_t \|G_t(t)\|_2 = \left\| \begin{bmatrix} 0_{2\times 2} & 0_{2\times 2} \\ -M_0^{-1} \begin{bmatrix} k_{\phi t} & 0 \\ 0 & 0 \end{bmatrix} & 0_{2\times 2} \end{bmatrix} \right\|_2 \leq k_{\phi t}\|M_0^{-1}\|_2 \,. \tag{12.28}$$

By Khalil [52, Theorem 4.10], the origin of the controlled system (12.23) is globally (uniformly) exponentially stable, as long as $\lambda_{\min}(N_t) > 2k_{\phi t}\lambda_{\max}(P_t)\|M_0^{-1}\|_2$ or

$$k_{\phi t} < \frac{\lambda_{\min}(N_t)}{2\lambda_{\max}(P_t)\|M_0^{-1}\|_2}.$$

The ratio $\lambda_{\min}(N_t)/\lambda_{\max}(P_t)$ is maximized by choosing $N_t = I_4$ [52]. Since we can choose the eigenvalues of $A_t - B_t K_p$ arbitrarily far into the left half-plane, we can (implicitly) choose $\lambda_{\max}(P_t)$ arbitrarily, as this value depends on the eigenvalues of $A_t - B_t K_p$ [13].

Thus, for any $k_{\phi t}$, we can find a controller such that the origin of the controlled system (12.23) is globally (uniformly) exponentially stable. □

If we take a closer look at the controller (12.16), it cancels the nonlinear tank damping. This damping is "good" damping; in the absence of the time-varying disturbance (setting $k_{\phi t} = 0$) it is fairly straight-forward to show that the origin of the system (12.15) is GAS by using the energy-like Lyapunov function $\bar{\mathcal{V}} = \dot{q}_{r_2}^{\mathrm{T}} M_0 \dot{q}_{r_2} + q_{r_2}^{\mathrm{T}} K_l q_{r_2}$ (via the Krasowskii–LaSalle theorem [52, Theorem 4.4]).

It is therefore reasonable to believe that this damping term is also beneficial in the presence of the time-varying disturbance ($k_{\phi t} \neq 0$). However, proving this has shown itself to be difficult, and the controller (12.16) is therefore canceling this term.

12.3 Simulation study

We simulated the plant Model XV both with and without the controller (12.16) to test the validity and the robustness of the controller. For comparison, we also simulated the controlled nominal system (12.23).

The tank functions y_t^b, z_t^b and A were given by (8.1)–(8.3). The tank state q_t was limited so that $|q_t| \leq q_{t,\max} = V_t/(2A_0)$ so that there is always tank fluid at the tank center point $\sigma = 0$.

Simulation parameters can be found in Table 12.1. The ship parameters J_{11}, $m_{A,44}$, d_{44}, k_{44}, $k_{\phi t}$ and k_{ϕ^3} were taken from Holden et al. [40, Experiment 1174]. The tank damping parameters are based on experimental values from Chapter 9 and formulas found in Holden et al. [42] and Lloyd [58]. The encounter frequency ω_e was chosen to be twice the natural roll frequency, when the system is known to parametrically oscillate.

Table 12.1: Simulation parameters.

Parameter	Value	Unit	Parameter	Value	Unit
J_{11}	1.4014E10	kg·m^2	A_r	30	m^2
$m_{A,44}$	2.17E9	kg·m^2	A_d	3.6145	m^2
d_{44}	3.1951E8	kg·m^2/s	w	27	m
d_{tt}	2.4618E3	kg·m/s	ϵ	1	m
$d_{tt,n}$	2.2742E5	kg·m	r_d	2	m
k_{44}	2.2742E9	kg·m^2/s^2	ς_0	17.5	m
$k_{\phi t}$	5.0578E8	kg·m^2/s^2	A_0	30	m^2
k_{ϕ^3}	2.974E9	kg·m^2/s^2	$\phi(t_0)$	5	°
m	7.64688E7	kg	$\dot{\phi}(t_0)$	0	°/s
z_g^b	−1.12	m	$q_t(t_0)$	0	m
g	9.81	m/s^2	$\dot{q}_t(t_0)$	0	m/s
ρ_t	1000	kg/m^3	$K_{p,1}$	3.9935E5	kg·m/s^2
ω_e	0.594	rad/s	$K_{p,2}$	7.2833E3	kg/s^2
α_ϕ	0	rad	$K_{p,3}$	−4.1664E5	kg·m/s
$q_{t,\max}$	5.6307	m	$K_{p,4}$	3.9916E5	kg/s

The uncontrolled nominal system (12.15) had eigenvalues

$$\lambda(A_t) \approx [-0.0049 \pm 0.3327i, -0.0051 \pm 0.2558i]$$

while the controlled system had eigenvalues

$$\lambda(A_t - B_x K_p) \approx [-0.0196 \pm 0.3327i, -0.0206 \pm 0.2558i] \ .$$

With the parameters of Table 12.1, the mass of the tank fluid m_t was computed to be $m_t \approx 337\,800$ kg. Per the standard rules of u-tank design [58], the tank is dimensioned so that the natural frequency of the tank (here, 0.2978 rad/s) is chosen to be approximately equal to the natural roll frequency (here, 0.2972 rad/s).

The results of the simulation study can be seen in Figures 12.1 and 12.2. We can clearly see that the system trajectory converges to the origin. Note also that the trajectory of the nominal system is almost identical to that of the true system.

From Figures 12.1(a) and 12.1(b), we can also see that a passive (uncontrolled) tank is capable of reducing the roll angle compared to not having a tank at all[2] (a reduction in maximum roll angle of approximately 21° to 7°). However, both roll and the tank fluid will end up in steady-state oscillations.

The issue of correctly tuning the natural frequency of the tank fluid bears some consideration. For a rectangular-prism tank (and a tank like the one used in the simulations in this chapter), the natural frequency can be changed by adjusting the fluid level ς_0 or the ratio of A_r and A_d (cross-sectional area of the reservoirs and the duct, respectively). The latter can of course only be done when the tank is constructed.

Unfortunately, the natural frequency has very low sensitivity to changes in ς_0 [58]. It is therefore almost impossible to change the natural frequency of the tank after it has been built. However, there can be quite some uncertainty in the natural roll frequency, which can also depend on loading conditions [20, 58].

If the natural frequency of the tank is not properly tuned, the effect of a passive tank can be drastically reduced. The more badly tuned it is, the less effective the tank is. However, as proven in Theorem 12.1, an active (controlled) tank will still be able to stabilize the origin of the system.

The power and energy consumptions of the control system is also worth noting. As can be seen from Figures 12.2(a) and 12.2(b), at peak the controller requires a force of about 250 kN and 210 kW. By integrating the power consumption (over 1 000 s), the total energy use can be found to be approximately 8 MJ.

These numbers require some context. If force on the tank fluid is applied by using high-pressure air in the reservoirs, the pressure difference in the two reservoirs has to be about 8.5 kPa, or 0.085 bar. When considering the maximum power consumption 21 kW, bear in mind that the actuator is moving 337.8 metric tons of fluid, and that the ship itself has a mass of 76 500 metric tons and is likely to have a quite large power system. The total energy consumption equals about 0.23 liters of gasoline (using 34.8 MJ/liter of gasoline [16]). All in all, the control system if fairly modest in scale.

[2] In Holden et al. [42] it was concluded that using a passive tank did not noticeably reduce the roll angle in parametric resonance, but this tank had a badly tuned natural frequency due to a calculation error; the ship's natural roll frequency is the square root of the value given in Holden et al. [42].

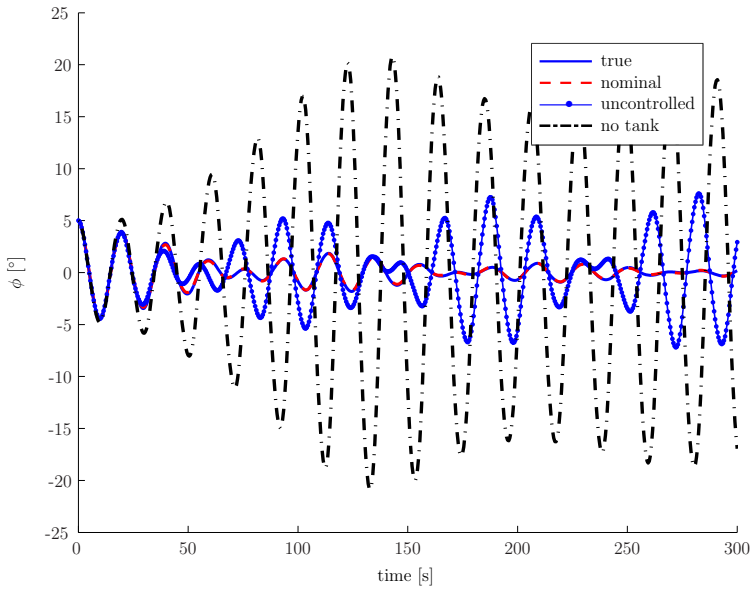

(a) Roll.

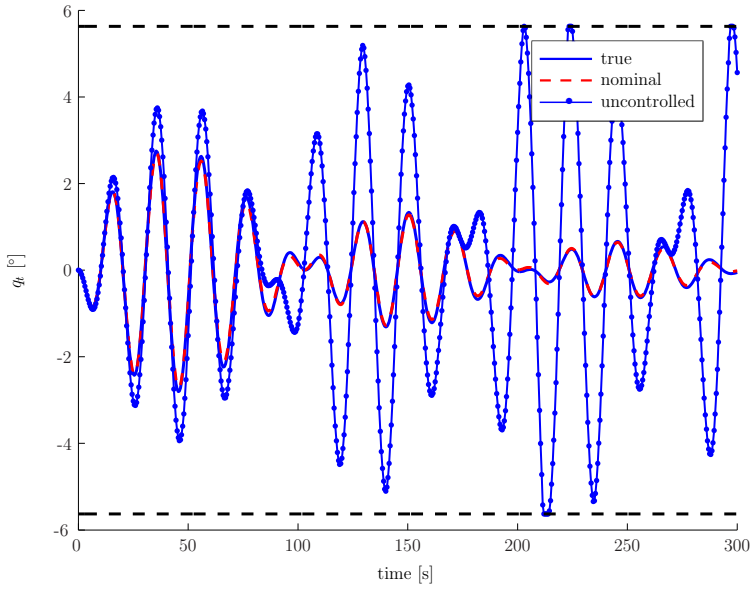

(b) Tank state.

Figure 12.1: Simulation of the closed- and open-loop system. True and nominal graphs are closed-loop simulations of Models XV and XVI, respectively. Uncontrolled is open-loop simulation of the plant Model XV.

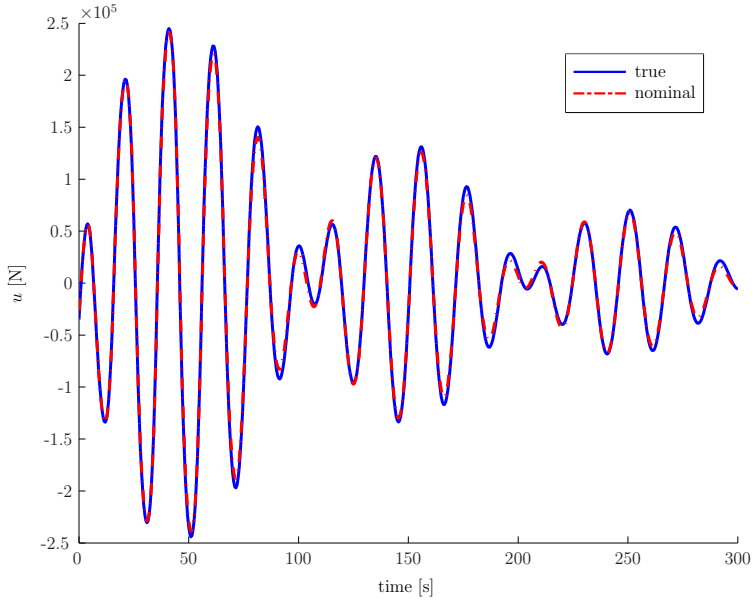

(a) Control input.

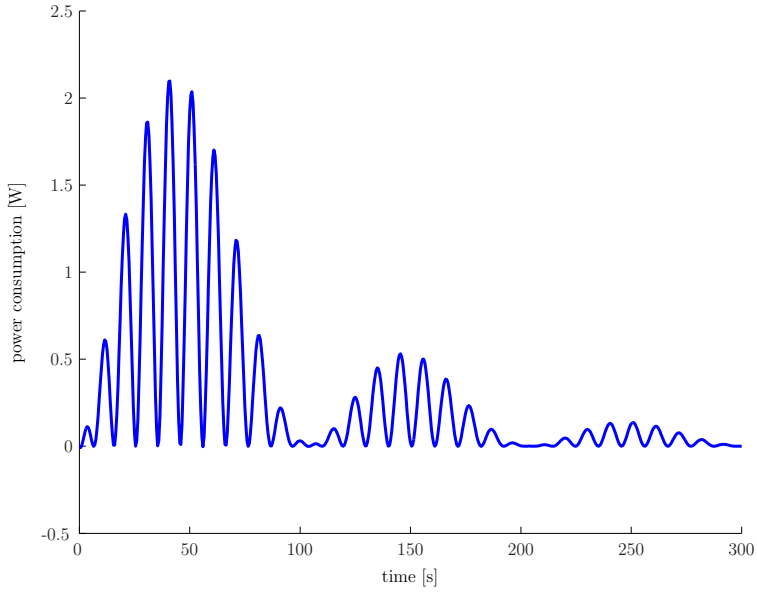

(b) Power consumption (true dynamics).

Figure 12.2: Simulation of the closed-loop system. True and nominal graphs are simulations of Models XV and XVI, respectively.

I have come to the conclusion, after many years of sometimes sad experience, that you cannot come to any conclusion at all.

Vita Sackville-West

Part IV

Closing remarks

Chapter 13

Conclusions and future work

This chapter lists the main conclusions drawn based on the thesis work. It also lists some possible avenues for future work.

13.1 Conclusions

The main goal of my PhD project has been to develop controllers capable of preventing or reducing parametric roll resonance, a dangerous resonance phenomenon afflicting especially container ships. Parametric roll is capable of causing damages for tens of millions of US dollars. Deriving, analyzing and simulating the controllers also necessitated the development of several novel models.

In this thesis, there have been six major contributions, four on modeling and two on control. They are listed here in their order of appearance in the thesis text.[1]

13.1.1 Six-DOF computer model for parametric roll

In Chapter 5, I presented a 6-DOF computer model for ships in parametric resonance (Model III). Unlike most models in literature, it is valid for both constant and changing velocity, allowing for both speed and course change.

The resulting model is a complex and accurate 6-DOF model. It considers the external forces due to the hydrostatic and hydrodynamic pressure field of the surrounding ocean. This includes the effect of waves. The restoring forces are calculated by integrating the pressure field over the instantaneous submerged part of the vessel, taking into account effects such as Doppler shift.

The model assumes that the pressure field is unchanged by the passage of the ship, and wave-induced forces are in practice limited to first-order approximations. The model is not analytical, and is therefore suitable only for simulation. We implemented the model in Matlab/Simulink using data from a specific, 281 m container ship.

The model has been published in Breu et al. [8].

[1] Note that the 3-DOF model described in Section 13.1.3 was, chronologically speaking, the first model derived during the PhD work. Its inability to describe the motion of ships with non-constant forward speed and/or course necessitated the development of further models.

13.1.2 One-DOF parametric roll model

In Chapter 5, I presented a 1-DOF analytical model for ships in parametric resonance (Model IV). Using a quasi-steady approach to compute heave and pitch motions, we derived a model that is suitable for ships with non-constant speed and course. Most existing models require the ship to be at constant forward speed and course.

We also showed that the more commonly used Mathieu equation is only valid if the speed and course of the vessel are constant. If these change, then the Mathieu equation is no longer able to accurately model the behavior of the ship.

The 1-DOF model was verified against the more complex 6-DOF Model III, and proved itself capable of capturing the dynamics of the ship across a wide range of conditions.

The model has been published in Breu et al. [8].

13.1.3 Three-DOF parametric roll model

In Chapter 6, I presented a 3-DOF (heave, roll, pitch) analytical model for ships in parametric resonance (Model VI). These three degrees of freedom are known to be coupled during parametric roll resonance.

The model is effectively a reduced-order, analytical version of the 6-DOF Model III described in Section 13.1.1. By Taylor-expanding the restoring forces to third order, an analytical model can be found. The parameters of the model can be computed from hull data. We used the same vessel as for the 6-DOF Model III.

The 3-DOF model was verified against experimental data gathered by Dr Ingo Drummen at SINTEF Marintek's towing tank in Trondheim, Norway. The model showed itself fairly capable of capturing the dynamics of the system, except in the borderland between no parametric resonance and parametric resonance. As this area is particularly vulnerable to small model uncertainties, this is to be expected.

One interesting thing to note is that, when plotting maximum roll angle against encounter frequency, the 3-DOF model shows high degree of similarity to that of both the 1-DOF Model IV and the 6-DOF computer Model III. As was shown in Chapter 11, this is due to the third-order restoring term in the 1-DOF and 3-DOF models. Unfortunately, the experiments show a somewhat different maximum roll to encounter frequency curve. This may indicate that a higher-order spring nonlinearity, or perhaps a trigonometric function, should be used instead of merely a third-order spring nonlinearity. Due to time constraints, this was not further investigated.

The model has been published in Holden et al. [40], Rodriguez et al. [77].

13.1.4 Seven-DOF model for ships with u-tanks

In Chapter 7, I presented a 7-DOF (6 DOFs for the ship, plus one for the tank) model for ships with u-tanks (Model VII). The model is suitable for both for ships suffering and not suffering parametric roll resonance.

Using Hamiltonian mechanics, a singularity-free model incorporating the intrinsic nonlinearities of the system was developed. The model is valid for u-tanks

of arbitrary shape, unlike most existing models, which are limited to u-tanks consisting of three connected rectangular prisms (one for the duct and one for each reservoir). The most restricting assumption in deriving the model is that the tank flow is one-dimensional. While technically not true, this is common practice in the literature. As we are most interested in the effect of the tank on roll, only the macroscopic motion of the tank fluid is interesting. Effects requiring partial differential equations to model are therefore of limited interest.

The model was experimentally verified, as detailed in Chapter 9, and compared to the commonly used model of Lloyd [57, 58] in Chapter 8. The model proved very capable of capturing the behavior of the tank fluid, significantly more so than existing models (having three orders of magnitude lower mean square error relative to experimental data). The experiments were conducted by me at SINTEF Marintek's facilities in Trondheim, Norway.

Most notable from the experimental verification was that the most significant nonlinearity in the system was the damping in the tank fluid. It was found that linear plus quadratic damping was sufficient to adequately model the damping. The effects of other nonlinearities was significantly smaller than that of the damping.

The model is not previously published, but is a generalization of the models found in Holden and Fossen [39], Holden et al. [44]. Experimental verification and comparison to the model of Lloyd [57, 58] has been published in Holden et al. [44].

13.1.5 Frequency detuning controller

A necessary (but not sufficient) criterion for the occurrence of parametric roll resonance is that the frequency of the waves as seen from the ship (the encounter frequency) is twice the natural roll frequency. Due to the Doppler effect, the encounter frequency is not necessarily the same as the actual frequency of the waves. This has the advantage that the encounter frequency can be changed by changing speed and/or course of the vessel. We have dubbed exploiting this to drive the encounter frequency away from potentially dangerous values "frequency detuning control".

In Chapter 11, I presented a frequency detuning controller capable of stopping parametric roll resonance.

The controller is derived based on the 1-DOF parametric roll model for non-constant speed and course, Model IV, mentioned in Section 13.1.2. The controller used only speed change. Using the 1-DOF Model IV, we proved mathematically that the frequency detuning controller is capable of stopping parametric roll resonance. The controller was verified in simulation, using both the 1-DOF Model IV and the higher-fidelity 6-DOF Model III. Simulation results confirmed the mathematical conclusions.

The control structure is quite simple, and requires no extra hardware or software on the ship. The main drawbacks of the controller are that it requires that the helmsman has ample warning about the onset of parametric roll (in practice probably requiring specialized detection software) and that the ship is capable of fairly rapid speed changes.

For high-inertia ships such as container ships, particularly the last drawback may prove critical. For smaller ships, such as fishing vessels, the problem is that

they often experience parametric roll when they are at rest. In those cases, it can take some time before the vessel is capable of effecting a significant speed change.

The effectiveness of the controller can in all likelihood be increased by changing course in addition to changing speed. However, this comes with the drawback that it will expose the ship to regular roll excitation. Due to time constraints, this was not further investigated during this PhD work.

The controller was published in Holden et al. [43].

13.1.6 Active u-tank-based controller for parametric roll

In Chapter 12, I presented an active u-tank-based controller capable of stopping parametric roll resonance.

We derived 2-DOF (roll and tank state) version of the 7-DOF u-tank Model VII mentioned in Section 13.1.4 and a further simplification of this 2-DOF model based on the conclusions as to which nonlinearities are important (see Section 13.1.4). Using the simplified 2-DOF model as control model, we derived a controller and proved mathematically that it is capable of stopping parametric roll. Zero roll angle and the tank fluid in it's equilibrium position was proven to be globally (uniformly) exponentially stable. The model was verified in simulation using both the control model and the more complicated 2-DOF model. Simulation results confirmed the mathematical conclusions, and showed that the control system uses almost negligible resources.

The controller uses an active u-tank. In simulation, a passive (i.e., uncontrolled) u-tank was also tested in the same conditions. The uncontrolled tank was capable of reducing the roll motion, but not driving it to zero as the controlled u-tank did. The effectiveness of the passive u-tank is also highly dependent on correct tuning of the tank's natural frequency. Ideally, it should match the ship's natural roll frequency. However, in practice, it is impossible to know the ship's actual roll frequency, and estimates are likely to be relatively inaccurate. Furthermore, it is effectively impossible to retune the tank after it has been installed on the ship. The controlled tank does not have any of these limitations. That, and the fact that the controller uses quite limited resources, indicates that an active control system is advantageous.

Combining the u-tank controller with the frequency detuning controller is quite possible, and would likely increase the effectiveness of the overall control scheme. Due to time constraints, this was not tested.

The controller was published in Holden and Fossen [39].

13.2 Future work

The time one has to work an a PhD is limited, and not all the could be done can be done in the time allotted. Thus, as always, there are several avenues that are open to further research. I list here some possibilities:

- The 6-DOF Model III should be verified against the same experimental data set that was used to verify the 3-DOF Model VI (and/or other against data sets).

- As mentioned in the conclusions, there is reason to believe that a third-order restoring moment nonlinearity in roll is not sufficient to get a more highly accurate model of roll during parametric resonance. Higher-order nonlinearities, or perhaps a trigonometric function, should be tested.
- The 7-DOF u-tank Model VII was verified using a specific rectangular-prism u-tank. Ideally, other u-tank shapes should also be tested in experiments.
- It is highly likely that the frequency detuning controller and the u-tank controller could be used effectively together. This would likely increase the effectiveness of the overall control scheme. This bears investigating
- The frequency detuning controller, on its own, could almost certainly be improved by also performing a course change rather than only a speed change. However, this does have the side effect that the ship would be subject to regular roll excitation, and should probably be used with caution. This should in any case be investigated.
- It is my belief that the stability properties of the u-tank using the more complicated 2-DOF model can be proven, rather than using a simplification. This should be examined further.
- Other active u-tank controllers could also be investigated.
- Ultimately, the controllers should be tested on model scale (or, preferably, full scale) ships.

[T]he appendix is small and has no known function.

New Oxford American Dictionary

Appendices

Appendix A

Matrix derivatives

The contents of this appendix are unpublished.

A.1 Useful operators

Before we define the derivatives of matrices, we need to define some useful operators.

We take the matrix $A = \{a_{i,j}\}_{\bar{a}_1 \times \bar{a}_2}$. We can take the vectorization $y = \operatorname{vec} A \in \mathbb{R}^{\bar{a}_1 \bar{a}_2}$ as $y_{\bar{a}_1(j-1)+i} = a_{i,j}$, i.e., stacking each column of A on top of each other to create y, or

$$y^{\mathrm{T}} = \begin{bmatrix} a_{1,1} & a_{2,1} & \dots & a_{\bar{a}_1,1} & a_{1,2} & a_{2,2} & \dots & a_{\bar{a}_1,\bar{a}_2} \end{bmatrix}. \tag{A.1}$$

The Kronecker product of to matrices $A = \{a_{i,j}\} \in \mathbb{R}^{\bar{a}_1 \times \bar{a}_2}$ and $B \in \mathbb{R}^{\bar{b}_1 \times \bar{b}_2}$ is given by

$$C = A \otimes B \triangleq \begin{bmatrix} a_{1,1}B & a_{1,2}B & \dots & a_{1,b}B \\ a_{2,1}B & a_{2,2}B & \dots & a_{2,b}B \\ \vdots & \vdots & \ddots & \vdots \\ a_{a,1}B & a_{a,2}B & \dots & a_{a,b}B \end{bmatrix} \in \mathbb{R}^{\bar{a}_1\bar{b}_1 \times \bar{a}_2\bar{b}_2}. \tag{A.2}$$

Lemma A.1 (Properties of the Kronecker product)**.** *For appropriately dimentioned matrices A, B, C and D and scalar k, the following hold:*

- $A \otimes 1 = 1 \otimes A = A$.
- $A \otimes 0 = 0 \otimes A = 0_{\dim A}$.
- $A \otimes (B + C) = A \otimes B + A \otimes C$.
- $(A + B) \otimes C = A \otimes C + B \otimes C$.
- $(kA) \otimes B = A \otimes (kB) = k(A \otimes B)$.
- $(A \otimes B) \otimes C = A \otimes (B \otimes C)$.
- $(A \otimes B)^{\mathrm{T}} = A^{\mathrm{T}} \otimes B^{\mathrm{T}}$.
- $(A \otimes B)^{-1} = A^{-1} \otimes B^{-1}$ *if A and B are invertible.*

- $(A \otimes B)(C \otimes D) = AC \otimes BD$.
- $\text{vec}\,(ABC) = (C^{\mathrm{T}} \otimes A)\text{vec}\,B$.

Proof. See Horn and Johnson [45], Strang [87] □

A.2 Matrix derivatives

We take a matrix function $M(x) = \{m_{i,j}(x)\}_{\bar{m}_1 \times \bar{m}_2}$ as a function mapping $\mathbb{R}^n$ to $\mathbb{R}^{\bar{m}_1 \times \bar{m}_2}$. The derivative of this matrix with respect to x_k is given by the matrix of the derivatives of the elements of M, or

$$\frac{\partial M}{\partial x_k} = \left\{ \frac{\partial m_{i,j}}{\partial x_k} \right\}_{\bar{m}_1 \times \bar{m}_2}. \tag{A.3}$$

We can take the derivative of a vector $y(x) \in \mathbb{R}^{\bar{y}}$ with respect to $x \in \mathbb{R}^n$ as a matrix

$$\frac{\mathrm{d}y}{\mathrm{d}x} \triangleq \begin{bmatrix} \frac{\mathrm{d}y_1}{\mathrm{d}x_1} & \frac{\mathrm{d}y_2}{\mathrm{d}x_1} & \cdots & \frac{\mathrm{d}y_{\bar{y}}}{\mathrm{d}x_1} \\ \frac{\mathrm{d}y_1}{\mathrm{d}x_2} & \frac{\mathrm{d}y_2}{\mathrm{d}x_2} & \cdots & \frac{\mathrm{d}y_{\bar{y}}}{\mathrm{d}x_2} \\ \vdots & \vdots & \ddots & \vdots \\ \frac{\mathrm{d}y_1}{\mathrm{d}x_n} & \frac{\mathrm{d}y_2}{\mathrm{d}x_n} & \cdots & \frac{\mathrm{d}y_{\bar{y}}}{\mathrm{d}x_n} \end{bmatrix} = \begin{bmatrix} \frac{\mathrm{d}y^{\mathrm{T}}}{\mathrm{d}x_1} \\ \vdots \\ \frac{\mathrm{d}y^{\mathrm{T}}}{\mathrm{d}x_n} \end{bmatrix} \in \mathbb{R}^{n \times \bar{y}}. \tag{A.4}$$

Note that this implies that the derivative of a scalar-valued function with respect to a vector is a column vector, and that $\frac{\mathrm{d}y^{\mathrm{T}}}{\mathrm{d}x} = \frac{\mathrm{d}y}{\mathrm{d}x}$.

Based on the derivative of a vector with respect to another, we can then take the derivative of M with respect to x as

$$\begin{aligned} \frac{\mathrm{d}M}{\mathrm{d}x} &\triangleq \begin{bmatrix} \frac{\mathrm{d}m_{1,1}}{\mathrm{d}x_1} & \frac{\mathrm{d}m_{2,1}}{\mathrm{d}x_1} & \cdots & \frac{\mathrm{d}m_{\bar{m}_1,1}}{\mathrm{d}x_1} & \frac{\mathrm{d}m_{1,2}}{\mathrm{d}x_1} & \cdots & \frac{\mathrm{d}m_{\bar{m}_1,\bar{m}_2}}{\mathrm{d}x_1} \\ \frac{\mathrm{d}m_{1,1}}{\mathrm{d}x_2} & \frac{\mathrm{d}m_{2,1}}{\mathrm{d}x_2} & \cdots & \frac{\mathrm{d}m_{\bar{m}_1,1}}{\mathrm{d}x_2} & \frac{\mathrm{d}m_{1,2}}{\mathrm{d}x_1} & \cdots & \frac{\mathrm{d}m_{\bar{m}_1,\bar{m}_2}}{\mathrm{d}x_1} \\ \vdots & \vdots & \ddots & \vdots & \vdots & \ddots & \vdots \\ \frac{\mathrm{d}m_{1,1}}{\mathrm{d}x_n} & \frac{\mathrm{d}m_{2,1}}{\mathrm{d}x_n} & \cdots & \frac{\mathrm{d}m_{\bar{m}_1,1}}{\mathrm{d}x_n} & \frac{\mathrm{d}m_{1,2}}{\mathrm{d}x_1} & \cdots & \frac{\mathrm{d}m_{\bar{m}_1,\bar{m}_2}}{\mathrm{d}x_1} \end{bmatrix} \\ &= \begin{bmatrix} \frac{\mathrm{d}(\text{vec}\,M)^{\mathrm{T}}}{\mathrm{d}x_1} \\ \vdots \\ \frac{\mathrm{d}(\text{vec}\,M)^{\mathrm{T}}}{\mathrm{d}x_n} \end{bmatrix} \in \mathbb{R}^{n \times \bar{m}_1 \bar{m}_2}. \end{aligned} \tag{A.5}$$

The ith row of the above matrix is the vectorization of M, differentiated with respect to x_i.

Lemma A.2 (Product rule)**.** *Let $M(x) = A(x)B(x) \in \mathbb{R}^{\bar{m}_1 \times \bar{m}_2}$, with $x \in \mathbb{R}^n$, $A(x) \in \mathbb{R}^{\bar{m}_1 \times \bar{a}_2}$ and $B(x) \in \mathbb{R}^{\bar{a}_2 \times \bar{m}_2}$. Then*

$$\frac{\mathrm{d}M}{\mathrm{d}x} = \frac{\mathrm{d}AB}{\mathrm{d}x} = \frac{\mathrm{d}A}{\mathrm{d}x}\left(B(x) \otimes I_{\bar{m}_1}\right) + \frac{\mathrm{d}B}{\mathrm{d}x}\left(I_{\bar{m}_2} \otimes A^{\mathrm{T}}(x)\right) \tag{A.6}$$

where $\otimes$ denotes the Kronecker product.

Proof. We let $l \in \{1, \ldots, n\}$, $k \in \{1, \ldots, \bar{m}_1\}$, $r \in \{1, \ldots, \bar{m}_2\}$.

We note that

$$\frac{\mathrm{d}m_{k,r}}{\mathrm{d}x_l} = \frac{\mathrm{d}}{\mathrm{d}x_l}\left[\sum_{j=1}^{\bar{a}_2} a_{k,j} b_{j,r}\right] = \sum_{j=1}^{\bar{a}_2}\left[\frac{\mathrm{d}a_{k,j}}{\mathrm{d}x_l} b_{j,k} + a_{k,j}\frac{\mathrm{d}b_{j,k}}{\mathrm{d}x_l}\right] \tag{A.7}$$

where the product rule (for scalars) has been used. From the definition of the derivative of a matrix with respect to a vector, $\frac{\mathrm{d}m_{k,r}}{\mathrm{d}x_l}$ is found in element $(l, \bar{m}_1(r-1)+k)$ of the matrix $\frac{\mathrm{d}M}{\mathrm{d}x}$.

We then look at element $(l, \bar{m}_1(r-1)+k)$ of the matrix $\frac{\mathrm{d}A}{\mathrm{d}x}\left(B(x) \otimes I_{\bar{m}_1}\right) + \frac{\mathrm{d}B}{\mathrm{d}x}\left(I_{\bar{m}_2} \otimes A^{\mathrm{T}}(x)\right)$. We define $C \triangleq \frac{\mathrm{d}A}{\mathrm{d}x}\left(B(x) \otimes I_{\bar{m}_1}\right) + \frac{\mathrm{d}B}{\mathrm{d}x}\left(I_{\bar{m}_2} \otimes A^{\mathrm{T}}(x)\right)$ with elements $c_{i,j}$. We then find

$$\begin{aligned} c_{l,\bar{m}_1(r-1)+k} &= \frac{\mathrm{d}(\mathrm{vec}\, A)^{\mathrm{T}}}{\mathrm{d}x_l}\begin{bmatrix} 0 \\ \vdots \\ b_{1,r} \\ \vdots \\ 0 \\ \vdots \\ b_{\bar{a}_2,r} \\ \vdots \\ 0 \end{bmatrix} + \frac{\mathrm{d}(\mathrm{vec}\, B)^{\mathrm{T}}}{\mathrm{d}x_l}\begin{bmatrix} 0 \\ \vdots \\ a_{k,1} \\ \vdots \\ a_{k,\bar{a}_2} \\ \vdots \\ 0 \end{bmatrix} \\ &= \frac{\mathrm{d}a_{k,1}}{\mathrm{d}x_l} b_{1,r} + \ldots + \frac{\mathrm{d}a_{k,\bar{a}_2}}{\mathrm{d}x_l} b_{\bar{a}_2,r} + \frac{\mathrm{d}b_{1,r}}{\mathrm{d}x_l} a_{k,1} + \ldots + \frac{\mathrm{d}b_{\bar{a}_2,r}}{\mathrm{d}x_l} a_{k,\bar{a}_2} \\ &= \sum_{j=1}^{\bar{a}_2}\left[\frac{\mathrm{d}a_{k,j}}{\mathrm{d}x_l} b_{j,r} + a_{k,j}\frac{\mathrm{d}b_{j,r}}{\mathrm{d}x_l}\right] \end{aligned} \tag{A.8}$$

which we see is equal to $\frac{\mathrm{d}m_{k,r}}{\mathrm{d}x_l}$. □

Note that $\frac{\mathrm{d}A}{\mathrm{d}x} \in \mathbb{R}^{n \times \bar{m}_1 \bar{a}_2}$, $B(x) \otimes I_{\bar{m}_1} \in \mathbb{R}^{\bar{m}_1 \bar{a}_2 \times \bar{m}_1 \bar{m}_2}$, $\frac{\mathrm{d}B}{\mathrm{d}x} \in \mathbb{R}^{n \times \bar{a}_2 \bar{m}_2}$ and $I_{\bar{m}_2} \otimes A^{\mathrm{T}}(x) \in \mathbb{R}^{\bar{a}_2 \bar{m}_2 \times \bar{m}_1 \bar{m}_2}$; so that $\frac{\mathrm{d}M}{\mathrm{d}x} \in \mathbb{R}^{n \times \bar{m}_1 \bar{m}_2}$ as it should be by the definition (A.5).

We can use Lemma A.2 to prove two corollaries.

Corollary A.3. *If $A = A^{\mathrm{T}} \in \mathbb{R}^{\bar{a} \times \bar{a}}$ is a constant and $b(x) \in \mathbb{R}^{\bar{a}}$ is a vector, then*

$$\frac{\mathrm{d}b(x)^{\mathrm{T}} A b(x)}{\mathrm{d}x} = 2\frac{\mathrm{d}b}{\mathrm{d}x} A b(x). \tag{A.9}$$

Proof. By Lemma A.2,

$$\begin{aligned} \frac{\mathrm{d}b^{\mathrm{T}} A b}{\mathrm{d}x} &= \frac{\mathrm{d}b^{\mathrm{T}}}{\mathrm{d}x}(Ab \otimes 1) + \frac{\mathrm{d}Ab}{\mathrm{d}x}(1 \otimes b) = \frac{\mathrm{d}b}{\mathrm{d}x} Ab + \frac{\mathrm{d}Ab}{\mathrm{d}x} b \\ &= \frac{\mathrm{d}b}{\mathrm{d}x} Ab + \frac{\mathrm{d}b}{\mathrm{d}x}(1 \otimes A^{\mathrm{T}})b = 2\frac{\mathrm{d}b}{\mathrm{d}x} Ab \end{aligned}$$

where function arguments have been dropped for brevity. □

Corollary A.4. *If $A = A^{\mathrm{T}} \in \mathbb{R}^{\bar{a}\times\bar{a}}$ is a function of x and $b \in \mathbb{R}^{\bar{a}}$ is a constant, then*

$$\frac{\mathrm{d}b^{\mathrm{T}}A(x)b}{\mathrm{d}x} = b^{\mathrm{T}}\frac{\mathrm{d}A}{\mathrm{d}x}b. \tag{A.10}$$

Proof. By Lemma A.2,

$$\frac{\mathrm{d}b^{\mathrm{T}}Ab}{\mathrm{d}x} = \frac{\mathrm{d}Ab}{\mathrm{d}x}(1 \otimes b) = \frac{\mathrm{d}A}{\mathrm{d}x}(b \otimes I_{\bar{a}})b = b^{\mathrm{T}}\frac{\mathrm{d}A}{\mathrm{d}x}b$$

where function arguments have been dropped for brevity. □

Further properties exist, but the ones listed are the only ones used in this thesis.

Appendix B

Hamilton's equations of motion

This appendix summarizes parts of Goldstein et al. [36], Lanczos [55], Shivarama [81], Shivarama and Fahrenthold [82], and is included here only for convenience.

We investigate a system with n degrees of freedom, with generalized coordinates $q \in \mathbb{R}^m$, $m \geq n$. If $m > n$, Lagrangian dynamics cannot be used. Hamilton's equations can still be used, however.

We assume that the system has potential energy $U(q) \in \mathbb{R}$ and complementary kinetic energy $T^*(q, \dot{q}) \in \mathbb{R}$.

We define the momentum of the system as

$$p \triangleq \frac{\partial T^*}{\partial \dot{q}} \in \mathbb{R}^m. \tag{B.1}$$

The complementary kinetic energy T^* and kinetic energy T have the same numerical value for all system states, but the kinetic energy is a function of q and p, while the complementary kinetic energy is a function of q and $\dot{q}$. That is,

$$T(q, p) = T^*(q, \dot{q}) \tag{B.2}$$

We can find T from this equation if we can find $\dot{q}$ as a function of p. We can also find the kinetic energy T from T^* via the Legendre transform as

$$T = p^{\mathrm{T}} q - T^* \in \mathbb{R}. \tag{B.3}$$

If T^* is quadratic in $\dot{q}$ and U is a conservative potential, then the Hamiltonian H is given by

$$H(q, p) = T(q, p) + U(q) \tag{B.4}$$

which is the total energy in the system.

If $m = n$, then the system dynamics are described by the equations

$$\dot{q} = \frac{\partial H}{\partial p} \tag{B.5}$$

$$\dot{p} = -\frac{\partial H}{\partial q} + \tau \tag{B.6}$$

where $\tau \in \mathbb{R}^m$ are external forces derived from some virtual work principle.

If $m > n$, then the states have to follow the algebraic constraints

$$\xi(q,p) = 0 \in \mathbb{R}^{m-n}. \tag{B.7}$$

The system dynamics are given by

$$\dot{q} = \frac{\partial H}{\partial p} + \frac{\partial \xi}{\partial p}\lambda \tag{B.8}$$

$$\dot{p} = -\frac{\partial H}{\partial q} - \frac{\partial \xi}{\partial q}\lambda + \tau \tag{B.9}$$

where $\lambda \in \mathbb{R}^{(m-n)\times 1}$ are some Lagrangian multipliers and $\tau \in \mathbb{R}^m$ are external forces derived from some virtual work principle.

Property B.1. If $m = n$ or $\xi = \xi(q)$, T and T^* satisfy

$$\frac{\partial T}{\partial q} = -\frac{\partial T^*}{\partial q}. \tag{B.10}$$

Proof. First, we note that $m = n$ or $\xi = \xi(q)$ and the fact that $H(q,p) = T(q,p) + U(q)$ implies that

$$\dot{q} = \frac{\partial H}{\partial p} = \frac{\partial T}{\partial p}. \tag{B.11}$$

From the Legendre transform (B.3)

$$T = p^{\mathrm{T}}\dot{q} - T^*. \tag{B.12}$$

The complimentary kinetic energy $T^* = T^*(q,\dot{q})$ has the total differential

$$\mathrm{d}T^* = \left(\frac{\partial T^*}{\partial q}\right)^{\mathrm{T}} \mathrm{d}q + \left(\frac{\partial T^*}{\partial \dot{q}}\right)^{\mathrm{T}} \mathrm{d}\dot{q}. \tag{B.13}$$

Therefore,

$$\begin{aligned}\mathrm{d}T &= p^{\mathrm{T}}\mathrm{d}\dot{q} + \mathrm{d}p^{\mathrm{T}}\dot{q} - \mathrm{d}T^* = p^{\mathrm{T}}\mathrm{d}\dot{q} + \mathrm{d}p^{\mathrm{T}}\dot{q} - \left(\frac{\partial T^*}{\partial q}\right)^{\mathrm{T}} \mathrm{d}q - \left(\frac{\partial T^*}{\partial \dot{q}}\right)^{\mathrm{T}} \mathrm{d}\dot{q} \\ &= \left(p - \frac{\partial T^*}{\partial \dot{q}}\right)^{\mathrm{T}} \mathrm{d}\dot{q} + \mathrm{d}p^{\mathrm{T}}\dot{q} - \left(\frac{\partial T^*}{\partial q}\right)^{\mathrm{T}} \mathrm{d}q.\end{aligned} \tag{B.14}$$

T also has the canonical form as a function of p and q, so

$$\mathrm{d}T = \left(\frac{\partial T}{\partial p}\right)^{\mathrm{T}} \mathrm{d}p + \left(\frac{\partial T}{\partial q}\right)^{\mathrm{T}} \mathrm{d}q. \tag{B.15}$$

Equating (B.14) and (B.15), we get

$$\left(\frac{\partial T}{\partial p}\right)^{\mathrm{T}} \mathrm{d}p + \left(\frac{\partial T}{\partial q}\right)^{\mathrm{T}} \mathrm{d}q = \left(p - \frac{\partial T^*}{\partial \dot{q}}\right)^{\mathrm{T}} \mathrm{d}\dot{q} + \mathrm{d}p^{\mathrm{T}}\dot{q} - \left(\frac{\partial T^*}{\partial q}\right)^{\mathrm{T}} \mathrm{d}q$$

$$\Downarrow$$

$$\left(\frac{\partial T}{\partial p} - \dot{q}\right)^{\mathrm{T}} \mathrm{d}p + \left(\frac{\partial T^*}{\partial \dot{q}} - p\right)^{\mathrm{T}} \mathrm{d}\dot{q} + \left(\frac{\partial T}{\partial q} + \frac{\partial T^*}{\partial q}\right)^{\mathrm{T}} \mathrm{d}q = 0.$$

Since the above must hold for all $\mathrm{d}p, \mathrm{d}\dot{q}, \mathrm{d}q$, this requires the relationships

$$\begin{aligned} \dot{q} &= \frac{\partial T}{\partial p} \\ p &= \frac{\partial T^*}{\partial \dot{q}} \\ \frac{\partial T}{\partial q} &= -\frac{\partial T^*}{\partial q}. \end{aligned}$$

We recognize the first equality as (B.11), the second equality as the definition of p, and the third statement as that which was to be proved. □

Appendix C

Numerical values for the parameters of Model VI

The results in this appendix are from Holden et al. [40].

The parameters can be found in Tables C.1–C.8. All numbers are given in the kg–m–s (SI) system. Note that α_3 and α_5 are given in radians.

Table C.1 contains the rigid body inertia matrix, and Table C.2 contains the body motion parameters. Table C.3 the added mass, while table C.4 contains the hydrodynamic damping parameters. Table C.5 contains the wave motion parameters for heave. Table C.6 contains the wave motion parameters for roll. Table C.7 contains the wave motion parameters for pitch. Table C.8 contains the external wave excitation parameters.

Table C.1: Inertia matrix M.

m	J_{11}	J_{22}
7.6654E7	1.4014E10	3.1045E11

Table C.2: Wave-independent restoring forces.

Heave	Roll	Pitch
$Z_z = 7.9882\text{E}7$	$K_\phi = 1.4340\text{E}9$	$M_z = 7.6622\text{E}8$
$Z_\theta = 7.6622\text{E}8$	$K_{\phi\phi\phi} = 2.9740\text{E}9$	$M_\theta = 4.1365\text{E}11$
$Z_{zz} = -1.5007\text{E}6$	$K_{z\phi} = -8.4268\text{E}7$	$M_{zz} = -1.2492\text{E}8$
$Z_{z\theta} = -2.4986\text{E}8$	$K_{\phi\theta} = -1.4090\text{E}10$	$M_{z\theta} = -4.9230\text{E}10$
$Z_{\phi\phi} = -1.4734\text{E}8$	$K_{zz\phi} = 1.3290\text{E}7$	$M_{\phi\phi} = -1.0307\text{E}10$
$Z_{\theta\theta} = -2.4615\text{E}10$	$K_{\phi\theta\theta} = 2.5667\text{E}10$	$M_{\theta\theta} = -2.4365\text{E}12$
$Z_{z\phi\phi} = 1.4408\text{E}8$		$M_{z\phi\phi} = 1.3526\text{E}10$
$Z_{\phi\phi\theta} = 1.3526\text{E}10$		$M_{\phi\phi\theta} = 2.0532\text{E}12$
$Z_{\theta\theta\theta} = 2.5540\text{E}8$		$M_{\theta\theta\theta} = 1.4277\text{E}11$

Table C.3: Added mass.

ω_e	$m_{a,33}$	$m_{a,35}$	$m_{a,44}$	$m_{a,53}$	$m_{a,55}$
0.5519	8.4377E7	5.2986E8	2.1700E9	2.2140E9	4.3227E11
0.5662	8.3596E7	6.8658E8	2.1700E9	2.0263E9	4.2368E11
0.5677	8.3515E7	5.7142E8	2.1700E9	2.1383E9	4.2519E11
0.5723	8.3266E7	6.5957E8	2.1700E9	2.0402E9	4.2169E11
0.5756	8.3077E7	5.9056E8	2.1700E9	2.1017E9	4.2161E11
0.5783	8.2935E7	6.3403E8	2.1700E9	2.0526E9	4.1972E11
0.5844	8.2604E7	6.0987E8	2.1700E9	2.0637E9	4.1775E11
0.5904	8.2273E7	5.8702E8	2.1700E9	2.0734E9	4.1579E11
0.5933	8.2112E7	6.2852E8	2.1700E9	2.0255E9	4.1376E11
0.5963	8.1955E7	5.6623E8	2.1700E9	2.0816E9	4.1392E11
0.6023	8.0509E7	5.2790E8	2.1700E9	2.0821E9	4.0685E11
0.6031	8.1568E7	6.4758E8	2.1700E9	1.9849E9	4.0935E11
0.6084	8.0003E7	5.0546E8	2.1700E9	2.0875E9	4.0410E11
0.6204	7.9811E7	4.7712E8	2.1700E9	2.1003E9	4.0240E11
0.6231	8.0481E7	6.8112E8	2.1700E9	1.9082E9	4.0059E11
0.6265	7.9714E7	4.6449E8	2.1700E9	2.1051E9	4.0155E11
0.6324	7.9491E7	4.5092E8	2.1700E9	2.1082E9	4.0014E11

Table C.4: Hydrodynamic damping.

ω_e	d_{33}	d_{35}	$d_{44,0}$	$d_{44,n}$	d_{53}	d_{55}
0.5519	4.6790E7	1.1900E9	3.1951E8	2.9939E8	2.6485E8	2.7431E11
0.5662	4.6121E7	1.1146E9	3.0467E8	3.7433E8	3.3617E8	2.7151E11
0.5677	4.6051E7	1.1830E9	3.1951E8	2.9939E8	2.6733E8	2.7254E11
0.5723	4.5838E7	1.1351E9	3.0962E8	3.4696E8	3.1392E8	2.7124E11
0.5756	4.5676E7	1.1795E9	3.1951E8	2.9939E8	2.6859E8	2.7166E11
0.5783	4.5554E7	1.1555E9	3.1456E8	3.2205E8	2.9184E8	2.7097E11
0.5844	4.5271E7	1.1757E9	3.1951E8	2.9939E8	2.6995E8	2.7071E11
0.5904	4.4987E7	1.1956E9	3.2445E8	2.7877E8	2.4824E8	2.7045E11
0.5933	4.4849E7	1.1717E9	3.1951E8	2.9939E8	2.7136E8	2.6973E11
0.5963	4.4714E7	1.2147E9	3.2921E8	2.6067E8	2.2754E8	2.7020E11
0.6023	4.4749E7	1.2312E9	3.3415E8	2.4348E8	2.1714E8	2.7166E11
0.6031	4.4383E7	1.1673E9	3.1951E8	2.9939E8	2.7292E8	2.6866E11
0.6084	4.4524E7	1.2498E9	3.3910E8	2.2779E8	1.9803E8	2.7167E11
0.6204	4.3839E7	1.2892E9	3.4898E8	2.0031E8	1.5198E8	2.7044E11
0.6231	4.3451E7	1.1585E9	3.1951E8	2.9939E8	2.7605E8	2.6654E11
0.6265	4.3497E7	1.3088E9	3.5393E8	1.8826E8	1.2903E8	2.6982E11
0.6324	4.3198E7	1.3274E9	3.5878E8	1.7741E8	1.0805E8	2.6943E11

Table C.5: Wave-dependent restoring moment, heave.

ω_0	$Z_{z\zeta c}$	$Z_{z\zeta s}$	$Z_{\theta\zeta c}$	$Z_{\theta\zeta s}$	$Z_{\phi\phi\zeta c}$	$Z_{\phi\phi\zeta s}$
0.4425	−2.3750E6	5.6977E5	−2.4465E8	1.9599E8	8.1275E7	−4.5080E7
0.4530	−2.5435E6	3.2979E5	−2.5538E8	1.5518E8	8.8517E7	−3.3157E7
0.4583	−2.6145E6	2.0307E5	−2.5920E8	1.3333E8	9.1601E7	−2.6808E7
0.4640	−2.6795E6	6.3346E4	−2.6201E8	1.0901E8	9.4449E7	−1.9766E7
0.4699	−2.7334E6	−8.4296E4	−2.6345E8	8.3036E7	9.6854E7	−1.2278E7
0.4764	−2.7763E6	−2.4951E5	−2.6320E8	5.3642E7	9.8827E7	−3.8388E6
0.4893	−2.8063E6	−5.8048E5	−2.5674E8	−6.3854E6	1.0049E8	1.3270E7

Table C.6: Wave-dependent restoring moment, roll.

ω_0	$K_{\phi\zeta c}$	$K_{\phi\zeta s}$
0.4425	−2.0159E8	5.0131E7
0.4530	−2.2088E8	2.9835E7
0.4583	−2.2955E8	1.9048E7
0.4640	−2.3800E8	7.0974E6
0.4699	−2.4571E8	−5.5988E6
0.4764	−2.5289E8	−1.9893E7
0.4893	−2.6271E8	−4.8841E7

Table C.7: Wave-dependent restoring moment, pitch.

ω_0	$M_{z\zeta c}$	$M_{z\zeta s}$	$M_{\theta\zeta c}$	$M_{\theta\zeta s}$	$M_{\phi\phi\zeta c}$	$M_{\phi\phi\zeta s}$
0.4425	−2.4465E8	1.9599E8	−4.1210E10	1.3418E10	1.2085E10	−8.3843E9
0.4530	−2.5538E8	1.5518E8	−4.3826E10	8.9360E9	1.2758E10	−6.7092E9
0.4583	−2.5920E8	1.3333E8	−4.4896E10	6.5627E9	1.3023E10	−5.8125E9
0.4640	−2.6201E8	1.0901E8	−4.5844E10	3.9408E9	1.3246E10	−4.8142E9
0.4699	−2.6345E8	8.3036E7	−4.6590E10	1.1646E9	1.3407E10	−3.7486E9
0.4764	−2.6320E8	5.3642E7	−4.7118E10	−1.9490E9	1.3496E10	−2.5428E9
0.4893	−2.5674E8	−6.3854E6	−4.7200E10	−8.2106E9	1.3384E10	−8.2023E7

Table C.8: External wave forces.

ω_e	$\lvert F_z\rvert$	α_z	$\lvert F_\theta\rvert$	α_θ
0.5519	1.1189E7	0.0000	2.9506E9	4.8904
0.5662	5.2714E6	−0.2025	5.2714E6	4.8730
0.5677	8.1228E6	−0.0750	8.1228E6	4.8817
0.5723	5.2225E6	−0.2147	5.2225E6	4.8730
0.5756	6.6526E6	−0.1361	6.6526E6	4.8765
0.5783	5.1755E6	−0.2269	5.1755E6	4.8712
0.5844	5.1300E6	−0.2391	5.1300E6	4.8695
0.5904	5.0859E6	−0.2496	5.0859E6	4.8695
0.5933	3.7086E6	−0.4189	3.7086E6	4.8642
0.5963	5.1571E6	−0.2478	5.1571E6	4.8712
0.6023	5.1384E6	−0.2548	5.1384E6	4.8695
0.6031	2.4887E6	−0.8186	2.4887E6	4.8573
0.6084	5.1053E6	−0.2653	5.1053E6	4.8695
0.6204	4.9566E6	−0.2950	4.9566E6	4.8660
0.6231	2.8160E6	−2.1398	2.8160E6	4.8381
0.6265	4.8859E6	−0.3107	4.8859E6	4.8642
0.6324	4.8381E6	−0.3229	4.8381E6	4.8642

Appendix D

Existence and uniqueness properties of (11.1)

In this appendix, we prove the existence and uniqueness properties of (11.1). These results are from Holden et al. [43].

From Nayfeh and Mook [63], we get the behavior of the system when ω_e is a constant, but not when it is changing. We need to guarantee a unique finite solution of (11.1) also for time-varying ω_e.

To prove the existence (and uniqueness) of the solution to (11.1), we will use the following theorem and lemma, written here for convenience:

Theorem D.1 (Khalil [52, Theorem 3.3]). *Let $f(t,x)$ be piecewise continuous in t and locally Lipschitz in x for all $t \geq t_0$ and all x in a domain $D \subset \mathbb{R}^n$. Let W be a compact subset of D, $x_0 \in W$, and suppose it is known that every solution of*

$$\dot{x} = f(t,x), \qquad x(t_0) = x_0$$

lies entirely in W. Then there is a unique solution that is defined for all $t \geq t_0$.

Lemma D.2 (Khalil [52, Lemma 3.2]). *If $f(t,x)$ and $\frac{\partial f}{\partial x}(t,x)$ are continuous on $[a,b] \times D$, for some domain $D \subset \mathbb{R}^n$, then f is locally Lipschitz in x on $[a,b] \times D$.*

If we take $x = [\phi, \dot{\phi}]^{\mathrm{T}}$, we can rewrite (11.1) as

$$\begin{aligned}
\dot{x} &= \begin{bmatrix} x_2 \\ -\frac{d_{44}}{m_{44}} x_2 - \frac{1}{m_{44}} \left[k_{44} + k_{\phi t} \cos\left(\int_{t_0}^{t} \omega_e(\tau)\, \mathrm{d}\tau + \alpha_\phi \right) \right] x_1 - \frac{k_{\phi^3}}{m_{44}} x_1^3 \end{bmatrix} = f(t,x) \\
&= \begin{bmatrix} 0 & 1 \\ -\frac{k_{44}}{m_{44}} & -\frac{d_{44}}{m_{44}} \end{bmatrix} x + \begin{bmatrix} 0 \\ -\frac{k_{\phi t}}{m_{44}} \cos\left(\int_{t_0}^{t} \omega_e(\tau)\, \mathrm{d}\tau + \alpha_\phi \right) x_1 - \frac{k_{\phi^3}}{m_{44}} x_1^3 \end{bmatrix} \\
&= Ax + g(t, x_1) \qquad \text{(D.1)}
\end{aligned}$$

with

$$f(t,x) \triangleq \begin{bmatrix} x_2 \\ -\frac{d_{44}}{m_{44}} x_2 - \frac{1}{m_{44}} \left[k_{44} + k_{\phi t} \cos\left(\int_{t_0}^{t} \omega_e(\tau)\, \mathrm{d}\tau + \alpha_\phi \right) \right] x_1 - \frac{k_{\phi^3}}{m_{44}} x_1^3 \end{bmatrix}$$

$$A \triangleq \begin{bmatrix} 0 & 1 \\ -\frac{k_{44}}{m_{44}} & -\frac{d_{44}}{m_{44}} \end{bmatrix}$$
$$g(t, x_1) \triangleq \begin{bmatrix} 0 \\ -\frac{k_{\phi t}}{m_{44}} \cos\left(\int_{t_0}^{t} \omega_e(\tau)\, \mathrm{d}\tau + \alpha_\phi\right) x_1 - \frac{k_{\phi^3}}{m_{44}} x_1^3 \end{bmatrix}.$$

Lemma D.3 (Existence and uniqueness of the solution of (11.1))**.** *There exists a unique solution of* (D.1) *(and thus* (11.1)*) defined for all* $t \geq t_0$.

Proof. It is clear that $f(t, x)$ of (D.1) is continuous in x for all $x \in \mathbb{R}^2$. It is also continuous in t for all $t \geq t_0$, as long as $\omega_e(t)$ is piecewise continuous. Our choice of ω_e (11.6) satisfies this.

The partial derivative of f with respect to x is given by

$$\frac{\partial f}{\partial x}(t, x) = A - \begin{bmatrix} 0 & 0 \\ \frac{k_{\phi t}}{m_{44}} \cos\left(\int_{t_0}^{t} \omega_e(\tau)\, \mathrm{d}\tau + \alpha_\phi\right) + 3\frac{k_{\phi^3}}{m_{44}} x_1^2 & 0 \end{bmatrix} \tag{D.2}$$

which, by the same argument, is continuous in x for all $x \in \mathbb{R}^2$ and $t \geq t_0$. By Khalil [52, Lemma 3.2], f is therefore locally Lipschitz in x for all $t \geq t_0$ and all $x \in \mathbb{R}^2$. The first part of Khalil [52, Theorem 3.3] is then satisfied.

To prove that the trajectories of the system are bounded, we use the Lyapunov function candidate

$$V = \frac{1}{2} x^{\mathrm{T}} P x + \frac{1}{4}\left(1 + \frac{m_{44}}{d_{44}}\right) k_{\phi^3} x_1^4 \tag{D.3}$$

with

$$P = \begin{bmatrix} d_{44} + k_{44}\left(1 + \frac{m_{44}}{d_{44}}\right) & m_{44} \\ m_{44} & m_{44}\left(1 + \frac{m_{44}}{d_{44}}\right) \end{bmatrix}. \tag{D.4}$$

The time derivative of V along the trajectories of the system (D.1) is given by

$$\begin{aligned} \dot{V} &= x^{\mathrm{T}} P \left(Ax + g(t, x)\right) + \left(1 + \frac{m_{44}}{d_{44}}\right) k_{\phi^3} x_1^3 x_2 \\ &= -\left(k_{44} + k_{\phi t} \cos\left(\int_{t_0}^{t} \omega_e(\tau)\, \mathrm{d}\tau + \alpha_\phi\right)\right) x_1^2 - d_{44} x_2^2 - k_{\phi^3} x_1^4 \\ &\quad - k_{\phi t} \cos\left(\int_{t_0}^{t} \omega_e(\tau)\, \mathrm{d}\tau + \alpha_\phi\right)\left(1 + \frac{m_{44}}{d_{44}}\right) x_1 x_2 \\ &\leq -\left(k_{44} - k_{\phi t}\right) x_1^2 - d_{44} x_2^2 - k_{\phi^3} x_1^4 + k_{\phi t}\left(1 + \frac{m_{44}}{d_{44}}\right) |x_1||x_2| \,. \end{aligned} \tag{D.5}$$

While $k_{44} > k_{\phi t}$, $\dot{V}$ is only negative definite for sufficiently small values of $k_{\phi t}$. If $k_{\phi t}$ *is* sufficiently small, then the origin of the system (D.1) would be globally uniformly exponentially stable, by Khalil [52, Theorem 4.10]. *A priori* we know that this is not the case; in parametric resonance, the origin is, in fact, unstable.

However, V can be used to prove that the trajectories of (D.1) are bounded. For $|x_1| \geq \mu > 0 \Rightarrow \|x\| \geq \mu$ it holds that

$$\begin{aligned}
\dot{V} &\leq -\left(k_{44} - k_{\phi t}\right) x_1^2 - d_{44} x_2^2 - k_{\phi^3} x_1^4 + k_{\phi t} \left(1 + \frac{m_{44}}{d_{44}}\right) |x_1||x_2| \\
&\leq -d_{44} x_2^2 - k_{\phi^3} \mu^2 x_1^2 + k_{\phi t} \left(1 + \frac{m_{44}}{d_{44}}\right) |x_1||x_2| \\
&= -(1-\delta) d_{44} x_2^2 - (1-\delta) k_{\phi^3} \mu^2 x_1^2 \\
&\quad + k_{\phi t} \left(1 + \frac{m_{44}}{d_{44}}\right) |x_1||x_2| - \delta d_{44} x_2^2 - \delta k_{\phi^3} \mu^2 x_1^2
\end{aligned} \tag{D.6}$$

for some $\delta \in (0, 1)$. Furthermore, the term

$$k_{\phi t} \left(1 + \frac{m_{44}}{d_{44}}\right) |x_1||x_2| - \delta d_{44} x_2^2 - \delta k_{\phi^3} \mu^2 x_1^2$$

is negative semidefinite if

$$k_{\phi t}^2 \left(1 + \frac{m_{44}}{d_{44}}\right)^2 \leq 4 d_{44} \delta^2 k_{\phi^3} \mu^2 \quad \Rightarrow \quad \mu \geq \frac{1}{2\delta \sqrt{d_{44} k_{\phi^3}}} k_{\phi t} \left(1 + \frac{m_{44}}{d_{44}}\right). \tag{D.7}$$

Therefore, for μ satisfying the above inequality,

$$\dot{V} \leq -(1-\delta) d_{44} x_2^2 - (1-\delta) k_{\phi^3} \mu^2 x_1^2 \tag{D.8}$$

which is negative definite. By Khalil [52, Theorem 4.18] the trajectories of (D.1) are bounded for any initial condition $x(t_0)$.

Therefore, the second condition of Khalil [52, Theorem 3.3] is satisfied, and there exists a unique solution of (D.1) (and thus (11.1)) that is defined for all $t \geq t_0$. □

References

[1] Assessment of parametric roll resonance in the design of container carriers. Technical report, American Bureau of Shipping, September 2004.

[2] S. L. Altmann. Hamilton, Rodrigues and the quaternion scandal. *Mathematics Magazine*, 62(5):291–308, 1989.

[3] J. Balchen, T. Andresen, and B. Foss. *Reguleringsteknikk*. Institutt for teknisk kybernetikk, 2003.

[4] R. F. Beck, W. E. Cummins, J. F. Dalzell, P. Mandel, and W. C. Webster. Motion in waves. In E. W. Lewis, editor, *Principles of Naval Architecture*, volume III, pages 1–187. SNAME, 1989.

[5] V. L. Belenky, H. Yu, and K. M. Weems. Numerical proceedures and practical experience of assessment of parametric roll in container carriers. In *Proceedings of the 9th International Conference on Stability of Ships and Ocean Vehicles*, 2006.

[6] W. Blocki. Ship safety in connection with the parametric resonance of the roll. *International Shipbuilding Progress*, 27:36–53, 1980.

[7] D. A. Breu and T. I. Fossen. Extremum seeking speed and heading control applied to parametric resonance. In *Proceeding of the IFAC Conference on Control Applications in Marine Systems*, 2010.

[8] D. A. Breu, C. Holden, and T. I. Fossen. Ship model for parametric roll incorporating the effects of time-varying speed. In T. I. Fossen and H. Nijmeijer, editors, *Parametric Resonance in Dynamical Systems*, chapter 8. Springer-Verlag, 2011.

[9] G. Bulian. *Development of analytical nonlinear models for parametric roll and hydrostatic restoring variations in regular and irregular waves*. PhD thesis, 2006.

[10] G. Bulian, A. Francescutto, and C. Lugni. On the nonlinear modeling of parametric rolling in regular and irregular waves. *International Shipbuilding Progress*, 51:173–203, 2004.

[11] G. Bulian, A. Francescutto, N. Umeda, and H. Hashimoto. Qualitative and quantitative characteristics of parametric ship rolling in random waves. *Ocean Engineering*, 35:1661–1675, 2008.

[12] S. M. Carmel. Study of parametric rolling event on a panamax container vessel. *Journal of the Transportation Research Board*, 1963:56–63, 2006.

[13] C.-T. Chen. *Linear System Theory and Design*. Oxford University Press, 1999.

[14] J. H. Conway and D. A. Smith. *On Quaternions and Ctonions*. A K Peters, Ltd., 2003.

[15] B. Cotton and K. J. Spyrou. Experimental and theoretical studies of large amplitude ship rolling and capsize. In *Proceedings of the 7th International Conference on Stability of Ships and Ocean Vehicles*, 2007.

[16] S. C. Davis and S. W. Diegel. *Transportation Energy Data Book*. Oak Ridge National Laboratory, 29th edition, 2010.

[17] I. Drummen. *Experimental and numerical investigation of nonlinear wave-induced load effects in constainerships considering hydroelasticity*. PhD thesis, NTNU, 2008.

[18] C. H. Edwards and D. E. Penney. *Calculus with Analytic Geometry*. Prentice Hall, 5th edition, 1998.

[19] O. Egeland and J. T. Gravdahl. *Modeling and Simulation for Automatic Control*. Marine Cybernetics, 2002.

[20] O. M. Faltinsen. *Sea Loads on Ships and Offshore Structures*. Cambridge University Press, 1998.

[21] O. M. Faltinsen and A. N. Timokha. *Sloshing*. Cambridge University Press, 2009.

[22] M. Faraday. On a peculiar class of acoustical figures; and on certain forms assumed by groups of particles upon vibrating elastic surfaces. *Philosophical Transactions of the Royal Society of London*, 121:299–340, 1831.

[23] D. Fathi. ShipX Vessel Responses (VERES). Marintek AS Trondheim, 2004.

[24] T. I. Fossen. *Handbook of Marine Craft Hydrodynamics and Motion Control*. Wiley, 2011.

[25] T. I. Fossen and H. Nijmeijer, editors. *Parametric Resonance in Dynamical Systems*. Springer-Verlag, 2011.

[26] H. Frahm. Results of trials of anti-rolling tanks at sea. *Transactions of the Institution of Naval Architects*, 53, 1911.

[27] W. N. France, M. Levadou, T. W. Treakle, J. R. Paulling, R. K. Michel, and C. Moore. An investigation of head-sea parametric rolling and its influence on container lashing systems. In *SNAME Annual Meeting*, 2001.

[28] A. Francescutto. An experimental investigation of parametric rolling in head waves. *Journal of Offshore Mechanics and Arctic Engineering*, 123:65–69, 2001.

[29] A. Francescutto and G. Bulian. Nonlinear and stochastic aspects of parametric rolling modelling. In *Proceedings of the 6th International Ship Stability Workshop*, 2002.

[30] W. Froude. On the rolling of ships. *Transaction of the Institution of Naval Architects*, 2:180–227, 1861.

[31] W. Froude. Remarks on Mr Scott Russel's paper on rolling. *Transactions of the Institution of Naval Architects*, 4(232–275), 1863.

[32] R. Galeazzi. *Autonomous Supervision and Control of Parametric Roll Resonance*. PhD thesis, DTU, 2009.

[33] R. Galeazzi and M. Blanke. On the feasibility of stabilizing parametric roll with active bifurcation control. In *Proceedings of the 7th IFAC Conference on Control Applications in Marine Systems*, 2007.

[34] R. Galeazzi, C. Holden, M. Blanke, and T. I. Fossen. Stabilisation of parametric roll resonance by combined speed and fin stabiliser control. In *Proceedings of the 10th European Control Conference*, 2009.

[35] S. Ginsberg. Lawsuits rock APL's boat. *San Francisco Business Journal*, 1998-11-22.

[36] H. Goldstein, C. Poole, and J. Safko. *Classical Mechanics*. Addison Wesley, 3rd edition, 2002.

[37] G. J. Goodrich. Development and design of passive roll stabilizers. In *Transactions of the Royal Institution of Naval Architects*, 1968.

[38] H. Hashimoto and N. Umeda. Nonlinear analysis of parametric rolling in longitudinal and quartering seas with realistic modeling of roll-restoring moment. *Journal of Marine Science and Technology*, 9:117–126, 2004.

[39] C. Holden and T. I. Fossen. A u-tank control system for ships in parametric roll resonance. In T. I. Fossen and H. Nijmeijer, editors, *Parametric Resonance in Dynamical Systems*, chapter 11. Springer-Verlag, 2011.

[40] C. Holden, R. Galeazzi, C. A. Rodríguez, T. Perez, T. I. Fossen, M. Blanke, and M. A. S. Neves. Nonlinear container ship model for the study of parametric roll resonance. *Modeling, Identification and Control*, 28(4), 2007.

[41] C. Holden, T. Perez, and T. I. Fossen. Frequency-motivated observer design for the prediction of parametric roll resonance. In *Proceedings of the IFAC Conference on Control Applications in Marine Systems*, 2007.

[42] C. Holden, R. Galeazzi, T. I. Fossen, and T. Perez. Stabilization of parametric roll resonance with active u-tanks via Lyapunov control design. In *Proceedings of the 10th European Control Conference*, 2009.

[43] C. Holden, D. A. Breu, and T. I. Fossen. Frequency detuning control by doppler shift. In T. I. Fossen and H. Nijmeijer, editors, *Parametric Resonance in Dynamical Systems*, chapter 9. Springer-Verlag, 2011.

[44] C. Holden, T. Perez, and T. I. Fossen. A Lagrangian approach to nonlinear modeling of anti-roll tanks. *Ocean Engineering*, 38:341–359, 2011.

[45] R. A. Horn and C. R. Johnson. *Topics in Matrix Analysis*. Cambridge University Press, 1991.

[46] J. J. Jensen and P. T. Pedersen. Critical wave episodes for assessment of parametric roll. In *Proceedings of the 9th International Marine Design Conference*, 2006.

[47] J. J. Jensen, J. Vidic-Perunovic, and P. T. Pedersen. Influence of surge motion on the probability of parametric roll in a stationary sea state. In *Proceedings of the 10th International Ship Stability Workshop*, 2007.

[48] J. J. Jensen, P. T. Pedersen, and J. Vidic-Perunovic. Estimation of parametric roll in stochastic seaway. In *Proceedings of IUTAM Symposium on Fluid-Structure Interaction in Ocean Engineering*, 2008.

[49] K. Kagawa, K. Fujita, M. Matsuo, H. Koukawa, and Y. Zensho. Development of tuned liquid damper for ship vibrations. In *Transactions of the West Japan Society of Naval Architects*, volume 78, page 251, 1989.

[50] K. Kagawa, K. Fujita, M. Matsuo, H. Koukawa, and Y. Zensho. Development of tuned liquid damper for ship vibrations. In *Transactions of the West Japan Society of Naval Architects*, volume 81, page 181, 1990.

[51] J. E. Kerwin. Notes on rolling in longitudinal waves. *International Shipbuilding Progress*, 2(16):597–614, 1955.

[52] H. Khalil. *Nonlinear Systems*. Prentice Hall, 3rd edition, 2002.

[53] E. Kreyszig. *Advanced Engineering Mathematics*. Wiley, 8th edition, 1999.

[54] S. H. Lamb. *Hydrodynamics*. Cambridge Mathematical Library, 6th edition, 1993.

[55] C. Lanczos. *The Variational Principles of Mechanics*. Dover, 4th edition, 1970.

[56] M. Levadou and L. Palazzi. Assessment of operational risks of parametric roll. In *SNAME Annual Meeting*, 2003.

[57] A. R. Lloyd. *Seakeeping: Ship Behaviour in Rough Weather*. Ellis Horwood Series in Marine Technology. Ellis Horwood, 1989.

[58] A. R. Lloyd. *Seakeeping: Ship Behaviour in Rough Weather*. ARJM Lloyd, 1998.

[59] E. Mathieu. Mémoire sur le movement vibratoire d'une membrane de forme elliptique. *Journal de Mathématiques Pures et Appliquées*, 13:137–203, 1868.

[60] F. Melde. Über erregung stehender wellen eines fadenförmigen körpers. *Annalen der Physik und Chemie*, 109:193–215, 1859.

[61] R. Moaleji and A. R. Greig. Inverse control for roll stabilization of ships using active tanks. In *Proceedings of 7th Conference on Manoeuvring and Control of Marine Craft*, 2006.

[62] R. Moaleji and A. R. Greig. On the development of ship anti-roll tanks. *Ocean Engineering*, 34:103–121, 2007.

[63] A. H. Nayfeh and D. T. Mook. *Nonlinear Oscillations*. Wiley, 1995.

[64] M. Neves and C. Rodriguez. A coupled third order model of roll parametric resonance. In *Maritime Transportation and Exploitation of Ocean and Coastal Resources: Proceedings of the 11th International Congress of the International Maritime Association of the Mediterranean*, page 243. Taylor & Francis, 2006. ISBN 0415390362.

[65] M. A. S. Neves. On the excitation of combination modes associated with parametric resonance in waves. In *Proceedings of the 6th International Ship Stability Workshop*, 2002.

[66] M. A. S. Neves and C. A. Rodríguez. On unstable ship motions resulting from strong non-linear coupling. *Ocean Engineering*, 33:1853–1883, 2006.

[67] M. A. S. Neves and C. A. Rodríguez. An investigation on roll parametric resonance in regular waves. In *Proceedings of the 9th International Conference on Stability of Ships and Ocean Vehicles*, 2006.

[68] M. A. S. Neves and C. A. Rodríguez. Influence of non-linearities on the limits of stability of ship rolling in head seas. *Ocean Engineering*, 34:1618–1630, 2007.

[69] M. A. S. Neves, N. A. Perez, and L. Valerio. Stability of small fishing vessels in longitudinal waves. *Ocean Engineering*, 26:1389–1419, 1999.

[70] I. G. Oh, A. H. Nayfeh, and D. T. Mook. Theoretical and experimental study of the nonlinearly coupled heave, pitch, and roll motions of a ship in longitudinal waves. In *Proceedings of the 14th Biennial Conference on Mechanical Vibration and Noise*, 1993.

[71] I. G. Oh, A. H. Nayfeh, and D. T. Mook. A theoretical and experimental investigations of indirectly excited roll motion in ships. *Philosophical Transactions: Mathematical, Physical and Engineering Sciences*, 358(1853–1881), 2000.

[72] M. Palmquist and C. Nygren. Recording of head-sea parametric rolling on a PCTC. Technical report, International Maritime Organization, 2004.

[73] J. Paulling. The transverse stability of a ship in a longitudinal seaway. *Journal of Ship Research*, 4(4):37–49, 1961.

[74] T. Perez. Patrol boat stabilizers. Technical report, ADI-Limited, Major Projects Group, 2002.

[75] T. Perez. *Ship Motion Control*. Advances in Industrial Control. Springer-Verlag, London, 2005.

[76] S. Ribeiro e Silva, T. A. Santos, and C. Guedes Soares. Parametrically excited roll in regular and irregular head seas. *International Shipbuilding Progress*, 51: 29–56, 2005.

[77] C. A. Rodriguez, C. Holden, T. Perez, I. Drummen, M. A. S. Neves, and T. I. Fossen. Validation of a container ship model for parametric rolling. In *Proceedings of the 9th International Ship Stability Conference*, 2007.

[78] N. E. Sanchez and A. H. Nayfeh. Nonlinear rolling motions of ships in longitudinal waves. *International Shipbuilding Progress*, 37(411):247–272, 1990.

[79] F. H. Sellars and J. Martin. Selection and evaluation of ship roll stabilization systems. *Marine Technology, SNAME*, 29(2):84–101, 1992.

[80] Y. S. Shin, V. L. Belenky, J. R. Paulling, K. M. Weems, and W. M. Lin. Criteria for parametric roll of large containeships in longitudinal seas. *Transactions of SNAME*, 112, 2004.

[81] R. A. Shivarama. *Hamilton's equations with Euler parameters for hybrid particle-finite element simulation of hypervelocity impact*. PhD thesis, University of Texas at Austin, 2002.

[82] R. A. Shivarama and E. P. Fahrenthold. Hamilton's equations with euler parameters for rigid body dynamics modeling. *Journal of Dynamic Systems, Measurement, and Control*, 126(1):124–130, 2004.

[83] K. J. Spyrou. On the parametric rolling of ships in a following sea under simultaneous nonlinear periodic surging. *Philosophical Transactions of the Royal Society of London*, 358:1813–1834, 2000.

[84] K. J. Spyrou. Designing against parametric instability in following seas. *Ocean Engineering*, 27:625–653, 2000.

[85] K. J. Spyrou. A comparison between the yaw and roll dynamics in astern seas and the effect of nonlinear surge on capsize. In *Proceedings of the 7th International Conference on Stability of Ships and Ocean Vehicles*, 2007.

[86] K. J. Spyrou, I. Tigkas, G. Scanferla, N. Pallikaropoulos, and N. Themelis. Predication potential of the parametric rolling behavior of a post-panamax container ship. *Ocean Engineering*, 35:1235–1244, 2008.

[87] G. Strang. *Linear Algebra and Its Applications*. Thomson Brooks/Cole, 4th edition, 2006.

[88] A. Tondl, T. Ruijgrok, F. Verhulst, and R. Nabergoj. *Autoparametric Resonance in Mechanical Systems*. Cambridge University Press, 2000.

[89] N. Umeda, H. Hashimoto, D. Vassalos, S. Urano, and K. Okou. Nonlinear dynamics on parametric roll resonance with realistic numerical modeling. *International Shipbuilding Progress*, 51:205–220, 2004.

[90] N. Umeda, H. Hashimoto, D. Vassalos, S. Urano, and K. Okou. An investigation of different methods for the prevention of parametric rolling. *Journal of Marine Science and Technology*, 13:16–23, 2008.

[91] F. M. White. *Fluid Mechanics*. McGraw Hill Text, 2002.